SHELL NACRE INTEGRATED BIOMATERIALS FOR BONE DEFECT MANAGEMENT

Bridget Jeyatha W.

PhD THESIS 2023

SREE CHITRA TIRUNAL INSTITUTE FOR MEDICAL SCIENCES AND

TECHNOLOGY, TRIVANDRUM

An Institution of National Importance established by an Act of the Indian Parliament
(Act No.52 of 1980)
Dept. of Science and Technology, Govt. of India
www.sctimst.ac.in

SHELL NACRE INTEGRATED BIOMATERIALS FOR BONE DEFECT MANAGEMENT

A THESIS PRESENTED BY

Bridget Jeyatha W.

TO

SREE CHITRA TIRUNAL INSTITUTE FOR MEDICAL SCIENCES AND TECHNOLOGY, TRIVANDRUM.

IN PARTIAL FULFILMENT OF THE REQUIREMENTS

FOR THE AWARD OF

DOCTOR OF PHILOSOPHY

2023

DECLARATION BY THE STUDENT

I, **BRIDGET JEYATHA W.** hereby declare that I had personally carried out the work depicted in the thesis titled, "**SHELL NACRE INTEGRATED BIOMATERIALS FOR BONE DEFECT MANAGEMENT**" except where due acknowledgement has been made in the text. No part of this thesis has been submitted for the award of any other degree or diploma prior to this date.

25.10.2023

Thiruvananthapuram

Bridget Jeyatha W.

2017/PhD/09

श्री चित्रा तिरुनाल आयुर्विज्ञान एवं प्रौद्योगिकी संस्थान, त्रिवेंद्रम, जैवचिकित्सकीय प्रौद्योगिकी स्कंध
पूजप्पुरा, तिरुवनन्तपुरम - 695 012, केरल, भारत
SREE CHITRA TIRUNAL INSTITUTE FOR MEDICAL SCIENCES AND TECHNOLOGY, TRIVANDRUM
BIO MEDICAL TECHNOLOGY WING
POOJAPPURA, THIRUVANANTHAPURAM - 695 012, KERALA, INDIA
(एक राष्ट्रीय महत्व का संस्थान, विज्ञान एवं प्रौद्योगिकी विभाग, भारत सरकार)
(An Institution of National Importance, Department of Science and Technology, Government of India)
टेलीफोन सं./Telephone No.: 0471-2340801/ 2520450 फैक्स/Fax: 0471-2341814
ई-मेल/E-mail: sct@sctimst.ac.in वेबसाइट/Website: www.sctimst.ac.in

Dr.Lizymol P.P.
Scientist G and in Charge,
Division of Dental Products,
Department of Biomaterial Science and Technology,
BMT Wing, SCTIMST.

CERTIFICATE

This is to certify that **Bridget Jeyatha W.** Division of Dental Products, Department of Biomaterial Science and Technology of this institute has fulfilled the requirements prescribed for the Ph.D. degree of the Sree Chitra Tirunal Institute for Medical Sciences and Technology, Trivandrum. The thesis entitled, "**Shell nacre integrated biomaterials for bone defect management**." was carried out under my direct supervision. No part of the thesis was submitted for the award of any degree or diploma prior to this date. Clearance was obtained from the Institutional Animal Ethics committees for carrying out the study.

Dr.Lizymol P.P
Scientist G
Scientist in Charge
Division of Dental Products
Biomedical Technology Wing
Sree Chitra Tirunal Institute for Medical Science & Technology
Poojappura,Thiruvananthapuram-695012

The thesis entitled

SHELL NACRE INTEGRATED BIOMATERIALS FOR BONE DEFECT MANAGEMENT

Submitted by

Bridget Jeyatha W.

for the degree of

Doctor of Philosophy

of

SREE CHITRA TIRUNAL INSTITUTE FOR MEDICAL SCIENCES AND TECHNOLOGY, THIRUVANANTHAPURAM

is evaluated and approved by

.....

Dr. Lizymol P.P.

(Research Supervisor)

.....

Dr. Santanu Dhara

(Thesis examiner)

ACKNOWLEDGEMENTS

First and foremost, I would like to praise and thank Lord for His grace and blessings in all my endeavours. I took this privilege to thank and acknowledge all who have helped me in accomplishing my PhD work.

First of all, I would like to express my heartfelt gratitude to my Guide Dr. Lizymol P.P. for accepting me as PhD student. I fail to gather words to express my deep sense of gratitude for her creative and expert guidance. Her ability to simplify the most challenging task., all promoting activities, provision of independent research, and the kindness which she always bestowed on me have paved the way for the successful completion of my work.

I am extremely grateful to my DAC members Dr. Anoop S Pillai, SUT Pattom, Dr. Kalliayanakrishnan, Former Dean and Head, SCTIMST, Dr. Manoj Komath, Head, Department of Biomaterial Science and Technology, Dr. Roy Joseph, Dean (Academic Affairs), SCTIMST for molding my PhD work, timely help, critical review and suggestions.

My vocabulary is insufficient to reflect my deep gratitude to Dr. Elena Jones, Supervisor Newton Bhabha PhD Placement Fellowship for her constant inspiration and support in making the placement possible. I sincerely thank her for all the initiatives for the immediate start of my experiment and all her support to finish the placement successfully. Furthermore, I thank her for all the comments and suggestions to make manuscripts and work better. I thank Dr. Hemant Pandit, LIRMM for all his immediate reply, support and inspiration.

I thank KSCSTE for the fellowship from 22.03.2017 to 15-10.2018 and thank ICMR, India for the ICMR SRF fellowship from 22.10.2018 -22.10.2022. I thank DBT, British Council, India and Newton fund, UK for the Newton Bhabha Ph.D. Placement Fellowship.

I sincerely thank the present Director Dr Sanjay Behari and former Directors of SCTIMST and The Head, BMT Wing for all the support and facilitation. I sincerely thank Dr.Kalliyanakrishnan, former Head of DBST, and Dr. Manoj Komath, Head, DBST for all the support and encouragement throughout the studies.

I sincerely thank the present Dean Dr.Roy Joseph, and former Deans for all the support. I thank present Associate Dean Dr. Uma Shankar and all former associate deans for all their support. I thank the present registrar Dr.Santhosh Kumar and former Registrars for all the support. I thank the present deputy registrar Ms. Radha M. and the former deputy registrars for all the support. I extend my thanks to all staff of Academic Affairs, SCTIMST. I thank all staff of library,customer service cell, network services cell, administration,Stores and Purchase, creche facility for all the support.

I sincerely thank Dr. Anil Kumar P.R. for all his support for the *in vitro* experiments particularly the osteogenesis study with rat BM-MSC through testing, project mode, and collaborative works. My special thanks to Ms. Deepa, Mr. Vinod, and all staff of TIC. I sincerely thank Dr. Mohanan P.V., Dr. Remya and all staff of toxicology for the timely execution of the biocompatibility studies. I sincerely thank Dr. Harikrishnan V.S., for the *in vivo* osseointegration studies. I also thank Mr. Manoj, Mr. Sunil, Mr. Prasanth, Mr.Pradeep and all members of DLAS I sincerely thank Dr. Sabareeswaran, Dr. Ariya, Mr. Joseph and all members of Histopathology lab for the explantation of implants and all histology work.

I sincerely thank Dr. Roy Joseph, for thermal analysis and all support comments and suggestions throughout the studies. I thank Mr. Willi Paul and all staff of CAF for helping with the studies. I thank Dr.Gijo Raj, Ms.Jasmine and all members of PMD. I thank Mr. RajKrishna, Ms.Bessy and all present and former members of IPC cell. I thank Dr. Prabha D Nair for contact angle studies and all members for DTERT. I thank Dr. Anughya Bhatt, Ms. Priyanka, Ms. Nimmy, Ms. Sasi Kala for rheology studies. I thank Dr. Uma Shankar, Dr. Sachin, Mr. Manoj for helping with x-ray radiography

I thank Prof. (Dr.) Anil Kumar T.V. for helping with critical review of my biology part, and helping with lyophilization. I thank Mr. Pratheesh and all members of experimental pathology. Dr. JayaSree R.S., Dr. Jibin, Ms. Dhanya and all members of Biophotonics for FTIR studies. I thank Dr. Rekha M.R. for helping with lyophilization, Ms. Rajalekshmi, Ms. Linchu and all members of BST

I sincerely thank Dr. Manoj Komath for helping with SEM, SEM-EDS, TEM, ICP-OES, FTIR, XRD analysis and *in vitro* experiments. Dr. Francis for cell culture studies, Dr. Suresh Babu for FTIR and XRD studies, Ms. Susan for TEM analysis of resins, Dr. Nishad for SEM studies, Dr.Remya, Dr. Nimmy, Dr. Eva, Ms. Gayathry, Ms. Saranya and all members of Bioceramics lab.

I sincerely thank The Director, and Deputy Director Dr. Hemant Pandit, LIRMM, Leeds for all the support and facilitation. I sincerely thank Dr. Payal Ganguly for all her experimental support and inspiration throughout the placement. I thank Dr. Heather Owston for all her support throughout the placement. I thank Dr. Neelam Iqbal for confocal training and all the support throughout the placement. I thank Mr. Michael Brookes for SEM-EDS training and allowing me to do ndependently and for timely help during the placement. I sincerely thank Dr. Payal Ganguly, Dr. Heather Owston and all for conducting the qPCR

experiment with fluidigm and helping me to accomplish my work after placement. I thank Prof. (Dr). Dennis McGonagle, Dr. Chi Wong, Ms. Rekha Parmer, Dr. James and all rheumatology and haematology lab members for the support.

I thank Dr. Shiny Velayudhan for helping with scaffold fabrications and all her technical inputs throughout my study. I thank Dr. Manju for helping with GPC for all her suggestions and comments. I thank Dr.Deepu, Ms. Saranya, Mr. Sreejith, Ms. Sajini and former members Dr.Vibha, Ms. Dhanya G R, Ms.Lakshmi, Ms. Deepa Mohan, Ms. Nithusha K, Ms. Shafna, Mr. Ajith, Mr. Paila Ravi Shankar, Ms. Anusree and all members of the lab for the friendship and support. I thank Ms. Kavitha, Scientist, Shell Fisheries Division, CMFRI for identifying the Pinctada fucata shells.

My PhD is not possible without the help of my husband Mr. Arul Mathan, who has been there with me every step of my way. I am eternally grateful to him and my children Johan and Joshan for all the adjustments, understandings and sacrifices they made to support my endeavours. I thank my parents Mr. Wilson Devaraj and Mrs. Paulin for their prayers, constant support and motivation throughout the study. I thank my sisters, brother, sister-in-law, and all my family members and friends for their support and inspiration.

I dedicate this thesis to Mr. Arul Mathan, Johan, Joshan, my parents and my guide

TABLE OF CONTENTS

LIST OF FIGURES

LIST OF TABLES

LIST OF ABBREVIATIONS

Abbreviation	Full Form
BCP	biphasic calcium phosphate
BHT	butylated hydroxytoluene
bis GMA	Bisphenol-A-glycidyl methacrylate
BM-MSC	Bone marrow mesenchymal stem cells
BMPs	bone morphogenetic proteins
BPO	benzoyl peroxide
CD	Cluster of differentiation
DMAPEA	2-4-(Dimethyl amino) phenyl ethanol
DMC	Dimethyl carbonate
DMEM	Dulbecco's minimal essential media
EDS	Energy dispersive spectroscopy
FBS	Foetal bovine serum
FTIR	Fourier transform infrared spectroscopy
HA	Hydroxyapatite
HOS	Human osteoblast sarcoma
JCPDS	Joint committee on powder Diffraction standards
MicroCT	Microcomputed tomography
MIMT	Masquelet induced membrane technique

MMA	Methyl Methacrylate
MTT	3-(4,5-Dimethyl thiazol-2-yl)-2,5- diphenyltetrazolium bromide
OES-ICP	Optical Emission Spectroscopy with Inductively Coupled Plasma
ORMOCER	Organically modified ceramic resin
PBS	Phosphate buffered saline
PCL	Polycaprolactone
PMMA	Polymethyl methacrylate
PVC	Polyvinylchloride
RUNX-2	Runt-related transcription factors-2
SBF	Simulation body fluid
SEM	Scanning electron microscope
TCP	tricalcium phosphate
TEGDMA	triethylene glycol dimethacrylate
TGA	Thermogravimetric analysis
TIPS	Thermal induced phase separation method
UHMWPE	ultra-high molecular weight polyethylene
XRD	X-ray Diffraction
DMEM	Dulbecco's minimal essential medium
SM Medium	Stem MACS Medium

SYNOPSIS

Bone is a specialized hard connective tissue that provides mechanical support, structural integrity, protects internal organs, facilitates locomotion, and serves as a reservoir of minerals. It is a dynamic load-bearing flexible tissue with an architecture of highly porous and elastic internal trabecular, and less porous, hard, and densely packed external cortical. The macro, micro, and nano-scale structures of the bone are fashioned with the organic matrix of collagenous and non-collagenous protein and the inorganic matrix of hydroxyapatite. The main engineers behind these superior structures are the bone-forming osteoblast, bone-resorbing osteoclast, and mechanosensory osteocytes. Bone is the only biomineralized composite with cellular compositions that enables it to regenerate without scar formation. Unfortunately, there are often situations like trauma, tumor resections, infection, osteoporosis, osteoarthritis, metabolic diseases, and many other conditions that cause bone defects.

The critical-sized bone defects are managed through bone grafting procedures and other techniques like the Masquelet-induced membrane technique. However, the deficiency of autografts occurs in the case of geriatric or pediatric patients or patients who couldn’t spare an iliac crest/reamer irrigator aspirator (RIA) graft/ or have a larger defect exceeding 5 cm. Furthermore, due to donor site morbidity of autografts; infections and rejection of allografts; heterotrophic bone formation, and high cost of bone morphogenetic proteins (BMPs), many new biomaterials have emerged in the field of orthopedics. Additionally, the report of 5.2 million bone grafting procedures (2020) in India has emphasized the dire need for affordable osteogenic, osteoconductive scaffold with suitable mechanical properties.

Another type of defect is bone voids (< 10 mm) which are met during revision arthroplasties or after tumor/infection resections. These bone voids are managed with bone cements such as polymethyl methacrylate (PMMA), calcium phosphate, calcium sulphate, and tricalcium phosphate cements, *etc*. However, the poor biological performance of PMMA-based cement and the lower mechanical performance of self-setting cement emphasize the critical need for a bioactive osteogenic low-shrinkage cement with good mechanical properties and minimal exotherm for load-bearing application.

The next major issue to consider is more than 50% of orthopedic surgeries are performed on elderly patients, aged over 65 years. This population faces major challenges such as slow recovery, delayed fracture healing, co-morbidities, and reduced mobility. Aging bone exhibits characteristic features, including empty osteocytic lacunae, shrunken osteocytes, osteoblast apoptosis, increased osteoclast activity, and increased bone marrow adiposity**,** ultimately leading to reduced bone formation and increased bone turnover. This shift toward adipogenesis instead of osteogenesis underscores the importance of considering the microenvironment of aging bone when designing any bone graft substitute. Therefore, the unmet clinical need is a cost-effective biomaterial with properties encompassing osteoconduction, osteogenesis, osseointegration, suitable mechanical properties, and consideration of the microenvironment of aging bone.

The field of orthopedics is exclusively dependent on high-cost synthetic calcium phosphate ceramics and the related materials for bone defect management. Natural materials like collagen, silk, chitosan, alginate, hyaluronic acid, cellulose

gelatine, rattan wood, pearl, shells, coral, *etc*., are investigated for osteogenic potential. All these materials are chemically transformed or combined with other inorganic calcium phosphate ceramics for osteogenesis and mechanical properties.

Shell nacre/mother of pearl is the inner nacreous layer of the pearl oyster shell. Among the other natural materials, better osteogenesis, radiopacity, osseointegration, high fracture toughness and strength, anti-osteoporotic activity, and angiogenesis property proved shell nacre as a suitable biomaterial for bone defect management. It is either investigated as a direct bone substitute or as a powder mixed with blood to fill bone voids. The major hurdle is that there is no proper processing method to obtain shell nacre powder with both organic and inorganic content. Further, no processing method is developed to set or mould shell nacre powder with suitable mechanical properties. So, the principal aim of the work is to develop a processing method to get shell nacre powder and development of shell nacre-based biomaterials for bone defect management using the shell nacre powder. This is followed by different physicochemical and biological evaluations as well.

With this background, the hypothesis of the thesis was

- Development of a processing method to obtain shell nacre powder with both inorganic and organic matrix
- Fabrication of porous, bioactive, osteoconductive, and osteogenic shell nacre scaffolds
- Setting and molding shell nacre into any osseous sites with defined anatomical forms as shell nacre cement

To prove the hypothesis, the framed four main objectives are

1. Shell nacre powder: Processing and characterization
2. Fabrication and characterization of shell nacre PCL composite scaffold
3. Development and characterization of shell nacre cement
4. *In vitro* osteogenesis of shell nacre integrated materials with bone marrow mesenchymal stem cells (BM-MSC) from young and older donor

The thesis is divided into eight main chapters. **Chapter 1** introduces the research topic and describes bone biology. Further, it familiarizes bone defect management, bone graft substitutes, bone cements, and briefly introduces natural materials. Further, it includes the need for osteogenic bone graft substitutes and bone void-filling cement, hypothesis and objectives.

Chapter 2 describes the detailed literature review of shell nacre and shell nacre-based materials. It also includes about bone tissue engineering, fabrication of scaffolds by thermal induced phase separation method. Further, it discusses about various resin matrix including organically modified ceramic resin and filler and its significance in bone cement systems. Finally, the chapter includes a literature search on changes in bone during aging.

Chapter 3 explains in detail about the materials and methods, results obtained, and the discussion of objective **1) Shell nacre powder: Processing and characterization** including the following sub-objectives

a) Removal of the outer prismatic layer of shell nacre

b) Processing of shells to obtain shell nacre powder and

c) Characterization of shell nacre powder.

In brief, pearl oyster shells were collected and the outer prismatic layer of shells were removed. Followed by the milling of nacreous shells and shell nacre powder was obtained and further characterized. The results were presented as graphs, images, and tables and discussed in relation to similar work, objectives, and hypotheses.

Chapter 4 includes the materials and methods, results obtained, and the discussion of **objective 2) Fabrication and characterization of shell nacre PCL composite scaffold** including the following sub-objectives

a) Fabrication by thermal induced phase separation method

b) Physico-chemical characterization

c) *In vitro* osteogenesis rat bone marrow mesenchymal stem cells

Shell nacre PCL composite scaffolds were fabricated by thermal-induced phase separation method. The effect of shell nacre was studied and two groups of scaffolds were fabricated with higher and lower concentrations of shell nacre. Based on compressive modulus, scaffolds SN-15 (14 wt%) and SN-150 (60 wt%) were selected for further studies. Physico-chemical characterizations and cytotoxicity studies were carried out. Further, the osteogenic potential of the scaffolds was studied with rat bone marrow mesenchymal stem cells. The *in vitro* osteogenesis of the scaffolds was compared with clinical control G-Bone and studied by alkaline phosphatase assay, quantitative PCR, and immunofluorescence staining. Further, the results obtained were presented as graphs, and images and discussed in the context of objectives, hypotheses, and related works.

Chapter 5 comprises the materials and methods, results obtained, and the discussion of the work carried out under **objective 3) development and characterization of shell nacre cement: Part I** including the sub-objectives

a) Synthesis of shell nacre containing ladder-structured siloxane methacrylate resin

b) Characterization of the resin.

Initially, shell nacre containing siloxane methacrylates (SNLSMs) was synthesized by the modified sol-gel method. The synthesized resins were characterized by Fourier transform infrared spectroscopy (FTIR), Raman spectroscopy, nuclear magnetic resonance spectroscopy (NMR) spectroscopy, thermogravimetry (TGA), and differential scanning calorimetry (DSC). Further, the viscosity and the ladder morphology of the resin were studied. The obtained results were presented as graphs, tables, and images and discussed in the background to similar literature.

Chapter 6 covers the materials and methods, results obtained, and the discussion of the work carried out under the **sub-objectives of objective 3 Part II**

c) Formulation of chemical cure compositions using the synthesized resin

d) Physico-chemical characterization of shell nacre cement

e) Biocompatibility evaluation and

f) Osseointegration of *in situ* setting shell nacre cement.

Shell nacre cement was formulated as a two-paste system A and B using the shell nacre powder and the synthesized SNLSM2. Both paste A and B included SNLSM2, triethylene glycol dimethacrylate, fumed silica, 4-methoxy phenol, and

shell nacre powder. Paste A specifically contained 2-4- (Dimethyl amino) phenyl ethanol (DMAPEA) as an activator whereas paste B contained benzoyl peroxide BPO) and butylated hydroxytoluene (BHT). Based on mechanical properties, setting, and working time, the best shell nacre cement was selected for further studies. After *in vitro* cytotoxicity studies, acute systemic toxicity, irritation test, and pyrogen test were carried out based on ISO 10993-1 standard. Shell nacre cement was *in situ* cured in a femoral cortical defect of 2 mm size in Sprague Dawley rats. After 6 and 12 weeks, X-ray imaging of the samples were carried out. The obtained results of each sub-objectives were presented as graphs, tables, and images and discussed in a milieu to the similar current literature on bonecement.

Chapter 7 contains the materials and methods, results, and the discussion of work carried out under **objective 4 - *In vitro* osteogenesis of shell nacre integrated materials with bone marrow mesenchymal stem cells from young and older donors** (Newton Bhabha PhD Placement - University of Leeds, UK) including the following sub-objectives

a) Cytotoxicity studies
b) Expansion and characterization of young and older donor BM-MSC
c) *In vitro* osteogenesis studies

After direct and indirect cytotoxicity of the shell nacre PCL composite scaffold and shell nacre cement with human BM-MSC, *in vitro* osteogenesis experiment with older and young donor BM-MSC was initiated. Donors of age less than 30 (n=3) were considered young and greater than 55 (n=3) were taken as the older group. Followed by the study of colony-forming unit fibroblastic assay and growth kinetics, the cultures

were pooled to minimize donor variation. The senescence of the pooled younger and older donor BM-MSC was studied by histochemical β-galactosidase staining. Pooled young and older donor MSCs were seeded into all three materials for 7, 14, and 21 days. After the attachment of cells (Day 7), the cells were induced with an osteo-differentiation medium for 14 days. The viability of the cells on the material was studied by live cell tracker green-confocal imaging studies. The osteogenic potential of the material was studied by scanning electron microscopy energy dispersive spectroscopy (SEM-EDS) and gene expression studies. The results were presented as graphs and images. The results were discussed in relation to similar studies and highlighted the significance of the present study.

Chapter 8 concludes and summarizes the thesis with respect to the outcomes of all the objectives. So, a processing method was developed to get shell nacre powder containing both organic and inorganic constituents. Shell nacre PCL composite scaffolds are porous, bioactive, non-cytotoxic, and osteogenic. Similarly, the shell nacre cement is a low shrinkage, biocompatible, osteogenic, and osseo-integrative with minimal exotherm generation. Although the older BMMSCs were more senescent than the young, shell nacre integrated cement and scaffolds promoted the microenvironment and osteogenesis. Therefore, shell nacre PCL composite scaffolds and shell nacre cement will be promising candidates for managing bone defects in the near future.

The citations of the work are included in the reference section using Zotero. Acknowledgments, table of contents, list of abbreviations, list of figures, list of tables, supplementary data, list of publications, patents, awards and brief CV are included.

1 INTRODUCTION

Bone is a remarkable and unique dynamic load-bearing tissue that possesses the ability to heal without scar formation. However, the maintenance of bone homeostasis relies on several essential factors, including viable cells such as osteoblasts, osteoclasts, stem cells and osteocytes, adequate vascularity, stability, the presence of growth factors, and a conducive matrix for growth. Regrettably, there are often situations like trauma, tumour resections, infection, osteoporosis, osteoarthritis, metabolic diseases, and many others where one or more of these conditions are inadequate and causes a bone loss/defect which requires surgical interventions like bone grafting, Masquelet technique, vertebroplasty, kyphoplasty, *etc*. The success of all these orthopaedic procedures is highly dependent on the quality of material used.

Bone defects are managed according to the defect size, site of the defect, age of patients, and other co-morbidities. Bone cement systems are mainly preferred for managing irregular bone voids in load-bearing sites and in geriatric patients. Polymethyl methacrylate (PMMA) is the most widely used material in orthopaedics. Despite the monomer-mediated toxicity, exotherm generation, and inertness, PMMA is used as bone void-filling cement only for its mechanical properties. Next to PMMA, calcium sulphate, calcium phosphate, and hydroxyapatite materials are used which lack structural support and undergoes either slow/rapid resorption. Similarly, porous bone void fillers/ bone graft expanders are used to manage critical-sized defects in old and young patients. In India alone, an astounding 5.2 million bone grafting procedures were reported in 2020. However, it is concerning that Indian orthopaedic surgeons rely

on imported bone substitute materials. This situation highlights the urgent and pressing need for the development of cost-effective bone substitute materials.

So, to develop an ideal material for managing bone defects, a thorough understanding of general bone biology, bone defects, bone grafts, bone substitutes, bone cement, natural biomaterials are discussed in detail below.

1.1 BONE BIOLOGY

Bone is a specialized hard connective tissue that provides mechanical support, imparts structural integrity, protects internal organs and facilitates locomotion. Additionally, bones act as reservoir of minerals with approximately 99% of calcium (1-1.5 kg) and 85% of phosphate are stored in the bones. The skeletal system carries out its function through two main components: the axial skeleton and the appendicular skeleton. The axial skeleton includes the vertebral column bones, thoracic cage, skull, and other related bones. The appendicular skeleton is connected to the axial skeleton and includes the bones of the pectoral girdle, pelvic girdle, upper limbs, and lower limbs. Based on shape, these bones are classified into long bones (*e.g.*, clavicle, humerus, radius, ulna, phalanges, femur, tibia, metacarpals), short bones (*e.g.*, carpals, patella, tarsus), flat bones (*e.g.*, cranial bones, rib bones, hip bones) and irregular bones (bones of the vertebra).

1.1.1 Macroscopic features of bone

All bones consist of both inner trabecular and outer cortical bones. The trabecular bone which makes up approximately 20% of the skeletal system, forms the inner architecture of the bones. The amount of trabecular bone can vary among

different bones such as the proximal femur (50-75%) and distal radius (25%). It has a highly porous structure, ranging from 50-90% resembling a spongy honeycomb or lattice-like pattern. This structure provides an increased surface area for red bone marrow, blood vessels and connective tissues to come in contact with the bone, facilitating process like haematopoiesis and mineral homeostasis. Trabecular bone also functions as an internal support by evenly distributing the load and absorbing energy, especially near joints. It is less dense, more elastic, and undergoes 25% remodelling annually (Bartl and Bartl, 2017).

Cortical bone forms the outermost layer of long bones and makes up 80% of the skeleton. The main function of the cortical bone is to provide mechanical strength and protection. It is hard, dense and nearly 90% calcified. It has a slow turnover rate and high resistance to bending and torsion. With a high matrix mass per unit volume and low porosity, it possesses the necessary compressive strength. Cortical bone undergoes 2.5% remodeling annually and contains micropores that facilitate vascularization, neural connection and nutrient delivery (Hadjidakis and Androulakis, 2006; Safadi et al., 2009).

1.1.2 Long bones

The macroscopic examination of long bone reveals epiphysis, diaphysis, metaphysis, and physis (seen in children). The epiphysis lies at the end and is situated between the epiphyseal growth plate and the articular cartilage. The diaphysis, also known as the midshaft refers to the middle hollow cylindrical portion of a tubular bone. The metaphysis is a wide transition zone between the middle diaphysis and the extreme epiphysis.

The long bones and the marrow have a rich vascular supply, receiving approximately 10-20% of the cardiac output through diaphyseal nutrient artery, metaphyseal artery, epiphyseal artery, and periosteal artery. Nerves are found in the articular extremities, including sensory, sympathetic, and vasomotor.

The periosteum is a thick fibrous membrane covering a bone's entire surface except for the articular cartilage. It consists of an outer fibrous connective tissue layer and the inner cambium (cellular) layer. The outer fibrous connective tissue layer provides structural integrity and includes the fibroblasts, collagen, elastin fibre, distinct nerves, and microvascular network. The inner cambium layer is a cellular osteogenic layer that consists of mesenchymal stem cells, osteogenic progenitor cells, fibroblasts, micro vessels, and sympathetic nerves. The endosteum, a single layer of bone lining cells and osteoblast, forms a membrane that encloses the bone marrow. This structure helps maintain the integrity of bones (Bartl and Bartl, 2017; Hadjidakis and Androulakis, 2006; Safadi et al., 2009).

1.1.3 Chemical compositions of bone

Bone is a composite calcified tissue of both organic and inorganic components. It includes 60% inorganic component, 10% water and 30% organic matrix. The inorganic component of the bone primarily consists of crystalline calcium hydroxyapatite $Ca_{10}(PO4)_6(OH)_2$. These hydroxyapatite crystals exhibit a small plate-shaped structure measuring 20-50 nm in length, 15 nm in width and 2-5 nm in thickness. Interestingly, these crystals are aligned parallel to collagen fibres within the bone matrix. This orientation maximizes the collagen's resistance to tensile (stretch)

forces while simultaneously enhancing the resistance of calcium hydroxyapatite crystal to compressive forces (Feng, 2009; Safadi et al., 2009).

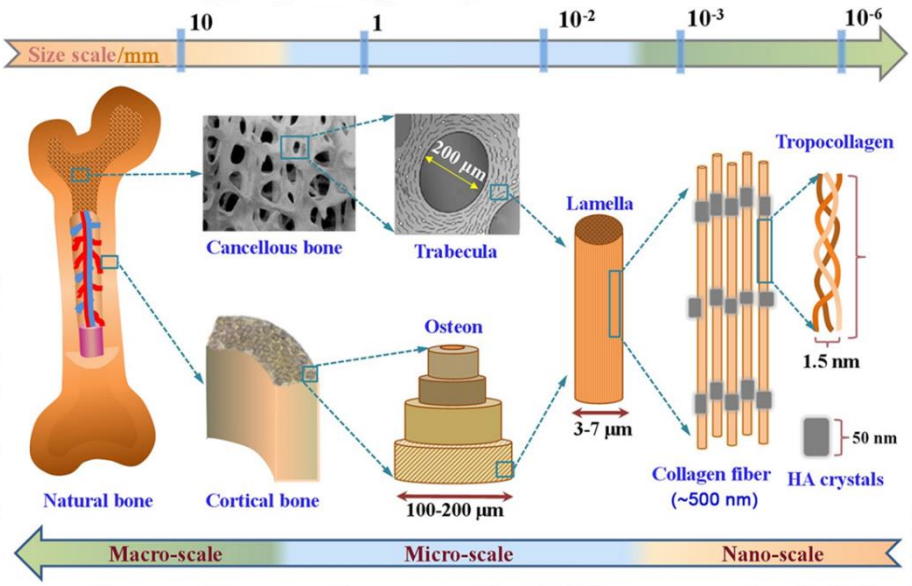

Figure 1.1 The chemical composition and multiscale structure of natural bone (Adopted from (Gao et al., 2017))

The organic component of bone primarily comprises type I collagen, which occupies 90% of the total composition and the remaining 10% consists of non-collagenous proteins. Type I collagen is a triple-helical molecule consisting of three polypeptide chains. These polypeptide chains are cross-linked, resulting in a linear molecule of ~ 300nm in length. These linear molecules are aligned together in a parallel fashion to form collagen fibrils, which are then grouped in bundles to produce collagen fibre. Type I collagen serves as the primary structural component within the bone matrix, providing strength and flexibility. In addition to collagen I, non-collagenous proteins represent the major structural component of the bone matrix. Nearly 30 non-collagenous proteins have been identified so far, which included the

ECM proteins, growth factors and cytokines such as fibronectin, osteopontin, osteocalcin and bone sialoprotein, decorin, biglycan *etc*. (Boskey, 2013; Feng, 2009).

1.1.4 Cellular compositions of bone

The main cellular components of the bone are osteoblasts, osteocytes and osteoclasts. Among this, osteoblasts and osteocytes are derived from mesenchymal stem cells, while osteoclasts are derived from hematopoietic stem cells.

1.1.4.1 Osteoblast

Osteoblasts are cuboidal-shaped bone-building cells that originate from mesenchymal stem cells (MSC) in the bone marrow. The commitment of MSC into the osteo-chondro progenitor lineage requires the expression of bone morphogenetic proteins (BMPs) and members of the Wingless (Wnt) pathways. Key transcription factors such as Runt-related transcription factors 2(RUNX-2), Distal-less homeobox 5 (Dlx5), and osterix (Osx) are crucial for osteoblast differentiation. In particular, Runx-2 is a master gene of osteoblast differentiation and upregulate genes such as collagen I, Alkaline phosphatase, bone sialoprotein, osteocalcin *etc*. The osteoblasts are responsible for producing bone matrix constituents. The process of bone formation occurs in three steps: osteoid matrix production, maturation of osteoid and mineralization of the matrix (Bartl and Bartl, 2017; Florencio-Silva et al., 2015; Hadjidakis and Androulakis, 2006).

1.1.4.2 Osteocytes

Osteocytes, also known as “bone maintainers” or “bone controllers,” are mature osteoblasts that became embedded within the osteoid matrix. They are the longest-living bone cell and have lower metabolic activity compared to osteoblasts. Osteocytes reside in small spaces within the bone called *lacunae* and establish connections with osteoblasts and other osteocytes through long cytoplasmic processes that pass through thin tunnels known as canaliculi. It possesses intracellular communication systems through the gap junction and extracellular communication system involving the lacuna-canalicular network. The quantity of osteocytes determines the bone mass. It plays a pivotal role in bone turnover and the functional adaptation of bone and called as mechanosensory cells of bone (Hadjidakis and Androulakis, 2006; Komori, 2013).

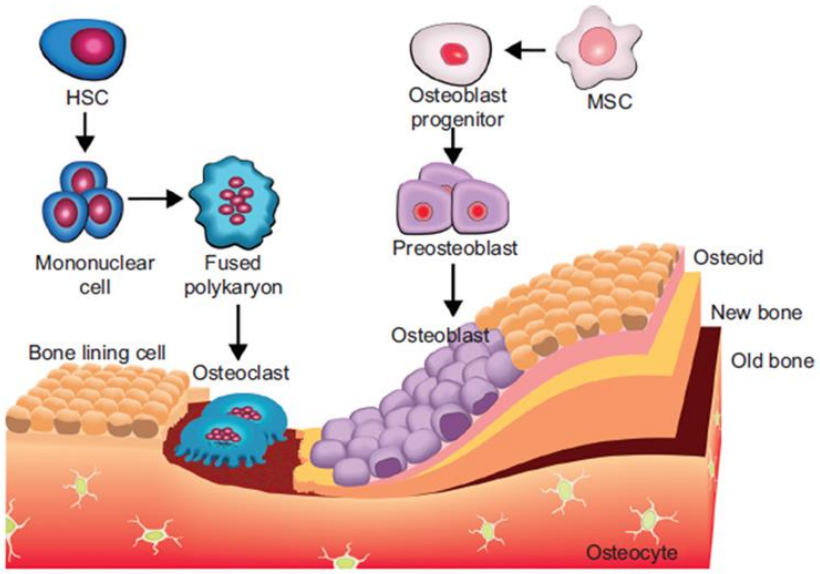

Figure 1.2 Diagram showing the evolution and function of osteoblasts and osteoclasts in bone formation (Adopted from (Rahman et al., 2015))

1.1.4.3 Osteoclast

Osteoclast are also known as bone carvers or bone breakers or bone resorbers. These are terminally differentiated multinucleated giant cells that lines up the bone. It has abundant Golgi complexes, mitochondria, and transport vesicles loaded with lysosomal enzymes. It induces the secretion of protons and lytic enzymes via the ruffled border into a sealed resorption pit. The secretion of protons causes acidification of the compartment. This activates tartrate resistant acid phosphatase and cathepsin K which degrades collagen and hydroxyapatite. It resorbs the weak, old and fractured bone in a short period of time (Florencio-Silva et al., 2015; Hadjidakis and Androulakis, 2006)

1.1.4.4 Endosteal lining cells

Endosteal lining cells, also known as bone "housekeepers", are flat inactive osteoblasts lining the internal surface of the bones and form a protective layer. It acts as a surveillance system and activates osteoclasts. It is actively involved in bone remodelling by removing the fragments of bone left by osteoclasts. It cleans the resorption pits and initiates new bone formation (Bartl and Bartl, 2017).

1.1.5 Development of bones

The flat bones of axial and long bones of appendicular skeleton are formed by intramembranous and endochondral ossification. In endochondral ossification, mesenchymal cells are differentiated into chondrocytes and then osteoblasts are formed. On the other hand, intramembranous ossification does not involve a chondrocyte intermediatory and osteoblasts are directly formed from the mesenchymal

stem cells. A key distinction between these two processes is the cartilage intermediatory.

1.1.5.1 Intramembranous ossification

During intramembranous ossification, a cluster of mesenchymal stem cells undergo condensation under the influence of fibroblast growth factors and bone morphogenetic proteins. This condensed mesenchyme then differentiates into osteoblast which secretes the matrix of collagen fibers called osteoid. Subsequently, this osteoid undergoes mineralization resulting in the formation of a woven bone. Over time, the woven bones are remodelled and gradually replaced with mature lamellar bone (Moreira et al., 2019; Safadi et al., 2009).

1.1.5.2 Endochondral ossification

Endochondral ossification is a process in which hyaline cartilage is gradually replaced by bone. The process begins with the commitment of MSC towards chondrocytes which occurs through the expression of transcription factors Pax1 and Scleraxis. These transcription factors activate cartilage genes, initiating the formation of cartilage. Subsequently, the committed mesenchymal stem cells differentiate into chondrocytes which rapidly proliferate and secrete the cartilage-specific extracellular matrix called hyaline cartilage to form the cartilage model of bone. The cartilage model includes the hyaline cartilage and the surrounding membrane perichondrium (Breeland et al., 2023; Safadi et al., 2009).

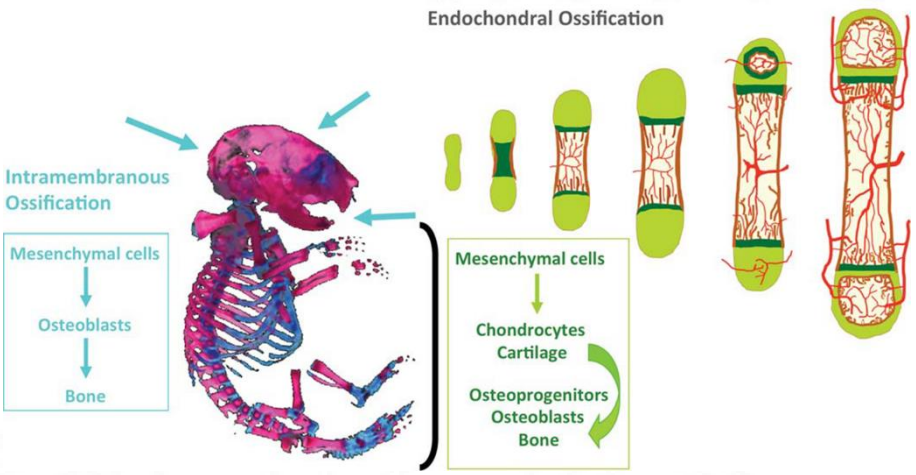

Figure 1.3 Mechanism of bone development. Different skeletal elements develop through intramembranous or endochondral ossification, as indicated on a skeletal preparation stained with alizarin red (bone) and alcian blue (cartilage) (Adopted from (Dirckx et al., 2013)).

The chondrocytes at the centre of this model become hypertrophic which secretes more collagen type X and fibronectin. This modified cartilage matrix allows calcification which prevents the entry of nutrients to chondrocytes. As a result, the chondrocytes undergo apoptosis and create spaces within the cartilage model. This space allows the invasion of blood vessels. The blood vessels further expand the spaces, which eventually combine and become the medullary cavity. The osteogenic cells are carried in by the blood vessels and trigger the transformation of the perichondrium to the periosteum. Further, the osteogenic cells are differentiated into osteoblasts, which built new bone matrix on the remnants of calcified cartilage (which acts as a scaffold). This newly formed bone forms the primary ossification centre which becomes the diaphysis of the bone. This method of bone formation spreads vertically in both directions from the primary ossification centre and eventually forms the secondary ossification centres at the ends of each bone. This secondary ossification centre becomes the epiphysis. The intervening cartilage between the primary and

secondary ossification centre forms the epiphyseal growth plate. Thus, the long bones of the skeleton are formed (Breeland et al., 2023; Galea et al., 2021; Moreira et al., 2019; Safadi et al., 2009).

1.1.6 Bone remodelling

Bone remodels and renews continually throughout life. Bone remodeling is a process of orchestrated cellular events involving the actions of osteoblast, osteoclast and osteocytes. It occurs in discrete foci called bone remodeling unit which is found throughout the skeleton. There are two types of bone remodeling: Haversian remodeling, which occurs in the cortical bone, and endosteal remodeling, which occurs along the trabecular bone surface. Both types of remodeling follow the sequence of activation, resorption, reversal and formation (ARRF). This process maintains and repairs the shape, architecture, density and microfractures of the bone (Moreira et al., 2019; Rowe et al., 2023; Safadi et al., 2009).

1.1.7 Bone healing

Bone healing is an intricate process which recapitulates the events of bone development and it can be considered a type of regeneration. During the process of bone healing, the damaged bone is restored to its pre-injury site, allowing for the resumption for the normal functioning. Bone healing occurs either by direct healing or indirect healing method.

1.1.7.1 Direct healing method

Direct bone healing is also known as primary bone healing which heals by intramembranous ossification. It requires precise alignment and complete anatomical reduction of the fracture ends without any gap. This direct healing is not a common occurrence method in the natural process of bone healing (Marsell and Einhorn, 2011).

1.1.7.2 Indirect bone healing method

Indirect bone healing also referred to as secondary bone healing which heals by both endochondral and intramembranous ossification. This is the most prevalent method observed in bone repair. Notably, indirect bone healing differs from direct as it does not require precise anatomical reduction or rigid stability conditions. In contrast, micro movements and load-bearing situations improve the bone healing (Marsell and Einhorn, 2011; Sheen et al., 2023).

Indirect bone healing includes a series of event that begins with an acute inflammatory response, followed by the recruitment of mesenchymal stem cells, which form a cartilaginous and periosteal bony callus. Subsequently, revascularized and neo-angiogenesis occur at the fracture site, followed by mineralization and resorption of the cartilaginous callus. Finally, bone remodelling occurs, and restoring the fracture site to its pre-injury state (Marsell and Einhorn, 2011; Sheen et al., 2023; Wang and Yeung, 2017).

1.1.8 Changes in bone during aging

The bone's physical, chemical, and biological features change gradually throughout life in relation to age. With increasing age, significant changes in bone

architecture, morphology and cellular microenvironment occur. This result in the reduction in bone mass and strength, increased susceptibility to fractures, and diminished bone healing capacity. The aging of bone is characterized by bone loss and the accumulation of bone marrow adiposity. The major molecular change observed is decrease in the osteogenic potential of the bone accompanied by an increase in adipogenesis.

1.2 BONE DEFECTS

1.2.1 Types of bone defects

The replacement of lost bone is the major challenge in the orthopedic surgery. Bone defects can be caused by trauma, gunshot or blast injuries, infections, tumours, congenital conditions, metabolic diseases, surgical interventions (tumour resections, revision arthroplasties) which can result in bone loss or damage. A universal classification categorizes long bone defect as limited defects (< 20%), bone fragments still have contact, segmental bone defects in which bone does not have contact, and complete articular defect (Solomin et al., 2022). Further, bone defects are classified as diaphyseal, metaphyseal, and articular defect, based on their anatomical locations (Keating, Simpson, and Robinson, 2005). Based on healing potential, the defects are categorized as critical and non-critical sized defects.

1.2.2 Critical sized bone defects

Critically sized bone defects are characterized by significant bone loss, those that do not heal spontaneously despite surgical stabilization or exhibit less than 10% bony regeneration and often require additional interventions like bone grafting. The

size or volume of a critical size bone defect is generally in the range of 1-2 cm or 2.0-2.5 times the diameter of the corresponding bone diaphysis. It is important to differentiate between a critical size defect and non-union. Non-union involves impaired cellular signalling and biomechanical instability, whereas in critical size defect, there may be an adequate stability and microenvironment, but an inability to replace the bone loss, which may be complicated by soft tissue and patient specific characteristics. The critical sized defects are commonly managed by bone grafting procedures, whereas the larger segmental defects are manged by Masquelet's induced membrane technique (Giannoudis et al., 2007; Nauth et al., 2018; Schemitsch, 2017).

1.2.2.1 Non-union

Non-unions are persistent defects that have been present for nine months, with no indications of healing even after three months. Hypertrophic non-unions occur when excessive motion is given at the defect site, although it retains the biologic properties with abundant callus formation (radiography). The mechanical stability required for healing a hypertrophic non-union is provided by internal fixation. On the other hand, atrophic non-union occurs due to inadequate mechanical and biological conditions. During radiography observation, no callus formation is seen. This is managed by internal fixation with bone grafting. The oligotrophic non-union exhibits both the hypertrophic and atrophic conditions whereas the septic non-union occurs due to infection. Bone grafts are needed for all the non-union other than hypertrophic non-union (Gillman and Jayasuriya, 2021; Thomas and Kehoe, 2023).

1.2.2.2 Mal-union

Mal-union occurs when bone heals in an incorrect orientation or location, resulting in an angular or rotational deformity exceeding five degree or bone shortening. The management of malunion involves fixation, osteotomies or bone grafting depending on specific nature of the defect(Gillman and Jayasuriya, 2021).

1.2.3 Metaphyseal bone defects

Metaphyseal bone defects often result from impression fractures occurring around a joint. These fractures are typically caused by a significant force or impact that leads to the indentation or depression of the bone rather than complete displacement. The main aim of managing metaphyseal bone defect is to provide mechanical support, filling of the defect and restoration of bone stock. Good vascularity and high bone turnover rate are the distinguishing features of metaphyseal region (Blokhuis, 2017), except the femoral head (Kumar et al., 2014). Although the metaphyseal defects can heal itself, the bone formation is limited without bone substitute (Malhotra et al., 2014; Voor et al., 2011). Previous studies proved the effect of calcium phosphate cement for managing tibial plateau fractures (Russell et al., 2008), calcaneal fractures (Schildhauer et al., 2000; Wee and Wong, 2009).

1.2.4 Diaphyseal bone defects

The diaphyseal defects are more challenging and the primary objective is to restore the continuity of the affected extremity, especially the cortical bone. Low vascularity and remodeling of the diaphyseal region demands more efforts rather than

filling the defects (Blokhuis, 2017). According to the diamond concept of bone healing, vascularity, cells, scaffolds, osteo-inductive signals, and a suitable mechanical environment are crucial for achieving diaphyseal healing (Giannoudis et al., 2007). The Masquelet's induced membrane technique is the most successful surgical intervention for managing these defects (Aurégan and Bégué, 2014; El-Alfy and Ali, 2015) .

1.2.5 Irregular Bone voids

Bone voids that are less than 5 mm or between 5 to 10 mm in size are treated with either bone cement or bone cement with screw augmentation (Hasandoost et al., 2020; Mancuso et al., 2017). These are defects which are met particularly during the surgical interventions such as revision arthroplasty defects, tumour or infection resection defects, geriatric defects *etc*., These bone voids are managed by bone cements which is the most preferred method. Generally, bone cements such as polymethyl methacrylate **(**PMMA), calcium phosphate and calcium sulphate are used.

1.3 BONE DEFECT MANAGEMENT

The management of bone defects depends on the size, shape, and location of the defect and on the patient's age and health. The critical sized defects and the segmental diaphyseal defects are managed by bone grafting procedures and induced membrane technique.

1.3.1 Bone grafting

Bone grafting is a promising strategy for managing bone defects. Large number of people regained their mobility and quality of life by this method. The primary objectives of the bone defect management include stabilization, restoring proper length and alignment as well as maintaining the optimum functions. Skeletal stabilization can be achieved by intramedullary nailing, plates or external fixation (Keating et al., 2005). Autograft is considered gold standard for managing bone defects which are less than 5 cm. The treatment options for the larger segmental defects may include vascularized fibular grafts, distraction osteogenesis, or the induced membrane technique depending on the patient' s health status and the expertise of surgeons. In addition to orthopedic applications, bone grafting procedures are applied in cranial and maxillofacial applications (Coots, 2012; Elsalanty and Genecov, 2009; Lu et al., 2022).

1.3.2 Induced membrane technique

Ilizarov's bone transport, vascularised bone graft and Masquelet induced membrane technique (MIMT) are different strategies for managing segmental bone defects. Among these methods, the Masquelet technique is considered simple, easy to perform and has recorded high success rate.

MIMT has shown effective in managing defects larger than 2 cm with low rate of complications. On average, it takes 1.24 months for a 1 cm defect to heal (Giannoudis et al., 2016). The first stage of MIMT involves a reconstructive stage which includes the radical debridement of soft and bone tissue, insertion of cement spacer into the bone defect, and stabilization of the bone. The cement spacer not only provides mechanical support, but also prevents fibrous in growth and promotes the formation of vascularised

membrane around the spacer. This induced membrane resembles the periosteum and enriched with multi-potent mesenchymal cells, as well as osteogenic and angiogenic factors.

In the second stage, once definitive soft tissue healing (4-8 weeks) occurs, the spacer is removed without disturbing the induced membrane. The membrane is then filled with cancellous autografts, typically sourced from iliac crest/ RIA (reamer irrigation aspirator) graft harvested from the intramedullary canal of the femur or tibia (Masquelet et al., 2000). MIMT is an efficient and the most successful methodology for the management of segmental defects in long bones. The key challenge is requirement of large volume of bone graft expanders to fill the defect in second stage.

1.3.3 Characteristics of bone graft or substitutes

An ideal bone graft or substitute should possess osteogenic, osteoconductive, osteo-inductive, osseo-integrative properties, along with the suitable structural characteristics. Osteogenesis refers to the process of bone formation, involving the activation and commitment of mesenchymal stem cells, their differentiation into osteoprogenitor cells and eventually maturation into osteoblast leading to bone mineralization. Osteo-conduction refers to the ability of the material to support bone growth on its surface or down into pores. Osteo-induction is the induction of osteogenesis by the graft material. Osseo-integrative is the ability of the graft to establish a bonding with the host bone (Albrektsson and Johansson, 2001; Giannoudis et al., 2005). In addition, porosity, biocompatibility and degradation of the material play significant roles in enhancing performance of the material. A bone graft substitute

should facilitate the normal healing process of the bone, promoting the regeneration and restoration.

1.3.4 Autografts

Autograft is the gold standard graft which is harvested from the different anatomical site of the same person. It possesses the properties of osteoconduction, osteoinduction, osteogenesis and osseointegration, housing all the necessary growth factors to promote accelerated healing of bone defects. The most commonly harvested from iliac crest, femoral greater trochanter, proximal-distal tibia, calcaneus and distal radius (Nandi et al., 2010). Recently, the reamer irrigator aspirator (RIA) system is used to collect bone graft from the medullary canal of the femur/tibia (Kovar and Wozasek, 2011). Similarly, vascularized bone grafts such as free fibula strut grafts, distal radius grafts, promote quick healing when carefully grafted preserving its mechanical stability, vascularity and cellular niche (Gillman and Jayasuriya, 2021). The major drawbacks of the autograft include limited availability and various associated complications such as donor site morbidity, chronic pain, blood loss, prolonged operative time, infection, haematoma formation, blood loss, nerve injury, hernia formation, infection, arterial injury, ureteral injury, fracture, pelvic instability, cosmetic defects *etc*., (Giannoudis et al., 2005).

Bone marrow aspirate and platelet rich plasma are combined with autografts. The bone marrow aspirate is effective in the treatment of non-unions and osseous defects and the harvesting is minimally invasive. Platelet rich plasma (PRP) is easy to prepare and it house all the growth factors that promote bone healing. However, the

individual variation in PRP and preparation method influence the outcome of PRP therapy (Campana et al., 2014; Gillman and Jayasuriya, 2021).

1.3.5 Allografts

The next option after autograft is allograft. Typically, allografts are rarely used fresh. They are commonly frozen or freeze dried, including both cortical and cancellous bone. It is processed to remove the surrounding soft tissues and then sterilized. Further, it is machined and customized in variety of forms such as dowel, chips, strips *etc*. The drawbacks of the allograft include cost, risk of infection, limited osteoinduction, low structural and biological properties.

1.3.6 Demineralized bone matrix (DBM)

DBM is a highly processed graft which undergoes mild acid treatment, potentially resulting in the removal of almost 40% of the bone mineral and matrix. It exhibits osteoconductive properties, while the property of osteoinduction relies upon the processing method employed. It is conveniently offered in different forms such as gel, malleable putty, flexible strips, mouldable or injectable paste. However, the significant drawback is poor structural properties (Giannoudis et al., 2005; Gillman and Jayasuriya, 2021).

1.4 BONE GRAFT SUBSTITUTES

The orthopaedic surgeons face a pressing need of bone graft substitutes in various clinical scenarios. These situations arise when there is a deficiency of autografts in geriatric or paediatric patients or when the clinical conditions prevent the use of iliac

crest/RIA graft or when the defect size exceeds 5 cm. Consequently, numerous bone substitutes have emerged including calcium phosphate ceramics, bioactive glass, polymer based composite materials, natural material, bone cements *etc*. These bone substitutes have been extensively investigated for their efficacy in managing bone defects.

1.4.1 Calcium phosphate ceramics

Calcium phosphate ceramics are highly crystalline materials that are made through sintering at high temperatures. It includes the tricalcium phosphate (TCP), biphasic calcium phosphate (BCP), hydroxyapatite (HA). The chemical composition of TCP closely resembles that of human bone. It exhibits osteoconduction, but the degradation is unpredictable. It is not suitable for load bearing applications. BCP is obtained by mixing both TCP and HA in different ratios. The synergism of TCP and HA tailor BCP with enhanced mechanical properties and controlled degradation. The chemical composition of HA is similar to that of bone. It possess both osteoconduction and osteoinduction but the degradation of HA is very slow(Campana et al., 2014; Moore et al., 2001).

1.4.2 Bioactive glass

Bioactive glass was developed by Larry Hench and is primarily composed of silica with other constituents such as calcium oxide, sodium oxide, phosphorus pentoxide. It has the ability to bond with both bone and soft tissue. It exhibits osteoconduction properties and can induce osteogenesis. However, bioactive glass is

brittle and possess low mechanical properties (Fernandez de Grado et al., 2018; Krishnan and Lakshmi, 2013).

1.4.3 Polymer based composites

Synthetic degradable polymers such as polycaprolactone (PCL), poly lactic acid (PLA), poly (lactic-co glycolic) acid (PLGA), polyethylene glycol (PEG), poly urethanes are the widely investigated materials for bone tissue engineering applications. These polymers are composited with hydroxyapatite, zirconia, titanium di oxide, tricalcium phosphate, graphene oxide, nano silica, bioglass *etc*., for mechanical properties and osteoconduction (Bharadwaz and Jayasuriya, 2020; Idumah et al., 2019).

1.5 NATURAL MATERIALS

Natural materials like collagen, silk, chitosan, alginate, hyaluronic acid, cellulose, gelatine, rattan wood, pearl, shells, coral, *etc*., were investigated for osteogenic potential. All these materials are either composited with other inorganic calcium phosphate ceramics or chemically transformed for osteogenesis and mechanical properties. In this section, the most investigated natural materials such as collagen, silk fibroin, chitosan, rattan wood, coral were discussed.

1.5.1 Collagen

Collagen I is the dominant extracellular matrix (ECM) of the calcified bone matrix which is synthesized and mineralized by osteoblasts (Chen, 2010). The triple helical structure of collagen imparts protection from proteases, favours cell adhesion

and assemble ECMs. Collagen is obtained from fish waste, marine animals and bovine sources (Bharadwaz and Jayasuriya, 2020). Although collagen possessed all the properties of a bone substitute, it lacks the required structural support and degrades very fast. Collagen is combined with HA and TCP to increase the mechanical properties and osteogenic properties of collagen scaffolds (Liu et al., 2009). Different composite collagen scaffold such as HA reinforced and cross-linked collagen scaffolds (Gleeson et al., 2010), nano HA crystallites precipitated in the interior of collagen (Liu et al., 2009), collagen scaffolds fortified with ultralong micro/nano ribbons of HA (Ying et al., 2019), collagen HA VEGF scaffolds enriched with carboxymethylcellulose spheres releasing BMP-2 sequentially (Dou et al., 2019) and electro-spun and rolled bone haversian like HA collagen implants (Bian et al., 2019) were investigated for the bone regenerative properties.

1.5.2 Silk fibroin

Silk fibroin is a protein extracted from the cocoon of the silk worm *Bombyx mori*. It has been studied for bone tissue engineering applications due to its biocompatibility and osteogenic properties (Sahu et al., 2015). Researchers have investigated various scaffolds for enhanced mechanical and bone regenerative properties, such as microparticle scaffold (Deshpande et al., 2022; Nisal et al., 2018; Parekh et al., 2017), and composite scaffolds of titanium dioxide (Johari et al., 2017), silk, collagen and HA (Chen et al., 2014), silk HA (Behera et al., 2017) *etc* .

1.5.3 Chitosan

Chitosan is a linear polysaccharide which is derived by the partial deacetylation of chitin. It is biodegradable, non-cytotoxic and can be easily modified. To overcome the poor mechanical nature, it is composited with HA, TCP, collagen and synthetic polymers (Bharadwaz and Jayasuriya, 2020; Kashirina et al., 2019)

1.5.4 Rattan wood

The rattan wood pieces of *Calamus manna* are used as a template which undergoes a series of thermal and hydrothermal process and chemically transformed to get a porous HA scaffold (Tampieri et al., 2009). This biomorphic transformed scaffold has a 3D bone like structure with non-sintered HA and TCP (Green bone). *In vitro*, *in vivo* and clinical studies demonstrated the osteogenic potential of the material (Alt et al., 2023; Kon et al., 2021).

1.5.5 Coral

Coral is composed of calcium carbonate in aragonite form along with organic matrix and other ions strontium, magnesium, fluoride *etc*. It possesses porosity, biocompatibility, and osteoconductivity. However, corals as such are brittle, lack mechanical strength and degrade rapidly. The properties and performance of the coral is enhanced by transforming into a hydroxyapatite through hydrothermal process. The coral-based products are available in the market, but the results have not been favourable always (Campana et al., 2014; Demers et al., 2002; Pountos and Giannoudis, 2016).

1.6 Commercially available bone graft substitute materials

The global market size of bone graft substitutes stood at $ 3.57 billion, and it is anticipated to grow from $3.78 billion in 2023 to reach $5.74 billion by 2030 exhibiting a compound annual growth rate (CAGR) of 6.2% (Fortune Business Insights, 2023a). The following is the list of commercially available bone graft substitute which includes either the HA, TCP, BCP or combination of all these. Clinically available bone graft substitutes are either hydroxyapatite/tricalcium phosphate/collagen/ combinations of all these. In India, G Bone and G grafts are the current commercially available material and various clinical studies reported the use of autografts, freeze-dried allografts, G-Bone, and Triosite during bone grafting procedures (Kasha et al., 2019; Sahu et al., 2019; Sivakumar et al., 2016).

Table 1.1 Commercially available bone graft substitutes

Product name	**Composition**	**Manufacturer**
Orthoss	Bovine bone derived HA with nanopores and macropores	Geistlich,Wolhusen, Switzerland
Allogran-R	Biphasic scaffold 40% β-tricalcium phosphate and 60% hydroxyapatite with 60-70% porosity	Biocomposite, UK
Bone Save	80% βTCP and 20%HA	Stryker,Kalamazoo,MI
INFUSE Bone Graft	Collagen sponge releasing recombinant BMP-2	Medtronic, Tennessee,USA
Mastergraft	85% β-TCP and 20%HA with 80% interconnected porosity	Medtronic, US
Chron OS	Pure β tri-calcium phosphate	Depuy Synthesis, USA
Orthoss Collagen	Xenograft with a combination of orthoss bovine HA and 10% porcine collagen	Geistlich, Switzerland

Vitoss	Synthetic β–TCPwith bovine collagen I	Stryker, Malvern, PA
G Bone	Low crystalline HA, TCP and other forms of calcium such as calcium carbonate and bicalcium phosphate.	Surgiwear, India
G Graft	Collagen HA	Surgiwear, India
ProOsteon	Layer of hydroxyapatite over a calcium carbonate core	ZimVie,US

1.7 BONE VOID FILLING CEMENTS

Polymethyl methacrylate (PMMA) cement, calcium phosphate, calcium sulphate materials are widely used for filling bone voids. Among this, PMMA is used mostly preferred for load bearing applications.

1.7.1 PMMA

Polymethyl methacrylate (PMMA) is an extensively used material in different formulations for orthopaedic applications. Bone cement serves multiple purposes, including acting acts as a grout for the fixation of prosthesis in hip, knee and other joint replacements; as a stabilizer for stabilizing the vertebral fractures during vertebroplasty, kyphoplasty and vertebral stenting procedures (restoring vertebral strength, function and relieving pain), as a filler for bone defects; as a spacer for the treatment of segmental defects in Masquelet technique; as a carrier for the treatment of bone tumor and infections and linker for the treatment of ossiculoplasty and cranioplasty procedures.

Bone cement can be categorized as plain, antibiotic or drug loaded. It consists of a liquid and a solid filler component. The solid part of an acrylic bone cement typically contains PMMA prepolymer or copolymers of acrylic acid, ethyl acrylate, methyl acrylate and styrene (80 wt%), an initiator such as benzoyl peroxide (0.75 to 2.5

wt%) and radiopacifier such as barium sulphate or zirconium dioxide powder (10 to 30 wt %). The liquid phase mainly consists of methyl methacrylate (MMA) monomer (95 wt %), an activator called N-N-dimethyl -p-toluidine (0.89 to 2.7 wt%) and an inhibitor hydroquinone to prevent premature polymerization (He *et al*., 2015).

PMMA is the most studied and clinically used materials. It is used for the management of fragility fractures (Piccirilli et al., 2022), vertebral compression fractures (He et al., 2015), revision arthroplasty defects, and bone voids after infection (Reito and Ylitalo, 2020), tumour resections (M Wu et al., 2018), tibial plateau defects of depth < 20mm after revision arthroplasty (Lotke et al., 1991), metaphyseal bone voids during proximal humerus fracture in the elderly patients (n=29 , average age-71.5 years) (Hristov et al., 2022) *etc.*

The PMMA bone cement is dense, non-porous, lacking bioactivity and functioning solely as a mechanical fixative. Lack of bioactivity, thermal and chemical necrosis as well as high polymerization shrinkage are the prime factors diminishing the performance of the bone cement (Vaishya *et al*., 2013, Orr et al., 2003 & Gilbert *et al*., 2000).

1.7.2 Calcium sulphate cement

Calcium sulphate, also known as “Plaster of Paris” or Gypsum was initially employed by Dreesman in 1892 for filling osteomyelitis defects. In 1959, Peltier reintroduced it with improved purity and crystallinity. Calcium sulphate is easy to prepare, cost-effective and exhibits osteoconductive properties. However, it has low strength, degrades rapidly, and can cause inflammation without bone formation (Thomas and Puleo, 2009).

1.7.3 Calcium phosphate cement

Calcium phosphate cement, invented by Chow and Brown in 1986, is made by mixing white calcium phosphate powder with a liquid to form a paste that can be easily moulded and shaped to fit the defect. The cement then hardens within approximately 20 min. It received FDA approval in 1996 for use in non-load-bearing applications. It is biocompatible, osteoconductive and bioresorbable. However, it possesses low mechanical properties (Bohner, 2000).

1.7.4 Commercially available bone void fillers and market status

The global market value of bone void fillers was valued at $3.09 billion in 2022 and it is expected to reach $3.27 billion in 2023 and further increase to $ 5.02 billion by 2030. This growth signifies a CAGR (compound annual growth rate) of 6.3% throughout the forecast period (Fortune Business Insights, 2023b).The following are the list of commercially available bone void fillers.

Table 1.2 Commercially available bone void fillers

Product Name	Composition	Manufacturer
QOSSHEALIHA	Calcium hydroxyapatite	G Surgiwear, India
HydroSet	Tetra Calcium Phosphate (73%) and Dicalcium Phosphate (23%)	Stryker, USA
Stimulan	Calcium Sulphate cement	Biocomposite, UK
Opus Mg Set	Magnesium phosphate	Orthofix, USA
Cerament	40% hydroxyapatite, 60% calcium sulfate and the radio-contrast agent iohexol	BoneSupport AB, Sweden

Cortoss	Bisphenol-a-glycidyl dimethacrylate, Bisphenol-a-ethoxy dimethacrylate, TEGDMA Boro-alumino silicate glass Combetite glass ceramic particles	Stryker,USA
Norian drillable bone void filler	Calcium phosphate with absorbable polylactide/glycolide copolymer fibers with solution of dilute sodium phosphate and sodium hyaluronate with	Depuy Synthesis, USA
DBX ™ Demineralized Bone Matrix	Granulated cortical bone (human) with sodium hyaluronate	Depuy Synthesis, USA

1.8 Major concerns of bone graft substitute

India lacks a uniform standard of healthcare across the country, particularly in rural areas where access to orthopaedic treatment is limited. In reality, traditional bone setters treat 60% of orthopaedic issues, often leading to complications such as mal-union, non-union, or an established infected non-union following an open fracture. As a result, hospitals encounter significant number of these non-unions than fresh factures. Unfortunately, amputation are still reported in India as a consequence of trauma injuries even in younger patients (Dar et al., 2023).

Bone grafting, specifically Masquelet's induced membrane technique (MIMT) is a clinically proven methodology that is successfully preventing amputations. Many individuals regained their mobility and improved their quality of life through these techniques. However, a significant challenge lies in the need of large volume of bone graft substitute to manage non-unions, tumour resections, compound/ comminute fractures with bone loss. The success of these orthopaedic procedures greatly relies on

the quality of bone graft substitute used. Unfortunately, in India, bone graft procedures rely on imported products, which are not affordable by all. Therefore, there is a pressing need for a cost-effective import substitute.

Bone graft substitute are scaffolds that mimic the skeletal niche and provide physical and biological support for bone cells to respond signals and promote bone formation. These scaffolds are three-dimensional, porous, interconnected, resorbable materials that are osteoconductive which promote the growth, attachment, proliferation and osteogenic differentiation of neighbouring skeletal stem cells. However, bone graft substitutes such as calcium phosphate ceramics, calcium sulphate, composite of collagen with calcium phosphate ceramics have shown unpredictable degradation, poor structural properties, and inflammatory reactions insisting the need of alternative materials. Particularly, there is a demand for a cost-effective bone graft substitute that possess all the properties of osteogenesis, osteoconduction, osteoinduction, biocompatibility, bioresorbable and structural properties.

1.9 Major concerns of bone void filling cements

Polymethyl methacrylate **(**PMMA) cement is the most studied and clinically used material for the management of fragility fractures (Piccirilli et al., 2022), vertebral compression fractures (He et al., 2015), revision arthroplasty defects (Hasandoost et al., 2020), and bone voids after infection (Reito and Ylitalo, 2020) / tumor resections (M Wu et al., 2018), *etc*. Apart from its inert application in arthroplasty, it is used for bone defect management, solely for its mechanical properties, regardless of the potential toxicity of the monomer, volumetric shrinkage

or the exotherm generated during polymerization (Vaishya et al., 2013; O'dowd-Booth et al., 2011; Soleymani Eil Bakhtiari et al., 2020).

Methyl methacrylate (MMA) and PMMA powder are the primary constituent of PMMA cement. In order to address the issues of polymerization shrinkage and exotherm generation, several organic matrices or combinations of organic matrices such as poly (propylene fumarate-co-ethylene glycol) oligomers (Jayabalan et al., 2000), urethane dimethacrylate, poly(ethylene) glycol dimethacrylate, triethylene glycol dimethacrylate (TEGDMA), bisphenol-A-glycidyl methacrylate (Bis GMA) (Deb et al., 2005; Kawanabe et al., 1993; G. X. Ni et al., 2006; Yamamuro et al., 1998), terpolymer (bisphenol-A-ethoxy methacrylate, Bis GMA, TEGDMA) (Boyd et al., 2008), as well as acrylic acid and styrene (Yang et al., 2017) *etc.* have been investigated, with the aim of replacing MMA. However, despite these efforts, the problem of exotherm generation, toxicity and polymerization shrinkage has not been completely addressed. Consequently, there is a need for an alternative resin matrix to overcome these challenges.

The next issue to address is the inertness of PMMA cement, which prevents it from bonding to the implanted bone. To overcome this limitation, with the concept of bioactivity, many researchers modified the cement formula with silanated glass (Kawanabe et al., 1993), apatite wollastonite glass ceramic (AW-GC) (Mousa et al., 2000), nano-sized titania particles (Goto et al., 2005), hydroxyapatite (HA) (Deb et al., 2005), strontium substituted HA (G. X. Ni et al., 2006), HA with BMP-2 (Liu et al., 2015), synthetic combeite glass-ceramic particles, barium boro aluminosilicate glass and silica particles (Erbe et al., 2001), borosilicate glass (Zhang et al., 2022), and

graphene oxide (Tan et al., 2023) *etc.* Similarly, bioactive self-setting cement such as calcium phosphate, calcium sulfate, tricalcium phosphate, calcium silicate and magnesium phosphate cement have also been investigated. However, these cements often exhibit brittleness, low mechanical properties, and faster resorption, which may not provide the long-term mechanical support required (Fillingham and Jacobs, 2016; Gu et al., 2022; Z Han et al., 2022; Z Liu et al., 2023; Marongiu et al., 2020; Moore et al., 2001; Nandi et al., 2010; Wang and Yeung, 2017). Additionally, bone cements based on oyster, clam and abalone shell powder have been studied, but none of these cements exhibited the required mechanical properties (Du et al., 2021; Ruan et al., 2018; Shen et al., 2014; Simu et al., 2018). Hence, the unsatisfactory biological performance of PMMA-based cements and the lower mechanical performance of the modified cements emphasize the critical need for an alternative cement that can offer both biological and physico-chemical properties together.

1.10 Selection of material

1.10.1 Shell nacre

Shell nacre from *Pinctada* species has been extensively investigated for its potential in bone regeneration. It is the inner nacreous layer of the pearl oyster shell. It is composed of calcium carbonate crystals arranged in aragonite form, with an organic layer inter-tiled between them. It was Camprasse *et al.* who first developed an artificial dental root made of shell nacre (Bioracine). Subsequently, Lopez group demonstrated the *in vitro* osteogenesis of shell nacre without any inducer (Camprasse et al., 1990; Lopez et al., 1992; Silve et al., 1992). *In vivo* comparison studies have shown that the shell nacre induced new bone formation whereas PMMA caused

necrosis and reduced bone mineralization (Lamghari, Berland, et al., 2001). Shell nacre possesses desirable properties such as osteogenesis, radiopacity, osseo-integration, high fracture toughness and strength, biodegradability, anti-osteoporotic activity and angiogenesis (Atlan et al., 1999; Berland et al., 2005; Gerhard et al., 2017; Kim et al., 2012; Lee et al., 2012).

1.10.2 Polycaprolactone

Polycaprolactone is an affordable synthetic polymer that has received FDA approval. It is known for its biocompatibility, biodegradability and favorable mechanical properties. It exhibits a long- duration degradation of 2 to 3 years. Therefore, PCL is well suited for bone tissue engineering applications. The thermal induced phase separation is a cost effective, straightforward approach to fabricate three-dimensional, interconnected porous scaffold. To address concerns of toxicity, a non-toxic green solvent dimethyl carbonate (freezing point of 2 to 4°C) is used.

1.10.3 Ladder structured siloxane methacrylate resin

Ormocer is a three-dimensional multifunctional inorganic-organic hybrid resin with inorganic siloxane backbone instead of organic carbon backbone. It is easily synthesized by modified sol gel method using methacrylate substituted alkoxysilanes through the process of hydrolysis and condensation to form the inorganic siloxane network whereas the methacrylate moieties remain intact (Wolter et al., 1992). It is widely investigated in the field of dental cements due to its non-cytotoxic nature, low polymerization shrinkage and higher mechanical properties (Lizymol, 2004a, 2010; Vibha and Lizymol, 2017, 2019), particularly the photocured cured composites of

ladder structured siloxane methacrylate resin (Bridget Jeyatha et al., 2022). However, there is no report of usage of this resin for orthopaedic applications to our knowledge. So, considering the low shrinkage properties, mechanical properties and non-cytotoxicity, we have selected the ormocer resin strategy.

1.11 In vitro osteogenesis with BM-MSC from Older donors

Senescence in bone is elicited by various factors such as oxidative stress, altered mitochondrial metabolism, aberrant epigenetic modification, DNA damage, telomere dysfunction, heterochromatin changes, mutation and oncogene expression. These factors collectively contribute to the aging of bone microenvironment (Chen et al., 2016; Pignolo et al., 2019; Ganguly et al., 2019). Both *in vitro* and *in vivo* studies have demonstrated a shift towards adipogenesis rather than osteogenesis in older BM-MSCs (Meunier et al., 1971; Justesen et al., 2001; Nuttall et al., 1998; Rodríguez et al., 2000; Stolzing et al., 2008; Zhou et al., 2008). This emphasises the need to consider the ageing bone microenvironment during the design and evaluation of any biomaterial. Furthermore, given that significant number of orthopaedic surgeries are performed on older individuals, it becomes crucial to evaluate the osteogenic potential of any bone substitute material using senescent BM-MSCs from older donors. Therefore, only after confirming the osteogenic potential with BM-MSCs of older donors, a bone substitute material would be considered truly osteogenic.

1.11.1 Gap area

Shell nacre is a superior composite material. Currently, research has focussed on studying the organic matrix of shell nacre as well as shell nacre pieces or powder,

to demonstrate the osteogenic potential. While shell nacre is commercially available as a bone substitute in powder form, pieces, or osteosynthesis devices (*MEGA BIOPHARMA*, n.d.), there is a void in research when it comes to exploring the use of shell nacre from *Pinctada fucata* for bone defect management. Furthermore, there is no established processing method to get shell nacre powder that retains both organic and inorganic content. Additionally, there is currently no method available to set and mould shell nacre powder into defined anatomical forms with suitable mechanical properties.

1.11.2 Unmet clinical need

The unmet clinical need is a cost-effective biomaterial with all the properties of osteoconduction, osteogenesis, osseointegration, suitable mechanical properties, and consideration of the microenvironment of aging bone.

1.11.3 Hypothesis

The hypothesis of the thesis is

- Development of a processing method to get shell nacre powder with both inorganic and organic matrix
- Fabrication of porous, bioactive, osteoconductive, and osteogenic shell nacre scaffolds
- Setting and molding shell nacre into any osseous sites with defined anatomical forms as shell nacre cement

1.12 OBJECTIVES

The main aim of the thesis is to develop shell nacre integrated biomaterials for bone defect management. In order to validate the hypothesis, the following specific objectives have been defined

1. **Shell nacre powder: Processing and characterization**

    a) Removal of the outer prismatic layer of shells

    b) Processing of nacreous shells

    c) Characterization of shell nacre powder

2. **Shell nacre PCL composite scaffold**

    a) Fabrication by thermal induced phase separation method

    b) Physico-chemical characterization

    c) *In vitro* osteogenesis rat bone marrow mesenchymal stem cells

3. **Development of shell nacre cement**

    a) Synthesis of shell nacre containing ladder-structured siloxane methacrylate resin

    b) Characterization of resin

    c) Formulation of chemical cure compositions using the synthesized resin

    d) Physico-chemical characterization of shell nacre cement

    e) Biocompatibility evaluation

f) Osseointegration of *in situ* setting shell nacre cement in a small animal model

4. ***In vitro* osteogenesis of shell nacre integrated biomaterials with human BM-MSC from older and young donors**

a) Cytotoxicity studies

b) Expansion and characterization of BM-MSC

c) *In vitro* osteogenesis studies

This thesis work is a systematic study on the development, physico-chemical and biological characterization of the shell nacre integrated biomaterials, which includes the following chapters.

Chapter 2 describes the literature search about shell nacre, scaffold fabrication, ormocer resins, bioactive bone cement. Chapter 3 explains in detail the materials and methods, results obtained, and the discussion of objective 1. Processing methods to get shell nacre powder and shell nacre powder characterization. Chapter 4 includes the materials and methods, results obtained, and the discussion of objective 2. fabrication and characterization of shell nacre PCL composite scaffold. Chapter 5 and 6 comprises the materials and methods, results obtained, and the discussion of the work carried out under objective 3 - development and characterization of shell nacre cement. Chapter 7 contains the materials and methods, results, and the discussion of work carried out under objective 4 - *In vitro* osteogenesis with geriatric human BMMSC at the University of Leeds, UK (Newton Bhabha PhD Placement). Chapter 8 summarizes and concludes the thesis with respect to the outcomes of all the objectives. The general outline of the work is shown below.

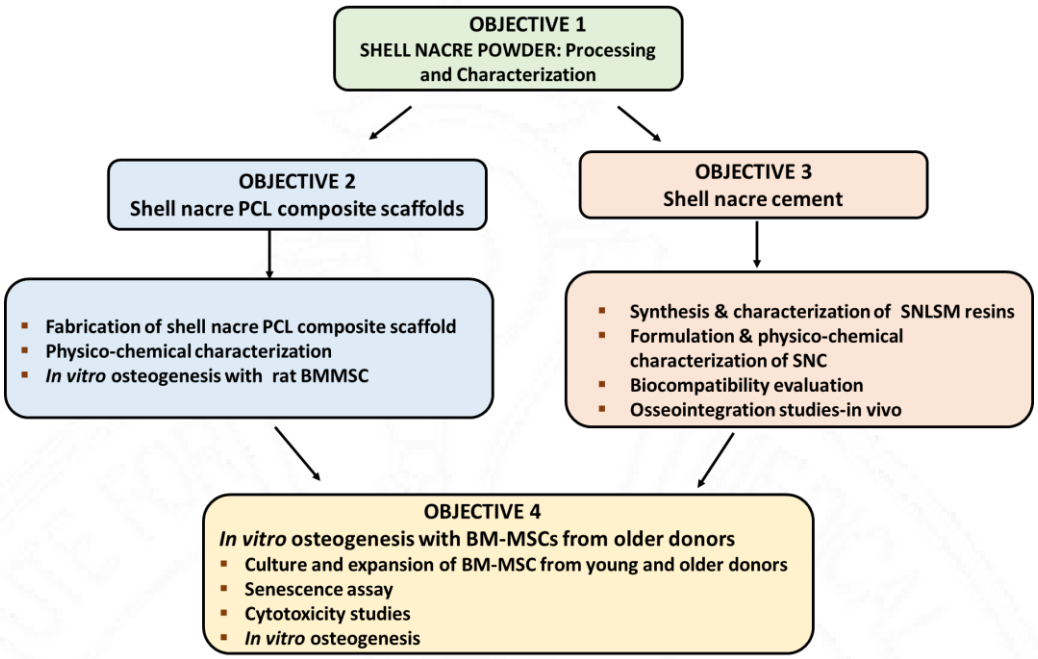

Figure 2.1 The general outline of the thesis work

2 LITERATURE REVIEW

Bone graft substitutes with properties such as osteogenesis, osteoconduction, osteoinduction, osseointegration will offer significant advantages. The first objective of the thesis is to develop a processing method to obtain shell nacre powder, followed by the characterization of the powder. The next objective is fabricating and characterising the porous three-dimensional composite scaffolds of shell nacre and PCL by thermal-induced phase separation. The third objective involves developing shell nacre cement based on ladder-structured ormocer resin, followed by physicochemical and biological evaluation. The final objective is to evaluate the osteogenic potential of the shell nacre PCL composite scaffolds and shell nacre cement using BM-MSC from older donors.

This chapter describes the literature search about the processing methods for shell nacre and shell nacre-based materials. It also provides details on scaffold fabrication by the thermal-induced phase separation method. Further, it includes a review of bone cement, regarding the modification of the resin matrix and filler part for better mechanical and biological properties. Finally, the chapter encompasses a literature search on changes in bone during ageing. Through this comprehensive literature review, valuable insights have been gathered and experimental strategies have been derived.

2.1 Pearl oysters

Pearl oysters are pearl-producing bivalve molluscs found in both marine and freshwater. *Pinctada* is a genus of marine pearl oysters of the family *Pteriidae. Pinctada maxima, Pinctada margaritifera, Pinctada radiata, Pinctada albina,* and *Pinctada fucata* are the different species of pearl-producing molluscs. *Pinctada fucata* is found in the Gulf of Mannar, Gulf of Kutch and Palk Bay region of Indian Coast. In the Gulf of Mannar, pearl oysters occur in large numbers on the submerged rocky or hard substrata known as paars (Behera, 2017). The shells of pearl oysters are made up of an outer prismatic layer and an inner nacreous layer. The outer prismatic layer is reddish or yellowish brown in colour with light-coloured radial rays. The thick inner nacreous layer is otherwise called as shell nacre or mother of pearl, which is lustrous with golden metallic colour. Shell nacre is an osteogenic, osteoconductive, osseo-integrative, radiopaque and biocompatible and a promising candidate for bone defect management.

2.2 SHELL NACRE

It is the inner lustrous layer of pearl oyster's shell. It is of calcium carbonate crystals in aragonite form with organic layer inter-tiled between them in brick-and-mortar fashion. It is a composite material with 95% inorganic and 5% organic layer. The aragonite crystals are arranged as pseudohexagonal tablets of diameter 5 to15 mm and thickness 0.5 mm. The aragonite tablets are arranged parallelly as a lamellar sheet and separated by an intra-lamellar organic matrix (Sun and Bhushan, 2012).

2.2.1 Organic matrix of shell nacre

Most of the studies either used shell nacre as a bone substitute or water-soluble matrix/ethanol-soluble matrix for bone tissue engineering applications. Organic matrix of shell nacre is comprised of the water-soluble matrix and the water insoluble matrix. The water-soluble matrix contains the acidic proteins and polysaccharides whereas the water-insoluble matrix contains the chitin, lipid and the alanine and glycine rich silk like proteins (de Muizon et al., 2022).

2.2.2 Earlier studies with shell nacre

Earlier studies by Bobbio reported the use of shell nacre as dental implants by the Mayans of the Honduras before 2000 years. Radiography results revealed that Mayan people fashioned three-nacre teeth which achieved perfect integration into the bone (Bobbio, 1972). The first developed biomaterial was Bioracine by the Camprasse group which was an artificial dental root made from the shell nacre of *Pinctada maxima*. This Bioracine matched the biological properties of bone and showed excellent osseointegration in humans (Camprasse et al., 1990). It was Lopez *et al* who first demonstrated the complete sequence of new bone formation without any chemical inducers when cultured human maxillary osteoblast with nacre chips (Lopez et al., 1992), and the osteogenesis was again confirmed by Silve (Silve et al., 1992).

2.2.3 Shell nacre as a direct bone substitute

Shell nacre was implanted into the cortico-cancellous, articular and intramedullary sites in the femur of sheep and after 3 months of implantation, no foreign body reaction was found and it showed excellent bonding to the bone (Delattre

et al., 1997). Similarly solid shell nacre bonded to the newly formed bone without any fibrous tissue, after 10 months of implantation within the cancellous bone of the epiphysis region of the femur in sheep (Atlan et al., 1999). Berland implanted raw shell nacre pieces of length 2 cm and 13 mm diameter into the diaphyseal femoral defect of sheep and showed that solid shell nacre underwent limited biodegradation after 9 months and the pattern of degradation depended on the bone microenvironment (Berland et al., 2005).

In vitro osteoclast degradation studies of shell nacre proved the resorption efficiency of shell nacre was limited when compared to bone (Duplat et al., 2007). Orthopaedic screws of shell nacre (*Pinctada maxima*) implanted in the upper tibial metaphysis of ewes to study the erosion and observed the presence of giant multinuclear macrophage derived cells which were involved in the process and reduced the fractal dimension with no inflammatory reaction and new bone opposition (Libouban et al., 2016). Osseointegration and erosion of shell nacre screws were studied up to 12 months by implanting them into the femoral condyle of Sprague Dawley rats. The study observed excellent osseointegration and erosion of the screw tip, which was in direct contact with the bone marrow, while the screw head remained intact (Kün-Darbois et al., 2021).

2.2.4 Shell nacre powder as a bone void filler

Shell nacre powder of size 50 to 100 µm from the shells of *Pinctada maxima* was mixed with autologous blood and applied to the defect area. Over the course of 6 months, shell nacre gradually dissolved and new bone formation was achieved after and restored the maxillary ridge bone of eight patients (Atlan et al., 1997). Similarly,

the upper lumbar vertebral defects were filled and after 12 weeks newly matured bone trabeculae was formed indicating the osteogenic potential of shell nacre powder (Lamghari et al., 1999). Shell nacre powder was injected into the upper lumbar vertebra of sheep. The shell nacre powder started degrading at 8 weeks and layer of new bone formation was observed until 12 weeks (Lamghari, Berland, et al., 2001). Shell nacre powder performed equivalent to that autologous bone graft during arthrodesis management in rabbit and started degrading from 5th week and induced endochondral bone formation (Lamghari, Antonietti, et al., 2001).

During a preclinical evaluation in sheep, shell nacre powder of mean particle size 42.7 µm was mixed with autologous blood to form a paste and the femoral condyle defects of diameter 10 mm and depth 5 mm were filled. After 8 weeks, complete degradation of shell nacre with a continuous new bone formation was observed (Iandolo et al., 2022).

2.2.5 Studies with organic matrix of shell nacre

Many studies proved that the organic matrix of shell nacre induced osteogenesis whereas synthetic aragonite exhibited lesser effect (Westbroek and Marin, 1998). Organic matrix of shell nacre was extracted by demineralization by decalcifying with hydrochloric acid or chelating with EDTA or by partial extraction with water and ethanol (de Muizon et al., 2022). Water soluble matrix of shell nacre induced the osteogenesis of rat bone marrow mesenchymal stem cells with enhanced alkaline phosphatase activity (Lamghari et al., 1999). WSM of shell nacre promoted the differentiation and maintained the survival of osteoblast which was understood by enhanced alkaline phosphatase activity and expression of anti-apoptotic protein Bcl-2

(Moutahir-belqasmi et al., 2001). Low molecular weight molecules of the water soluble extract of nacre induced mineralization of the pre-osteoblast MC3T3 cells (Rousseau et al., 2008). The water-soluble matrix of shell nacre restored the angiogenesis of deep burn injury of porcine skin (Lee et al., 2012). This was the first study reported demonstrating the angiogenesis of WSM of nacre. Followed by this, it was proved that ethanol soluble matrix (ESM) of nacre induced angiogenesis of human cord blood-derived endothelial progenitor cells (Willemin et al., 2019).

2.2.6 Scaffolds based on shell related products

Liu *et al*. fabricated a porous scaffold of PLLA and pearl powder -60%, 70% and 80% (fresh water *Hyriopsis cumingi*) by freeze dry method using the solvent dioxane (Liu et al., 2013). Hydrogel containing shell nacre induce differentiation of human bone marrow mesenchymal stem cells with evidence of hydroxyapatite mineralization (Flausse et al., 2013). Composite scaffolds of pearl PLA were fabricated by solvent casting method (Dai et al., 2015). Zhang *et al.* 3D printed composite scaffolds of PCL and pearl powder of *Hypriopsis cumingi* and *Cristaria plicata* (Zhang et al., 2018) whereas Xiao et al., fabricated a hollow composite scaffold of PLA and nacre and investigated the repair of segmental bone defects in rabbit (Xiao et al., 2012). Didekhani *et al*. fabricated a electrospun PCL composite scaffolds with oyster shell powder (Didekhani et al., 2020). Kim *et al.* fabricated a 3 D printed PCL scaffold and then deposited abalone shell particles by thermal method, whereas Pan *et al.* fabricated composites scaffolds with abalone shell powder (Kim et al., 2021; Pan et al., 2022), Many other studies investigated the effect of shell derived HA or nacre derived hydroxyapatite (Megat Abdul Wahab et al., 2020).

Table 2.1 Summary of shell nacre (*Pinctada* species) related studies

SHELL NACRE-BASED STUDIES	REFERENCE
Osteogenesis of shell nacre chips *in vitro*	Lopez *et al.* 1992, Silve *et al.,* 1992
Reconstructive surgery of human alveolar ridge bone using Shell nacre powder (50-100 µm)	Atlan *et al.* 1997
Water soluble matrix (WSM) of nacre - rBMSC and Sheep	Lamghari *et al.* 1997
Shell nacre as a bone substitute in sheep	Delatree *et al.* 1997
Comparison with titania and HA composite	Liao *et al.* 1997
Comparison between shell nacre and autograft in rabbit	Lamghari *et al*. 2001
Bone substitute – sheep	Berland *et al*. 2005
Organic matrix of nacre water soluble matrix of nacre	Kim *et al. 2002,* Lopez *et al. 2003,* Milet *et al. 2004,* Zhang *et al. 2006,* Lao *et al. 2007,* Wang *et al. 2007,* Rouseau *et al. 2008,* Kim *et al. 2012,* Chaturvedhi *et al. 2013,* Green *et al. 2015,* Brion *et al. 2015,* Zhang *et al. 2016*
Angiogenesis of human cord blood derived endothelial progenitor cells using ethanol soluble matrix of nacre	Willemin *et al 2019*
Shell nacre screws implanted in upper tibial metaphysis of ewes	Libouban *et al., 2016*
Shell nacre implanted in femoral condyle defect of Sprague Dawley rats	Kün-Darbois *et al., 2021*
Shell nacre powder implanted in sheep	Iandolo *et al., 2022*

2.2.7 Bone cements based on shell related products

Shen *et al*. engineered a composite calcium sulphate cement with oyster shell after removing the entire organic content (Shen et al., 2014), whereas Simu *et al.* formulated a bone cement with clam shell powder and propolis extract (Simu et al., 2018). Ruan *et al.* developed a composite calcium phosphate cement with 25% and 50% nacre powder to improve the biological properties(Ruan et al., 2018). Du *et al* utilized entire abalone shell powder as a precursor for the synthesis of calcium sulphate cement (Du et al., 2021).

2.2.8 Characterization of shell nacre powder

Many researchers have studied the inner nacreous layer of pearl oyster shells and explained that brick and mortar structure of shell nacre (Rousseau et al., 2005; Sun and Bhushan, 2012). Shell nacre powder from *Pinctada maxima* was first characterized by Balmain group. In their study, detailed analysis using FTIR, XRD, and TGA analysis was conducted which revealed the organic and inorganic constituent of shell nacre powder (Balmain et al., 1999). Furthermore, both *in vitro* and *in vivo* studies with the water soluble matrix, shell nacre pieces or shell nacre powder demonstrated the biocompatibility of shell nacre (Agarwal et al., 2014; Atlan et al., 1997, 1999; Lamghari, Antonietti, et al., 2001; Lamghari et al., 1999).

2.3 BONE TISSUE ENGINEERING

The concept of bone tissue engineering proposed by Crane is a widely accepted method, in which a scaffold or a conduit of natural or synthetic material is used for cell transplantation to guide new bone growth (Crane et al., 1995). The *in vitro*

expanded cells are seeded onto the scaffold and subsequently, the scaffold with cells is implanted into the bone defects. These exogenous seed cells suffer nutrient deficiency, inflammatory response and poor adhesion to the scaffold. These limitations significantly hinder the performance of tissue engineered materials. Moreover, the inflammatory reactions triggered by the apoptosis of seeded cells further prevents the bone repair process (Cao et al., 2020). Nonetheless, the translation of *in vitro* tissue engineering into clinical therapies is accompanied by various technical and regulatory challenges and requires sophisticated *in vitro* facilities. So, to overcome these challenges, *in situ* bone tissue engineering method has been introduced, which utilizes the inherent regenerative potential of the bone to heal.

In situ bone tissue engineering approaches are often focused on using a scaffold or growth factor-based cues which recruits endogenous stem cells to the injury site and promote the healing and restoring to preinjury state. The three-dimensional scaffold plays a crucial role in mimicking the bone's architecture and providing the necessary microenvironment and extracellular factors for healing. The bone ECM like architectural features and the bioactive composition of the bone triggers the inherent healing process of the bone which involves the stimulation of endogenous stem cells and growth factors present in the host tissue. Consequently, the endogenous stem cells and growth factors migrate to the surface and interior of the scaffold, promoting proliferation and osteogenic differentiation. This orchestrated process effectively repairs bone defects and facilitates new bone formation (Cao et al., 2020; Sengupta et al., 2014).

2.3.1 Properties of scaffolds

The first requirement of a scaffold is non-cytotoxicity and good cytocompatibility. The scaffold should not generate any toxic degradation products and provoke any inflammatory reactions. It should be porous with interconnected and the size of the pores should be less than 300 μm to favour the attachment and proliferation of cells, nutrient flow and vascularization (Zhao et al., 2016). The scaffolds should contain the bioactive factors that recruits the mesenchymal stem cells, decrease the pro-inflammation and promote healing. Biodegradation and control of biodegradation are the crucial properties of the scaffold. An ideal scaffold can be customized to provide the optimum structural support for regeneration while facilitating the efficient biological clearance to minimize foreign body response. This approach ensures that regeneration takes place where it is needed and concluded once the defect is healed. The degradation of the scaffold can be dynamically tailored to regulate porosity and mechanical properties (Babensee et al., 1998).

2.3.2 Fabrication of scaffolds

Fabrication of a 3D scaffold with interconnected porous structure poses a significant challenge, but it can be achieved by different fabrication methods. When selecting a processing method, it is crucial to ensure that it does not affect the properties of material. The chosen fabrication method should fulfil certain criteria such as being easily reproducible, and cost and time effective. Various fabrication methods such as freeze drying, phase separation, gas foaming, electrospinning, 3D printing, stereolithography, fused deposition modelling etc., are reported. The TIPS method is

simple to perform and a 3D scaffold is fabricated with interconnected porous structures.

2.3.3 Thermal induced phase separation

In this technique, the temperature of the polymer solution is quenched below the freezing point of the solvent. This decrease in temperature act as a driving force, causing phase separation as the system becomes thermodynamically unstable and separated into two phases: A polymer rich phase and a solvent rich phase (polymer lean) phase with varying polymer concentration. The solvent in the polymer lean phase is then removed through extraction or sublimation. Once the solvent is removed, the polymer lean phase form pores, while the polymer rich phase transform into a porous structure (Capuana et al., 2021; Nam and Park, 1999).

The TIPS process relies on how the polymer and solvent interact and the phase separation can occur through two mechanisms: Liquid-Liquid separation and a solid-liquid separation. Liquid-liquid separation occurs before the solvent freezes, whereas the solid-liquid separation occurs after the solvent is completely frozen. A high freezing point for solvent and strong compatibility between the polymer and the solvent causes solid-liquid phase separation. By cooling the polymer solution, the solvent crystallizes causing the polymer to separate from the crystallization front. Once the solvent is removed by sublimation, the resulting foam exhibits pores that resemble the shape of solvent crystals. The structure of the scaffold is determined by various factors including, crystallization of the solvent, polymer concentration, solvent type, thermal quenching strategy *etc* (Cao et al., 2006; Nam and Park, 1999; Zeinali et al., 2021).

2.3.4 Composite PCL scaffolds by TIPS method

PCL is the most extensively investigated material for bone tissue engineering applications. It is a biodegradable FDA approved polymer which is cost effective. It is hydrophobic, semi-crystalline polymer with melting point ranging between 59 to 64°C. PCL dissolve in almost all the solvent at room temperature (Siddiqui et al., 2018). Dioxane is one of the most widely used solvent (Yao et al., 2020), followed by tetrahydrofuran (Wang et al., 2013) for scaffold fabrication by TIPS method. However, the toxicity of the solvent is the major concern. Dimethyl carbonate is a green solvent with freezing point of 2 to 4°C and the solvent is easily removed by lyophilization (Cao et al., 2006; Fabbri et al., 2010).

The slow degradation nature is one of the reasons for its use in bone tissue engineering applications. The strength of the scaffold depends on the molecular weight and the porosity (Guarino et al., 2014). The degradation of the PCL is adjusted by altering the porosity and molecular weight. Similarly, it is blended with natural polymers or any bioactive materials for tailored degradation and mechanical properties. PCL HA composite scaffold fabricated by the TIPS method exhibited higher mechanical properties with the addition of HA (Goonasekera et al., 2016; Sultana and Hayat Khan, 2013). Similarly, bioglass PCL scaffolds were fabricated with the aim of bioactivity and enhanced mechanical properties (Fabbri et al., 2010). Composite scaffolds of PCL and nano HA exhibited reduction in compressive strength with increasing amount of HA (Díaz et al., 2014). Similarly, the addition of multiwalled carbon nanotubes to the PCL HA scaffold altered the degradation and mechanical properties (Díaz et al., 2021).

Moreover, PCL has been modified with drug, bioactive molecular for enhanced osteogenesis. For instance, Nair *et al.,* fabricated a PCL laponite composite scaffold with strontium ranelate (drug for osteoporosis) which demonstrated increased osteogenic potential (Nair et al., 2016). In another study, Korbut *et al.,* fabricated composite scaffolds by incorporating HA whiskers, lysine into PCL, resulting in improved cell adhesion and young's modulus (Korbut et al., 2021). These findings indicated that PCL can be tailored with desirable characteristics by blending or forming composite scaffolds.

2.3.5 Characterization of scaffolds

One of the first desirable property of scaffold is porosity which is mainly studied by SEM and rarely by MicroCT (Wang et al., 2013; Yao et al., 2020). Next, the chemical constituent of scaffold are studied by FTIR and TGA (Abdelrazek et al., 2016; Elzein et al., 2004). The next property studied is compressive modulus and most scaffolds exhibited compressive modulus less than 5 MPa (Goonasekera et al., 2016; Korbut et al., 2021). Several studies reported aging of the scaffolds in PBS and its impact on the mechanical properties (Díaz et al., 2014; Remya et al., 2018). Furthermore, *in vitro* bioactivity studies are conducted by soaking the scaffolds in SBF according to ISO 23317 (ISO 23317, 2014). This indirectly demonstrated the osseointegration ability of the bones (Kokubo and Takadama, 2006). Another essential requirement of scaffold is non-cytotoxic nature and cytocompatibility. The cytotoxicity evaluation is conducted according to ISO 10993-5 (ISO 10993-5, 2009). Finally, the osteogenesis of the scaffold is studied using BM-MSC and the osteogenesis is proved by ALP assay, immunofluorescence, gene expression *etc*.,

2.4 BONE VOID FILLING CEMENTS

A bioactive material is one that elicits a specific complex orchestrated cellular, physiochemical, mechanical responses at the implanted site which facilitates osteointegration, osteoconduction, osteoinduction and finally osteogenesis. Bone like apatite formation in the simulated body fluid is an essential property making the synthetic material bioactive. The silanol (Si–OH) group and calcium ions are effective components for inducing apatite nucleation (Miyazaki & Ohtsuki 2008) and can bond to the implanted bone.

2.4.1 Modifications of resin matrix

Many different organic matrices or combination of organic matrices have been investigated to address the issues polymerization shrinkage and exotherm generation of composite bone cement. For example, Kawanabe *et al.,* 1993 used bisphenol A glycidyl methacrylate (bis GMA) and triethylene glycol dimethacrylate (TEGDMA) based cement. However, the toxicity of TEGDMA and volumetric shrinkage of bisGMA remained the same (Tamura et al., 1995). Yamura *et al.,* formulated a composite bone cement with bis GMA resin matrix, which exhibited less adhesiveness to polyethylene, poor ductility and high rigidity (Yamura et al., 1998). Ni *et al.,* included the resin matrix of Bis GMA, TEGDMA and poly (ethylene) glycol methacrylate in the composition of strontium-HA bioactive bone cement (G.X. Ni et al., 2006), while Deb *et al.,* 2005 developed a two-paste bioactive bone cement with the monomers urethane dimethacrylate, bisphenol glycidyl methacrylate, and triethylene glycol dimethacrylate. High exotherm, cytotoxicity and excessive elastic modulus are the problems associated with commercially available cortoss bone

cement, which contained the terpolymer of bisGMA, bisphenol-a-ethoxy dimethacrylate (bis-EMA) and TEGDMA resins (Boyd *et al*., 2008). A hydrophilous PMMA cement based on acrylic acid and styrene was synthesized which exhibited volumetric swelling and reduced compressive strength than PMMA (Yang et al., 2017). It is proved that a resin matrix highly influences the properties of composite bone cement. Despite efforts to replace MMA by bis GMA, bis EMA and TEGDMA and combination resins, the problem of exotherm generation and toxicity due to free monomer release has not been fully addressed. Therefore, there is a need for an alternative resin matrix.

2.4.2 Ormocer

Organically modified ceramic resin (ORMOCER) are the emerging three-dimensional class II hybrids with organic and inorganic portions (Owens et al., 2016). It is a multifunctional inorganic-organic hybrid material used in the field of dental cements for non-cytotoxic nature, low polymerization shrinkage and mechanical properties (Lizymol, 2004a, 2010; Vibha and Lizymol, 2017, 2019). This glass like inorganic- organic hybrids are easily synthesized by modified sol gel method using methacrylate substituted alkoxysilanes through the process of hydrolysis and condensation to form the inorganic siloxane network whereas the methacrylate moieties remain intact (Wolter et al., 1992). Later the methacrylate groups undergoes photo/chemical curing to form the organic network (Haas, 2000). Cage/random/ladder structured siloxane network is formed depending upon the catalyst used (Dirè et al., 2018) (Kim et al., 2018a). Among this, ladder structures have higher inorganic siloxane network density which introduced improved physico-chemical properties

when compared to the other molecular architectures (Kim et al., 2018b). In our previous study, it was reported that photocured cement of ladder structured siloxane methacrylate (LSM) resin exhibited low shrinkage properties (Bridget Jeyatha et al., 2022). However, there is no report of usage of this resin for orthopaedic applications to our knowledge.

2.4.3 Modification of filler part

Many researchers modified the cement composition with novel bioactive fillers to improve the mechanical properties, reduce shrinkage and exotherm and enhance bioactivity, biocompatibility *etc*. Kokubo *et al.,* 1992 developed bioactive cement, which includes glass powder containing calcium as a main constituent and a hardening liquid ammonium phosphate. Kawanabe *et al.,* 1993 developed a composite bioactive bone cement containing equal parts of bis GMA and TEGDMA and glass powder (70%), which exhibited higher compressive strength, exotherm temperature and volumetric shrinkage. Composite bone cement with bisGMA resin matrix and apatite wollastonite glass ceramic (AW-GC) exhibited less adhesiveness to polyethylene, poor ductility and high rigidity (Yamura et al., 1998). Mousa *et al.,* 2000 developed AW-GC (50%/70%) containing bioactive bone cement with PMMA and it exhibited good bioactivity. Osseointegration without any fibrous tissue was observed after the implantation of Strontium-HA bioactive bone cement with filler composition of Sr-HA -97.5%, fumed silica – 2.5% and BPO-0.5% (Ni et al., 2006).

Goto *et al.,* 2005 used nano-sized titanium particles, silanized titanium powder with PMMA for bioactive bone cement preparation. But this titanium containing cement does not release calcium ions and the cement get degraded gradually. The

commercially available cortoss bone cement which included the terpolymer resins reinforced with synthetic combeite glass-ceramic particles, barium boro aluminosilicate glass and silica particles (Boyd et al., 2008). PMMA cement modified with calcium deficient nano hydroxyapatite exhibited increase mechanical properties and the exotherm generated was lower than PMMA (Jayasree and Sampath Kumar, 2015). Wu *et al*., used amphiphilic raspberry particles as bioactive fillers to enhance cell adhesion and the bone-cement interface(T Wu et al., 2018a).

Addition of graphene to the composition of styrene and acrylic acid, increased the compressive strength to 99 MPa but lowered it to 75 MPa when soaked in PBS. GO modification improved the physicochemical properties but the exothermic reaction was not satisfactory (Tan *et al*., 2023).

2.4.4 Formulation of bone void filling cement

The bone void filling cements can be either injectable or packable and the composition is optimized accordingly. Generally, bone cement is formulated as a powder-liquid system which takes longer mixing time and sometimes poor mixing reduces the mechanical properties. Sometimes, the two-paste system is preferred (Deb et al., 2005) and the main advantage of two paste system is as follows

- Control of the setting time of the cement. Both the paste can be mixed immediately before use.
- Enable faster mixing
- Enhanced mechanical properties.

In the two-paste system, the initiator and the accelerator are usually separated. The most commonly used initiator is benzoyl peroxide and the accelerator is dimethyl Para toluidine. Concerning the toxicity of DMPT, the activator DMAPEA is sometimes used in the experimental cements during optimization (Mathew et al., 1997). To reduce the toxicity of left free radicals during curing, free radical scavenger, BHT is used in the dental cements to prevent the premature and spontaneous polymerization (Yehye et al., 2015). It is also used to prolong the working time (Grohmann et al., 2022).

2.4.5 Characterization of bone cements

In addition to the characterizations mentioned in 2.3.5, the specific characterizations such as linear polymerization shrinkage, exotherm studies, radiopacity, compressive and flexural strength are studied for the cement systems. After curing, the cement undergoes shrinkage and the simple method to study shrinkage is measurement of diameter of the samples before and after curing to calculate linear polymerization shrinkage (%) (Lizymol, 2010). The exotherm generation is studied by isothermal DSC (Ormsby et al., 2011; Paz et al., 2017; Watson et al., 1990). The radiopacity of the cement is studied according to ASTM standard with the aluminum wedge (ASTM F640, 2023).

Generally, biocompatibility of the cements are studied according to ISO 10993-1 (ISO 10993-1, 2018: 10993). Acute systemic toxicity, irritation test and pyrogen test were studied during the evaluation of BioCas cement (Sandhya et al., 2017) and Chitra CPC cement (Fernandez et al., 2006). According to Blokhuis, the metaphyseal defect differs from diaphyseal defect in biological and mechanical aspects (Blokhuis, 2017).

Diaphyseal defect is considered, being easy to access and set the cement, Tarafder *et al.,* implanted 3D printed tricalcium phosphate scaffold in femoral defect (diameter 3mm) of Sprague Dawley rats (Tarafder et al., 2013). Similarly, Fielding & Bose, 2013 implanted scaffolds to investigate osteogenesis in femoral defect model of size 2.5 mm diameter (Fielding and Bose, 2013). It is understood that the osseointegration of the *in situ* setting cement can be studied in the diaphyseal femoral defect model. Further, the gross examination, radiography and histology can prove the osseointegration.

2.5 AGING OF BONE

Age-related changes occur in the cellular and microenvironment of the bone, which causes a reduction in bone mass and mineral content, an increase in bone marrow adiposity, and changes in bone morphology and structural constituents, reducing the performance and function of the bone.

2.5.1 A shift towards adipogenesis

Histomorphometry analysis of the iliac crest biopsies of osteoporosis patients confirmed the reduction in the trabecular bone and an increase in the bone marrow adipose tissue (Meunier et al., 1971) (Justesen et al., 2001). Further, the reduction in the expression of transforming growth factor β (TGF-β) and deficient of collagen I in the extracellular matrix produced by *in vitro* cultured BM-MSCs of osteoporotic patients indicated the adipogenic nature of BM-MSCs instead of osteogenesis (Rodríguez et al., 2000) and similar conclusions were recorded during the *in vitro* experiments with human trabecular bone cells (Nuttall et al., 1998). Zhou *et al.* proved the reduction in the proliferation and osteogenic potential and increase in the

senescence-associated β-galactosidase positive cells and apoptosis in human MSCs from older donors (>55 years) (Zhou et al., 2008). Thus, senescence causes a decline in the ability of BM-MSCs to proliferate, form smaller colonies and self-renew, accompanied by the loss of osteogenic potential and shifting towards adipogenesis, leading to a reduction in osteoblast numbers and increase in osteoclast activity, which impacting the bone formation and bone resorption process (Corrado et al., 2020; Ganguly et al., 2019; Singh et al., 2016; Tiede-Lewis and Dallas, 2019).

2.5.2 Changes in bone microenvironment

Senescence-associated secretory phenotype by senescent osteocytes and deterioration of the lacuna-canalicular network system of the osteocytes also leads to reduced bone formation and increased bone resorption (Farr and Khosla, 2019) (Infante and Rodríguez, 2018). Further changes occur in the crystallinity of bone minerals, collagen and its crosslinking, and non-collagenous protein, which affects the mechanical environment of the bone leading to the formation of fragile bone (Burr, 2019) (Boros and Freemont, 2017). It is well understood that alterations occur in the cellular and extracellular matrix of ageing bone. This influence the bone quality and increase the susceptibility to fractures and bone loss (Clarke and Khosla, 2010) (Rolvien and Amling, 2016). Therefore, emphasising the need to consider the ageing bone microenvironment during the design and evaluation of any biomaterial, as more than 50% of orthopaedic procedures are performed in older patients (Quatman et al., 2018).

2.5.3 Characterization of older donor BM-MSC

Generally, the population doubling time of the older donor BM-MSC is longer and this can be easily studied from passage 0 to 5 respectively. Further, the colony forming ability is reduced in the BM-MSC of older donors (Ganguly et al., 2019). This is studied by CFU-F assay and the colony area and density can be further evaluated using Image J analysis. Similarly, the BM-MSC from older donors exhibit a flattened morphology, which is easily studied by microscopic observation.

β- galactosidase serves as an indicator of cellular senescence. SA-β gal assay is a widely used method for investigating the senescence of various cell types (Debacq-Chainiaux et al., 2009). It was reported that β-gal positive cells showed the characteristics of senescence-like shortening of telomeres and higher expression of phosphorylated inhibitor of cyclin depended kinase 4A ($p16^{INK4a}$) (Liu et al., 2020). Further, the detailed investigation of osteogenesis is crucial, as older BM-MSC shows adipogenesis than osteogenesis. Hence the influence of aging on the function of the BM-MSC can be well understood through gene expression studies (Ganguly, El-Jawhari, et al., 2022; Ganguly, Fiz, et al., 2022).

3 SHELL NACRE POWDER: PROCESSING AND CHARACTERIZATION

Pinctada fucata is a pearl producing marine mollusc of the genus *Pinctada* and family *Pteriidae*. This bivalve possesses an outer prismatic layer and thick inner nacreous layer commonly referred to as shell nacre or mother of pearl. Shell nacre holds significant value in biomedical applications within the fields of cosmetics and orthopaedics. Notably, it has been reported to exhibit osteogenic, angiogenic, anti-osteoporotic, anti-inflammatory as well as radiopacity and superior mechanical properties (Gerhard et al., 2017). However, there exists a research gap concerning the utilization of shell nacre from *Pinctada fucata* for bone defect management studies. The development of definitive processing method to obtain shell nacre powder comprising both organic and inorganic constituents, has not been adequately demonstrated. Hence, the primary objective of this chapter is to establish a processing method to obtain shell nacre powder and subsequent characterization, including the sub-objectives a) removal of the outer prismatic layer of shells b) processing of nacreous shells and c) characterization of shell nacre powder.

3.1 MATERIALS AND METHODS

3.1.1 Identification and collection of shells

Pinctada fucata shells which were discarded after the fishing activities were collected from the Kayalpattinum coast of Gulf of Mannar. It was identified by the reddish or brown coloured shells with light-coloured radial rays.

3.1.2 Characterization of inner nacreous layer

The shells were washed in running water and the external impurities like tunicates and deposited dirt were removed mechanically. Followed by the detergent wash, the shells were dried at 37°C. The inner nacreous layer was observed using scanning electron microscopy (SEM) (FEI Quanta 200, Netherlands).

3.1.3 Removal of outer prismatic layer

Two different methods were used to remove the outer prismatic layer. In the first method, 6N HCl was used to scrub the outer prismatic layer. After the removal of outer prismatic layer, acid impurities were removed by washing in distilled water multiple times and the shells were dried. In the next method, shells were soaked in 15 to 20% acetic acid with 5%NaCl. After 1 h of soaking, the external prismatic layer was scrubbed out. Shells were sonicated in distilled water to remove the acid impurities and then dried. Both the dried nacreous shells were observed in SEM (FEI Quanta 200, Netherlands).

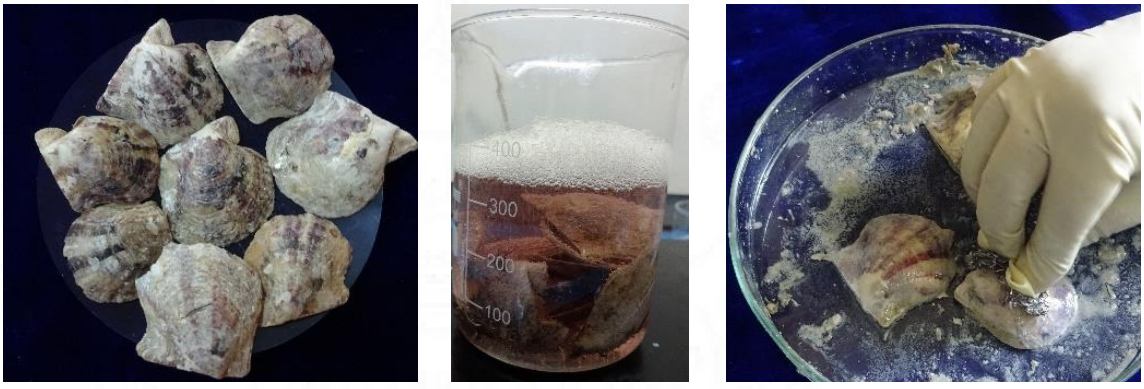

(a) (b) (c)

Figure 3.1 Processing of pearl oyster shells: (a) Shells of *Pinctada fucata*; (b) Soaking of shells in acetic acid and NaCl solution and (c) scrubbing the outer prismatic layer

3.1.4 Processing method for shell nacre powder

Nacreous shells were broken into small pieces and powdered using a planetary ball mill (Retsch, Germany) and sieved using a vibrational sieve (Retsch, Germany). Shell nacre powder collected through a 20 μm sieve was washed in deionized water for 3 h by stirring with intermittent water changes by decanting. Finally, shell nacre powder was freeze dried to get fine powder.

Shell nacre powder obtained from different batches were pooled together and then characterized.

3.1.5 Characterization of shell nacre powder

The size and morphology of shell nacre powder was studied by scanning electron microscopy. Shell nacre powder was mixed with potassium bromide (KBr) in the ratio 1:400 and the FTIR spectrum was recorded from 400 to 4000 cm^{-1}at a resolution of 4 cm^{-1}(FTIR Carry 600, Agilent technologies). Raman spectrum of shell nacre powder was recorded using confocal Raman microscopy (alpha 300RA, Witec, Germany) with a 532 nm laser. X-ray Diffraction Spectrum (XRD) (Bruker, D8 Advance, Germany) was measured in the 2θ range 10° to 70°C with CuKά radiation in the incremental step of 5° and peaks were identified using the JCPDS (Joint committee on powder Diffraction standards) database. Thermogravimetric analysis of shell nacre powder was carried out using SDT-2960, TA Instruments and heated from room temperature to 1000°C (heating rate-10°C/min) in a nitrogen atmosphere. Trace elements like Cu, Fe, Mg, Mn, Zn, Cd, Pb, Hg, and Se were estimated using Optical Emission Spectroscopy with Inductively Coupled Plasma (OES-ICP) (Perkin Elmer,

US). All the spectrums were drawn using Origin Pro software (OriginLab Corporation, USA).

3.1.6 *In vitro* studies

3.1.6.1 Direct contact

Shell nacre powder was made into a pellet of diameter 10 mm, using uniaxial press uniaxial press (X press 3630) under the pressure of 8 ton with holding and releasing time of 1 min respectively. The prepared pellets were handled carefully and steam sterilized. The direct contact study was carried out based on ISO 10993-5 (ISO 10993-5, 2009). Human osteoblast sarcoma (HOS) cells (American Type Culture Collection) were cultured in Dulbecco's minimal essential media (DMEM; Gibco, USA), supplemented with 10% foetal bovine serum (FBS, Gibco, USA) and 1% penicillin-streptomycin (Gibco, USA). The positive control used was stabilized polyvinylchloride (PVC) disc, while the ultra-high molecular weight polyethylene (UHMWPE) served as a negative control. Cells were seeded in a 24-well plate at a density of $3x10^4$ cells/ well and incubated at 37°C with 5% CO_2 until they reached sub-confluency. Subsequently, three replicates of shell nacre powder pellet (SNP) and the controls were placed on the monolayer. After 24 h of contact with the material, the response around the materials was observed using a phase contrast microscope. Qualitative changes such as cell morphology, zone of lysis, vacuolization, detachment, and membrane disintegration were graded on a scale of 0-none, 1-slight, 2-mild, 3-moderate and 4-severe.

3.1.6.2 Cell adhesion study

Cell adhesion study of the shell nacre powder pellet (SNP) was performed using HOS cell line. Cells were sub-cultured and seeded on SNP at density of $1x10^4$ cells/cm^2 and incubated for 48 h at 37±1°C under humidified atmosphere containing 5% CO_2. After 48 h cell seeded test material and glass cover slides were fixed in 4% paraformaldehyde for 48h. The dried samples were observed in SEM.

3.2 RESULTS AND DISCUSSION

3.2.1 Identification of *Pinctada fucata* shells

Pinctada fucata shells were identified by the reddish or brown coloured shells with radial rays of light coloured which formed the outer prismatic layer. Meanwhile, the inner nacreous layer exhibited a golden metallic hue. Both the external and internal features of shells were in agreement to the description of the *Pinctada fucata* as reported (Behera, 2017).

3.2.2 Characterization of inner nacreous layer

The inner nacreous layer of the *Pinctada fucata* shells was observed in SEM (Figure 3.2.1). It revealed the characteristic brick and mortar structure where aragonite tablets act as brick and the inter-tiled organic layer as mortar. Aragonite tablets were of pseudo-hexagon shaped and each aragonite tablets were glued by organic matrix to form a lamellar sheet. The cross-section analysis showed that each lamella was arranged in a parallel manner and placed one above the other. The parallel lamellar sheet with brick-and-mortar organization was clearly evidenced from the SEM analysis. The structure of the shells were similar to the structure of *Pinctada maxima*

as reported by Rousseau's group (Rousseau et al., 2005) and hierarchical structure of nacre as reviewed by Sun and Bhushan (Sun and Bhushan, 2012).

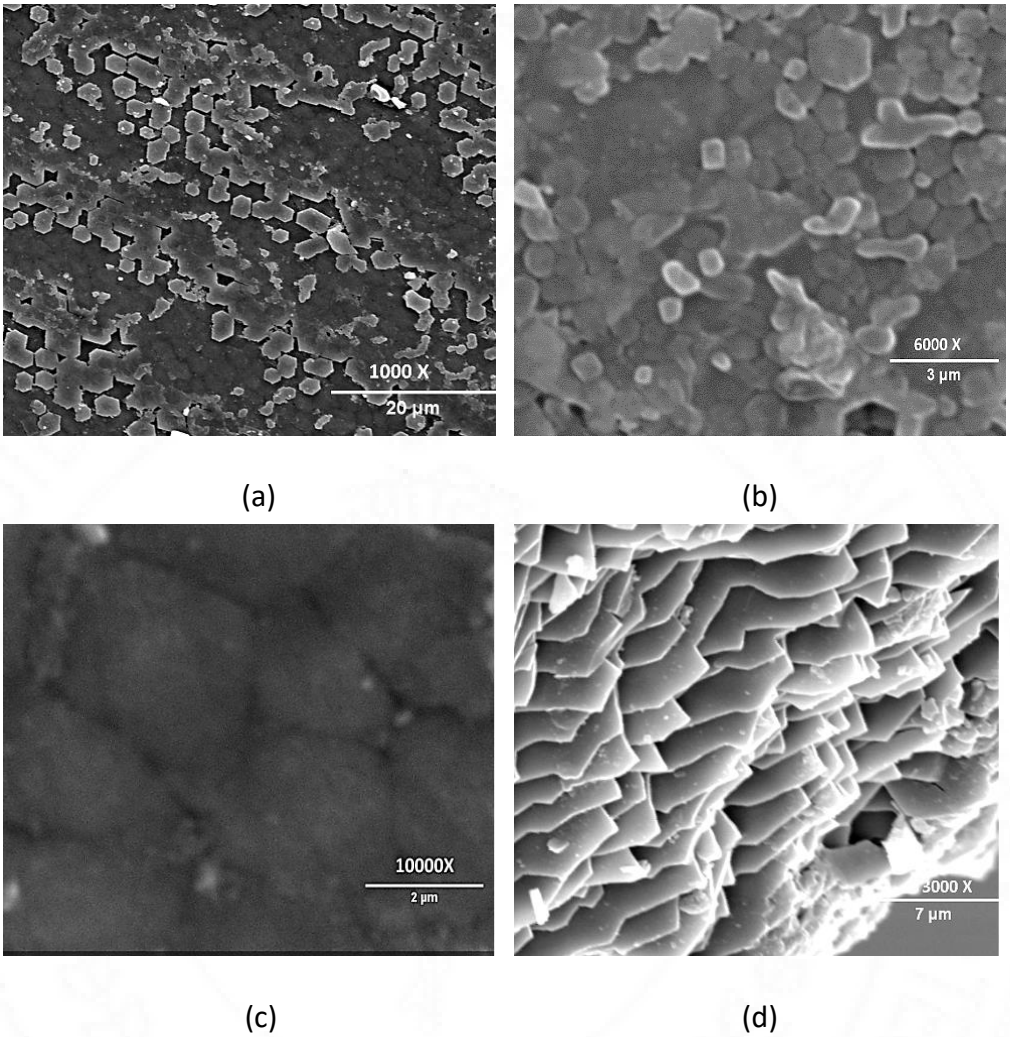

Figure 3.2.1 SEM observation of inner nacreous layer of *Pinctada fucata*. (a,b,c) Surface morphology view revealing the brick and mortar structure. (d) Cross-sectional view revealing the lamellar arrangement. Scale bar represents a) 20 µm b) 3 µm c)2 µm and d)7µm

3.2.3 Removal of outer prismatic layer

The main objective of this work is to get shell nacre powder with both organic and inorganic content. Several methods to remove the prismatic layer have been reviewed by Pei *et al*., such as mechanical separation, acid hydrolysis with 5%HCl and

hydrogen peroxide, alkali hydrolysis with NaOH *etc*. The amount of organic content of the shell nacre powder was depended on the processing method used (Pei et al., 2021). To achieve the goal of obtaining shell nacre powder with both inorganic and organic matrix together, both the HCL based method and a mild acetic acid along with NaCl was attempted.

During the SEM observation of HCL treated shells (Figure 3.2.2), the surface layer had been significantly disrupted, resulting in the loss of characteristic brick-and-mortar arrangement. It became apparent that HCl treatment had penetrated deeply, potentially even removing the organic layer. However, the outer prismatic shell had to be scrubbed out with 6N HCl, the method proved to be time consuming, and laborious.

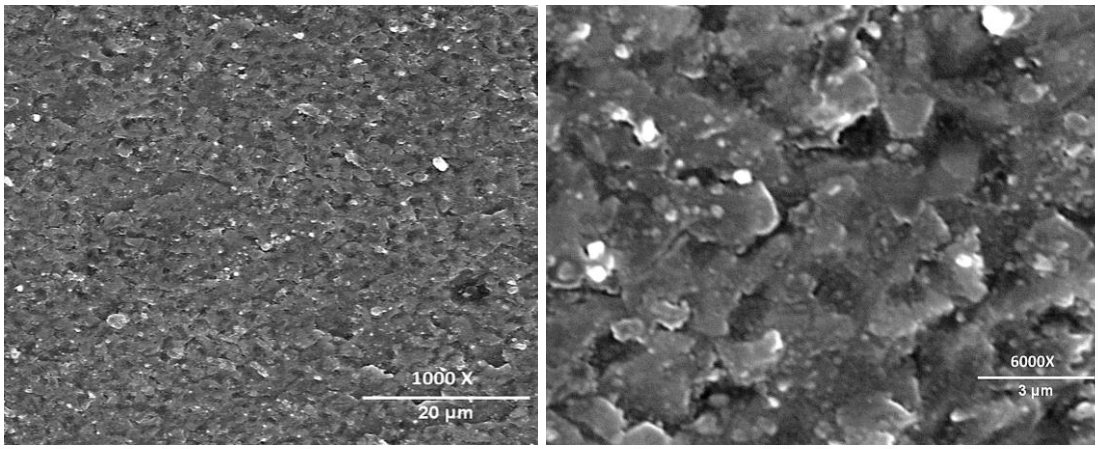

(a) (b)

Figure 3.2.2 Microstructure of inner nacreous layer of *Pinctada fucata* after HCl treatment. Scale bar represents a) 20 µm b) 3 µm.

In the next method, the shells were soaked in acetic acid and NaCl solution, which enabled the faster removal of calcite with brisk effervescence. Further manual scrubbing, removed the outer prismatic layer completely and obtained nacreous shells. The nacreous shells were lustrous with a golden metallic hue as previously described

(Behera, 2017). SEM observation of the acetic acid and NaCl treated shells (Figure 3.2.4) revealed the characteristic brick and mortar structure wherein the polygonal aragonite crystals were surrounded by the organic layer. This confirmed the removal of prismatic layer without disturbing the organic layer of nacreous shell.

Figure.3.2.3 Nacreous shells after prismatic layer removal

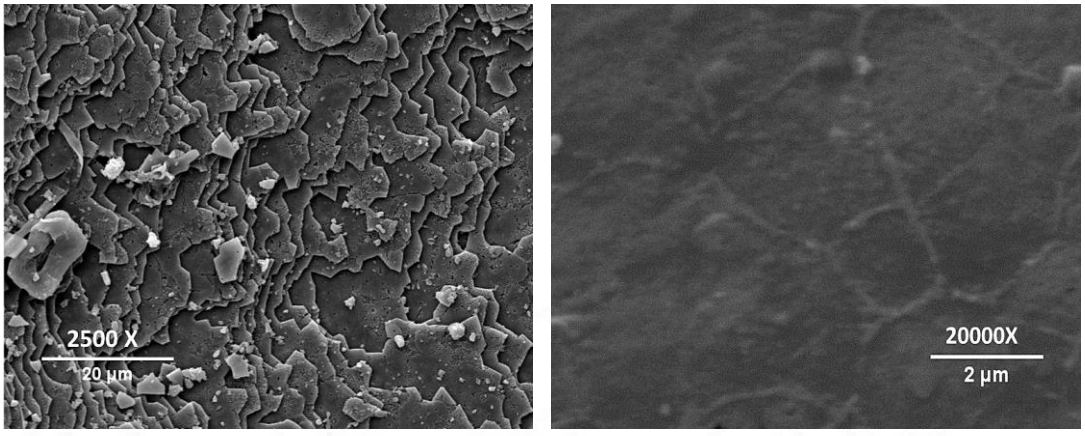

(a) (b)

Figure 3.2.4 Microstructure of inner nacreous layer of *Pinctada fucata* after acetic acid and NaCl treatment. Scale bar represents a) 20 µm b) 3 µm

3.2.4 Characterization of shell nacre powder

The lustrous nacreous shells were ball milled and sieved to get the shell nacre powder (Figure 3.2.5 a). SEM analysis of the shell powder (Figure 3.2.5 b) revealed

an irregular morphology with different sizes less than 0.5 µm (Image J analysis), whereas other studies reported shell nacre powder of larger sizes, such as 42.5 µm (Iandolo et al., 2022) and 50 to 100 µm (Atlan et al., 1997) respectively.

(a) (b)

Figure 3.2.5 Shell nacre powder; (a) Macroscopic appearance of shell nacre powder (b) SEM observation of shell nacre powder. Scale bar represents 10 µm

3.2.4.1 FTIR analysis

FTIR analysis of shell nacre powder is shown in Figure 3.2.6. The presence of peaks for the internal vibration modes of CO_3^{2-} ions of calcium at 714 cm^{-1},862 cm^{-1}, 1083 cm^{-1} and 1480 cm^{-1} and a splitting peak at 714 cm^{-1} confirmed the aragonite form. The strongest peak of the spectrum was at 1480 cm^{-1} which was due to the overlap of peaks of organic matrix and carbonate ions. The broad peak at 3463 cm^{-1} was the stretching modes of OH/NH of organic matrix or the adsorbed water molecules as reported (Balmain et al., 1999; Verma et al., 2006, 2007). A strong peak at 2920 cm^{-1} were attributed to the CH stretching modes of the organic matrix. The peaks of -OH of HCO_{3-} groups in the crystal lattice or at the mineral/organic interface groups of carboxylic groups were observed at 2522 cm^{-1} and stretching of carbonyl groups of

acidic proteins at 1788 cm^{-1}. Peaks at 1656 and 1526 cm^{-1} were attributed to the amide I / amide II bonds of proteins of organic matrix. A shoulder at 1065 cm^{-1} were assigned to the C-O stretching of carbohydrates present in the organic matrix and further, the peak also indicated the SO_{3-} vibration of the sulphated glycosaminoglycans. Similar observations were recorded during the investigation of organic polymers of venus clams (Agbaje et al., 2021).

It was reported that organic matrix of shell nacre is comprised of the water-soluble matrix and insoluble matrix. The water-soluble matrix contains the acidic proteins and polysaccharides whereas the water-insoluble matrix contains the chitin, lipid and the alanine and glycine rich silk like proteins (de Muizon et al., 2022). In the present study, FTIR spectra of shell nacre powder showed the peaks of aragonite, proteins, carbohydrates, and water. Results were consistent with the findings of Balmain *et al.,* and Zouari *et al.,* during the investigation of organic content of the shell nacre of *Pinctada maxima* shells (Balmain et al., 1999) and *Pinctada radiata* shells (Bellaaj-Zouari et al., 2011). Thus, the FTIR study confirmed the presence of both organic and inorganic constituents in the shell nacre powder.

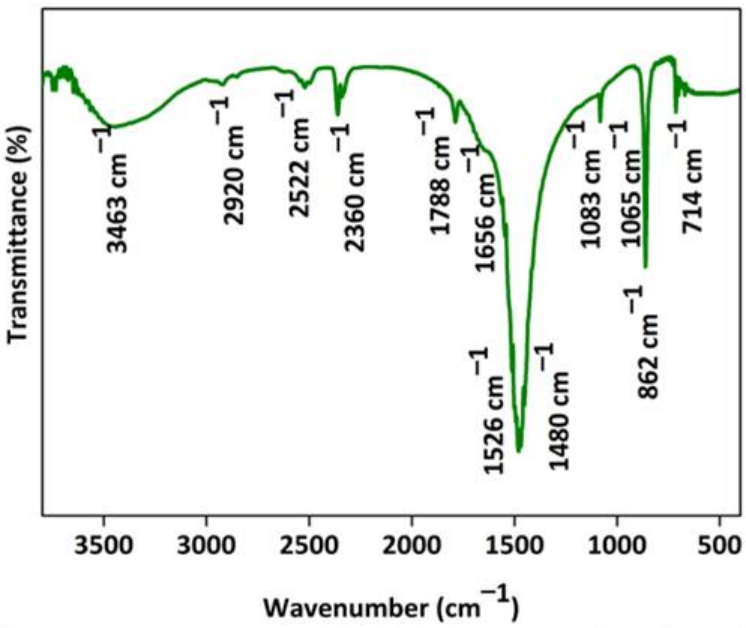

Figure 3.2.6 FTIR spectrum of shell nacre powder from 400 to 3750 cm^{-1}

3.2.4.2 TGA analysis

The thermogram of shell nacre powder is shown in Figure 3.2.7. The initial loss of water content was observed at 266°C, followed by the degradation of organic content at 596°C and the transformation of the aragonite to calcite. The gradual major loss (40%) occurred between 596°C to 735°C during the conversion of calcite to calcium oxide with the release of CO_2 and left with final residue of calcium oxide (56%) at 1000°C. During TGA analysis degradation of organic molecules occurred at high temperature 596°C as it is complexed with aragonite. Once the organic content was lost, aragonite crystal got transformed to calcite and gradually the entire calcite got degraded, which was finally left with 56% calcium oxide residues from 735°C. Thus, it was found that shell nacre powder comprised of 5% organic and 95% inorganic content which was determined from the thermogravimetry changes. The similar TGA results were reported by Balmain *et al.*, and Zouari *et al.*, during the

investigation of organic content of *Pinctada maxima* shells (Balmain et al., 1999) and *Pinctada radiata* shells (Bellaaj-Zouari et al., 2011).

3.2.4.3 Micro -Raman and XRD studies

Micro-Raman spectrum (Figure 3.2.8) exhibited the characteristic carbonate stretching vibrations of aragonite at 1084 cm^{-1} and lattice vibrations modes of aragonite at 155 cm^{-1}, 208 $cm^{-1}$and 706 cm^{-1}. X ray diffraction pattern (Figure 3.2.9) of shell nacre powder matched with the aragonite crystals of JCPDS 01-071-2392 (Figure 3.2.10) and had characteristic sharp diffraction lines of well crystallized aragonite of single mineral phase. Both the Raman and XRD study of shell nacre powder proved the aragonite form of the calcium carbonate as reported (Balmain et al., 1999). During the analysis, a calcite peak at 276 $cm^{-1}$and a diffraction line of calcite at 29.4° was noted, which may be due to the heat generated during the milling of shell nacre powder or may be traces of external prismatic layer or due to presence of calcite in shell nacre itself (Balmain et al., 1999; Bellaaj-Zouari et al., 2011; Ramesh et al., 2018).

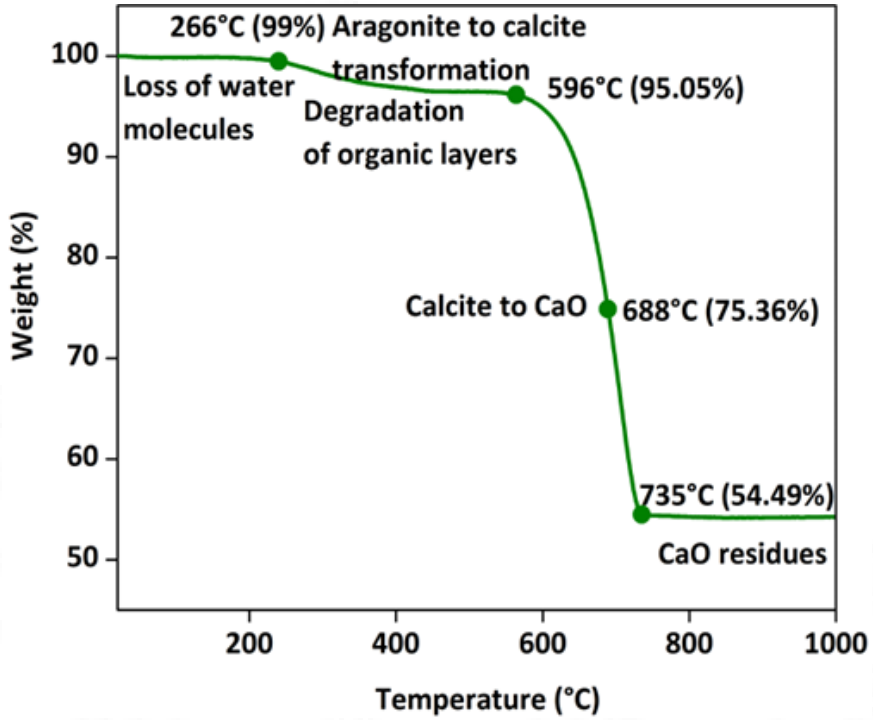

Figure 3.2.7 Thermogram of shell nacre powder from RT to1000°C

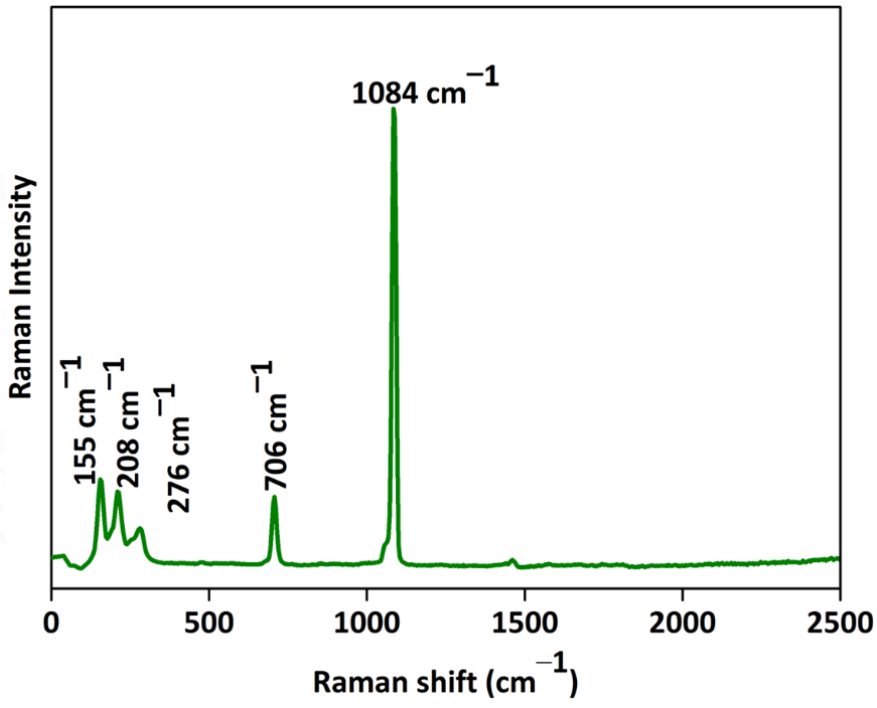

Figure 3.2.8 Micro Raman spectrum of shell nacre powder

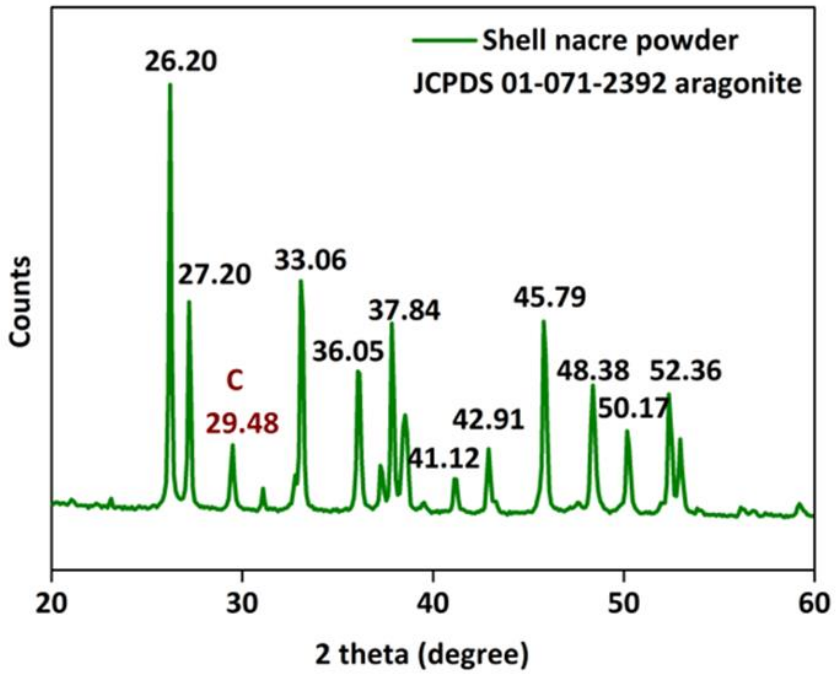

Figure 3.2.9 X-ray diffraction pattern of shell nacre powder

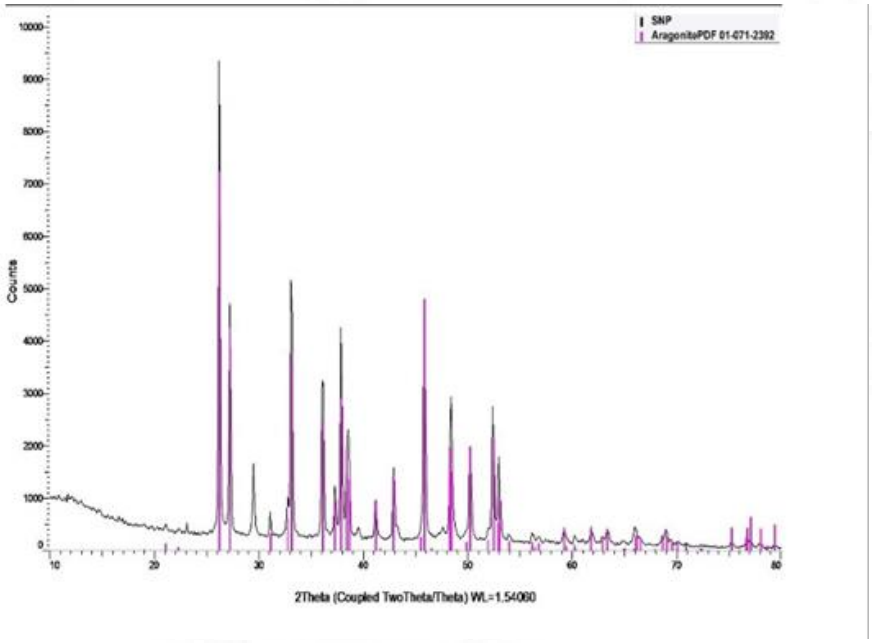

Figure 3.2.10 Matching of XRD pattern of shell nacre powder with aragonite JCPDS 01-071-2392

3.2.4.4 ICP-OES analysis

Table 3.1 ICP OES analysis of shell nacre powder

S.No.	Elements analyzed	Total amount (ppm)
1	Cu	BDL[1]
2	Fe	5.889
3	Mg	102.87
4	Mn	0.772
5	Zn	0.4827
6	Cd	BDL[1]
7	Pb	0.772
8	Hg	1.4
9	Se	BDL[1]

[1] BDL Below the lower detection limit for Cu - 0.0097 ppm, Cd - 0.0027 ppm Se - 0.0750 ppm.

Table 1 presents the result of the trace element analysis of shell nacre powder. Copper was not detected, while manganese and zinc were present at very low levels (0.772 and 0.4827 ppm) respectively. Iron was detected at 5.889 ppm and the magnesium was found at concentration of 102.87 ppm. Among the deleterious heavy metals, cadmium and selenium were below the detection limit, while mercury and lead were present at the levels of 1.4 ppm and 0.772 ppm, respectively. Further the trace element analysis was concluded based on ASTM standards (ASTM F1609-08, 2014; ASTM F2103, 2018), which specify that the permissible limit of mercury and lead are 5 and 30 ppm respectively, and the total content of harmful heavy metals should be less than 50 ppm. In the present study, shell nacre powder contained mercury and lead which were below the permissive limit and other heavy metals cadmium, selenium, and copper were below the detection limit. The total content of harmful heavy metals in the shell nacre powder was below 50 ppm. Therefore, the shell nacre powder obtained through the acetic acid-based method is suitable for use in biomedical

applications, as it contains both organic and inorganic content, and free of harmful heavy metals.

3.2.5 *In vitro* studies

3.2.5.1 Direct contact studies

Direct contact of shell nacre powder pellet was evaluated based on the ISO standard (ISO 10993-5, 2009). After 24 h contact with the shell nacre powder pellet (Figure 3.2.11), HOS cells showed no features of cytotoxicity like change in morphology, detachment and zone of lysis *etc.*, The cells attached well to the sample and the same was observed in the case of negative control UHMWPE, whereas the positive control exhibited the features of cytotoxicity.

3.2.5.2 Cell adhesion study

Cell adhesion of shell nacre powder pellet was studied by SEM. During SEM observation, a layer of cells was attached over the shell nacre powder pellet (Figure 3.3.2 a) revealing typical spindle morphology (Figure 3.2.12). The cells spread over the shell nacre powder pellet which was understood by the presence of both filopodial and lamellipodial extensions. This exhibited the cytocompatible nature of the shell nacre powder pellet.

Previous study by Agarwal *et al.*, observed that higher concentrations of shell nacre powder was-cytotoxic and recommended low concentration for aesthetic formulations (Agarwal et al., 2014). In contrast, in the present study, shell nacre powder was non-cytotoxic and cyto-compatible in direct contact with shell nacre powder pellet. Similarly, many *in vivo* studies of shell nacre powder and pieces

demonstrated the biocompatibility of shell nacre powder (Atlan et al., 1997, 1997; Lamghari, Antonietti, et al., 2001; Lamghari, Berland, et al., 2001).

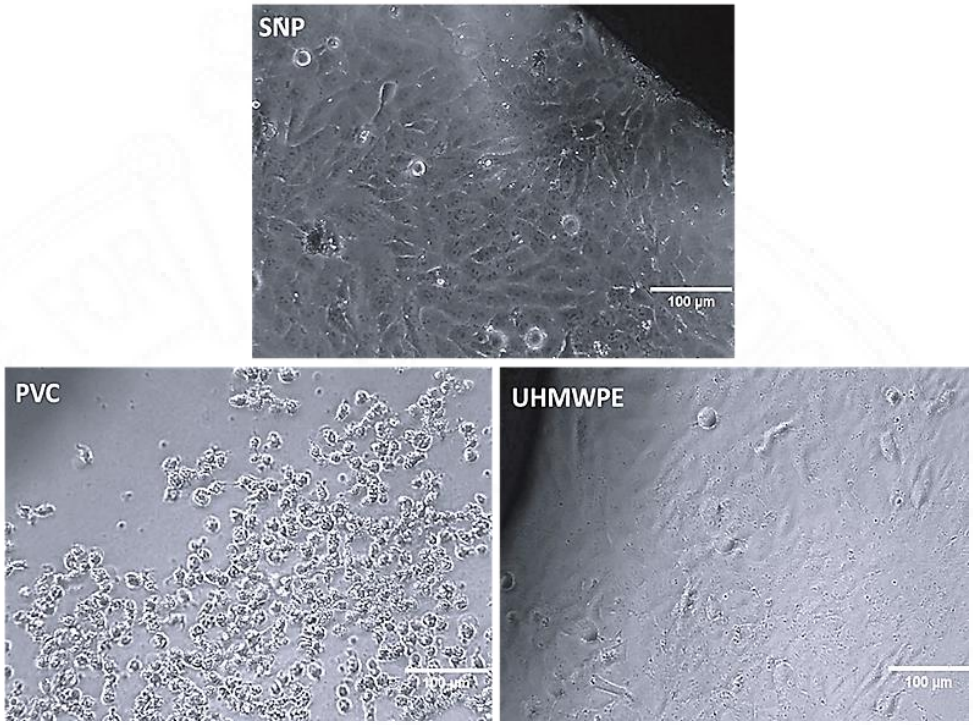

Figure 3.2.11 Direct contact of sterile shell nacre powder (SNP) pellet, a) SNP b) Stabilized PVC and c) UHMWPE with human osteosarcoma cell line (HOS) for 24 h. Scale bar represents 100 µm.

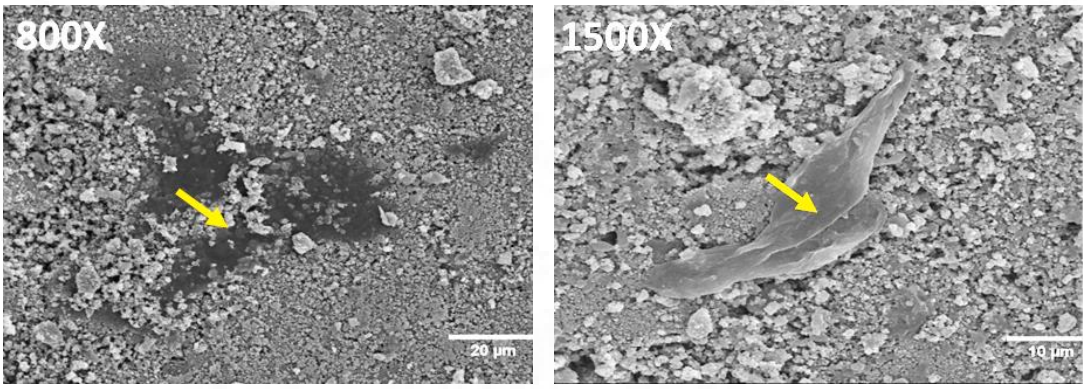

(a) (b)

Figure 3.2.12 Cell adhesion: SEM images showing the adhesion of HOS cells with shell nacre powder pellet after 48 h. Scale bar represents a) 20 µm and b) 10 µm

Overall, in this study, shell nacre powder was processed from the shells of Pinctada fucata using the acetic acid and NaCl method. Shell nacre powder comprised of both organic and inorganic constituents and it was found to be free of harmful heavy metals. Furthermore, it lacks cytotoxicity and exhibited cyto-compatible properties.

4 FABRICATION AND CHARACTERIZATION OF SHELL NACRE PCL COMPOSITE SCAFFOLDS

Composite scaffolds of shell nacre powder and PCL were fabricated, employing a thermal induced phase separation (TIPS) method. Notably the use of green solvent dimethyl carbonate enhanced the versatility of the process. This shell nacre PCL composite scaffold is distinct from other reported composite scaffolds which utilized oyster shell powder (Didekhani et al., 2020), abalone particles (Kim et al., 2021; Pan et al., 2022), nacre derived hydroxyapatite (Megat Abdul Wahab et al., 2020), pearl powder (Zhang et al., 2018) *etc*. Two different types of scaffolds were fabricated in this study. One with lower concentration of shell nacre powder and the other with higher concentration of shell nacre powder. From each type, one with higher compressive modulus was selected for further evaluation. The selected scaffolds were subjected to comprehensive analysis to assess the physico-chemical properties, cytotoxicity and osteogenic potential with rat BM-MSCs. Overall, this study aimed to gain insights into the performance and potential of shell nacre PCL composite scaffolds.

4.1 MATERIALS AND METHODS

4.1.1 Fabrication of scaffolds

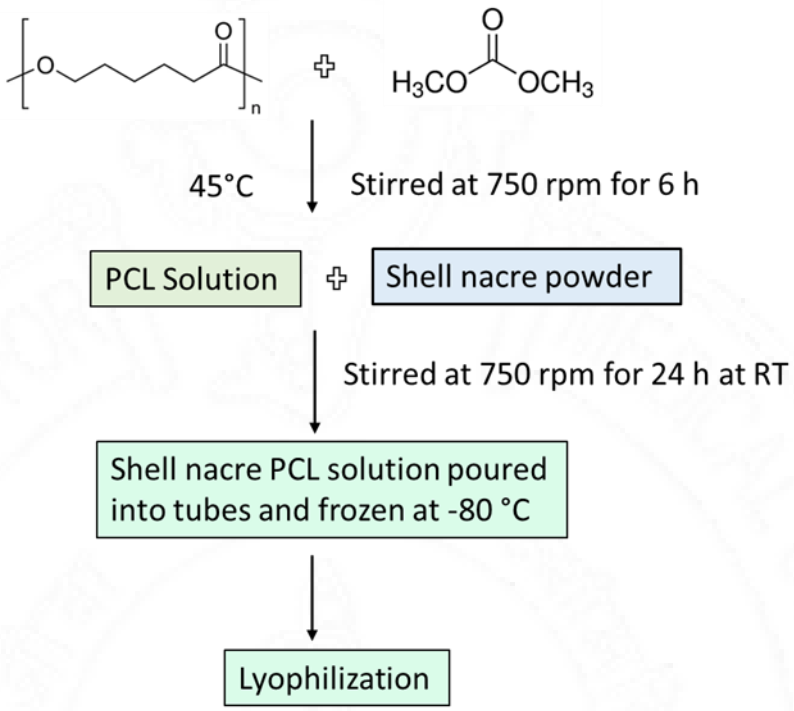

Figure 4.1 Steps in the fabrication of shell nacre PCL composite scaffolds

Shell nacre polycaprolactone (PCL) scaffolds were fabricated by the thermal induced phase separation method. PCL (average Mn-80,000, Merck, Germany) (12% w/v) was dissolved in dimethyl carbonate (DMC) (Spectrochem, India) for 6h at 45°C by magnetic stirring. Two sets of scaffolds were fabricated: One with lower concentrations of shell nacre powder (5%, 10%, 15% weight of PCL) and the other with high concentrations of shell nacre powder (50%, 100% and 150% weight of PCL) was fabricated. Shell nacre powder was added to the PCL solution and the mixture was stirred at 750 rpm for 24 h. Shell nacre PCL composite solutions were then poured into tubes and frozen at -80°C. After 24 h, the frozen solution was subjected to lyophilization for 16 h to obtain a porous scaffold.

Figure 4.1.1 Fabrication of shell nacre PCL composite scaffolds

4.1.2 Evaluation of compressive strength

Samples of size 6mm diameter and 12 mm height were prepared and the compressive modulus of the shell nacre PCL composite samples were evaluated using a universal testing machine (Instron, Model 1011, UK) with a crosshead speed of 5 mm/min respectively. Statistical analysis was done using GraphPad Prism Software. Ordinary one-way ANOVA was performed. * - $p < 0.05$, **** - $p < 0.0001$. Data is shown as mean and standard deviation of the mean (n= 3).

4.1.3 Characterization of scaffolds

4.1.3.1 SEM

The surface morphology of the scaffolds (PCL, SN-15 and SN-150) was studied by SEM imaging.

4.1.3.2 Micro-computed tomography

The scaffolds were scanned using a microCT desktop scanner (Scanco Medical AG, Switzerland) at 6 µm voxel resolution, using x-rays of energy 45 keV and intensity 177 mA (detector–charged couple device). The system-generated 2D slice images were then contoured and 3D images were reconstructed using in-built software. This facilitated the estimation of each scaffold's pore size and porosity (%). The porosity (%) was calculated using the formula (TV-BV)/TV *100 whereas the TV represents the total volume and BV represents the void (pores) volume.

4.1.3.3 FTIR analysis

FTIR analysis of the scaffolds (PCL, SN-15 and SN-150) were carried out using a Thermo Nicolet 5700 spectrometer in attenuated total reflection (ATR) mode in the range of 3500 to 600 cm^{-1} (resolution - 4 cm^{-1}).

4.1.3.4 TGA of scaffolds

TGA analysis of the scaffolds (PCL, SN-15 AND SN-150) was carried out using SDT Q600, TA instruments. The scaffolds were heated from RT to 750°C at a heating rate of 10°C/min.

4.1.3.5 PBS aging studies

Samples with a diameter of 6 mm diameter and 12 mm height were immersed in phosphate-buffered saline (PBS) for 0, 30, 60 and 150 days. Compressive modulus was evaluated on these specific time points following the procedure mentioned in section 4.1.2.

4.1.3.6 In vitro bioactivity studies

In vitro bioactivity was studied following the procedures based on ISO standard (ISO 23317, 2014). The scaffolds SN-15 and SN-150 were immersed in SBF for 0, 2, 7 and 14 days respectively. The scaffolds were observed using SEM (Hitachi model S2400) along with EDAX Genesis XM 4.

4.1.4 Cytotoxicity studies

4.1.4.1 Direct contact

Direct contact of the scaffolds (PCL, SN-15 AND SN-150) was studied based on ISO standard (ISO 10993-5, 2009) using human osteoblast (HOS) cell line following the procedure mentioned in 3.1.6.1.

4.1.4.2 MTT assay

MTT assay was performed (ISO 10993-5) at the end of the direct contact method to measure the metabolic activity of cells. After 24 h contact with HOS cell line, sterile samples (PCL, SN-15 and SN-150), positive control and negative controls were removed. The culture medium was replaced with 400 µl MTT solution (1mg/ml of serum-free DMEM media) wrapped with aluminum foil and incubated at 37±1°C.

During the incubation, metabolically active cells will produce mitochondrial reductase which reduced the yellow-colored tetrazolium salt 3-(4,5-Dimethyl thiazol-2-yl)-2,5-diphenyltetrazolium bromide (MTT) to purple-colored formazan crystal. After 2h, the MTT solution was removed and 800 µl of isopropanol was added and swayed the plates to dissolve the formazan crystals and the purple color developed was read at 570 nm using a spectrophotometer (Biotek, USA). The percentage metabolic activity of the cells was calculated using the formula: (OD test/OD cell control) *100.

4.1.5 Isolation and characterization of rat BM-MSC

The Institute Animal Ethics Committee (SCT/IAEC-387/November/2020/107) was obtained before experiments. Male Sprague Dawley rats of weight 140 –180 g was used for this experiment. Mesenchymal stem cells were isolated from bone marrow stroma of the femur. Rats were euthanized by CO_2 asphyxiation. Aseptically, the femur was cut at the epiphysis level using a sterile bone cutter. The bone marrow was flushed out from the femur using αMEM containing Penicillin-Streptomycin antibiotics. This was done by a syringe connected with a 20-gauge needle. The collected marrow was then pipetted several times to dislodge any clusters present. Subsequently, it was centrifuged at 600g for 10 min. The supernatant was decanted and the cell pellet was collected and suspended in fresh αMEM supplemented with 10% FBS and antibiotics. The resulting cell suspension was transferred to a T25 culture flask and incubated undisturbed for three days at 37°C with 5% CO_2. On the third day, the first medium change was performed and subsequent medium changes were carried out every three days. For subculturing, 0.25% Trypsin-0.02% EDTA solution was used to detach the cells. BM-MSC were then maintained in αMEM

supplemented with 10% FBS and antibiotics. BM-MSCs at the second or third passage were used for experiments.

4.1.5.1 Characterization of rat BM-MSC

According to international society for cellular therapy (ISCT) (Dominici et al., 2006), rat BM- MSCs were characterized for the mesenchymal stem cell marker (CD90 and CD105) and hematopoietic stem cell marker (CD34). BM-MSCs in passage 2 were used for characterization by flow cytometry and immunostaining.

4.1.5.2 Immunostaining

BM-MSCs were seeded on cover glasses measuring of 1x1 cm in size. The cells were then allowed to adhere and grow for 2 days until reaching confluency.

CD90: The confluent cells on the cover glasses were fixed in 80% cold methanol for 5 min. Then, washed thrice with PBS to remove methanol. Subsequently, the cells were permeabilised with 0.1% Triton X-100 in PBS for 5 min. BM-MSCs were rinsed thrice with PBS and then blocked with 1% BSA in PBS for 1h. After blocking, the cells were then incubated with Alexa Fluor 488 conjugated anti-mouse CD90 (Sigma) at 1:1000 dilution for 1h. After incubation, the antibody was removed and nucleus was counter stained with Hoechst 33258. Finally, the BM-MSCs were observed under an inverted fluorescence microscope (Leica DMI6000B, Germany).

CD105 and CD34: The confluent cells on the cover glasses were fixed with 4% paraformaldehyde (PFA) for 20 min for CD105 and CD34. The monolayer was washed thrice with PBS to remove the fixative. After permeabilization with 0.1% Triton X-100 in PBS for 5 min, cells were rinsed thrice with PBS. Then the BM-MSCs

were blocked with 1% BSA in PBS for 1h. Subsequently, the cells were then incubated separately with primary mouse anti-CD105 and anti-CD34 antibodies at 1:1000 dilution for 1h. Followed by the washes with PBS (3 times), Alexa Fluor 488 conjugated anti-mouse secondary antibody (1:100) was added and incubated for 1h. After incubation, the secondary antibody was removed and the nucleus was counter-stained with Hoechst 33258 for 1 min. The cells were observed under a fluorescence microscope.

4.1.5.3 Flow cytometry

The cell suspension of BM-MSC at passage 2 was used for flowcytometry analysis. For CD90 marker, BM-MSCs were fixed in 80% cold methanol for 5 min. For CD105 and CD34 marker, cells were fixed with 4% Paraformaldehyde (PFA) for 20 min. Then, washed thrice with PBS at 2000 rpm for 2 min to remove the fixatives. Cells were permeabilized by resuspending in 0.1% Triton X-100 for 5 min and again rinsed with PBS for three times. Subsequently, BM-MSCs were blocked with 1% BSA in PBS for 1h. After blocking, methanol fixed cells were incubated with anti-mouse CD90 conjugated with Alexa flour 488 at 1:1000 dilution for 1h. PFA fixed BM-MSCs were taken as two aliquots and incubated with the primary antibodies anti-CD105 and anti-CD34. Followed by PBS wash (thrice), BM-MSCs were incubated with anti-mouse secondary antibody conjugated with Alexa flour 488. The flow cytometric analysis was performed using flow cytometer (Cytoflex, USA). The cell data was collected by gating the dot plot obtained from forward and side scatter measurements and a minimum of 5000 events were acquired. The acquired data was then processed and analyzed using the software Cytoflex.

4.1.6 *In vitro* osteogenesis of the scaffolds

In vitro osteogenesis of the scaffolds SN-15 and SN-150 was studied using rat BM-MSC over a period of 7, 14 and 21 days. At passage 3, the BM-MSC monolayer was sub-cultured into 12, 24 and 6 well plate at a density of 3×10^4 cells per well. After 24 h of cell adherence to the plate surface, scaffolds SN-15, SN-150 and G-Bone were placed carefully over the cells. The negative control was cells cultured in αMEM with 10%FBS and 1% antibiotics. The positive control was the cells cultured in StemPro™ Osteogenesis Differentiation medium (Invitrogen). Media change was performed on every third day. The controls and the medium used were as follows

Tables 4.1 Samples, controls and the treatment medium used in *in vitro* osteogenesis study

S.No	Groups	Treatment medium
1.	Positive control (PC)	Stem Pro™ Osteogenesis Differentiation Medium
2.	Negative control (NC)	α-MEM Medium
3.	SN-15	α-MEM Medium
4.	SN-150	α-MEM Medium
5.	Clinical control GBone, Surgiwear	α-MEM Medium

4.1.6.1 Alkaline Phosphatase (ALP) assay

The ALP assay was carried out by fluorimetry method using the ALP assay kit (Abcam). The principle behind the assay is that ALP cleaves the phosphate group of a non-fluorescent substrate called 4-methylumbelliferyl phosphate disodium salt (MUP). This cleavage results in the production of a fluorescent signal with specific

excitation and emission wavelength (Ex/Em = 360nm/440nm) when the substrate is dephosphorylated.

At 7, 14 and 21 days, cells from tests and controls were rinsed with ice cold PBS. Subsequently, the cells were re-suspended in 100 µl of assay buffer provided in the kit. To ensure proper homogenization, the cells were quickly pipetted up and down for few times. Following this, the samples were centrifuged at 13000 g at 4ºC for 3 min to remove insoluble materials. The resulting supernatant was stored at -85ºC until further use. On the day of analysis, the reagents were freshly prepared and sequentially mixed within prelabelled wells of 96 well plates as follows.

Table 4.2 Reaction mix for ALP assay

Components	**Standard (**µl)	**Test (**µl)
Sample	-	110
MUP substrate 2 µl + assay buffer 18 µl	20	20
Incubate for 30 min		
Stop solution	20	20

Standard solutions were prepared by diluting a 50µM MUP standard to 0.1 to 0.5 nmol/well using assay buffer. All the reaction mixes were measured at an excitation /emission wavelength of 360/440nm using spectrofluorimeter (Biotek Synergy, USA).

4.1.6.2 Gene expression studies

RNA Isolation

On the day of 7, 14 and 21, the medium of the rat BM-MSCs treated with test samples and controls was removed. The cells were then rinsed once with ice cold PBS.

Cells were lysed by adding 1 ml of TRI reagent (Thermo Fisher Scientific) (1 ml /10 cm^2) and scraping with cell scraper. The lysate was kept at −85ºC until analysis. On the day of analysis, lysate was allowed to stand at room temperature for 5 min. Afterwards, it was subjected to centrifugation at 12,000 x g for 15 min at 4ºC. The process was repeated by adding 200 µl of chloroform to the supernatant and centrifuged at 12000 rpm for 5 min.

RNA was precipitated by adding 0.5 ml isopropyl alcohol per 1 ml of TRI reagent used and kept at room temperature for 10 min and then centrifuged at 12,000 g for 10 min at 4ºC. The supernatant was decanted and the RNA precipitate was washed with 75% ethanol, vortexed and then centrifuged at 7,500 g for 5 min at 4ºC and the washing step was repeated again. The ethanol was decanted and the RNA pellet was air dried for 5-10 min. The RNA was dissolved in diethyl pyrocarbonate (DEPC)-treated water and quantified using spectrophotometer (Biophotometer, Eppendorf, Germany).

cDNA synthesis

cDNA was synthesized using GoScript™ Reverse Transcription System (Promega) according to the manufacturer's protocol. The required quantity of RNA, Oligo DT Primer (0.5µg/reaction) - 1µl, and nuclease free water were combined to a final volume of 5µl. The reaction mix was then heated to 70°C in a preheated heat-block for 5 min and chilled on ice for 5 min. The tubes were subsequently centrifuged for 10 seconds in a micro centrifuge to collect the condensate and maintain the original volume. Tubes were kept at ice until the reverse transcription reaction mix was added. RT reaction mix was prepared according to table 4.3.

The RT reaction step included the following steps: annealing at 25°C for 5 min. extension at 42°C for 1 h and final inactivation at 70°C for 15 min. After inactivation, the reaction was held at 4ºC. The cDNA was amplified using GoTaq®qPCR kit (Promega). following the manufacturers protocol and the following primers (table 4.4) (Jia et al., 2019; Weng et al., 2019; Wu et al., 2016), components (Table 4.5) and conditions (Table 4.6) using Bio-Rad Q PCR.

Table 4.3 RT reaction mix

Components	Volume
GoScript™ 5X reaction buffer	4 µl
$MgCl_2$	4 µl
PCR Nucleotide Mix	2 µl
Recombinant RNasin®Ribonuclease inhibitor	1 µl
GoScript™ reverse transcriptase	1 µl
Nuclease free water	(to final vol of 15 µl)
RNA Primer mix	5 µl

The cycle threshold (ct) values of the gene of interest were normalized to the housekeeping gene, and the fold expression of the genes was calculated using the formula $2^{-\Delta\Delta Ct}$ where $\Delta\Delta CT = \Delta CT$ of the target gene of the test - ΔCT of the target gene of control (negative control). Hierarchical gene clustering was done by complete linkage (Spearman Correlation method) using cluster 3.0 and Java Tree view software

Table 4.4 List of primers

S.No.	Name	Primer Sequence	Primer length	T_m	Product size
1.	GAPDH- F	CCTGCACCACCAACTGCTTA	20	60.54	120

	GAPDH-R	GGCCATCCACAGTCTTCTGAG	21	60.41	
2	RUNX 2-F	AAGGTTGTAGCCCTCGGAGA	20	60.25	128
	RUNX2-R	TTGAACCTGGCCACTTGGTT	20	60.03	
3.	BMP-2 F	GAAGCCAGGTGTCTCCAAGAG	21	60.34	122
	BMP-2 R	GTGGATGTCCTTTTCCGTCGT	21	60.61	
4.	OCN F	GGTGCAGACCTAGCAGACACCA	22	64.21	173
	OCN R	AGGTAGCGCCGGAGTCTATTCA	22	62.98	
5.	COL-I F	GCCTCCCAGAACATCACCTA	20	58.80	82
	COL-I R	GCAGGGACTTCTTGAGGTTG	20	58.47	
6.	ALP-F	GGTTACTGCTGATCACTCCCA	21	59.44	112
	ALP-R	TGTGAAGGGCTTCTTGTCCG	20	60.25	

Table 4.5 Real time PCR components

S. No	Component	Volume
1	GoTaq®qPCR Master Mix, 2X	30 µl
2	Reverse primer	4.8 µl
3	Forward primer	4.8 µl
4	cDNA	3 µl
5	Nuclease free water	7.4 µl

Table 4.6 Real time PCR steps

Step	Cycles	Temperature	Time
GoTaq® Hot Start Polymerase activation	1	95°C	2 min
Denaturation	40	95°C	15 s
Annealing and extension		60°C	1 min

4.1.6.3 Immunostaining (ALP, OCN)

To perform immuno-staining of the cell monolayer at different time intervals after contact with test materials and controls for 7, 14 and 21 days the following steps were caried out: The monolayer was washed thrice with PBS to remove the media.

The cells were then fixed with 4% PFA for 20 min at room temperature. After fixation the cells were rinsed thrice with PBS. The cells were permeabilized with 0.1% triton X-100 for 5 min and then rinsed with PBS for three times. The cells were subsequently blocked with 1% BSA for 1h. The cells were then incubated with 1:1000 dilution of anti-mouse primary antibodies against ALP, and osteocalcin for 1h. After incubation, the primary antibodies were removed and cells were washed with PBS for three times. Then, treated with secondary antibody (anti-mouse Alexafluor 488) for 1h. After 1h secondary antibody was removed and washed with PBS. The nucleus was counter stained with Hoechst 33258. The cells were then viewed under inverted fluorescent microscope (Leica DMI 6000E) using filters for Alexa fluor 488 (I3) and Hoechst (A).

4.1.7 Statistics and spectrums

All statistical analysis were performed using GraphPad Prism software (version 9.5.1) (GraphPad, USA). All the spectrums were drawn using OriginPro software (OriginLab Corporation, USA).

4.2 RESULTS AND DISCUSSION

4.2.1 Fabrication of shell nacre PCL composite scaffold

The shell nacre PCL composite scaffolds were fabricated using the TIPS technique. DMC was selected as a solvent based on the freezing point 2-4°C and less toxicity (Cao et al., 2006). In this process, the PCL solution was prepared by heating the PCL-DMC mix at 45°C for 6 h. This step aimed to completely dissolve the PCL. Subsequently, the shell nacre powder was added to the PCL solution and stirred for 24 h at 37°C. This extended mixing was necessary to ensure the thorough mixing of shell

nacre powder within the PCL solution. Then, it was cooled below the freezing point of DMC which resulted in the phase separation of a polymer rich phase and a solvent rich phase. PCL rich phase solidified whereas the DMC rich phase crystallized. During the lyophilization process, the solvent crystals underwent sublimation, leaving behind a porous structure. Thus, the shell nacre PCL composite scaffolds with low and high concentration of shell nacre powder were fabricated.

4.2.2 Compressive modulus of shell nacre PCL composite scaffold

The compressive modulus of SN-15 was ~6 MPa (Figure 4.2) which was the highest among the scaffolds with a lower concentration of shell nacre powder. Furthermore, it was significantly higher than the PCL scaffold. In the higher concentration group, SN-150 exhibited compressive modulus of ~11 MPa (Figure 4.2). The compressive modulus of the scaffolds exhibited an upward trend with increasing concentration of shell nacre powder which is consistent with the previous findings involving the addition of HA in composite PCL scaffold fabricated by the TIPS method (Goonasekera et al., 2016; Sultana and Hayat Khan, 2013). It is known that mechanical property and porosity of the scaffolds exhibit an inverse relationship (Guarino et al., 2007). In other words, as the porosity of scaffold decreases, its mechanical properties tend to increase. In the present study, the observed increase in compressive modulus indirectly suggested a reduction in porosity of the scaffolds. Based on their respective compressive modulus values, SN-15 from the lower concentration group and SN-150 from the higher concentration group were chosen for further studies.

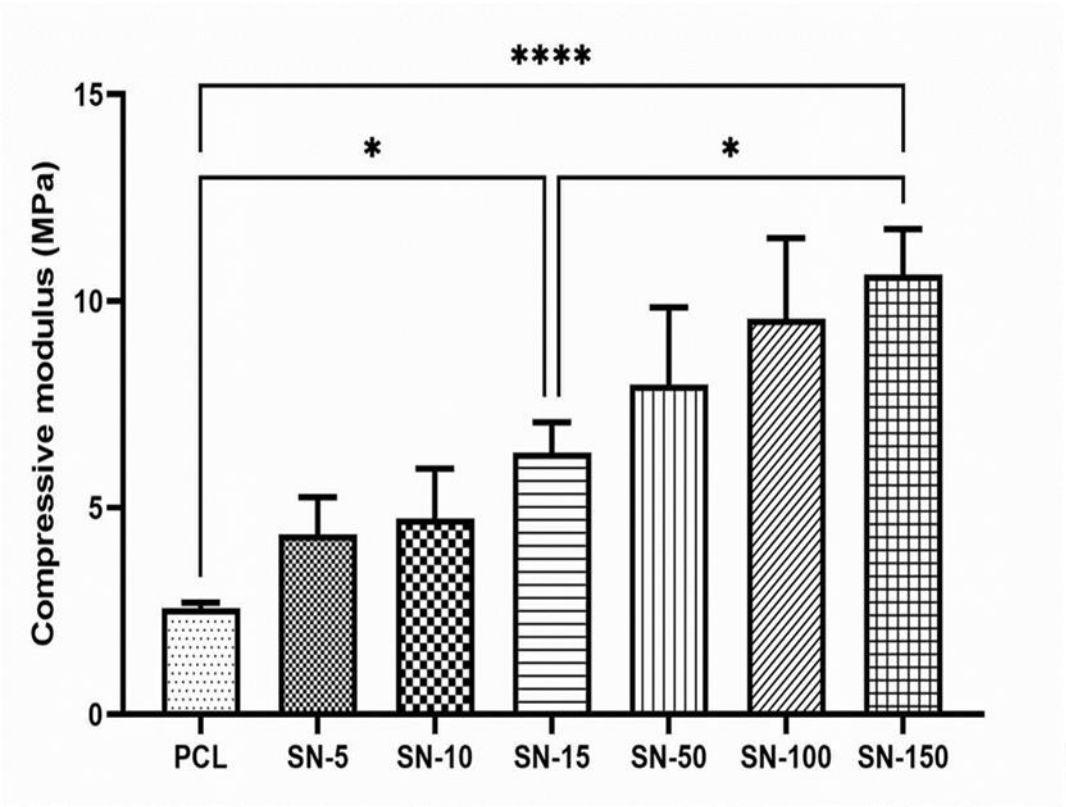

Figure 4.2 Compressive modulus of shell nacre PCL composite scaffold. Ordinary one-way ANOVA. * - $p < 0.05$, **** - $p < 0.0001$. Data is shown as mean and standard deviation of the mean (n= 3).

4.2.3 Characterization of scaffolds

4.2.3.1 SEM imaging

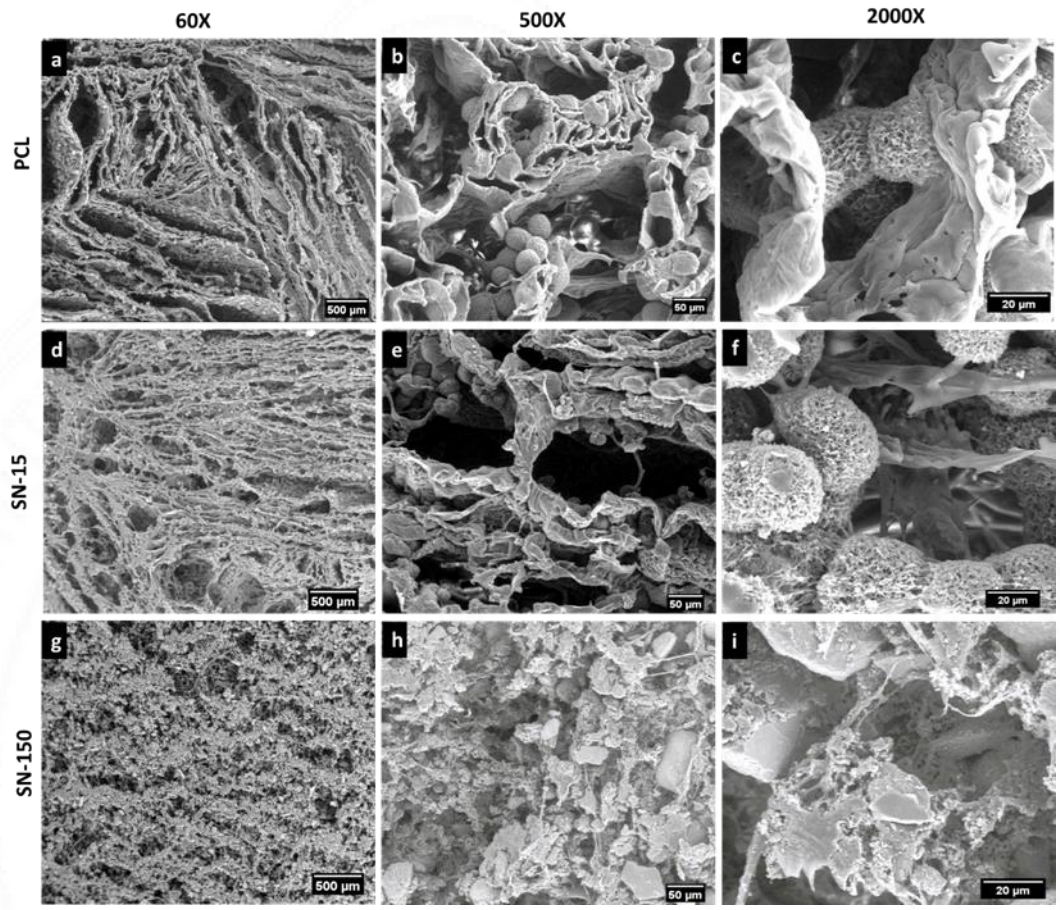

Figure 4.2.1 SEM images of the PCL (a-c), SN-15 (d-f), and SN-150 (g-i) scaffolds. Scale bar represents 500 µm in 60 X, 50 µm in 500 X, and 20 µm in 2000 X.

SEM images of the scaffolds (Figure 4.2.1) revealed an interconnected porous lamellar structure of PCL, SN-15 and SN-150 scaffolds with pore size of 150-200 µm. Microspheres of diameter 32 µm (Image J analysis) was observed in PCL scaffolds (Figure 4.2.1 a-c) and SN-15 scaffold (Figure 4.2.1 d-f). The SN-150 scaffold exhibited a random porous structure with no microspheres (Figure 4.2.1 g-i). SN-150 had 60 wt% of shell nacre powder and 40 wt% of PCL. Hence, the microspheres were not formed, due to the higher amount of shell nacre powder in SN-150. In the case of

SN-15, which contained 14 wt% shell nacre powder and 86 wt% PCL, this quantity of shell nacre powder did not interfere the microsphere formation. Furthermore, the microspheres were porous and interconnected which made them unique from other reported microspheres. Yao *et al.,* fabricated aggregated microporous microspheres (size 126 µm) containing PCL scaffolds with dioxane and water as solvent (Yao et al., 2020). Similarly, Wang's group fabricated PCL scaffolds with aggregated microspheres ranging in size from 170-816 µm using tetrahydrofuran as a solvent. They further concluded that the size of microsphere is depended on the solution temperature before freezing, with higher temperature above 37 °C resulting in large microspheres (Wang et al., 2013). In contrast, the microspheres were smaller in PCL and SN-15 scaffold when compared to the above discussed works. The microsphere formation is depended on the PCL concentration, solvent, freezing temperature and lyophilization.

4.2.3.2 MicroCT

The PCL scaffold exhibited a 90% porosity with a pore size ranging from 40-250 µm (Figure 4.2.2 a, b). On the other hand, SN-15 scaffold showed a porosity of 70%, accompanied by a pore size ranging from 30-150 µm (Figure 4.2.2 c, d). In contrast, SN-150 scaffold demonstrated a porosity (%) of 35% with pore size ranging from 10-200 µm as shown in figure 4.2.2 e and f. The porosity and the pore size reduced with an increasing concentration of shell nacre powder. The higher the addition of shell nacre powder, the lower the porosity and the inverse relationship between porosity and mechanical property is once again reflected here (Guarino et al., 2007).

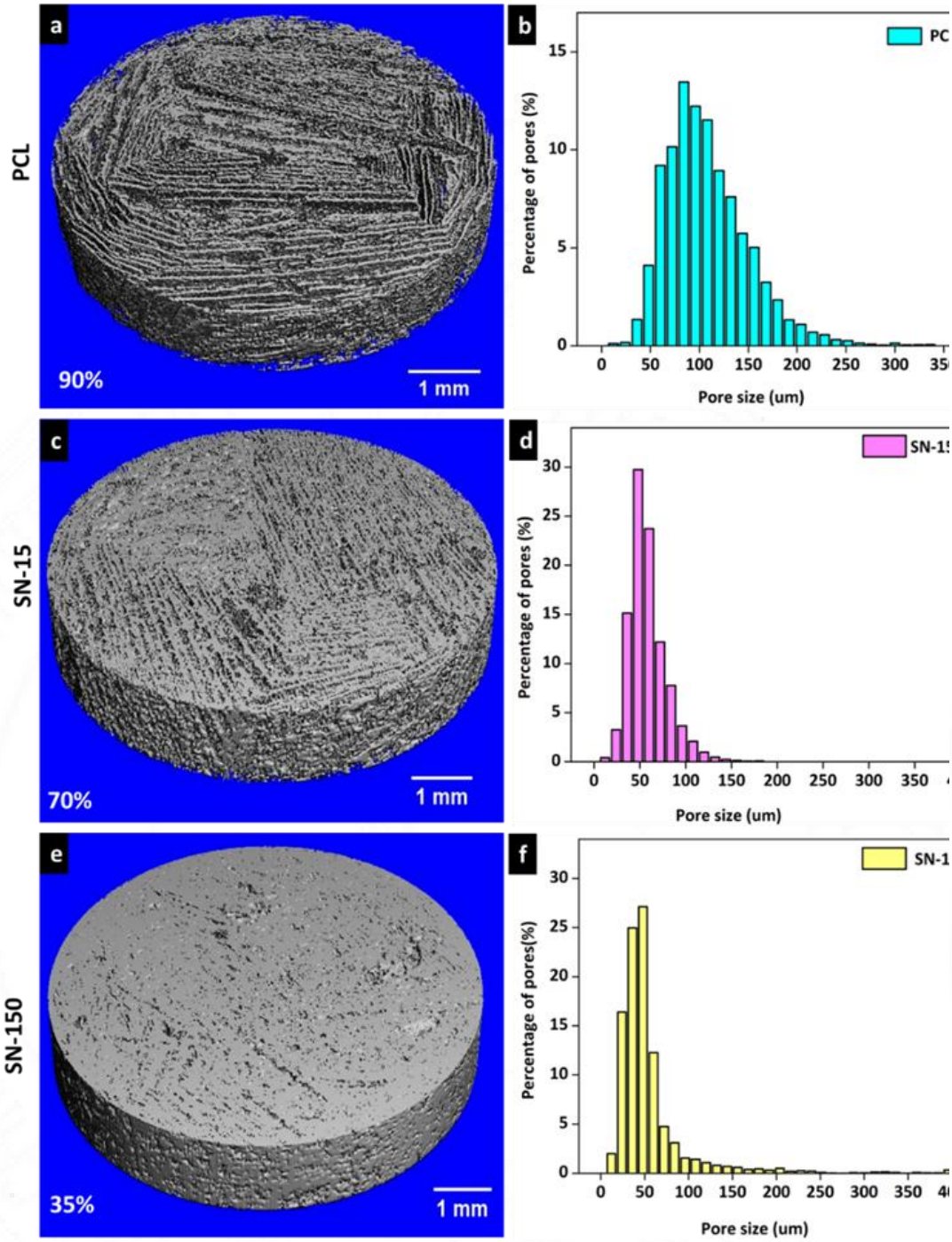

Figure 4.2.2 Micro CT images and pore size distribution of PCL, SN-15 and SN-150 scaffolds. Scale bar represents 1 mm.

4.2.3.3 FTIR analysis

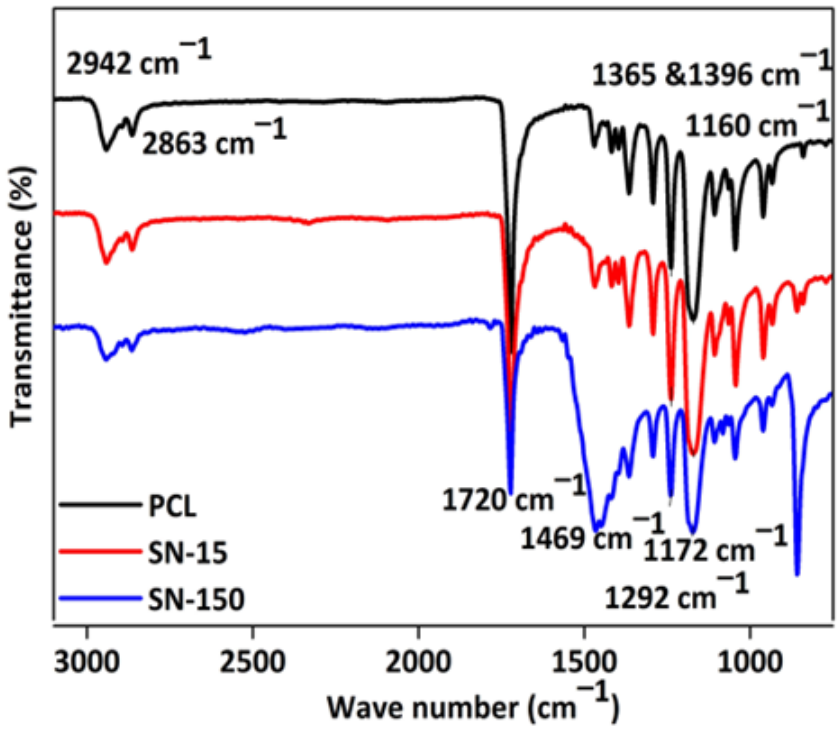

Figure 4.2.3 FTIR analysis of PCL, SN-15 and SN-150 scaffold

The FTIR spectrum of SN-15, SN-150 and PCL scaffolds is shown in the figure 4.2.3. The prominently seen peaks were 2942, 2863, 1720, 1469, 1396, and 1365 cm^{-1}. The peaks at 2942 & 2863 cm^{-1} were attributed to asymmetric and symmetric CH_2stretching vibration of PCL, respectively. The strong peak at 1720 cm^{-1} was assigned to the C=O stretching vibration of PCL. Similarly, the peaks at 1469, 1396, 1365 cm^{-1} were attributed to the CH_2bending vibrations, while the peaks at 1160 and 1292 cm^{-1} were assigned to C-O stretching and C-C stretching vibrations. All the scaffolds revealed the characteristic PCL peaks and similar peaks have been reported in previous studies (Abdelrazek et al., 2016; Elzein et al., 2004).

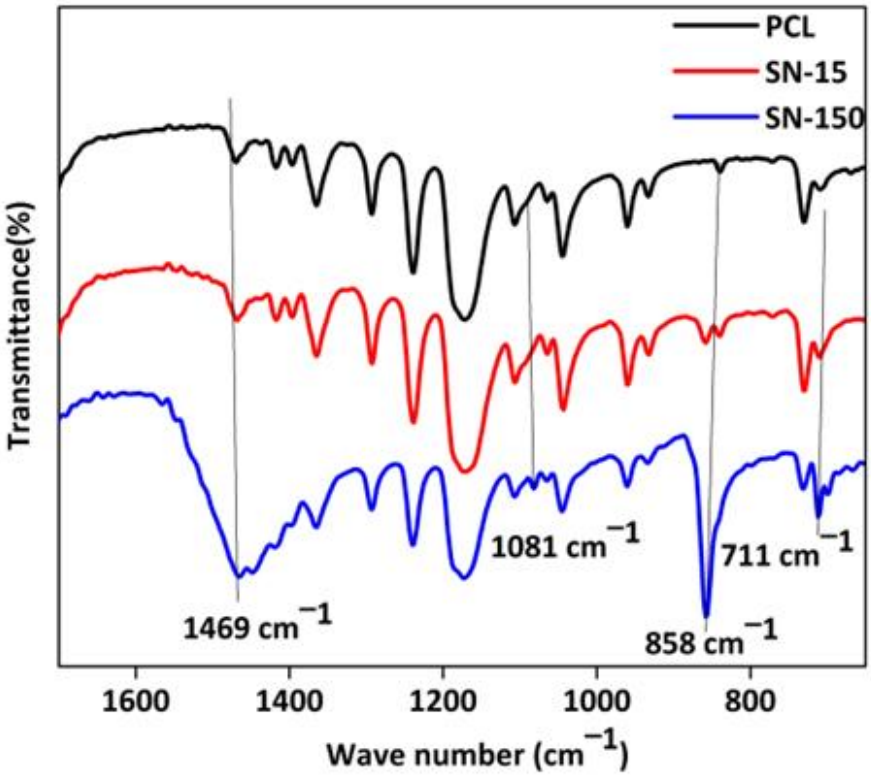

Figure 4.2.4 FTIR spectrum of the scaffolds from 1700-650 cm^{-1}

The peak at 1469 $cm^{-1}$was broadened and new peaks emerged at 1081, 858 & 711 cm^{-1} in SN-150 whereas only smaller shifts were observed in SN-15 (Figure 4.2.4). These peaks indicated the vibrations of carbonate ions of shell nacre and similar peaks have been documented in previous studies with shell nacre powder (Balmain et al., 1999). SN-150 contained high amount of shell nacre which exhibited clear peaks of shell nacre, while SN-15 contained 14 % shell nacre powder and showed only minor changes in the spectrum. Thus, the FTIR analysis confirmed the presence of both PCL and shell nacre peaks in SN-15 and SN-150 scaffolds.

4.2.3.4 Thermogravimetry (TGA) analysis

Thermogram of the PCL, SN-15 and SN-150 scaffolds is shown in figure 4.2.5. At 466° C, T_{100} was observed for PCL scaffold, T_{86} for SN-15 scaffold, and T_{36} for

SN-150 scaffold. PCL scaffold was completely degraded at 466°C whereas SN-15 and SN-150 scaffold underwent 86% and 36% degradation. SN-15 and SN-150 scaffold contained 86% and 40% PCL. The PCL present in all the three scaffolds were degraded at 466°C.

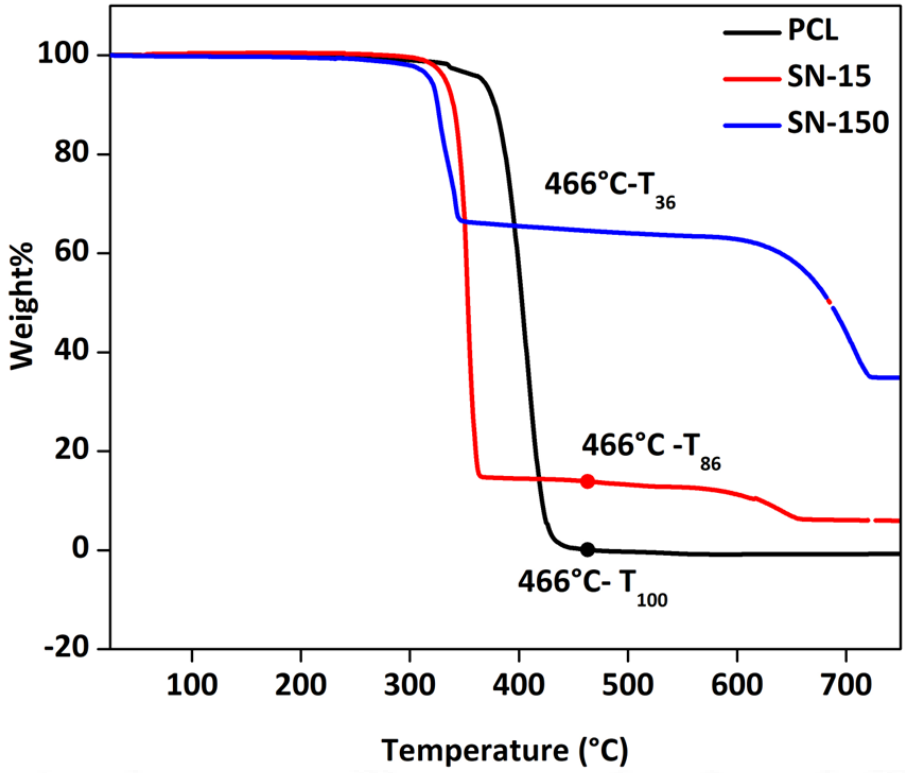

Figure 4.2.5 TGA analysis of the scaffolds from RT to 750°C

These results were in consistent with the previous studies with PCL composites of hydroxyapatite (HA) and lysine (Korbut et al., 2021) and PCL HA composites (Salerno and Domingo, 2015). Both SN-15 and SN-150 showed changes in the amount of left over residues which indicated the calcium oxide residue of shell nacre powder. The higher the amount of shell nacre powder, higher the thermal stability and residues left at 750°C. Previous TGA analysis of shell nacre powder alone, showed the presence of more than 45% calcium oxide residues (Balmain et al., 1999). Thus, the TGA

analysis confirmed the presence of shell nacre powder and the quantity of shell nacre powder added and estimated from the thermogram were nearly the same and in agreement.

4.2.3.5 PBS aging studies

The degradation of the scaffold can be indirectly understood with change in mechanical properties. The compressive modulus of the scaffolds were decreased by 0.75% for PCL, 16.5% for SN-15 and 50% for SN-150 scaffolds after 30 days in PBS. Additionally, after 60 days, the compressive modulus of the scaffolds was reduced by 5% for PCL, 42.8% for SN-15 and 55.9% for SN-150 scaffolds. Finally, a significant decrease in compressive modulus was observed after 150 days, with reductions of 30.8% for PCL, 51.2% for SN-15 and 75.8% for SN-150 scaffolds (Figure 4.2.6).

During PBS aging studies, the compressive modulus of all three scaffolds decreased over time. After 30 days, PCL scaffolds showed very slight reduction, SN-15 exhibited a moderate decline and SN-150 demonstrated a significant reduction of compressive modulus. The compressive modulus of all the scaffolds were further reduced after 60 days, with SN-15 experiencing a highest reduction, followed by SN-150 and PCL After 150 days, there was a substantial decrease in compressive modulus of all the scaffolds, with SN-150 showing the highest reduction followed by SN-15 and PCL. PCL scaffolds showed a slower degradation pattern, compared to SN-15 and SN-150, which degraded more rapidly. The results indicated that the higher the amount of shell nacre powder, greater the reduction in compressive strength. These findings were in consistent with the previous studies in which the addition of higher HA reduced the compressive strength of PCL/nHA composites after 16 weeks of PBS

aging (Díaz et al., 2014). In contrast, PCL/nHA/multi-walled nano carbon tube composites showed only 20% reduction after 8 weeks of PBS aging (Díaz et al., 2021).

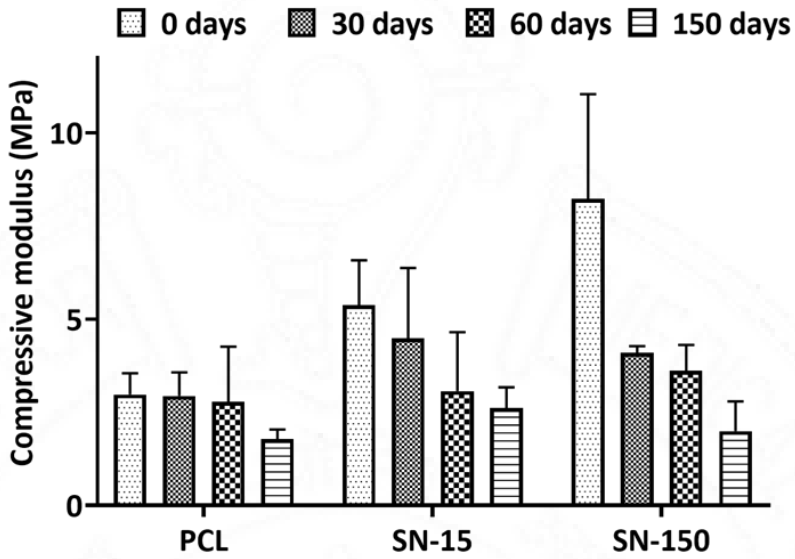

Figure 4.2.6 PBS ageing studies of the scaffolds for up to 150 days

4.2.3.6 In vitro bioactivity studies

Bioactivity refers to the ability of the material to bond with living bone, which is an essential feature for any bone substitute material. In order to study the bioactivity, the material is typically immersed in SBF, a solution with composition equivalent to that of human blood plasma. A bioactive material will utilize the calcium and phosphorus ions from the SBF and form the bone like apatite crystals on its surface which is further confirmed with SEM EDS, XRD *etc*. (Kokubo and Takadama, 2006). In the present work, *in vitro* bioactivity studies were carried out based on ISO 23317(ISO 23317, 2014). SN-15 scaffolds did not show any mineralization prior soaking in SBF (Figure 4.2.7 a). During 2 and 7 days of SBF treatment, SN-15 evidenced the presence of many globular accretions of apatite formation on the

scaffolds with calcium and phosphorus peaks (Figure 4.2.7 b, c). Further, these mineralized structures fused together to form large mineralized structures after 14 days with the proof of calcium and phosphorus peaks (Figure 4.2.7 d). Similarly, SN-150 scaffolds did not exhibit any signs of mineralization before soaking in SBF (Figure 4.2.8 a). Remarkable intense apatite mineralization was observed in SN-150 starting from day 2 with calcium and phosphorus peaks (Figure 4.2.8 b). Similarly, mineralization continued to be observed after 7 and 14 days in SBF (Figure 4.2.8 c, d). Overall, the results indicated both the SN-15 and SN-150 scaffolds demonstrated a rapid onset of apatite mineralization with calcium and phosphorus peaks after soaking in SBF.

Both SN-15 and SN-150 exhibited intense apatite mineralization from day 2 and this mineralization is appreciated and matched with apatite formation observed on silica and titania gel as reported in the leading opinion of Kokubo and Takadama (Kokubo and Takadama, 2006). Although both SN-15 and SN-150 showed dense mineralization, there was noticeable difference in the size of the globular accretions formed. The globular accretions seen on SN-15 was larger compared to those seen on SN-150 scaffolds. This difference in size may be attributed to the microsphere structure of SN-15 which have large surface area available for the apatite formation. This larger surface area facilitated the formation of larger mineralized structures. A similar observation was recorded during the bioactivity studies conducted with microsphere aggregated scaffolds (Yao et al., 2020).

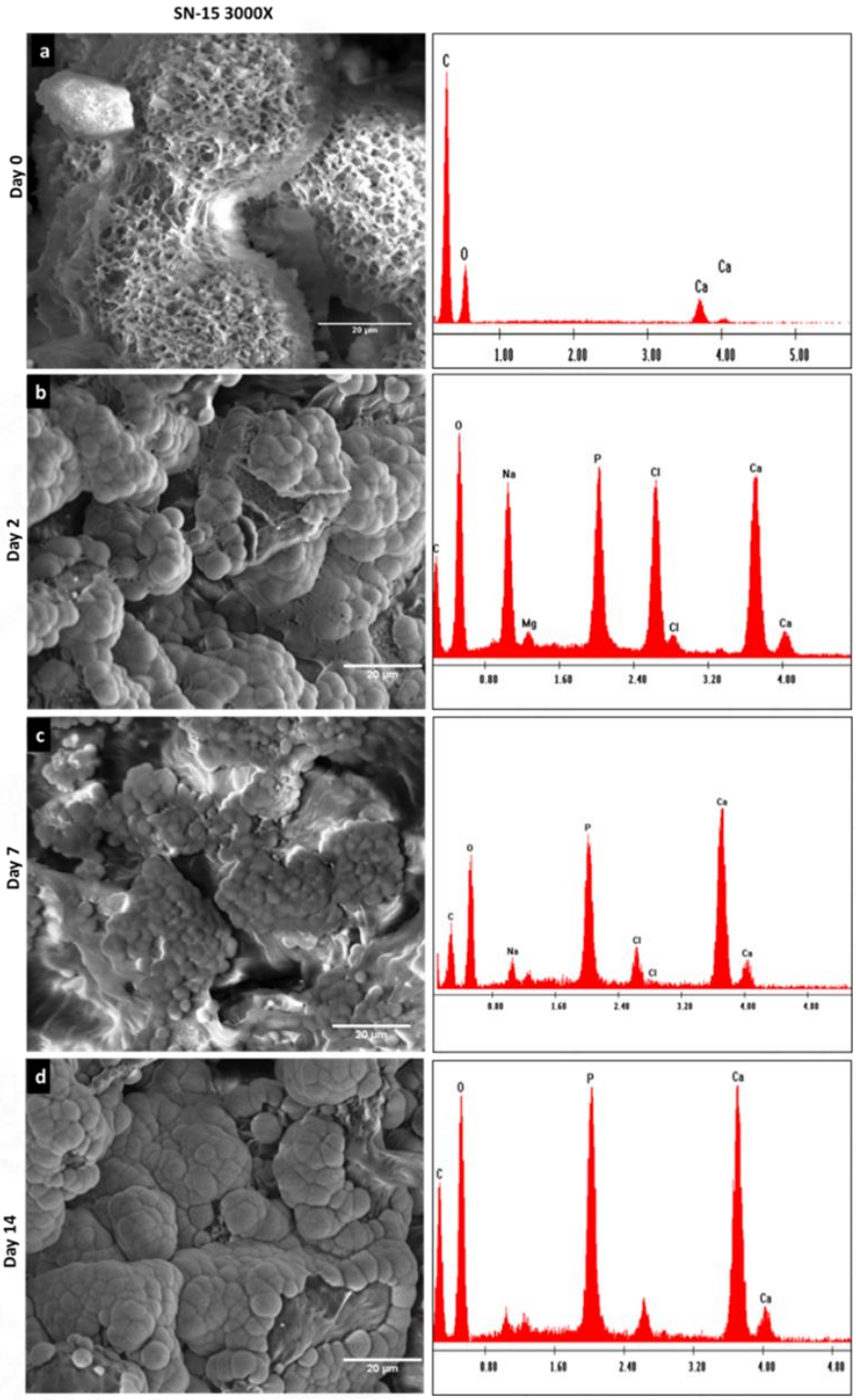

Figure 4.2.7 SEM EDS study of SN-15 scaffolds after SBF treatment for 0, 2, 7 and 14 days. Scale bar represents 20 µm.

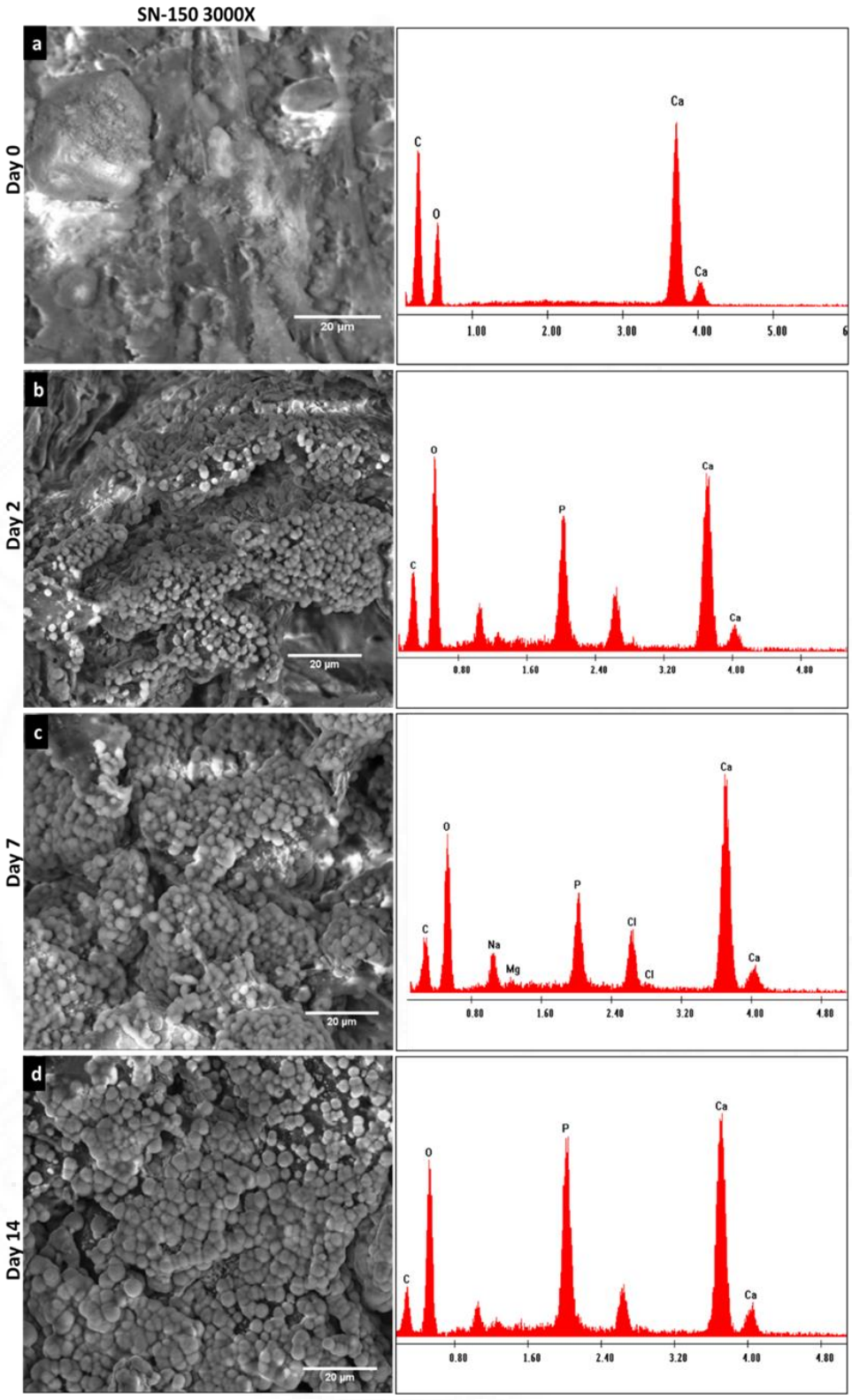

Figure 4.2.8 SEM EDS study of SN-150 scaffolds after SBF treatment for 0, 2, 7 and 14 days. Scale bar represents 20 µm.

4.2.3.7 Cytotoxicity studies

The cytotoxicity test conducted was direct contact with MTT assay according to ISO standard, which determined the eligibility of the material for biomedical applications (bone substitute). During the direct contact of PCL, SN-15 and SN-150 scaffolds with HOS cells, the cells were observed in close proximity with the samples and the cells retained the morphology with no signs of toxicity observed (Figure 4.2.9 c, d, e). Similarly, the negative control UHMWPE showed no features of cytotoxicity (Figure 4.2.9 b), whereas the positive control exhibited severe toxicity (Figure 4.2.9 a) as expected. These findings confirmed the non-cytotoxic nature of PCL, SN-15 and SN-150 scaffolds. Furthermore, during MTT assay all the samples PCL, SN-15 and SN-150 showed more than 90% cell viability (Figure 4.2.10). This again confirmed the non-cytotoxic nature of SN-15 and SN-150 samples. Although SN-150 contained high amount of shell nacre powder, SN-150 and SN-15 performed equivalent to that of PCL scaffolds.

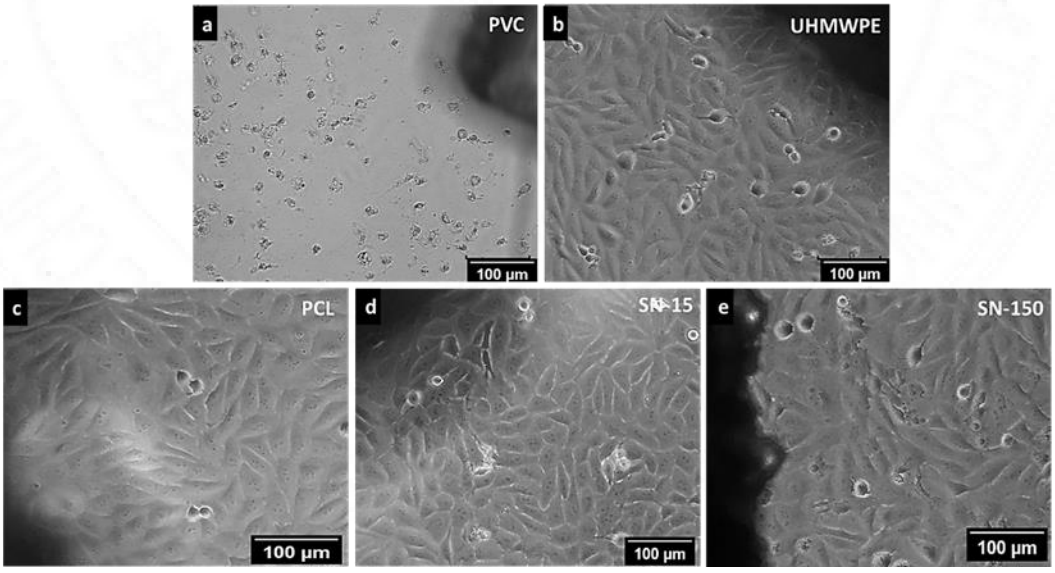

Figure 4.2.9 Direct contact of PCL, SN-15 and SN-150 scaffolds with HOS cell line for 24 h

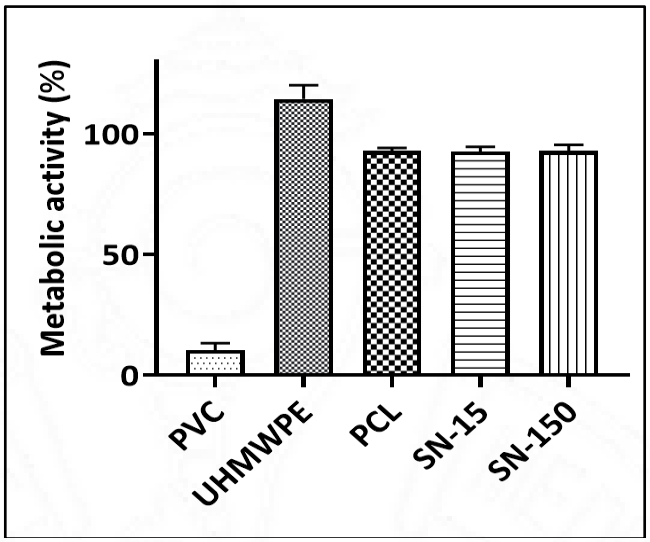

Figure 4.2.10 MTT assay after direct contact of stabilized PVC disc (PVC), UHMWPE, PCL, SN-15 and SN-150 scaffolds with HOS cell line for 24 h.

4.2.4 Characterization of rat BM-MSCs

Rat BM-MSCs were isolated and cultured which exhibited the typical spindle shaped morphology and plastic adherent. During the flow cytometry analysis of rat BM-MSCs at passage 2, showed more than 85% positivity for the mesenchymal stem cell marker CD90 and CD105 and only 11% positivity for the haematopoietic stem cell marker CD34 (Figure 4.2.11). Similarly, the immunostaining of rat BM-MSCs exhibited the expression of CD90 and CD105 (green colour) and no signal for CD34 (Figure 4.2.12).

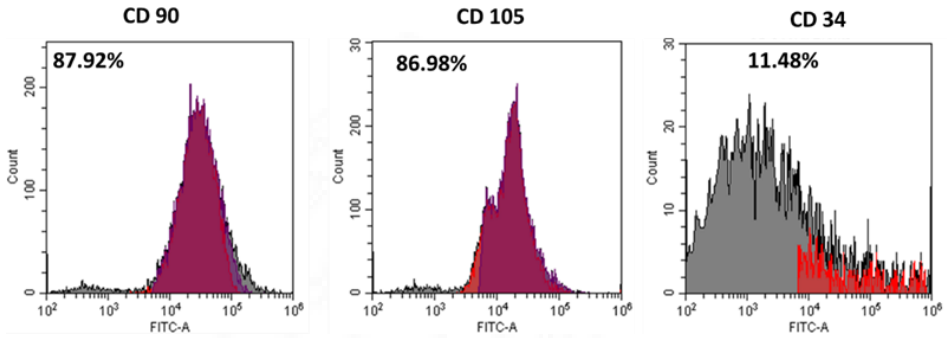

Figure 4.2.11 Flow cytometry analysis of rat BM-MSCs

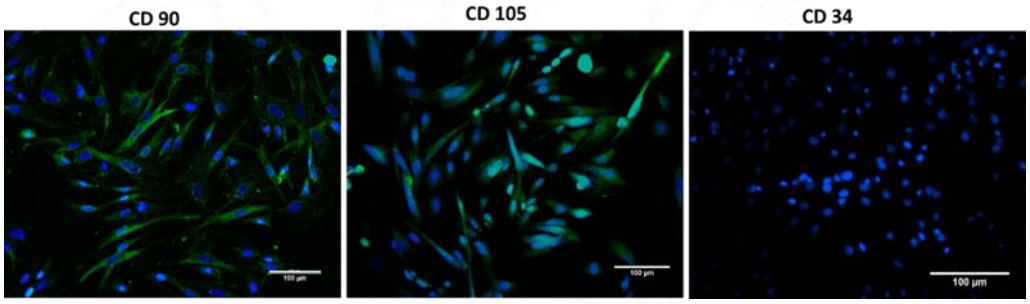

Figure 4.2.12 Immunostaining of rat BM-MSCs

4.2.5 *In vitro* osteogenesis of the scaffold

4.2.5.1 ALP assay

Alkaline phosphatase is a marker of osteoblast activity and confirms the differentiation of rat BM-MSC into osteoblast (Christenson, 1997; Sabokbar et al., 1994). In this study, ALP activity of rat BM-MSCs was studied after contact with SN-15, SN-150, G-Bone, positive control (osteo-differentiation medium) and negative control (α-MEM medium) over a period of 7, 14 and 21 days. The rat BM-MSCs in all the groups were cultured in α-MEM medium, except for the positive control group, which was cultured in an osteo-differentiation medium. During day 7 and day 14, SN-15, SN-150 and G-Bone showed similar ALP activity to that of positive control. Interestingly, SN-15 and SN-150 showed higher ALP activity than positive control

whereas G-Bone showed minimal activity that of negative control during day 21(Figure 4.2.13). These results confirmed that both SN-15 and SN-150 possessed the potential to enhance the differentiation of rat BM-MSCs into osteoblast. It is important to note that the higher the osteoblast typically correlates with increased osteoblast activity. Therefore, the ALP assay demonstrated the osteogenic potential of SN-15 and SN-150, which is equivalent to that of positive control and superior to that of the clinical control.

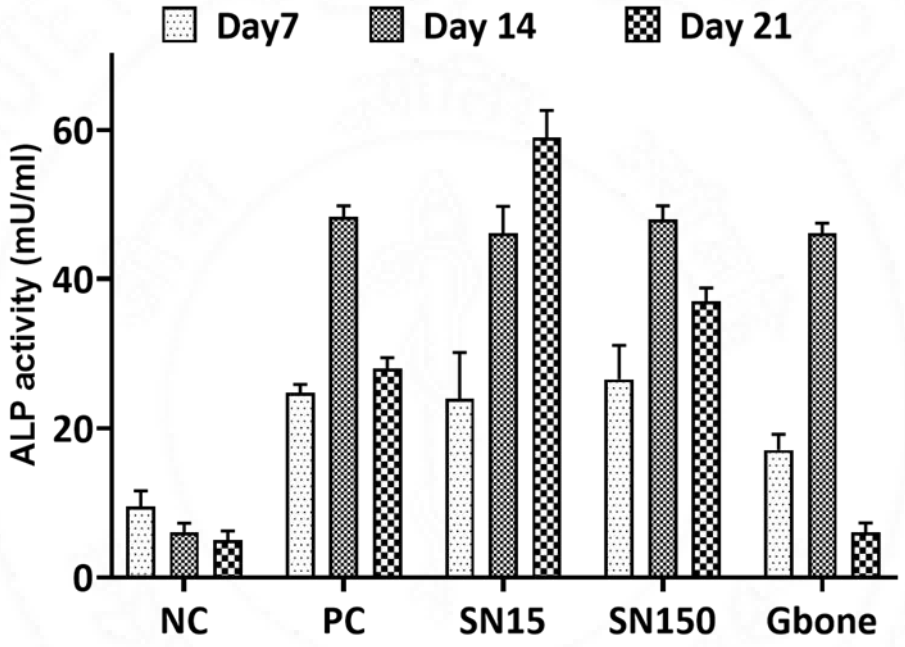

Figure 4.2.13 Alkaline Phosphatase activity of rat BM-MSCs for 7, 14 and 21 days. PC - positive control, NC - negative control cultured in normal medium. All values were normalized with volume of sample and time of incubation

4.2.5.2 Gene expression

The effect of SN-15, SN-150, G-Bone on the gene expression of rat BM-MSCs was studied over the period of 7, 14 and 21days. The fold expression was calculated by the ΔΔ CT method and the fold expression of the test was normalized with GAPDH

gene and target gene of the negative control. Hierarchical gene clustering was performed by complete linkage method using the similarity metric - Spearman rank correlation method. Three sample clusters and two gene clusters were seen. In the first gene cluster (shown in pink box), BMP-2 was the highly expressed gene, followed by RUNX-2. In the second gene cluster (shown in purple box), ALP was the highly expressed gene, followed by osteocalcin and collagen I.

The first sample cluster in yellow box included the SN-15, SN-150, G-Bone as well as PC of day 7 and day 21 all of which showed the expression of BMP-2. The middle sample cluster consisted of the day 14 samples of PC, SN-15 and SN-150 which all exhibited the expression of RUNX-2 except G Bone. The third sample cluster comprised the G Bone of day14 and day 21 samples of SN-15, SN-150 and G-Bone showing the expression of collagen I, ALP and Osteocalcin (Figure 4.2.14). Overall, Q PCR analysis confirmed the osteogenic potential of SN-15 and SN-150 with the expression of the regulators BMP-2, RUNX-2, osteoblast marker – ALP and the extracellular matrix proteins collagen I and osteocalcin.

BMP-2 plays a significant role in the commitment of mesenchymal stem cells to osteo-chondroprogenitor cells. Subsequently, the osteo-chondroprogenitor cells undergo commitment towards osteogenesis by the activation of RUNX-2. These committed osteoprogenitor cells then differentiate into pre-osteoblasts with the expression of collagen I, ALP and osteocalcin (Ponzetti and Rucci, 2021). In this work, both the SN-15 and SN-150 showed high expression of BMP-2, similar to that of G-Bone and PC on day 7. This indicated the commitment of the rat BM-MSCs of all the samples on day 7 towards the common osteo-chondroprogenitor cells. RUNX-2 is the

master controller of osteogenesis (Schroeder et al., 2005). Furthermore, the expression of RUNX-2 on day 14 cells of SN-15 and SN-150 confirmed the osteogenic potential, while G-Bone showed no expression of RUNX-2. ALP is a marker of osteoblast activity (Christenson, 1997; Siffert, 1951) and all the samples of SN-15, SN-150 and G-bone showed higher expression of ALP. This results further confirmed the osteogenic potential of SN-15 and SN-150. Additionally, the expression of extracellular matrix protein genes such as collagen I and osteocalcin further validated the inherent osteogenic potential of SN-15 and SN-150 without the need for osteo-differentiation medium.

4.2.5.3 Immunostaining

During the immunostaining of ALP, the PC, SN-15 and SN-150 groups showed high expression of ALP, while the G-Bone groups showed lower expression of ALP on day 14. No signal was detected in the negative control throughout the treatment period (Figure 4.2.15). Further, the immunostaining of osteocalcin, PC showed signal for osteocalcin on both day 14 and 21 whereas the negative control did not show any signal throughout the treatment period. SN-150 and G-Bone showed maximum expression of osteocalcin on day 14, which continued up to day 21. However, SN-15 showed expression of osteocalcin specifically on day 21 (Figure 4.2.16). Thus, the immunostaining of ALP and osteocalcin, confirmed the osteogenic potential of SN-15 and SN-150. Overall, ALP assay, q-PCR and immunostaining proved the osteogenic potential of SN-15 and SN-150, which performed on par with PC and superior than the clinical control G-Bone.

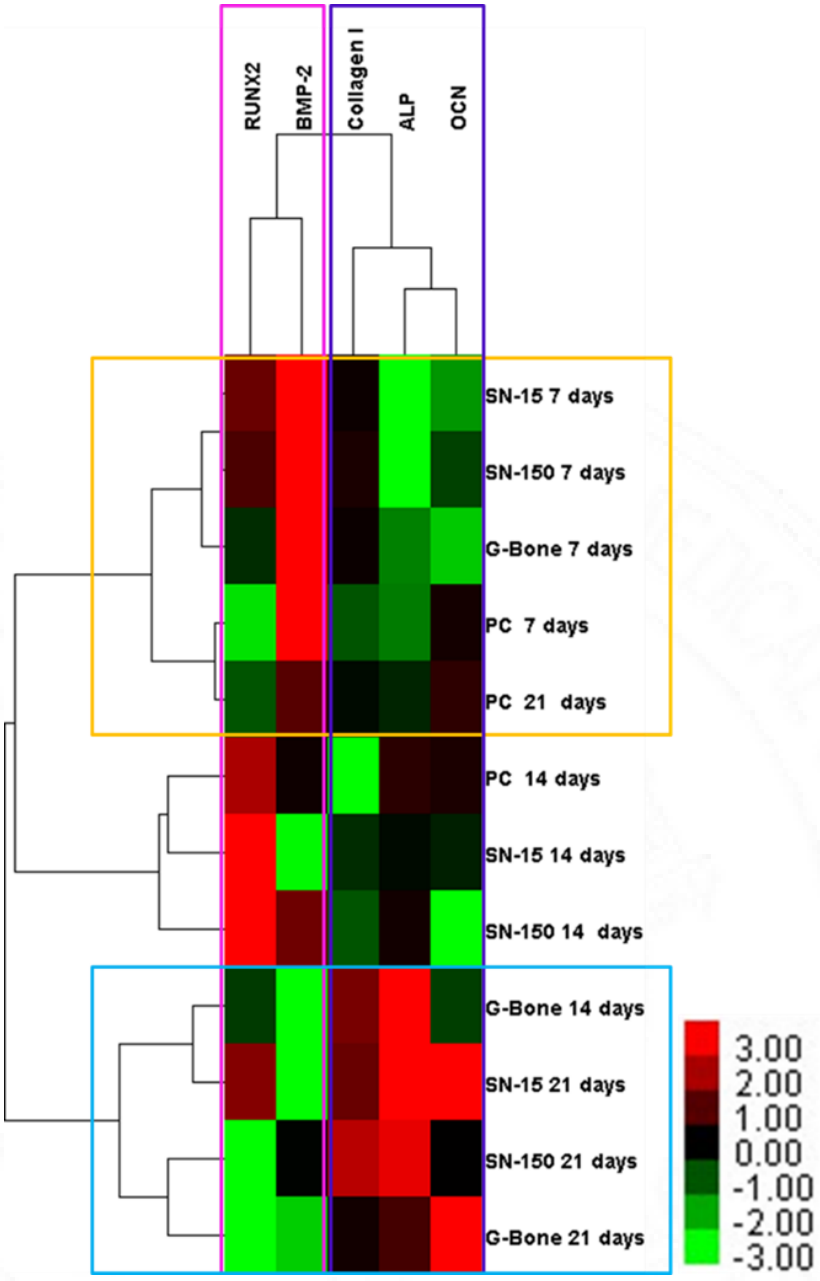

Figure 4.2.14 Hierarchical gene clustering by complete linkage (Spearman rank correlation method). Each columns represents gene and the gene names are shown on the top. Each row represents samples and sample names are shown on the right side. The gene expression levels are represented by colour scale, ranging from red for the highest and green for the lowest expression. Data shown as heat map with average value (n=2) of fold expression

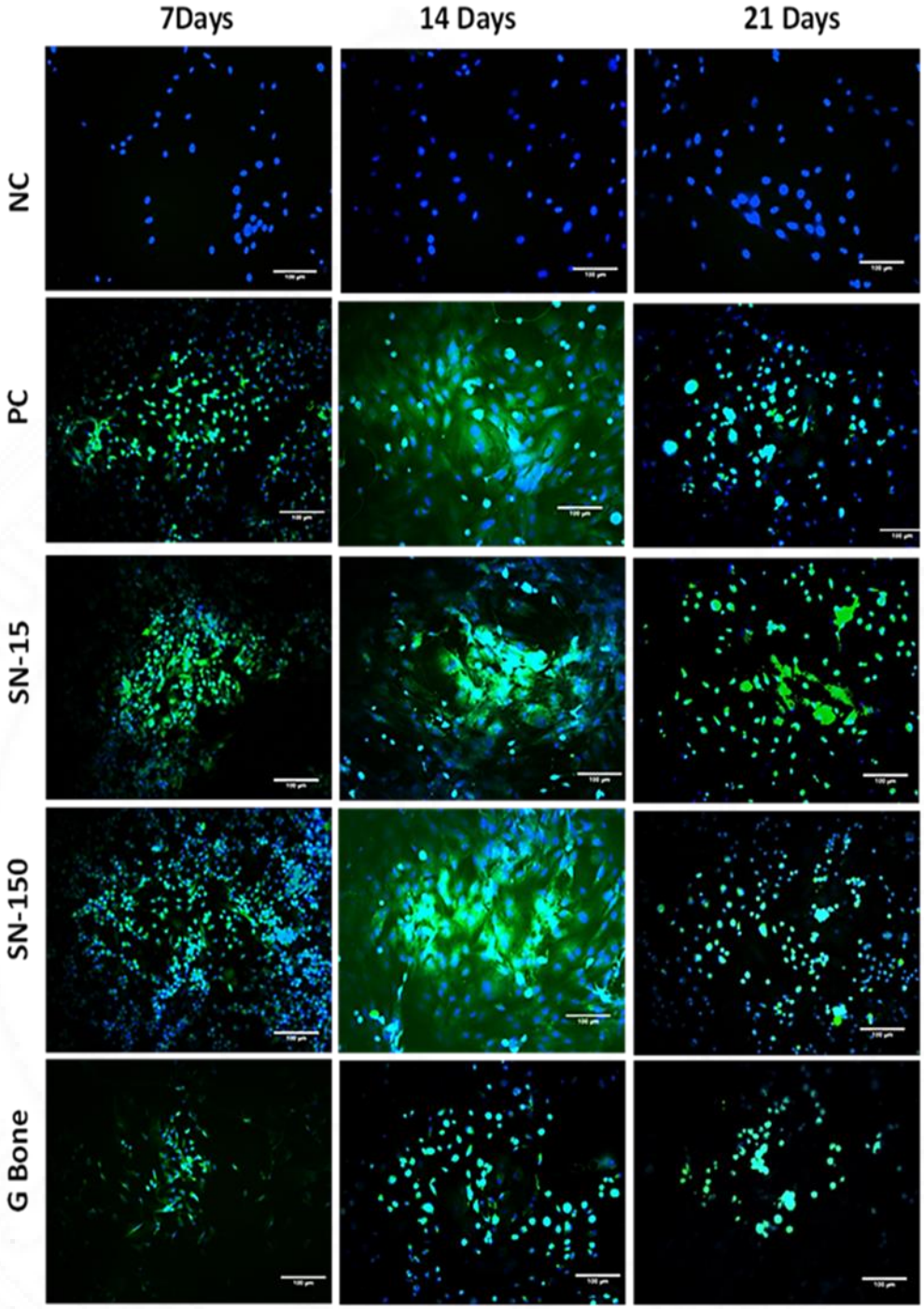

Figure 4.2.15 Fluorescent microscopy images of rat BM-MSCs (after contact with SN-15, SN-150, G-Bone, NC, and PC for 7,14, and 21 days) stained with ALP antibody followed by anti-mouse secondary antibody with Alexa fluor 488(green). The nucleus was stained with Hoechst (blue). The scale bar represents 100 µm.

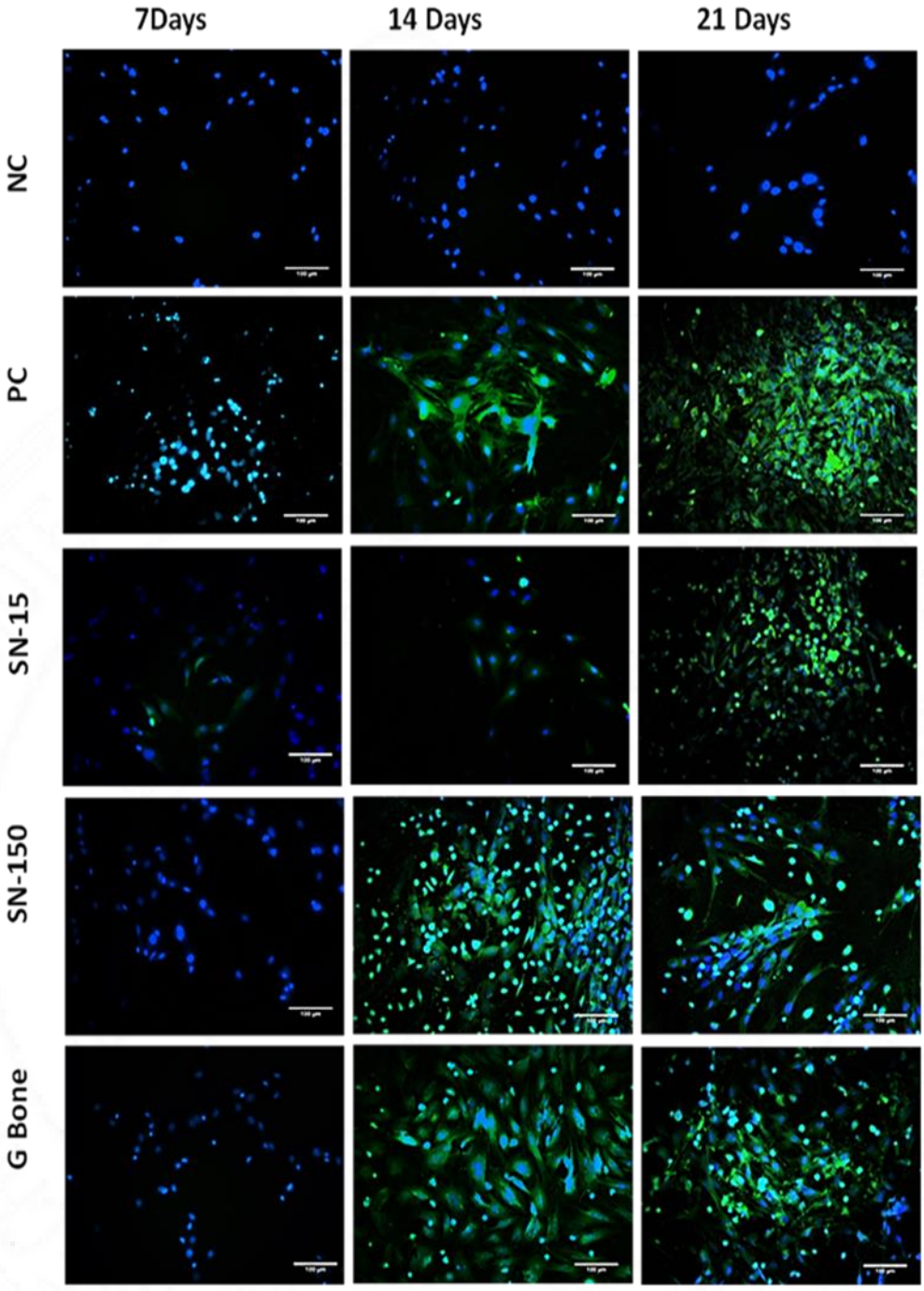

Figure 4.2.16 Fluorescent microscopy images of rat BM-MSCs (after contact with SN-15, SN-150, G-Bone, NC, and PC for 7,14, and 21 days) stained with osteocalcin antibody followed by anti-mouse secondary antibody with Alexa fluor 488(green). The nucleus w stained with Hoechst (blue). The scale bar represents 100 µm.

Thus, the shell nacre powder, processed from the shells of pearl oysters was impregnated into the polymer matrix of polycaprolactone. Highly porous microsphere

structured scaffold and randomly aligned less porous scaffolds were fabricated by TIPS method using a green solvent dimethyl carbonate. The porosity and structure of the scaffold were depended upon the quantity of shell nacre and the polymer, which were further influenced by the solvent used. Both SN-15 and SN-150 scaffolds exhibited non-cytotoxicity, bioactivity and osteogenic potential. These composite scaffolds will be a promising candidate for bone defect management.

DEVELOPMENT AND CHARACTERIZATION OF SHELL NACRE CEMENT: PART I

5 SYNTHESIS AND CHARACTERIZATION OF SHELL NACRE CONTAINING LADDER STRUCTURED SILOXANE METHACRYLATE RESIN

Organic monomers like methyl methacrylate, bisphenol A glycidyl methacrylate, and triethylene glycol dimethacrylate have been traditionally used in the composition of bone cement to improve mechanical and handling properties. However, the use of these monomers has been associated with cytotoxicity, volumetric shrinkage, and exotherm generation, which have limited the success of the cement. This insisted on the need for an alternative resin matrix with low polymerization shrinkage, non-cytotoxicity, and minimal exotherm generation. This chapter covers the materials and methods, results, and discussion related to the sub-objectives of main objective 3, “Synthesis and characterization of shell nacre containing ladder-structured siloxane methacrylate resin”.

5.1 MATERIALS AND METHODS

5.1.1 Synthesis of ladder-structured siloxane methacrylate (LSM) and shell nacre containing ladder-structured siloxane methacrylate (SNLSM) resins

Figure 5.1 Experimental setup for ormocer resin synthesis

The first step in the synthesis was hydrolysis of the precursor 3-trimethoxysilyl propyl methacrylate (Sigma Aldrich) with deionized water in a ratio of 1:3. After 30 mins of hydrolysis, 6N NaOH, and diethyl ether were added and the reaction was continued for 8 h to synthesize LSM resin. The same procedure was followed for the synthesis of SNLSMs. After hydrolysis, 6N NaOH, shell nacre powder (1%,2%, 5%, and 10%), and diethyl ether were added and the reaction was continued for 8 h to

synthesize SNLSM1, SNLSM2, SNLSM5, and SNLSM10 resin. Later the reaction mix was washed and separated with distilled water and diethyl ether to remove the alkali. Then, the ether phase containing the resin was collected, evaporated, and dried at 37°C till the complete removal of water.

5.1.2 Characterization of resins

5.1.2.1 Refractive Index (RI)

The refractive index of the resins was measured using an Abbey refractometer. A drop of the resin was placed onto the sample holder and fixed to the centre of the main prism so that the drop of the sample spread into a thin film. Upon illumination and viewing through the eyepiece, the colour compensate knob was turned to get a boundary line between the upper red and lower blue regions. The boundary line was then aligned with the intersection of the crossed line in the refraction field of vision and the scale reading was noted as the refractive index of the resin at room temperature.

5.1.2.2 Fourier Transform infrared spectroscopy (FTIR)

FTIR spectrums of the resins were recorded using the FTIR Carry 600 (Agilent Technologies), The thin layer of resin was applied and the spectrum was recorded from 400 to 4000 cm^{-1} at a resolution of 4 cm^{-1}.

5.1.2.3 Micro-Raman analysis

A thick layer of resin was applied on a glass slide and the Raman spectrum was recorded using confocal Raman microscopy (alpha 300RA, Witec, Germany) with a 532 nm laser.

5.1.2.4 Thermogravimetry analysis

Thermal stability of the resins was evaluated by heating from room temperature to 1000°C based on ASTME-1131-98 by using SDT-2960, TA Instruments. The heating rate used was 10°C/min, in a nitrogen atmosphere.

5.1.2.5 Differential scanning calorimetry

Based on ASTM standard D3418-15, glass transition temperature (Tg) and melting temperature T_m of the resins were measured from -90°C to 100°C at a ramp rate of 10°C/min, in a nitrogen atmosphere.

5.1.2.6 Transmission electron microscope (TEM) imaging

The LSM and SNLSM2 resin (in methanol) was drop-casted onto formvar coated 200 mesh copper grids (EM sciences, USA), and allowed to dry overnight. The grid was then observed in TEM (Hitachi H-7650 Tokyo, Japan) at an accelerated voltage of 80kV.

5.1.2.7 Nuclear Magnetic Resonance Spectroscopy (NMR)

Resins (LSM and SNLSM2) were dissolved in dimethyl sulphoxide. ^{13}C spectrum of the resins was recorded with a Bruker AMX 500 spectrometer. Chemical shifts were expressed in parts per million.

5.1.2.8 Viscosity of SNLSM2

The viscosity of SNLSM2 was measured using a modular compact rheometer (MCR 302, Anton Parr) by the parallel plate method with a 25 mm diameter plate and

a 1 mm measurement gap. A temperature sweep was carried out from 20°C to 45°C to analyze the viscosity changes. Additionally, the change in viscosity was studied at a constant temperature of 25°C and a shear rate of 1/s.

5.1.3 Spectrums

All the spectrums were drawn using OriginPro software (OriginLab Corporation, USA) and chemical structures were drawn using ChemDraw (Perkin Elmer).

5.2 RESULTS AND DISCUSSIONS

5.2.1 Synthesis of resins

All the ormocer resins were synthesized using the precursor 3-TMSPM at room temperature, following the alkali mediated modified sol gel method. During the hydrolysis step, the precursor was partially hydrolyzed by the replacement of methoxy group of silicon atoms of 3-TMSPM with –OH groups. Subsequently, the alkali catalyst NaOH was added, which further promoted the hydrolysis of partially hydrolyzed precursors and induced the polycondensation process (Artaki et al., 1985a). During the process of polycondensation, followed by the deprotonation of -OH groups, the precursors underwent polycondensation and an intense Si-O-Si siloxane network was formed. The siloxane network can be tailored as cage, random or ladder structure, which is depended on the catalyst used. Alkali catalyst promote the formation of ladder structured siloxane network (Dirè et al., 2018; Jena et al., 2018). In an organic silica network, being a tetravalent silicon act as a network builder, it can promote the growth of network. In contrast, calcium is a divalent, which cannot form

networks. Hence, the addition of shell nacre modified the siloxane network and prevent the growth of the siloxane network. After 8 h of reaction, the alkali catalyst was removed by multiple washing and separation with water and ether. Finally, the ether based organic phase was collected, which was then evaporated at fume hood and then kept at 37°C. Finally, a transparent glass like resin was synthesized.

5.2.2 Characterization of resins

5.2.2.1 Refractive index

Table 5.1 Refractive index of the resin

S.No	Name	RI
1.	LSM	1.4794
2.	SNLSM1	1.4812
3.	SNLSM2	1.4808
4.	SNLSM5	1.4796
5.	SNLSM10	1.481

All the resins exhibited transparency and the refractive index of all the resin was found to be almost similar to that of the control resin LSM. The synthesized resins SNLSMs showed no change in refractive index ~1.47 after the addition of shell nacre powder and similar RI were recorded for the ormo-resins (Lizymol, 2004b), zirconium containing resin (Vibha and Lizymol, 2019) and strontium containing resin (Vibha and Lizymol, 2017)

5.2.2.2 FTIR analysis

The molecular architecture of the siloxane is identified by FTIR analysis, which reveals distinct peaks in the 1000–1200 cm^{-1} region. A random structure is

characterized by multiple peaks, cage structure by a single sharp peak and a ladder structure by bimodal peaks (Brown, 1963). FTIR analysis (Figure 5.2.1 and 5.2.2) of all the resins proved the presence of bimodal peaks at 1101 cm^{-1} and 1033 cm^{-1} and confirmed the polycondensation and formation of ladder structured inorganic siloxane backbone. It was reported that alkali catalyst favoured the formation of ladder structured siloxane and the results were in agreement with the previous studies (Bridget Jeyatha et al., 2022; Dirè et al., 2018; Kim et al., 2018a). A shift in the peak from 980 to 987 cm^{-1} in all the resins confirmed the presence of Si-O-Ca in the network. Further, the presence of Ca-O (Figure 5.2.2) in the siloxane network of all the resins, except LSM was evidenced by a band at 862 cm^{-1} and the findings were consistent with the previous studies (Owens et al., 2016). All the resins retained the characteristic acrylate groups C=C at 1637 cm^{-1} and C=O at 1716 cm^{-1}. Thus, the FTIR analysis confirmed the presence of shell nacre integrated ladder structured siloxane skeleton with methacrylate side-chain.

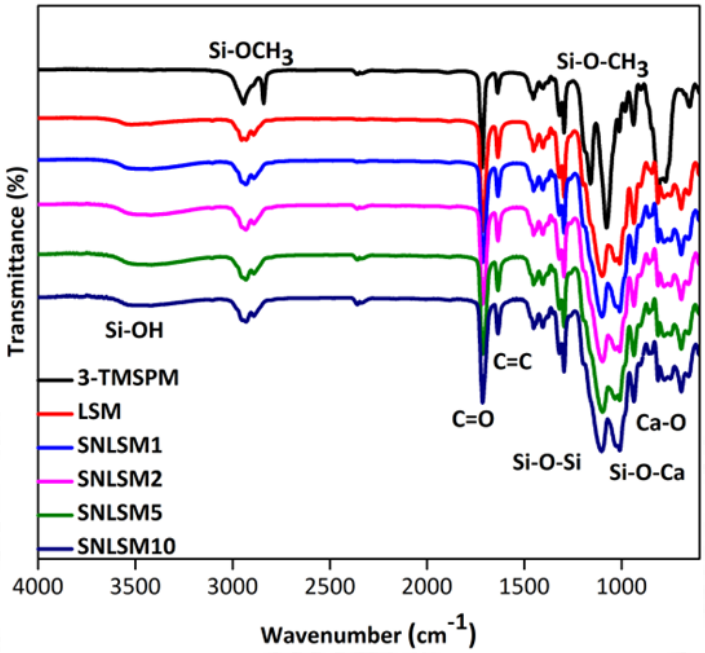

Figure 5.2.1 FTIR analysis of resins

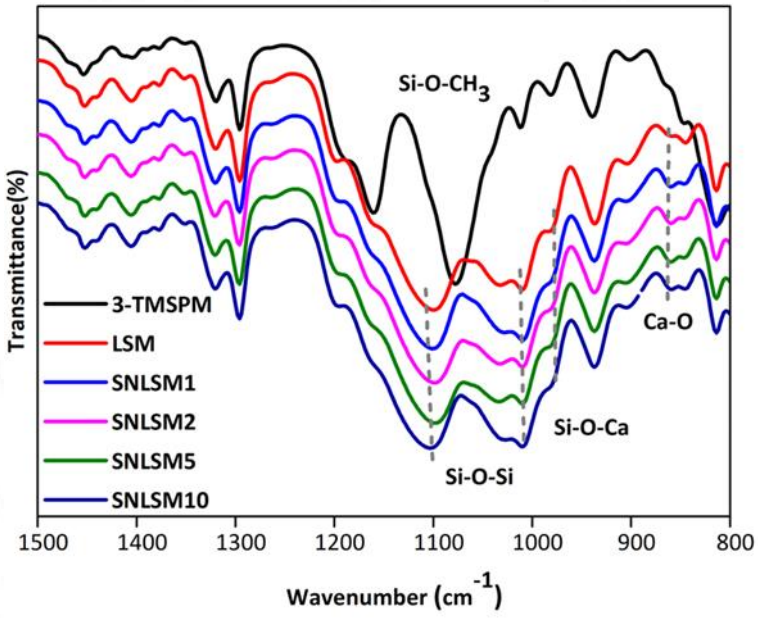

Figure 5.2.2 FTIR spectrum of resins from 800 to 1500 cm^{-1}

5.2.2.3 Micro-Raman analysis

Raman analysis of the resins as shown in Figure 5.2.3 proved that the siloxane unit was four membered, which was confirmed by the presence of peak at 598 cm^{-1}

and similar results were documented in a previous study (Baatti et al., 2017). Additionally, a broad shoulder observed at 440 cm^{-1} indicated the symmetric bending vibrations of the Si-O-Si linkage with oxygen motion perpendicular to the Si-Si line. Further, the siloxane network formation was understood by a peak around 829 cm^{-1} as reported by the Artaki group (Artaki et al., 1985b). Again, the integration of shell nacre was confirmed by the shift in siloxane peaks at 598 cm^{-1},846 cm^{-1},900 cm^{-1},975 cm^{-1} and 1008 cm^{-1} in all the resins except for LSM and these findings were consistent with the previous research (Kalampounias, 2011).

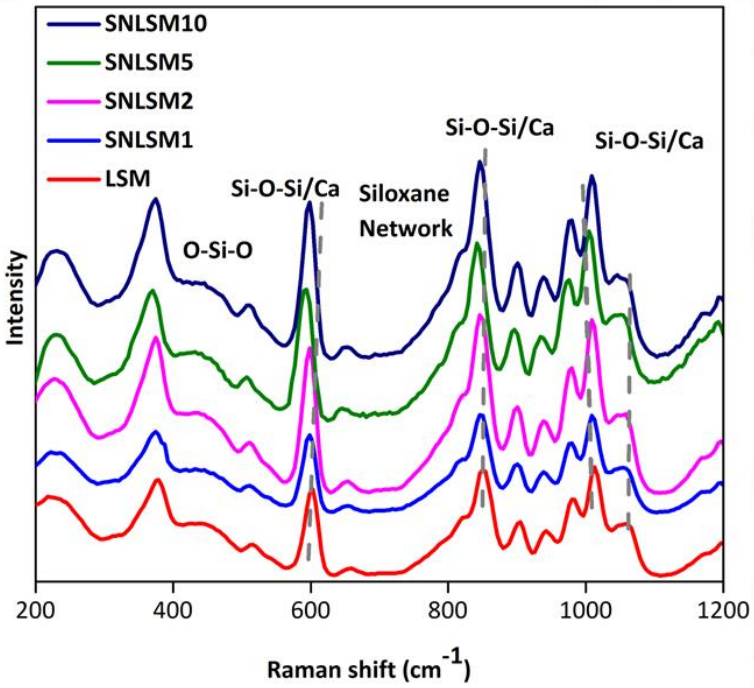

Figure 5.2.3 Raman spectrum of resins

5.2.2.4 Thermogravimetric analysis

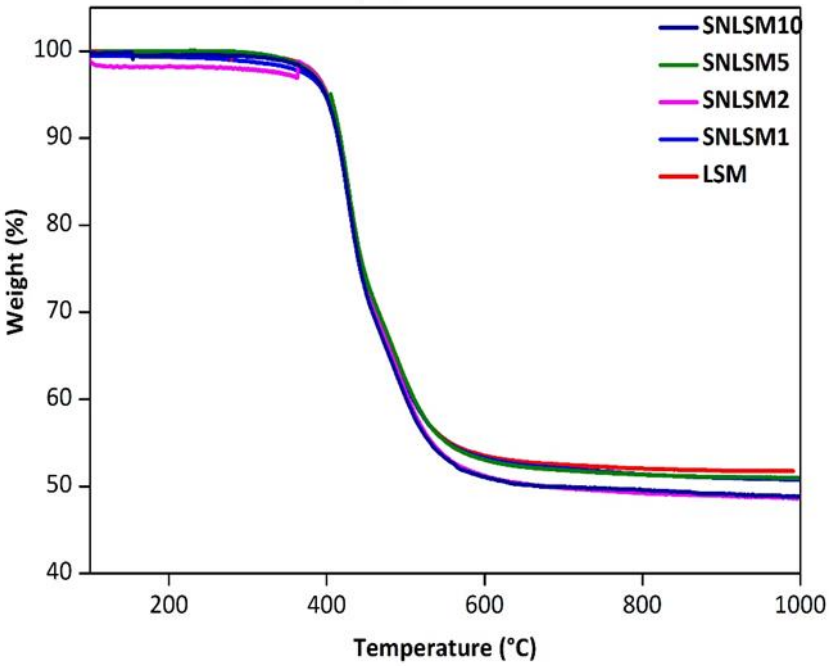

Figure 5.2.4 TGA analysis of resins

Table 5.2 Thermogravimetric analysis of resins

Weight %	Temperature ° C				
	LSM	SNLSM1	SNLSM2	SNLSM5	SNLSM10
T_5	400	397	399	399	398
T_{25}	444	444	443	446	442
T_{50}	-	-	672	-	675
Residue at 900°C	51.81	51.12	49	51.07	49.18

Figure 5.2.4 shows the thermogram of the resins which were carried out from 25°C to 1000°C. The initial degradation started around 400°C in all the resins. SNLSM2 and SNLSM10 exhibited T_{50} (the temperature at which 50% degradation occurred) at 672°C and 675°C whereas no T_{50} was noted for the other resins (Table

5.2). All the resins were left with more than 50% residues other than the SNLSM2 and SNLSM10. The ladder structured siloxane methacrylate (LSM) is known for its exceptional thermal stability and superior thermal properties when compared to cyclic siloxane (Unno et al., 2013). This was attributed due to the intense siloxane backbone (Kim et al., 2018a) present in LSM. In the present study, LSM resin withstand the temperature up to 1000°C and left with residue of ~52% which was already reported (Bridget Jeyatha et al., 2022). Pure siloxane LSM resin can withstand up to 1000°C without any record of T_{50}. Both the SNLSM2 and SNLSM10 had ~49% residue with T_{50} at around 675°C. In contrast, ormoresin R17 with calcium hydroxide and silica exhibited T_{50} at 435°C (Lizymol, 2004b). TGA results of SNLSM1 and SNLSM5 were similar with the earlier study of ladder structured siloxane methacrylate, which was also left with ~52% residue (Bridget Jeyatha et al., 2022). This revealed that addition of shell nacre had not modified the siloxane network of SNLSM1 and SNLSM5 whereas in the case of SNLSM2 and SNLSM10, shell nacre modified the siloxane network.

5.2.2.5 DSC analysis

During the DSC investigation of resins (Figure 5.2.5), a low Tg of approximately -50°C was observed for LSM and the other SNLSM resins. Both LSM and SNLSM10 exhibited almost similar T_g values, while SNLSM1 and SNLSM5 had comparable T_g values, specifically, T_g value of SNLSM2 was -47°C respectively. Pure siloxanes are highly flexible which is understood by the record of low glass transition temperature (Mark, 2004). In the present DSC analysis, a low T_g was recorded for all the resins. The low T_g proved the flexibility of the siloxane chains. (Crystal E. Porter

and Frank D. Blum, 2000). However, the T_g of all the resins were almost same, indicating that the shell nacre did not affect the molecular mobility or its transition from a glassy to a rubbery state. Based on all investigations, SNLSM2 evidenced shell nacre integration and hence selected for further characterization.

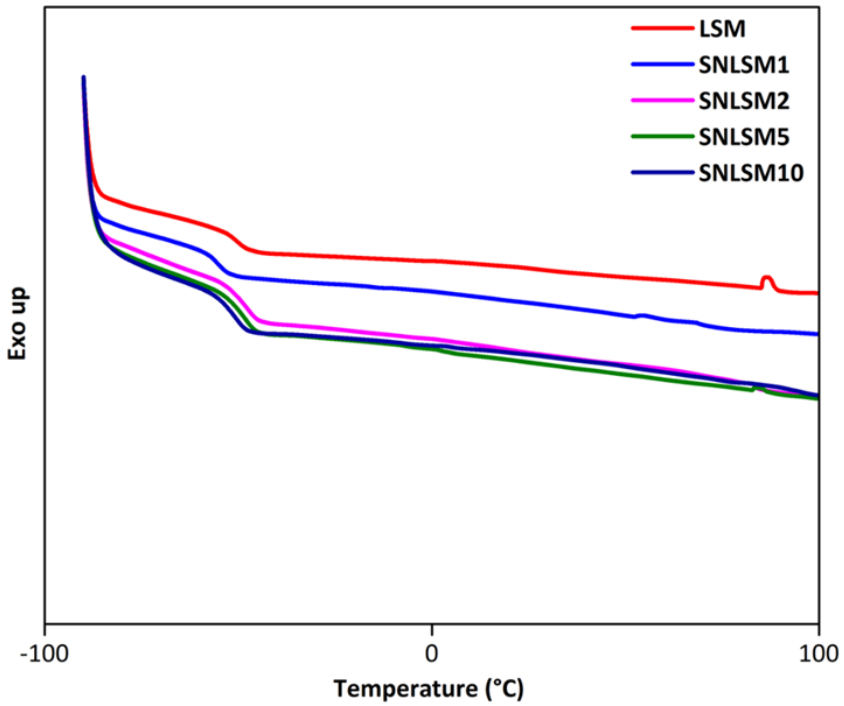

Figure 5.2.5 Differential scanning calorimetry analysis of resins

Table 5.3 Glass transition and melting temperature of resins

Name of the resin	Tg (°C)
LSM	-50.36
SNLSM1	-47.48
SNLSM2	-47.39
SNLSM5	-48.39
SNLSM10	-50.74

5.2.2.6 NMR analysis

The absence of an O-CH_3 peak at δ=55.31 ppm in ^{13}C NMR (Vibha, C., 2018) of both LSM (Figure 5.2.6) and SNLSM2 (Figure 5.2.8) confirmed the condensation of silanol moieties and the formation of siloxanes. ^{13}C NMR of LSM (Figure 5.2.7) (500 MHZ, DMSO): 8.45 -9.01 -g_1 (m, α-CH_2), 22.36 – f_1 (br, β CH_2), 66.26 - e_1 (s, γ CH_2), 136.35-b_1(s, C=C), 125.81-a1 (q, C=CH_2), 166.86- c_1, d_1 (s, C=O). ^{13}C NMR of SNLSM2 (Fig. 5.2.9): 8.45 -9.01 -7 (m, α-CH_2), 22.36 – 6 (br, β CH_2), 66.26 - 5 (s, γ CH_2), 136.36- 2 (s, C=C), 125.69 -1 (q, C=CH_2), 166.84- 3,4 (s, C=O).

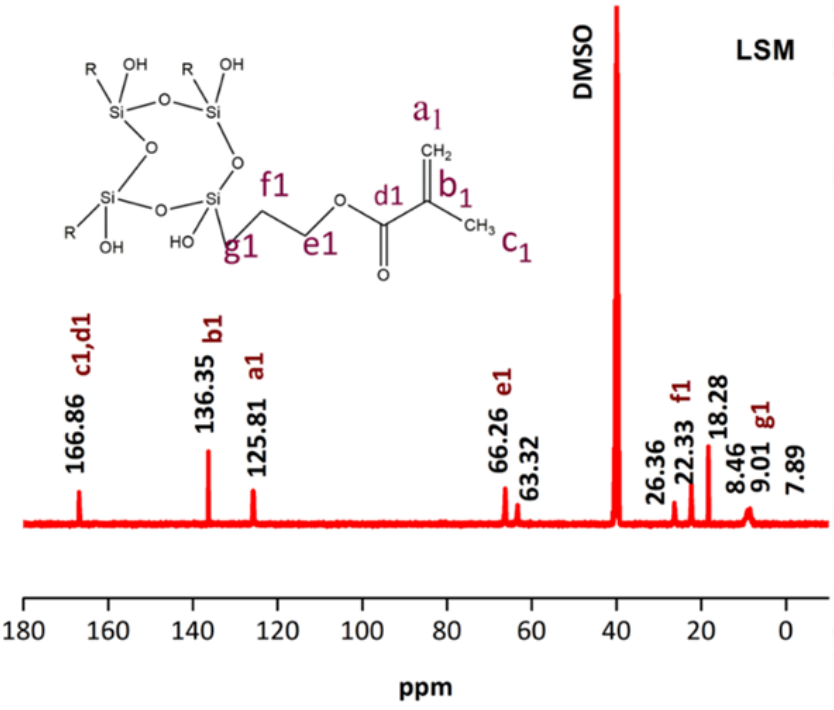

Figure 5.2.6 ^{13} C NMR spectrum of LSM resin

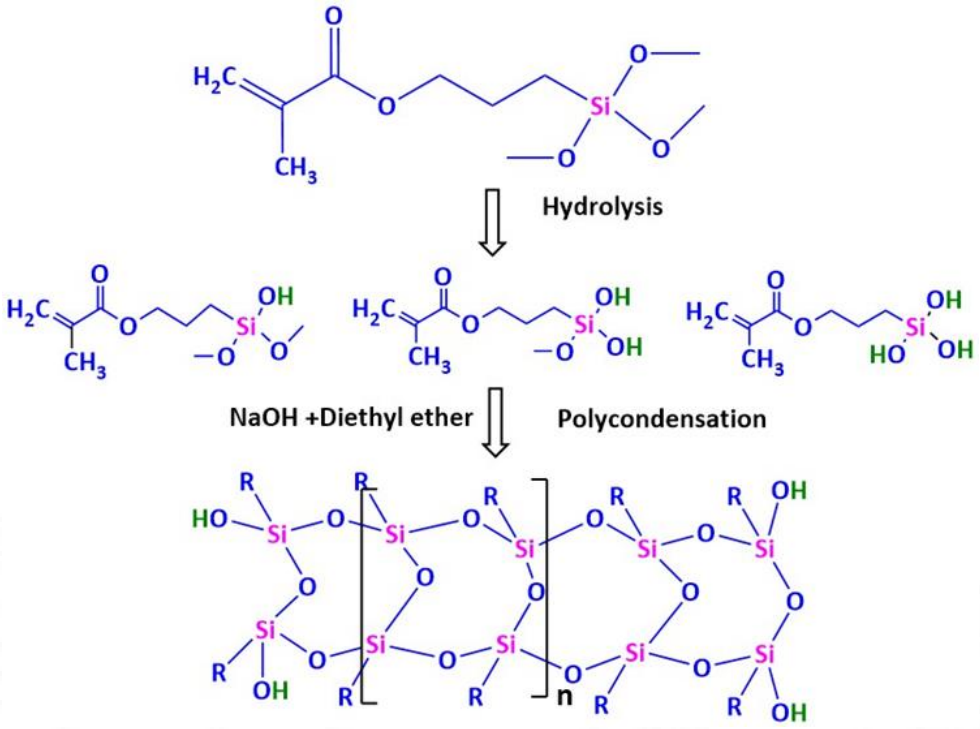

Figure 5.2.7 Schematic representation of the synthesis of LSM resin

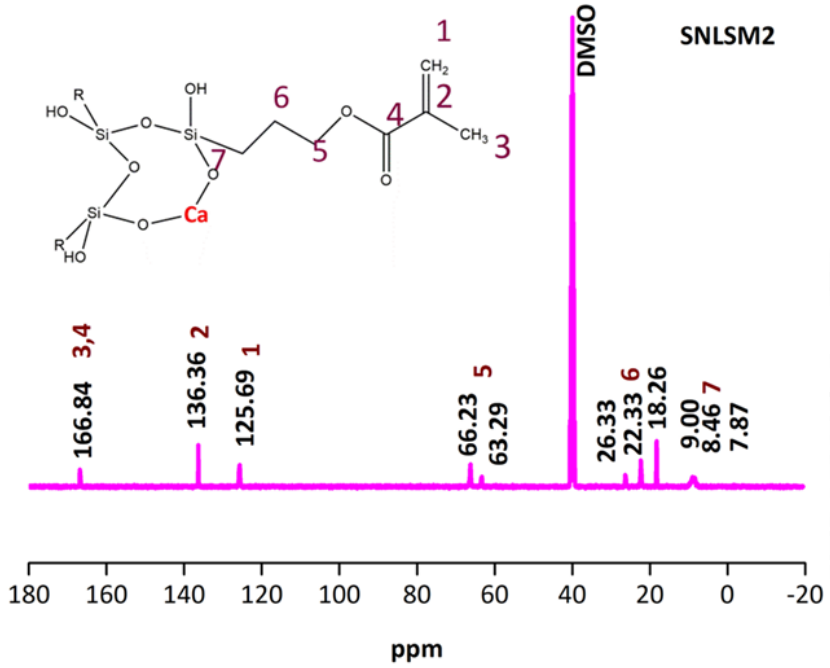

Figure 5.2.8 ^{13}C NMR spectrum of SNLSM2 resin

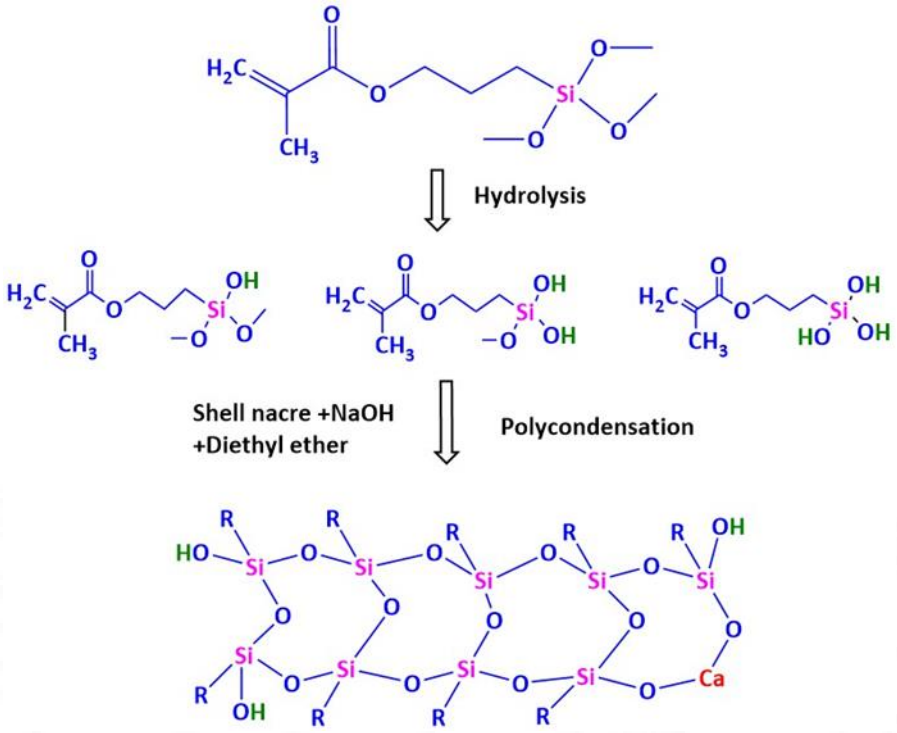

Figure 5.2.9 Schematic representation of the synthesis of SNLSM2 resin

5.2.2.7 TEM imaging

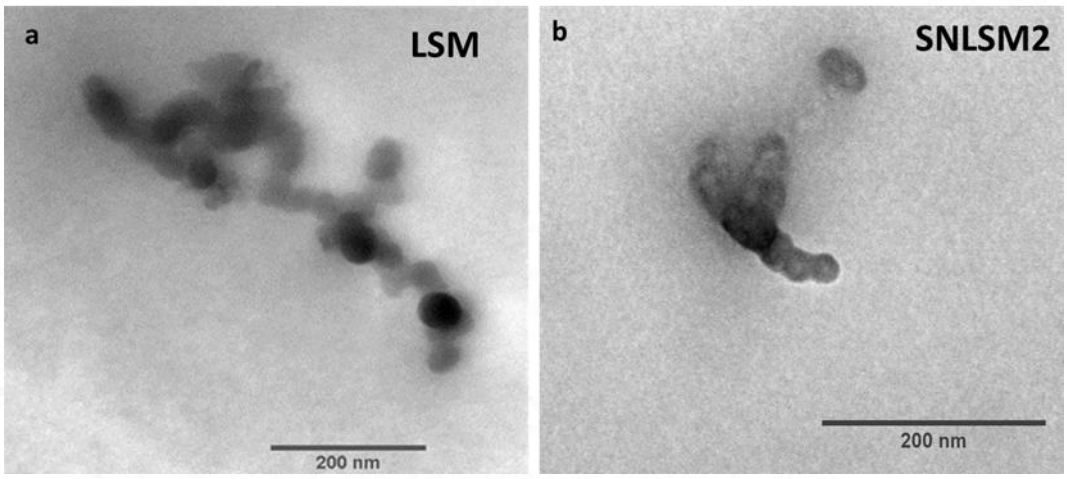

Figure 5.2.10 TEM image of a) LSM b) SNLSM2 resin; scale bar represents 200 nm

The TEM image (Figure 5.2.10 a) of LSM clearly showed the continuous growth of the Si-O-Si network as a ladder structure. Each siloxane unit was seen as

small dots of size approximately 10 nm. Notably, the structure exhibited interconnections between the siloxane units and with few silica clusters (darkened) overlapping them. On the other hand, SNLSM2(Figure 5.2.10 b), exhibited a shorter chain compared to the LSM resin, but a continuous network of ladder-structured siloxane was observed. TEM image of the both LSM and SNLSM2 was highly appreciated where the clear connections between each siloxane was observed and revealed the ladder structured morphology. This report of clearly seen ladder structure image was first of its kind whereas Jena *et al*., reported the structure of siloxanes which showed only few connections (Jena et al., 2018).

5.2.2.8 Viscosity of the resin

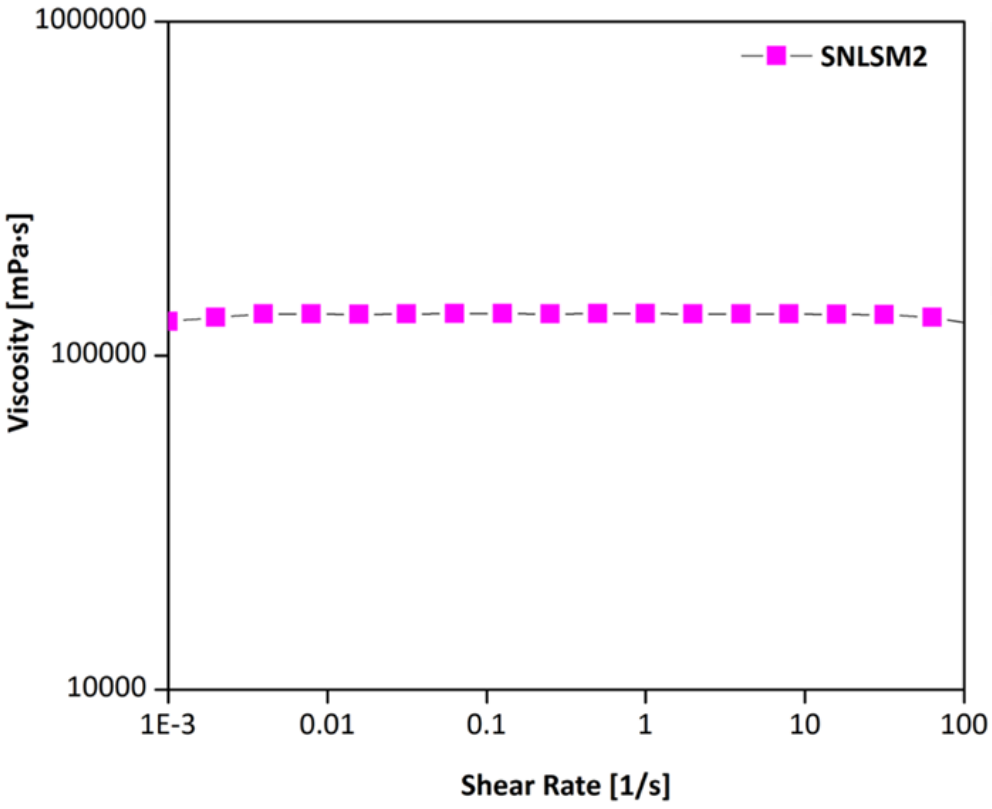

Figure 5.2.11 Viscosity curve of the SNLSM2

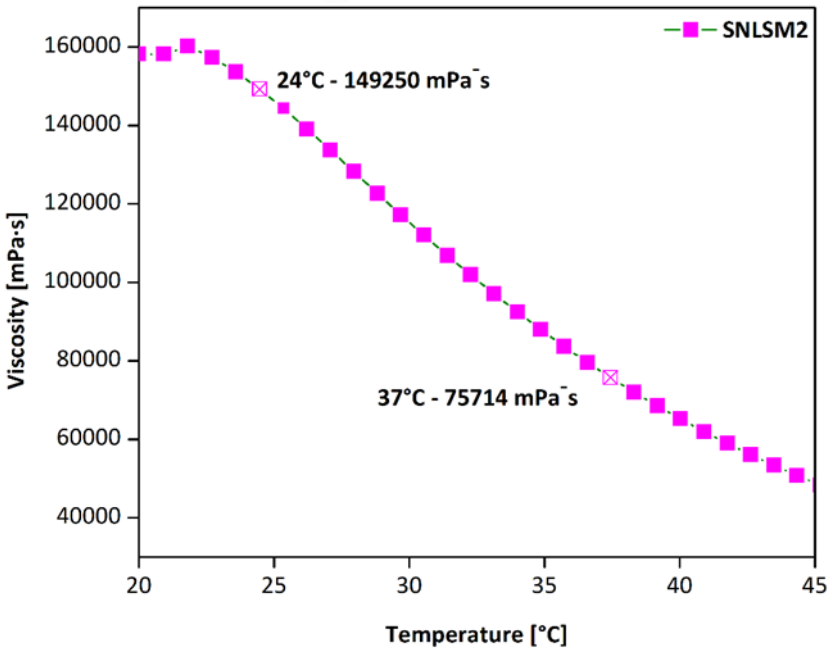

Figure 5.2.12 Temperature sweep test of SNLSM2

The viscosity of the SNLSM2 remained constant with an increase in shear rate, exhibiting the Newtonian property (Figure 5.2.11). During the temperature sweep test, the viscosity of the resin decreased as the temperature increased. At 25°C, the viscosity of the resin was 144.32 Pa s, whereas at 37°C, it was reduced to 75.714 Pa s (Figure 5.2.12).

Finally, the viscosity of the resin was studied, as it is one of the essential properties of the resin to be utilized for cement formulation. A high viscosity resin is always difficult to handle and limits the reinforcement of filler. MMA is very low viscous which was behind the bone cement post implantation syndromes (Vaishya et al., 2013). In contrast, the viscosity of bis GMA was 910 Pa s and several modifications were tried to reduce the viscosity (Alrahlah et al., 2021) (Al-Odayni et al., 2019). In the present study, the viscosity of SNLSM2 was 144.32 Pa s, which was

very low when compared to BisGMA and exhibited good handling property when diluted with equal amount of triethylene glycol dimethacrylate (TEGDMA) (Lizymol, 2004a)

Thus, shell nacre containing siloxane methacrylate resin was synthesized. FTIR, Raman, DSC, TGA, NMR of the resins proved that SNLSM2 comprised of ladder structured siloxane backbone and methacrylate side chain. TEM images exhibited the ladder structured siloxane backbone. SNLSM2 was transparent with medium viscosity of 144 $Pa\bar{}s$ and it was selected for bone void filling cement formulation.

DEVELOPMENT AND CHARACTERIZATION OF SHELL NACRE CEMENT:PART II:

6 FORMULATION, PHYSICOCHEMICAL, BIOCOMPATIBILITY AND OSSEOINTEGRATION EVALUATION

This chapter covers the materials and methods, results, and discussion related to the sub-objectives of main objective 3. Formulation, physicochemical characterization, biocompatibility evaluation and osseointegration study of *in situ* setting shell nacre cement. The main objective of this study is to develop shell nacre cement (SNC) with desirable characteristics such as low polymerization shrinkage, minimal exotherm, excellent mechanical properties, bioactivity, biocompatibility and osseointegration. The SNC was formulated by combining the synthesized SNLSM2 resin with shell nacre powder at different concentrations (24, 48 and 72%) along with the other additives. The resulting cement compositions were assessed for radiopacity, linear polymerization shrinkage and mechanical properties. The exothermic behaviour of the cement was studied by isothermal DSC and bioactivity by SEM-EDS. The cytotoxicity of the cement was studied with L929 cells. Acute systemic toxicity, irritation and pyrogen test were carried out based on ISO 10993-1. Finally, osseointegration of the cement was studied in a small animal model. Through these comprehensive evaluations, this study aims to provide valuable insights into the

physicochemical and biological properties of shell nacre cement, highlighting the synergistic action of shell nacre powder and the ormocer resin.

6.1 MATERIALS AND METHODS

6.1.1 Formulation of shell nacre cements

Shell nacre cement was formulated as a two-paste system A and B with the shell nacre powder and the synthesized SNLSM2. Paste A included SNLSM2 (12%), triethylene glycol dimethacrylate (TEGDMA) (12%) (Sigma Aldrich), dimethyl amino phenyl ethanol (DMAPEA) (Sigma Aldrich, US), fumed silica (FS) (3%), 0.03% 4-methoxy phenol (4-MP) (Sigma Aldrich, US), and shell nacre powder (24/48/ 72%). Paste B included SNLSM2 (12%), TEGDMA (12%), recrystallized (ice cold chloroform and methanol) benzoyl peroxide (BPO) (Merck, Germany), 0.1% butylated hydroxytoluene (BHT) (Merck, Germany) and 4-MP (0.03%), FS (3%), and shell nacre powder (24/48/72%). All the percentages mentioned were weight percentage and indicated as (wt.%). The amount of BPO, DMAPEA, BHT and shell nacre powder was optimized.

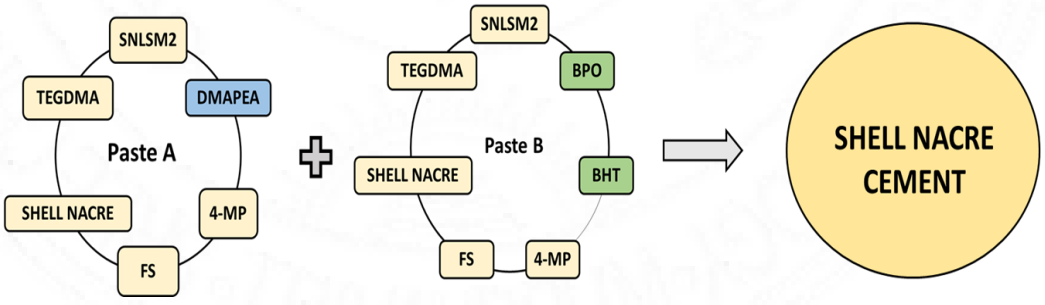

Figure 6.1 Representation of the composition of the paste A and paste B

6.1.1.1 Preparation of paste A and paste B

First step in the preparation of paste A was thinning of SNLSM2 with TEGDMA to form the resin matrix. DMAPEA was added next, followed by 4-MP, which were allowed to dissolve completely in the resin matrix. Subsequently, fumed silica was added and mixed well. Finally shell nacre powder was added slowly and mixed thoroughly to form the paste A. Similarly, paste B was prepared by completely dissolving BPO, BHT and 4-MP to the resin matrix. Afterward fumed silica was added, and lastly, shell nacre powder was added to form the paste B.

6.1.1.2 Effect of DMAPEA, BPO and BHT

Different weight (%) of DMAPEA (0.12,0.24,0.36 and 0.48%) and BPO (0.48, 0.72 and 0.96 %) were added and the effect on working time, setting time and compressive strength was studied. After optimizing the percentage of DMAPEA and BPO, different percentages of BHT (0.06, 0.08, 0.1) was added and the working and setting time was optimized. An equal amount of paste A and paste B was mixed for 30 sec by hand spatulation. After mixing, the cement was allowed to polymerize and the time before it started to get set was recorded as the working time. The time required for the complete setting of the cement (which was understood by the non-sticky nature of the cement) was noted as setting time. and the cured/set samples of required dimensions were prepared according to the need of experiments.

6.1.2 Physico-chemical characterization of shell nacre cement

Different weight (%) of shell nacre powder 24, 48 and 72% (SNC 24/48/72) were added to the paste A and B. An equal amount of paste A (SNC 24/48/72) and

paste B (SNC 24/48/72) was mixed for 30 sec by hand spatulation. After mixing, the cement was allowed to polymerize and cured/set samples of required dimensions were prepared according to the need of experiments.

6.1.2.1 Evaluation of radiopacity

Radiopacity of the cement was studied based on the ASTM standard (ASTM F640, 2023). Scout images of SNC samples (6mm diameter and 3mm height) and the reference material aluminium step wedge (aluminium alloy EN 1050 containing 99.5% of Al) was acquired using microcomputed tomography (µCT Scanco 40, Switzerland). Using image J, the grayscale intensity of the samples was analysed (n=6). A standard curve was plotted with thickness of Al wedge (0.5, 1, 1.5, 2, 2.5 and 3 mm) against mean grayscale intensity of the Al wedge. Radiopacity of the cement samples equivalent to the thickness of the Al wedge (mm)was determined from the standard curve.

6.1.2.2 Evaluation of linear polymerization shrinkage (LPS)

Shell nacre cement was packed in a 6 mm diameter and 3 mm height stainless steel mould and allowed to cure. The sample was then released from the mould and the internal diameter of the mould was calculated accurately using a digital calliper with an accuracy of 0.01 mm (Mitutoyo, Japan). The diameter of the cured sample was measured at six points in all directions and the mean value was calculated. The measurement was repeated for six samples and the percentage linear polymerization shrinkage was calculated using the formula LPS (%) = (Internal diameter of the mould-sample diameter)/ Internal diameter of the mould) *100 (Lizymol, 2010).

6.1.2.3 Evaluation of mechanical properties

Compressive strength samples were prepared using the brass mould of 3 mm diameter and 6 mm depth. The mould was placed on a strip of the transparent sheet on a metal plate and the shell nacre cement pastes A and B were mixed and packed into the mould. The second strip of the transparent sheet was placed on the top followed by a second metal plate. The mould and strip of film between the metal plates were pressed to displace excess material and allowed to cure for 30 mins. Similarly, flexural strength test specimens were prepared using the mould of 25 mm length, 2 mm depth, and 2mm thickness. The cured samples were removed from the mould and incubated in distilled water at 37 ± 1^0C for 23±1 h and 22 ± 2^0C for 1 h before testing. Using the corresponding jigs, compressive strength and flexural strength were determined using a universal testing machine (Instron, Model 1011, UK) with a crosshead speed of 5 mm/min and 1 mm/min respectively.

6.1.2.4 Investigation of exotherm generated

Exotherm generation of the curing SNC 72 cement was studied by isothermal DSC (Universal V4.5A, TA Instruments Inc, USA) at 24°C and 37°C for 30 min and the enthalpy change (δH) was recorded.

6.1.2.5 In vitro bioactivity studies

Based on ISO standard (ISO 23317, 2014), samples were soaked in simulation body fluid (SBF) for 14 days for remineralization with periodic change of SBF in alternative days. Surface morphology of the samples after remineralisation were studied using scanning electron microscope (Carl Zeiss EVO 18, Germany). The

elemental composition of the scanned surfaces was identified with Energy dispersive x-ray spectroscopy (Oxford instruments, X-Max).

6.1.2.6 PBS and SBF aging of SNC 72

SNC 72 samples (n=12) of size 4mm x 6mm were soaked in simulated body fluid and PBS at 37°C for 0, 4, 8 and 12 months. The media was changed every 14 days. After the specified time periods, the compressive strength of the samples was evaluated using the methodology described in 6.1.2.3

6.1.3 Cytotoxicity evaluation

Cytotoxicity test of the sterile SNC 72 cement sample was performed based on ISO standard (ISO 10993-5, 2009) using L929 cell line (ATCC), following the procedures mentioned in 3.1.6.1.

6.1.4 Biocompatibility studies

6.1.4.1 Ethical clearance and maintenance of animals

Table 6.1 IAEC approvals

S.No.	Name of the study	IAEC approvals
1.	Acute systemic toxicity test	SCT/IAEC-411/July/2021/110
2.	Animal intracutaneous reactivity test	SCT/IAEC-416/July/2021/110
3.	Pyrogen test	SCT/IAEC-420/July/2021/110

All experimental procedures and protocols were conducted as per the guidelines and recommendations of Committee for the Purpose of Control and Supervision of Experiments on Animals (CPCSEA), India and with the prior approvals

of the Institutional Animal Ethics Committee (IAEC) as mentioned in the table above. All the animals used in the following three studies were acclimatized for 5 days, maintained at 22 ± 3°C, humidity 30-70%, light/dark cycle for 12h, 15 fresh air/h, and fed with commercial mice / rabbit feed and filtered water *ad libitum*

6.1.4.2 Acute systemic toxicity

The detrimental effects of a single exposure of the extracts of shell nacre cement SNC 72 in mice model were studied based on ISO 10993-11: 2017(E) Annexure A 7 and 8 (ISO 10993-11, 2017). Both the cottonseed oil and physiological saline were used for extraction and as control. 4 g of the cured sterile shell nacre cement samples were incubated in 20 ml of physiological saline/cotton seed oil at 37°C ± 1°C for a period of 72 ± 2 h with 50 rpm agitation.

20 healthy adult Swiss albino mice of either sex were acclimatized for 5 days, housed 2-3 mice/cage, maintained at 22 ± 3°C, humidity 30-70%, light/dark cycle for 12h, 15 fresh air/h, and fed with commercial mice feed and filtered water *ad libitum* **(SCT/IAEC-411/July/2021/110).** The aqueous physiological saline extract of the sample and the control physiological saline was injected intravenously (5 for test and 5 for control) at a dose of 50 ml/kg. Similarly, the non-aqueous cotton seed oil extract and the control cotton seed oil were injected intraperitoneally. The animals were observed immediately and at 24, 48, and 72 h for any abnormalities in clinical signs/mortality/reduction in body weight. Clinical sign includes respiratory, motor, convulsion, reflexes, ocular signs, cardiovascular signs, salivation, piloerection, analgesia, muscle tone, gastrointestinal, and skin.

6.1.4.3 Animal intracutaneous (intradermal) reactivity test

The local irritation potential of the shell nacre cement sample SNC 72 was studied based on ISO 10993-10: 2021-Biological evaluation of medical devices - Part 10 (ISO 10993-10,2021) **(SCT/IAEC-416/July/2021/110)**. Three New Zealand rabbits of weight 2 to 2.2 kg were caged individually and maintained as stated above. The physiological saline and cottonseed oil extract of the shell nacre cement was prepared similarly to the acute systemic toxicity test and the extracts were aseptically injected into 5 sites (0.2ml/site) of the upper left and right-hand side of 3 animals. Similarly, the controls were injected into the lower left and right-hand sides of the same rabbits. The signs of erythema and oedema caused by the shell nacre cement and controls were recorded at 24, 48, and 72h. The grading system followed was 0- no erythema, 1- very slight, 2- well defined, 3- moderate, and 4 –severe erythema; similarly, oedema was graded and the possible score for irritation was 8. After final grading at 72 h, all erythema grades and oedema grades (24 h, 48 h and 72 h) were totally added separately for SNC or control for each individual animal. To calculate the irritation score of a test sample or control on each individual animal, divide each of the totals by 15 (3 scoring time points *5 extract injection sites). The requirements of the test are met if the final average irritation score of the sample is one or less.

6.1.4.4 Pyrogen test

The pyrogenicity was investigated based on annexure G information on material mediated pyrogens ISO 10993-11 (ISO 10993-11, 2017). Healthy and adult New Zealand white rabbits of weight 2-2.1kg (3 Nos.) were chosen and housed individually in a rabbit restrainer for 7 days at 22 $\pm$ 3°C. The daily rectal temperature

of the rabbits was recorded for seven days using a calibrated thermometer. Rabbits whose temperature varies less than 1°C and exceeded not more than 39.8°C were selected for the study. 20g of the sterile shell nacre cement samples were extracted in 100 ml of sterile physiological saline at 37°C for 1 h. Extract preparation and injection were done sterile and pyrogen free. The rectal temperature before 30 min of injection was recorded as base temperature. At a dose of 10 ml/kg, SNC 72 extract were injected into the marginal ear vein of the rabbit within 10 min. Change in rectal temperature was noted between 1 and 3 h at 30 min interval and the rise in temperature with respect to the base temperature was calculated.

6.1.5 Osseointegration of *in situ* setting shell nacre cement

6.1.5.1 Ethical clearance

Animal surgical procedures were carried out at Division of Laboratory Animal Science (DLAS), BMT Wing, SCTIMST. All experimental procedures and protocols were conducted as per the guidelines and recommendations of CPCSEA, India and with the prior approval of the IAEC B Form No. SCT/IAEC-285/Sep/2018/97 extension dated 15.05.2021.

6.1.5.2 Cortical femoral defect surgery

Male Sprague-Dawley rats (390–510 g) of age 15-18 weeks were used for the implantation studies. Animals were grouped into PMMA (clinical control -Surgical Simplex P cement, Stryker) and shell nacre cement group SNC 72 for 6 and 12 weeks with n=3 in each group. Prior to surgery, the rats were housed in individual cages with alternating 12-hour cycles of light and dark in temperature and humidity-controlled

rooms. Following acclimatization, all animals underwent metaphyseal cortical defect surgery in the femur (2 mm diameter) (Figure 6.1.1). Under general intraperitoneal anaesthesia (xylazine 5 mg/kg and ketamine 80 mg/kg), the right hindlimb was aseptically prepared and the animals were placed in a lateral position. The defect was created in the mid shaft of femur by means of a 2 mm drill bit. The cavity was rinsed with physiological saline to wash away remaining bone fragments. Both the PMMA and shell nacre cement was set into the defect using cement filling tools like spoon shaped excavator and condenser. Following implantation, synthetic absorbable surgical suture was used to close the muscle layer and 3-0 braided silk to close the skin. Meloxicam 1.0mg/kg body wt was administered subcutaneous for 3 days post operation once daily. Cephtriaxone@ 15mg/kg Od was administered intramuscular for 3 post operative days. At 6- and 12-weeks post-surgery, rats were euthanized and samples were collected for analysis like gross morphology and x-ray radiography.

6.1.5.3 Gross examination

Animals were euthanized at 6- and 12-week post implantation. The implant site along with the femur bone was explanted and fixed in 10% NBF. Gross examination of the retrieved explants was carried out.

6.1.5.4 Radiography

After gross examination, scout images of explants containing PMMA and SNC 72 were captured using microct (µCT Scanco 40, Switzerland).

6.1.6 Graphs, Statistics and spectrums

All line and bar graphs were drawn using Microsoft excel. All statistical analysis were performed using GraphPad Prism software (version 9.5.1) (GraphPad, USA). Ordinary one-way ANOVA was performed along with Tukey's multiple comparisons test. The differences between mean were statistically significant only if $p \leq 0.05$. The level of significance was indicated as *ns* - $p>0.05$, * - $p\leq 0.05$, ** - $p<0.01$, *** - $p<0.001$, **** - $p<0.0001$. All the spectrums were drawn using OriginPro software (OriginLab Corporation, USA).

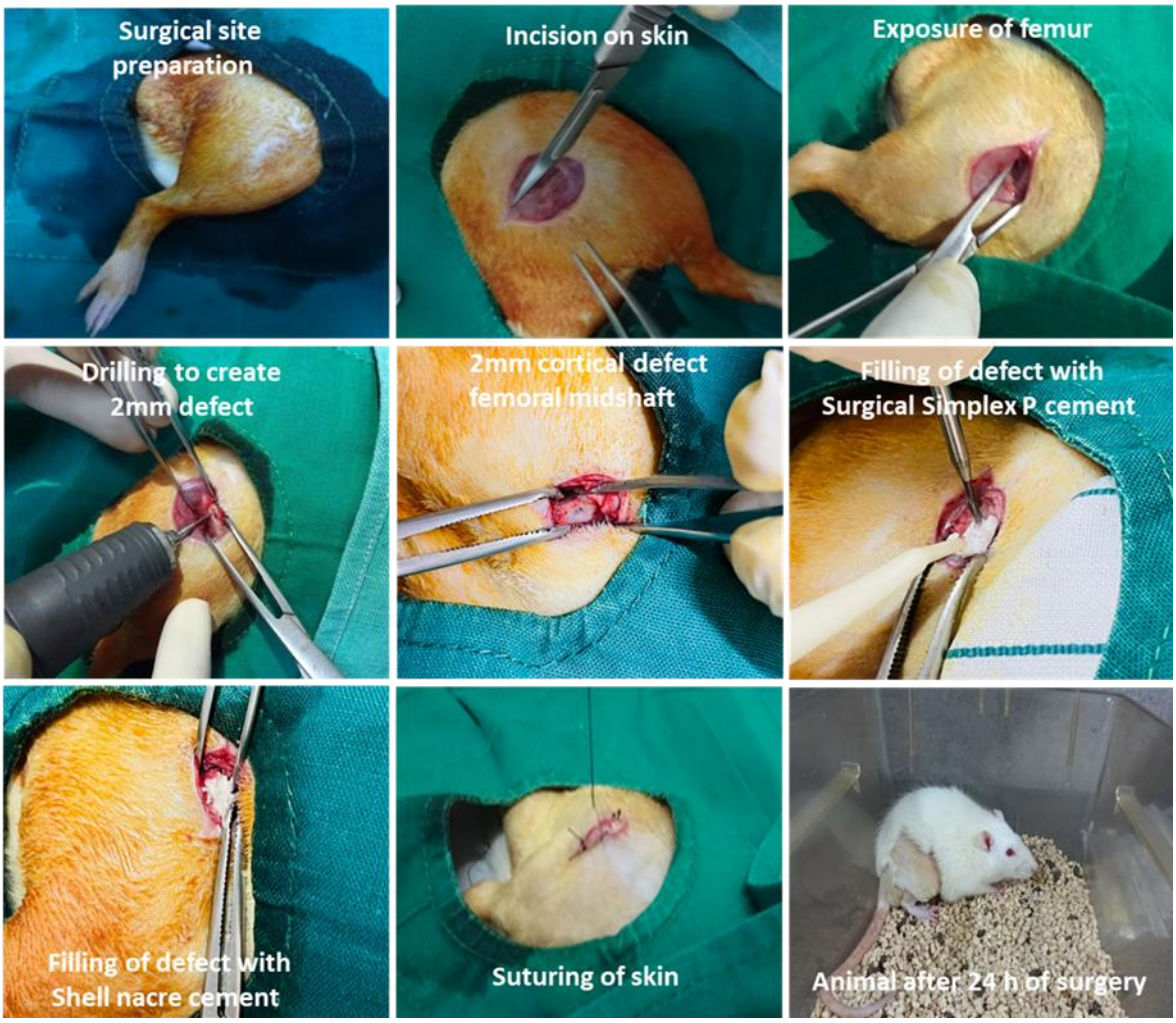

Figure 6.1.1 Surgical procedure for femoral cortical defect and filling with cements

6.2 RESULTS AND DISCUSSION

There is a growing interest in biomedical field towards natural material and shell nacre is an emerging bone substitute with superior properties. However, there is a gap area where the usage of shell nacre from *Pinctada fucata* is not fully explored for bone defect management, particularly as a bone void filling cement. There are two novelties in this cement; one was usage of shell nacre containing ladder structured siloxane methacrylate resin and the other was shell nacre powder. This unique *in situ* curing composite cement composition has not been reported in previous studies, which utilized oyster powder (unnamed) (Shen et al., 2014), nacre powder (unspecified) (Ruan et al., 2018), clam shell powder (Simu et al., 2018) or whole abalone shell powder (Du et al., 2021) for composite cement preparation. Therefore, to our knowledge, this is the first bone void filling cement of its kind.

Shell nacre cement was formulated as paste A and paste B and during the mixing of both paste A and paste B, BPO along with DMAPEA promoted the polymerization of the organic network by breaking the C=C bond of the methacrylate moieties of the resin and TEGDMA and the chain growth was continued. The amount of BPO, DMAPEA and BHT was optimized. Different formulations of cements were prepared by varying the amount of shell nacre powder (24, 48 and 72wt%). The best cement SNC 72 was selected for further studies, based on radiopacity, LPS (%), and mechanical properties. Furthermore, isothermal DSC of exotherm generation, bioactivity PBS and SBF aging, cytotoxicity, biocompatibility, and osseointegration of SNC 72 was studied.

6.2.1 Formulation of shell nacre cement

SNLSM2 (12%) was diluted with equivalent amount of TEGDMA (12%) and formulated as a two paste with initiator, activator, stabilizers, fumed silica, and shell nacre powder. The activator DMAPEA was included in the paste A whereas the initiator BPO was included in the paste B and the polymerization began only during the mixing of both paste A and B. The amount of both BPO and DMAPEA influenced the working and setting time as well as mechanical properties (Nussbaum et al., 2004).

6.2.1.1 Effect of BPO

The amount of BPO and DMAPEA have significant effect on the properties of the cement. First, the effect of BPO (0.48, 0.72,0.96%) was studied with 0.36% and 0.48% DMAPEA. With both the concentration of DMAPEA (0.36% and 0.48%), the working and setting time was reduced with increasing concentration of BPO (Figure 6.1.2 a, b). However, the compressive strength increased with increasing concentration of 0.72% BPO with 0.36% DMAPEA but reduced with 0.96%BPO (Figure 6.1.2 c). Similarly, compressive strength increased with increasing concentration of BPO with 0.48% DMAPEA but reduced with 0.96%BPO (Figure 6.1.2 d). The similar observation of reduced working and setting time but increased compressive strength was reported by Przeslawski's group (Przesławski et al., 2022).

6.2.1.2 Effect of DMAPEA

The effect of DMAPEA (0.12, 0.24, 0.36%) was studied with 0.48% and 0.72% BPO. With both 0.48% and 0.72% BPO, the working and setting time (Figure 6.1.3 a, b) were reduced with increasing concentration of DMAPEA. However, the

compressive strength increased with increasing concentration of DMAPEA with 0.48% BPO (Figure 6.1.3c), but reduced with 0.72%BPO (Figure 6.1.3 d). The similar results of reduced working and setting time was reported by Mathew's group (Mathew et al., 1997).

Finally, the paste A with 0.36%DMAPEA and paste B with 0.72 % BPO with working time of 60 sec, setting time of 120 sec and compressive strength of 100 MPa was selected for further optimization.

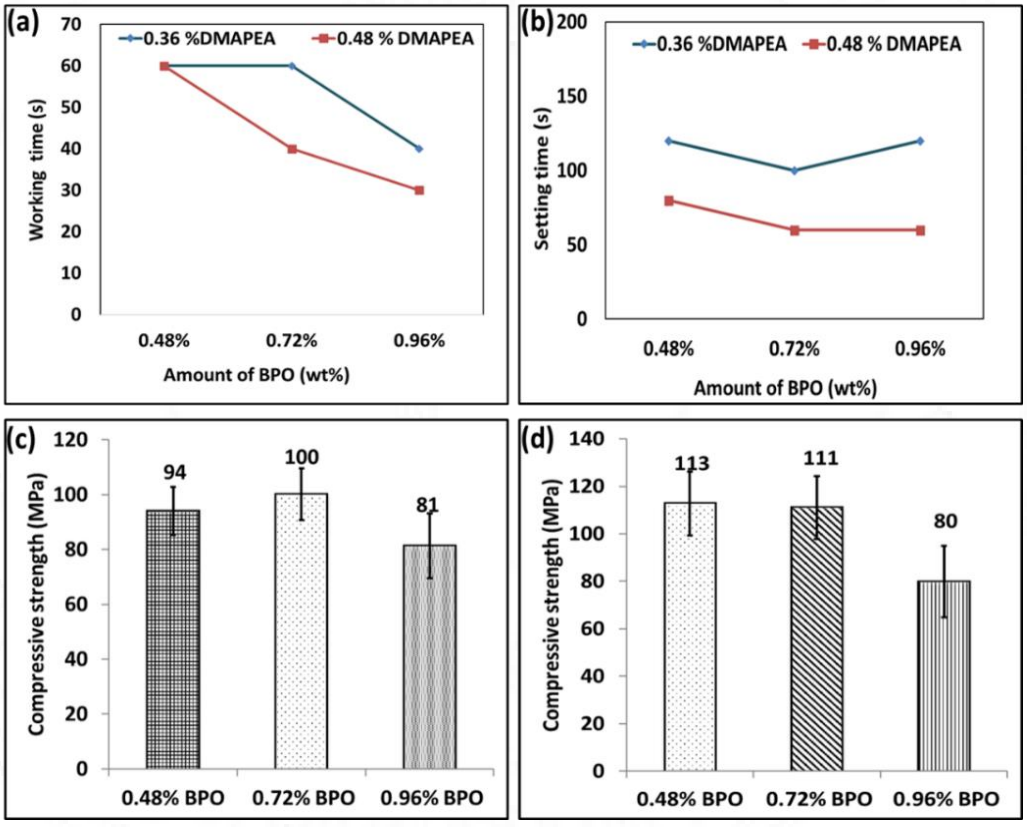

Figure 6.1.2 Effect of 0.48, 0.72 and 0.96% BPO (paste B) with 0.36% and 0.48% DMAPEA (paste A) on the working time(a), setting time , (b) compressive strength with 0.36% DMAPEA and d) compressive strength with 0.48% DMAPEA.

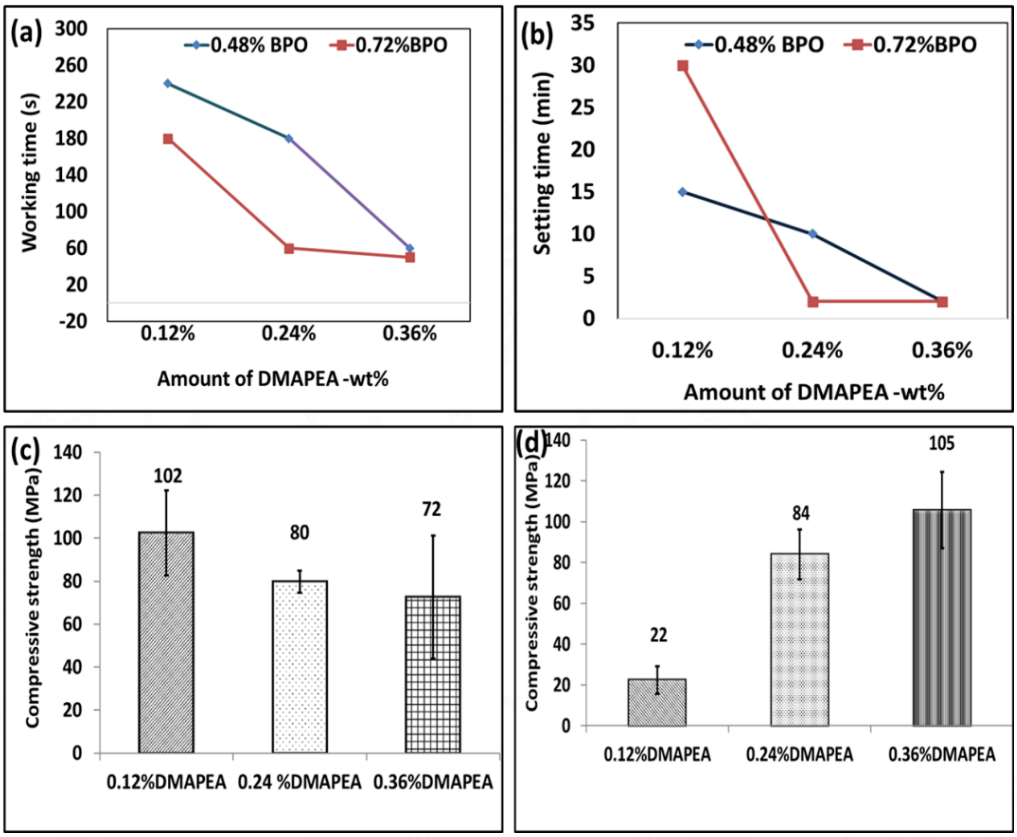

Figure 6.1.3 Effect of 0.12, 0.24 and 0.36% DMAPEA (Paste A) with 0.48% and 0.72% BPO (Paste B) a) on the working time, b) setting time, c)compressive strength with 0.48%BPO and d) compressive strength with 0.72% BPO.

6.2.1.3 Effect of BHT on working and setting time

BHT is a free radical scavenger (Yehye et al., 2015), used in the dental cements to prevent the premature and spontaneous polymerization and to increase the working time(Grohmann et al., 2022). The working and setting time were reduced with increasing concentration of BHT with 0.36% DMAPEA and 0.72% BPO composition. However, with 0.1% BHT, both the working (150 sec) and setting time (420 sec) increased sharply (Figure 6.1.4).

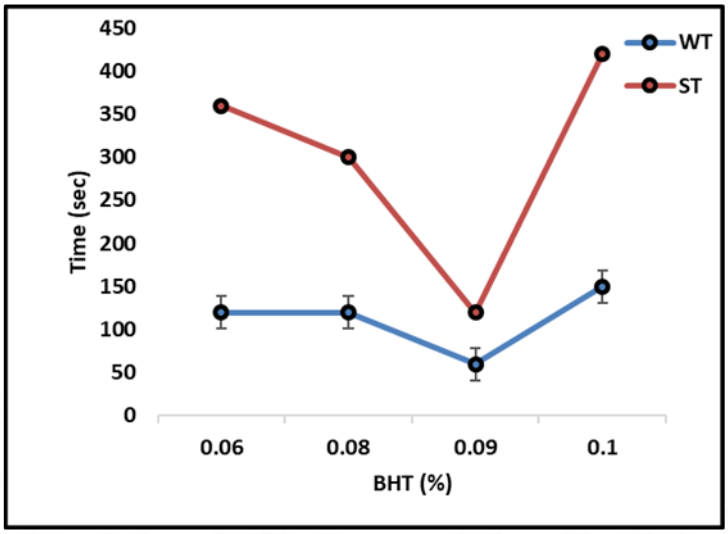

Figure 6.1.4 Influence of BHT (006,0.08,0.09,0.1%) on the working and setting time of paste with 0.36% DMAPEA and 0.72 % BPO

6.2.2 Physico-chemical characterization of SNC

Based on working time, setting time and compressive strength, the final shell nacre cement was optimized with 0.36% DMAPEA, 0.72% BPO, 0.1% BHT. The working time of the cement was 3 min with setting time of 6 min.

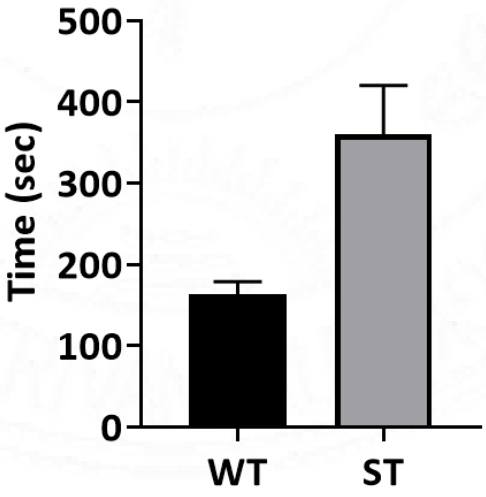

Figure 6.1.5 The working and setting time of the optimized formulation

6.2.2.1 Radiopacity evaluation

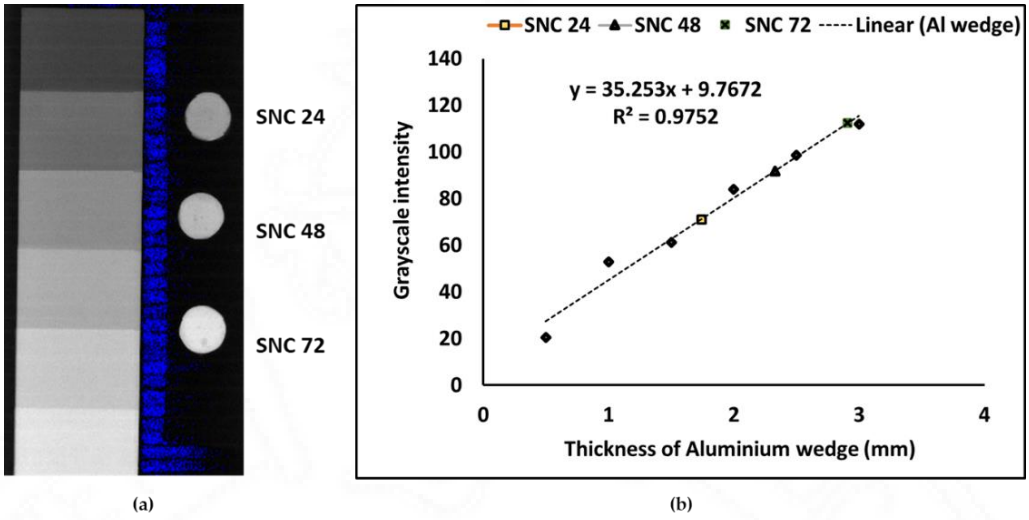

Figure 6.2 Radiopacity evaluation; (a)Scout images of shell nacre cement SNC 24, 48 and 72 with Aluminium wedge obtained using micro computed tomography (b) A standard curve was plotted with the thickness of each step of the Al wedge against mean grayscale intensity of the Al step wedge

Different cement compositions were prepared with increasing quantity of shell nacre powder SNC 24, SNC 48 and SNC 72. Radiopacity is an essential property for bone cements used in clinical settings, as it allows for monitoring the material's position and distribution. Barium sulphate and zirconium dioxide are the commonly used radiopacifier in the clinically available PMMA cement. However, these materials have been found to have negative effects on the toxicity and mechanical properties of the cement. As a result, researchers have explored alternative radiopacifier such as triphenyl bismuth, tantalum powder, bismuth salicylate, iodine containing co-polymer as powder and as liquid, bromine containing co-polymer (Lewis, 2008), and gold (Jacobs et al., 2016) *etc*. In the present study, the radiopacity values of SNC 24, SNC 48 and SNC 72 were 1.74, 2.3, 2.9 mm equivalent to the thickness of Aluminium wedge (Figure 6.2). Radiopacity was enhanced with increasing concentration of shell

nacre and the inherent radiopacity of shell nacre contributed to the radiopacity of the cement. SNC 72 exhibited higher radiopacity equivalent to 2.9 mm thickness of aluminium wedge.

6.2.2.2 Evaluation of LPS

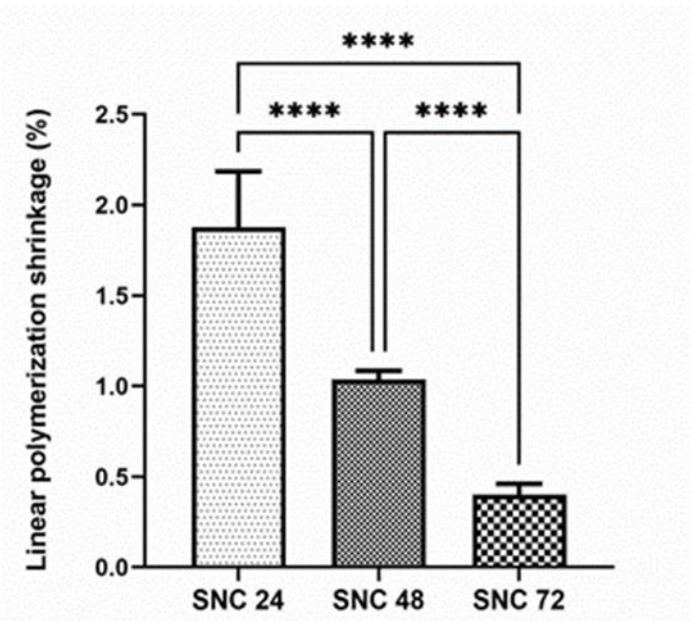

Figure 6.2.1 Evaluation of linear polymerization shrinkage (n=6); Ordinary one-way ANOVA. Tukey's multiple comparisons test. * P< 0.05, ** P<0.01, **** P<0.0001. Data are shown with mean and standard deviation of the mean

The linear polymerization shrinkage of commercially available bone cements is a major concern with values typically in the range of 5-10% (Gilbert et al., 2000). Additionally, the exotherm generated by the polymerization of the PMMA cement is very high at 52kJ/mole of PMMA, which is another major drawback of the cement (Soleymani Eil Bakhtiari et al., 2020). The healing of any bone defect is influenced by various factors including, stability, lack of cytotoxicity and mechanical support. Therefore, the development of bone void filling cement with synergistic properties like

mechanical property, non-cytotoxicity, minimal shrinkage and exotherm is necessary. This synergism can be achieved by altering either the resin matrix or the filler part of the cement. Both the strategies were attempted in SNC cement by modifying the organic resin matrix with ormocer SNLSM2 and introducing shell nacre (24%, 48% and 72 %) in the filler part.

Linear polymerization shrinkage percentage of the cements decreased with increasing shell nacre content with values of 1.8, 1.03 and 0.4% (Figure 6.2.1) for the 24, 48 and 72% compositions, respectively. Interestingly, even the minimal shell nacre containing cement exhibited shrinkage of 1.8%, which is significantly lower than many of the existing composites, reflecting the multi-functionality of SNLSM2. Thus, the synergistic action of both the SNLSM2 and shell nacre led to the reduction in the linear polymerization shrinkage of the SNC compositions.

6.2.2.3 Evaluation of mechanical properties

SNC 72 exhibited average compressive and flexural strength of ~110 MPa (Figure 6.2.2) and ~35 MPa (Figure 6.2.3). Previous studies by Shen *et al*., and Du *et al.,* reported that the compressive strength of calcium sulphate composites of oyster powder and abalone shell powder was only ~11 MPa (Shen et al., 2014) and ~5 MPa (Du et al., 2021) respectively. Another study with calcium phosphate cement, showed that increasing concentration of nacre reduced the compressive strength (Ruan et al., 2018). In contrast, the compressive strength of the current SNC 72 composite was ~110 MPa which was 10 to 20 times higher than the reported calcium sulphate composites, and the mechanical properties were further enhanced with increasing shell nacre content. Previous studies by Wu *et al.,* reported that addition of amphiphilic

raspberry particles to the PMMA reduced the compressive strength (T Wu et al., 2018b).

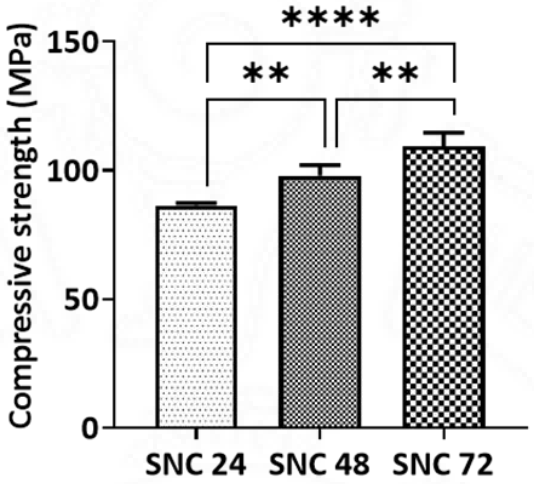

Figure 6.2.2 Evaluation of Compressive strength (n=6). Ordinary one-way ANOVA. Tukey's multiple comparisons test. * P< 0.05, ** P<0.01, **** P<0.0001. Data are shown with mean and standard deviation of the mean

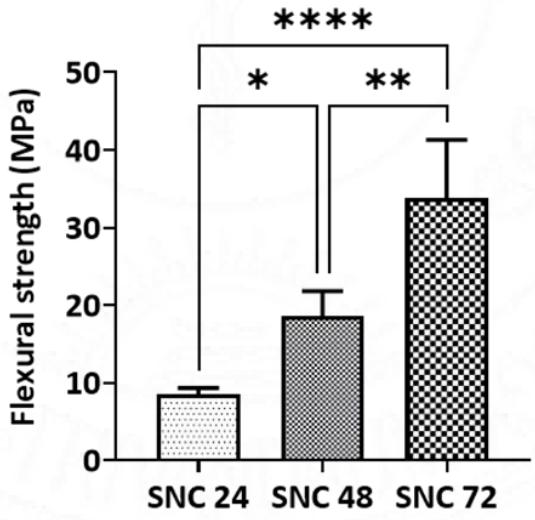

Figure 6.2.3 Evaluation of flexural strength analysis (n=6). Ordinary one-way ANOVA. Tukey's multiple comparisons test. * P< 0.05, ** P<0.01, **** P<0.0001. Data are shown with mean and standard deviation of the mean

In another study, addition of magnesium oxide reduced the mechanical properties of the cement (Khandaker et al., 2014). However, in the shell nacre cement compositions, the mechanical properties were improved by the bonding of shell nacre powder with the SNLSM2 resin. A study by Yang *et al.,* found that use of acrylic acid and styrene in PMMA cement lowered the compressive strength than PMMA (Yang et al., 2017). But in the present cement, SNLSM2 imparted good compressive strength even to the cement with low concentration of shell nacre powder (24 wt%). Being an inorganic-organic hybrid filler, shell nacre was incorporated to the cement compositions without any silanization. Both the ormocer SNLSM2 and shell nacre contributed to the mechanical properties, as evidenced by the increase in both compressive and flexural strength with increasing shell nacre content.

6.2.2.4 Investigation of exotherm generation

Compared to other formulations, SNC 72 exhibited better mechanical property, radiopacity and low linear polymerization shrinkage and so selected for further studies. As curing is affected by temperature, both the room temperature of the surgery room and the human body temperature was considered and isothermal DSC was carried out at both 24°C and 37°C. The exotherm generated by SNC 72 at 37°C and 24°C was 2.227J/g and 0.5781J/g (Figure 6.2.4) respectively. Although the heating rate and other conditions were similar, variations in enthalpy change, δH was noticed during curing of SNC 72 in two different temperatures

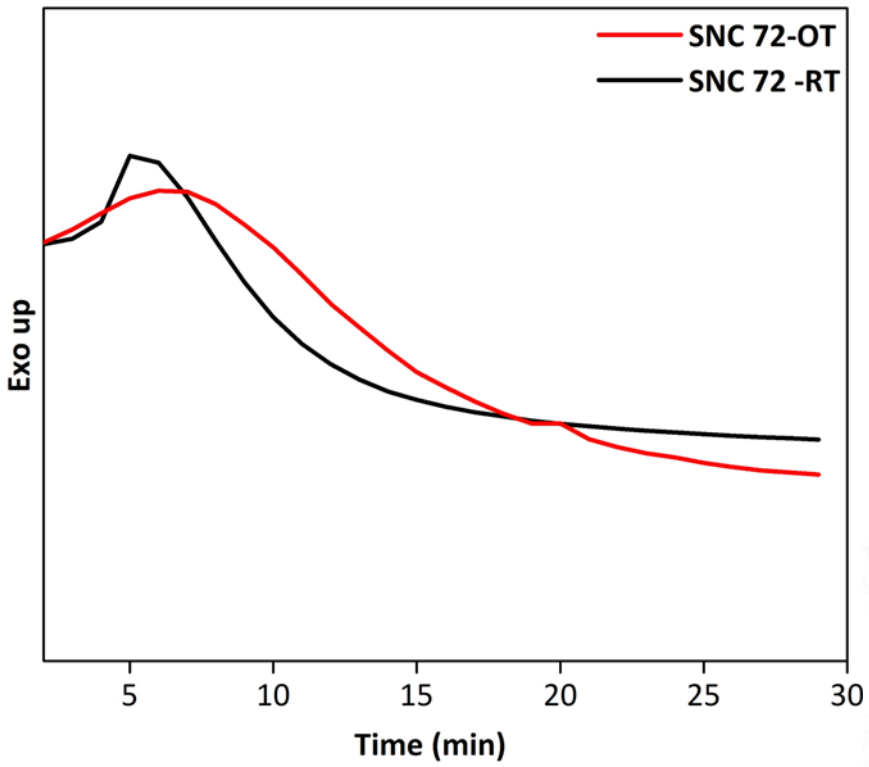

Figure 6.2.4 Thermal study of SNC 72: (a) Isothermal DSC at 24°C and (b) 37°C showing the exotherm generated during the curing of SNC 72

A previous study reported no significant change in maximum polymerization temperature of Palacos cement after modification with 2-hydroxyethyl methacrylate, calcium chloride and sodium carbonate (Wolf-Brandstetter et al., 2013). Similarly, addition of graphene and graphene oxide powders to PMMA showed no changes in exotherm generation (Paz et al., 2017). In contrast, combination of shell nacre powder and SNLSM2 resulted in the significant reduction of exotherm to low value, compared to the commercially available cements and experimental cements.

6.2.2.5 In vitro bioactivity of SNC 72

Bone like apatite formation in the simulated body fluid is a desirable property that are intended for use in bone substitute applications. This is because the formation

of apatite similar to bone within the SBF indicates that the material has the ability to bond within the surrounding tissue. The silanol (Si–OH) group and calcium ions are effective components for inducing apatite nucleation (Miyazaki & Ohtsuki 2008) and can bond to the implanted bone. Many researchers modified the cement formula with glass powder (Kawanabe et al., 1993; Kokubo et al., 1991), apatite wollastonite glass ceramic (AW-GC)(Mousa et al., 2000), barium boro-alumino-silicate glass and silica particles (Erbe et al., 2001), nano-sized titania particles (Goto et al., 2005), hydroxyapatite (Deb et al., 2005), strontium substituted hydroxyapatite (G. X. Ni et al., 2006), hydroxyapatite along with BMP-2 (Liu et al., 2015), synthetic combeite glass-ceramic particles, borosilicate glass (Zhang et al., 2022) and graphene oxide (Tan et al., 2023) *etc.* for bioactivity. *In vitro* mineralization studies of SNC 72 were conducted based on ISO 23317. SEM-EDS analysis of SNC 72 after 21 days in SBF evidenced globular accretions of hydroxyapatite mineralization with Ca and P peaks whereas no mineralization was observed in day 0 SNC 72 samples (Figure 6.2.5). The SEM-EDS analysis of SNC 72 after 21 days revealed the significant formation of apatite on the surface, as evidenced by the presence of Ca and P peaks. This confirmed the bioactive nature of the shell nacre cement.

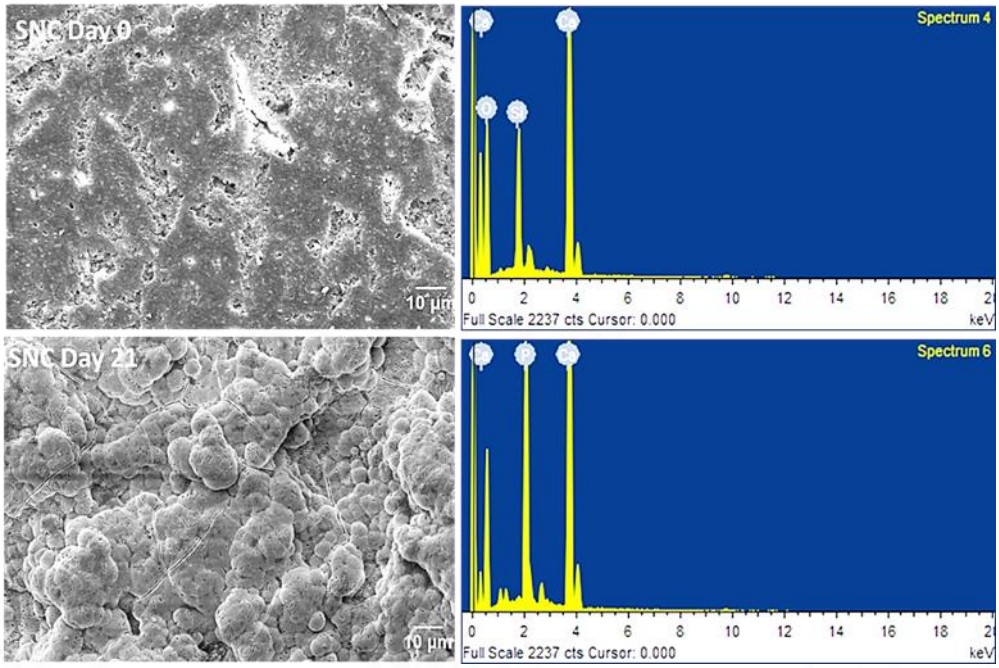

Figure 6.2.5 *In vitro* bioactivity studies; SEM-EDS analysis of the SNC 72 after immersing in SBF for 0 and 21 days. Magnification 1500 X - Scale bar 10 µm

6.2.2.6 PBS and SBF aging of SNC 72

Another essential property for any bone void filling cement is matching of degradation with bone formation. The right degradation of the cements is crucial for facilitating bone repair, as it makes space for the new bone formation. In the present study, degradation of SNC 72 was understood indirectly from the reduction in CS. After PBS aging, 0%, 11% and 40% reduction in CS was noted after 4, 8 and 12 months. After SBF aging, 3%, 10% and 28% reduction in CS was recorded after 4, 8 and 12 months (Figure 6.2.6). This indicated the slow degradation pattern of shell nacre cement.

SNC 72 retained the strength and no change in CS was observed after four months in both PBS and SBF. However, after eight months, subtle changes of

approximately 10% were noted and after a year, reduction of 40% (in PBS) and 28% (in SBF) was recorded.

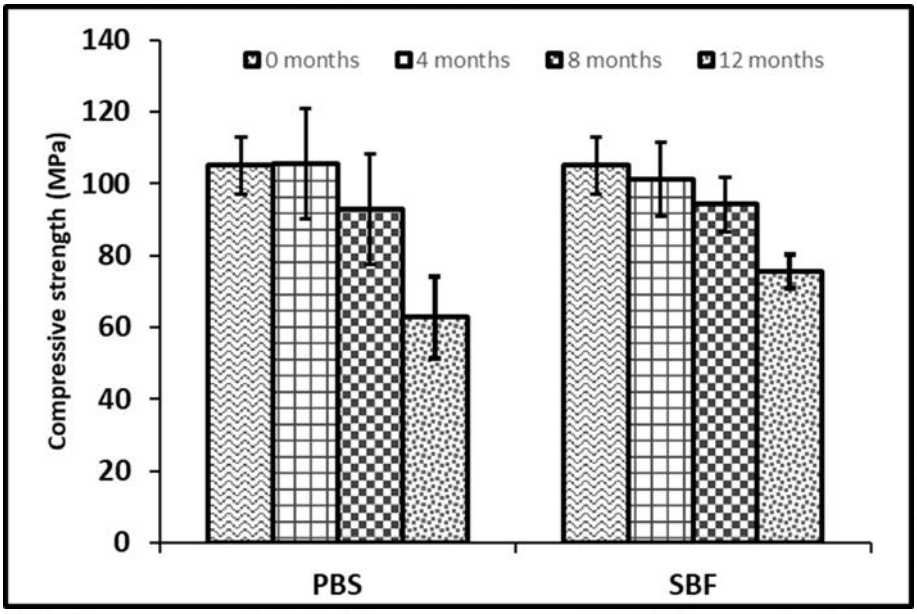

Figure 6.2.6 Compressive strength of SNC 72 after PBS and SBF aging of shell nacre cement for 0,4,8 and 12 months

In contrast, Ma *et al.,* observed a 6.5% increase in compressive strength of N-acetyl-L-cysteine modified nanohydroxyapatite/magnesium phosphate cement over 28 days in SBF (Ma et al., 2023). Whereas Duan *et al*., observed a 44% reduction in compressive strength of composite magnesium alloy rods reinforced bioglass cements after 6 weeks in SBF (Duan et al., 2020). Similarly, Lin *et al.*, observed a 20% reduction in compressive strength of magnesium modified acrylic bone cement (Lin et al., 2019) in Tris HCl solution for 60 days. The findings from the present study demonstrated the gradual degradation of SNC 72 overtime which make it as a right choice for load bearing application.

6.2.3 Non-cytotoxic nature of SNC

The cytotoxicity evaluation of SNC 72 was conducted in accordance with ISO 10993-5 using mouse fibroblast cell line L929. During contact with the cured sterile SNC cement sample, L929 cells maintained the spindle morphology and no cytotoxicity features were observed as shown in figure 6.2.7 a. The negative control also showed similar observations (Figure 6.2.7 b) and both samples were zero graded After 24h contact with the positive control stabilized PVC disc, L929 cells showed severe cytotoxicity as expected (Figure 6.2.7 c) with a grading of 4. This confirmed the non-cytotoxic nature of the cured shell nacre cement samples.

SNC 72 comprised 72wt% of shell nacre, 12wt% of SNLSM2 and TEGDMA and the complete curing of the cement favoured the non-cytotoxic behaviour. L929 cells retained the spindle morphology after 24 h contact with the cured SNC 72 cement and the observations were very similar to that of negative control. A previous study found that addition of increasing amount of calcium sulphate (40% by weight) to PMMA cement resulted in the reduction of cell viability (Chiang et al., 2021). On the other hand, addition of 72 wt% shell nacre to SNC 72 did not cause any toxicity issues due to the non-cytotoxic and cyto-compatible nature of shell nacre powder.

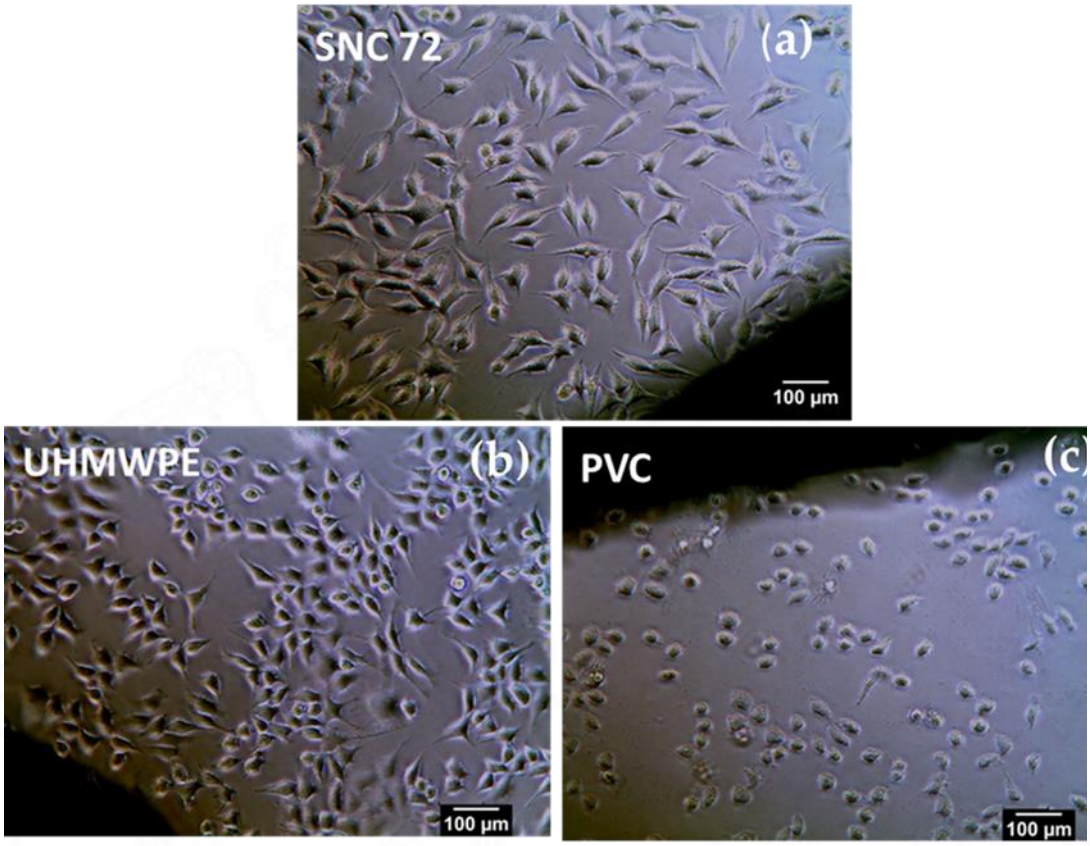

Figure 6.2.7 Cytotoxicity studies: Direct contact of SNC with L929 cells for 24 h based on ISO 10993-5(a) Shell nacre cement (SNC 72); (b) Negative control- ultra high molecular weight polyethylene (UHMWPE); (c) Positive control- Stabilized Poly Vinyl Chloride disc (PVC). Magnification 20 X. Scale bar 100 µm

6.2.4 BIOCOMPATIBILITY EVALUATION

6.2.4.1 Acute systemic toxicity

All the Swiss albino mice stayed healthy and the animals did not show any abnormalities in clinical signs after the intravenous and intraperitoneal injection of aqueous physiological saline extract (Table 6.1 and 6.2) and cotton seed oil extract (Table 6.1 and 6.2) of the SNC 72 cement sample. No mortality was recorded and increase in body weight was noted after 72 h.

Table 6.2 Common clinical signs and observation sheet–physiological saline extract of SNC 72

Clinical observation	Animals	PS of SNC 72				
		1♂	2♂	3 ♂	4♀	5♀
Body weight (g)	**Initial**	22.15	22.05	21.70	19.95	20.7
Vol. of injection	**mL**	1.1	1.1	1.1	1.0	1.0
Respiratory	**4/24/48/72 h**	N	N	N	N	N
Motor	**4/24/48/72 h**	N	N	N	N	N
Convulsion	**4/24/48/72 h**	N	N	N	N	N
Reflexes	**4/24/48/72 h**	N	N	N	N	N
Ocular signs	**4/24/48/72 h**	N	N	N	N	N
Cardiovascular signs	**4/24/48/72 h**	N	N	N	N	N
Salivation	**4/24/48/72 h**	N	N	N	N	N
Piloerection	**4/24/48/72 h**	N	N	N	N	N
Analgesia	**4/24/48/72 h**	N	N	N	N	N
Muscle tone	**4/24/48/72 h**	N	N	N	N	N
Gastrointestinal	**4/24/48/72 h**	N	N	N	N	N
Skin	**4/24/48/72 h**	N	N	N	N	N
Body weight (g)	**Final**	**24.35**	**25.6**	**24.10**	**22.85**	**22.75**

Table 6.3 Common clinical signs and observation sheet –physiological saline only

Clinical observation	Animals	PS				
		6♀	7♀	8♀	9♂	10♂
Body weight (g)	**Initial**	21.2	20.2	20.65	21.40	22.05
Vol. of injection	**mL**	1.1	1.0	1.0	1.1	1.1
Respiratory	**4/24/48/72 h**	N	N	N	N	N
Motor	**4/24/48/72 h**	N	N	N	N	N
Convulsion	**4/24/48/72 h**	N	N	N	N	N
Reflexes	**4/24/48/72 h**	N	N	N	N	N
Ocular signs	**4/24/48/72 h**	N	N	N	N	N
Cardiovascular signs	**4/24/48/72 h**	N	N	N	N	N
Salivation	**4/24/48/72 h**	N	N	N	N	N
Piloerection	**4/24/48/72 h**	N	N	N	N	N
Analgesia	**4/24/48/72 h**	N	N	N	N	N
Muscle tone	**4/24/48/72 h**	N	N	N	N	N
Gastrointestinal	**4/24/48/72 h**	N	N	N	N	N
Skin	**4/24/48/72 h**	N	N	N	N	N
Body weight (g)	**Final**	**22.95**	**22.90**	**22.05**	**24.50**	**25.05**

Table 6.4 Clinical signs and observation sheet; cotton seed oil extract of SNC 72

Clinical observation	Animals	CSO of SNC				
		1♂	2♂	3 ♂	4♀	5♀
Body weight (g)	**Initial**	22.15	21.85	21.60	20.90	20.95
Vol. of injection	**mL**	1.1	1.1	1.1	1.0	1.0
Respiratory	**4/24/48/72 h**	N	N	N	N	N
Motor	**4/24/48/72 h**	N	N	N	N	N
Convulsion	**4/24/48/72 h**	N	N	N	N	N
Reflexes	**4/24/48/72 h**	N	N	N	N	N
Ocular signs	**4/24/48/72 h**	N	N	N	N	N
Cardiovascular signs	**4/24/48/72 h**	N	N	N	N	N
Salivation	**4/24/48/72 h**	N	N	N	N	N
Piloerection	**4/24/48/72 h**	N	N	N	N	N
Analgesia	**4/24/48/72 h**	N	N	N	N	N
Muscle tone	**4/24/48/72 h**	N	N	N	N	N
`Gastrointestinal	**4/24/48/72 h**	N	N	N	N	N
Skin	**4/24/48/72 h**	N	N	N	N	N
Body weight (g)	**Final**	**25.45**	**23.15**	**24.60**	**24.25**	**23.45**

Table 6.5 Clinical signs and observation sheet; cotton seed oil only

Clinical observation	Animals	CSO				
		6♀	7♀	8♀	9♂	10♂
Body weight (g)	Initial	18.35	20.60	19.95	22.05	22.10
Vol. of injection	mL	0.9	1.0	1.0	1.1	1.1
Respiratory	4/24/48/72 h	N	N	N	N	N
Motor	4/24/48/72 h	N	N	N	N	N
Convulsion	4/24/48/72 h	N	N	N	N	N
Reflexes	4/24/48/72 h	N	N	N	N	N
Ocular signs	4/24/48/72 h	N	N	N	N	N
Cardiovascular signs	4/24/48/72 h	N	N	N	N	N
Salivation	4/24/48/72 h	N	N	N	N	N
Piloerection	4/24/48/72 h	N	N	N	N	N
Analgesia	4/24/48/72 h	N	N	N	N	N
Muscle tone	4/24/48/72 h	N	N	N	N	N
`Gastrointestinal	4/24/48/72 h	N	N	N	N	N
Skin	4/24/48/72 h	N	N	N	N	N
Body weight (g)	Final	20.55	23.45	21.70	25.70	25.55

6.2.4.2 Animal intracutaneous (intradermal) reactivity test

Table 6.6 Observation sheet

Sl. No.	Animal No/ID	Erythema/ Oedema	Observation at		
			24 h	48h	72h
1.	399 ♂	Erythema	Test site CSO: 1,1,1,1,1 PSO:0,0,0,0,0	CSO:1,1,1,1,1 PSO:0,0,0,0,0	CSO: 0,0,0,0,0 PSO:0,0,0,0,0
			Control site CSO: 0,0,0,0,0 PSO:0,0,0,0,0	CSO:0,0,0,0,0 PSO:0,0,0,0,0	CSO: 0,0,0,0,0 PSO:0,0,0,0,0
		Oedema	Test site CSO: 0,0,0,0,0 PSO:0,0,0,0,0	CSO:0,0,0,0,0 PSO:0,0,0,0,0	CSO: 0,0,0,0,0 PSO:0,0,0,0,0
			Control site CSO: 0,0,0,0,0 PSO:0,0,0,0,0	CSO:0,0,0,0,0 PSO:0,0,0,0,0	CSO: 0,0,0,0,0 PSO:0,0,0,0,0
2.	420 ♀	Erythema	Test site CSO: 1,1,1,1,1 PSO:0,0,0,0,0	CSO:1,1,1,1,1 PSO:0,0,0,0,0	CSO: 0,0,0,1,1 PSO:0,0,0,0,0
			Control site CSO: 0,0,0,0,0 PSO:0,0,0,0,0	CSO:0,0,0,0,0 PSO:0,0,0,0,0	CSO: 0,0,0,0,0 PSO:0,0,0,0,0
		Oedema	Test site CSO: 0,0,0,0,0 PSO:0,0,0,0,0	CSO:0,0,0,0,0 PSO:0,0,0,0,0	CSO: 0,0,0,0,0 PSO:0,0,0,0,0
			Control site CSO: 0,0,0,0,0 PSO:0,0,0,0,0	CSO:0,0,0,0,0 PSO:0,0,0,0,0	CSO: 0,0,0,0,0 PSO:0,0,0,0,0
3.	406♂	Erythema	Test site CSO: 1,1,1,1,1 PSO:0,0,0,0,0	CSO:1,1,1,1,1 PSO:0,0,0,0,0	CSO: 1,0,0,0,1 PSO:0,0,0,0,0
			Control site CSO: 0,0,0,0,0 PSO:0,0,0,0,0	CSO:0,0,0,0,0 PSO:0,0,0,0,0	CSO: 0,0,0,0,0 PSO:0,0,0,0,0
		oedema	Test site CSO: 0,0,0,0,0 PSO:0,0,0,0,0	CSO:0,0,0,0,0 PSO:0,0,0,0,0	CSO: 0,0,0,0,0 PSO:0,0,0,0,0

			Control site CSO: 0,0,0,0,0 PSO:0,0,0,0,0	CSO:0,0,0,0,0 PSO:0,0,0,0,0	CSO: 0,0,0,0,0 PSO:0,0,0,0,0

Table 6.7 Average irritation score

Animal No/ID	**Extract**	**Irritation score**	
		Control	SNC
1. 399 ♂	PS	0	0
	CSO	0	0.66
2.420 ♀	PS	0	0
	CSO	0	0.80
3.406♂	PS	0	0
	CSO	0	0.80
Overall Mean Score	PS	0	0
	CSO	0	0.75
Final Score		**0**	**0.75**

The intradermal injection of the physiological saline extracts of the SNC 72 sample did not cause any oedema or erythema and the average irritation score was zero. The cotton seed oil extract of the SNC 72 sample did not cause any oedema with slight erythema and the average irritation score was '0.75' (Table 6.5 and 6.6). Thus, the SNC 72 cement sample met the requirement of the test and the extracts did not cause any irritation immediately or after 24 h/48h/ 72h.

6.2.4.3 Pyrogen test

Marginal ear vein injection of the physiological saline extract of SNC 72 sample did not cause an individual rise of 0.5°C of rectal temperature which were recorded in every 30 min between 1-3 h after injection.

Table 6.8 Record of rectal temperature

Particulars	391 ♂	415♀	417 ♀
Animal body weight (g)	2010	2060	2015
Temperature 30' prior to injection °C	39.12	38.97	39.36
Volume of injection (ml)	20.10	20.60	20.15
Temperature 60' after injection °C	38.99	38.96	39.30
Temperature 90' after injection °C	38.97	39.02	39.43
Temperature 120' after injection °C	38.93	38.93	39.46
Temperature 150' after injection °C	38.97	38.84	39.41
Temperature 180' after injection °C	39.10	39.28	39.67
Rise in Temperature °C	0	0.31	0.31

Biocompatibility is ability and performance of material within in a host for the intended application(ISO 10993-1, 2018). According to the ISO standard, biological risk assessment of the SNC 72 was conducted, which involved evaluating the irritation test, material mediated pyrogen test and acute systemic toxicity. Both the physiological saline and cotton seed oil extract of SNC 72 did not induce any acute systemic toxicity in mice. In contrast, physiological saline extract of the BioCaS cement showed a transient reduction in motor activity of the mice immediately after injection and

recovered soon (Sandhya et al., 2017) whereas the Chitra CPC cement did not evoke any systemic toxicity (Fernandez et al., 2006). Further, the intradermal injection of the SNC 72 extracts did not cause any erythema or oedema in rabbits. These results were in consistent with the findings of Chitra CPC and BioCaS cement (Fernandez et al., 2006; Sandhya et al., 2017). Additionally, the PS extract of the material did not evoke any rise in rectal temperature, similar to that of BioCaS (Sandhya et al., 2017). Thus, the end points of biological safety evaluation test indicated that the SNC 72 was a biocompatible non-toxic, non-irritant and non-pyrogenic cement.

6.2.5 Osseointegration of SNC72

Both the shell nacre cement and PMMA cement were *in situ* set in the femoral cortical defect. At definite time points, animals were euthanized and the cement filled femoral bones were explanted.

6.2.5.1 Gross examination

During gross examination, it was observed that SNC 72adhered well to the bone, whereas the PMMA was loosely found in the implanted site on both 6 and 12 weeks. Similarly, no fibrous tissue or any signs of infection was seen at the implanted site of all the time periods (Figure 6.2.8).

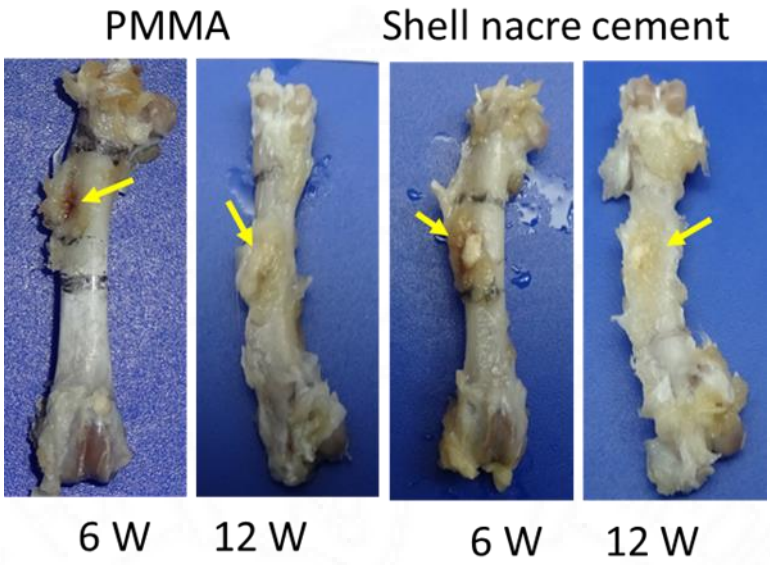

Figure 6.2.8 Gross examination of explants

6.2.5.2 Radiography

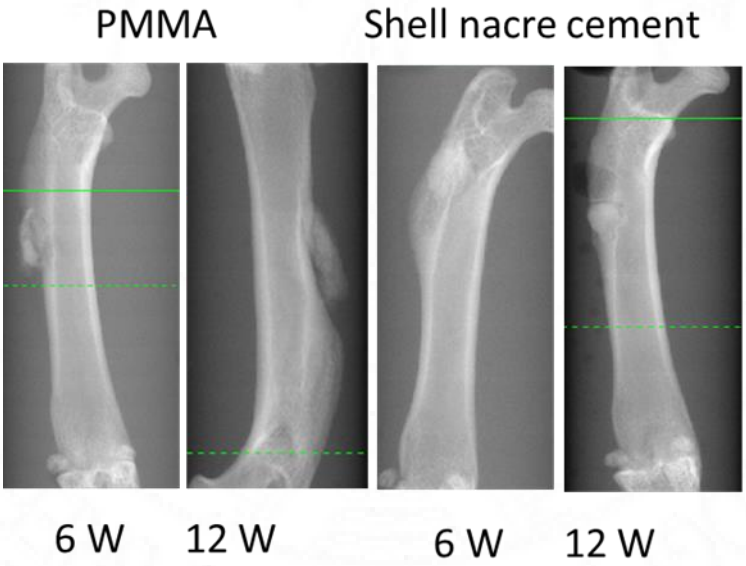

Figure 6.2.9 Radiography analysis after 6 and 12 weeks of surgery

Radiography analysis proved the osseo-integration of SNC with no radiolucent line between SNC and bone, whereas in the case of PMMA a clear radiolucent line

was seen between PMMA and bone of both 6 and 12 weeks (Figure 6.2.9). The *in situ* setting of SNC 72 in the 2mm femoral cortical defect of rats demonstrated the successful osseointegration of the material. SNC 72 adhered firmly to the bone and no signs of inflammation and infection were observed. In contrast, the clinical control PMMA cement showed evidence of poor adhesion during gross evaluation. Further, the radiography analysis confirmed the osseointegration of SNC where no radiolucent lines was observed between SNC 72 and bone. In the case of PMMA, a clear radiolucent line was observed between PMMA and bone. Similar observations were reported during the *in vivo* study of tetracalcium phosphate and whitlockite incorporated bone cement (Q Liu et al., 2023) and strontium containing borate bioactive glass incorporated bone cement (Cui et al., 2017).

SNC is biocompatible, osseo-integrative, bioactive, radiopaque, non-cytotoxic, with higher mechanical properties and exhibited low linear polymerization shrinkage and minimal exotherm generation. Therefore, the findings from the study proved that the shell nacre cement will be a potential bone void filling cement for bone defect management.

7 *IN VITRO* OSTEOGENESIS OF SHELL NACRE INTEGRATED MATERIALS WITH HUMAN BONE MARROW MESENCHYMAL STEM CELLS FROM YOUNG AND OLDER DONORS

The main objective of this study is to investigate the *in vitro* osteogenic potential of shell nacre cement (SNC) and shell nacre scaffolds SN-15 and SN-150 with BM-MSCs collected from older donors and young donors. The study began with an investigation into the cytotoxic and cytocompatibility of the samples with BM-MSC. The population doubling time and colony forming ability of all the older (n=3) and young (n=3) donors were then evaluated. Next the BM-MSCs of the older donors were pooled and similarly, the BM-MSCs from the younger donors were pooled and their cell morphology was observed. The senescence of the pooled older and younger donor BM-MSC was then studied by SA-β Gal assay. Pooled BM-MSCs from the old and young are seeded separately into SNC, SN-15 and SN-21 samples for 21-days. The presence of viable cells on the material was studied by Live cell tracker green staining. Further, the osteogenic potential of the materials was studied by scanning electron microscope- energy dispersive spectroscopy (SEM-EDS). Further, the influence of the material on the gene expression of both young and older BM-MSCs was evaluated by Q-PCR.

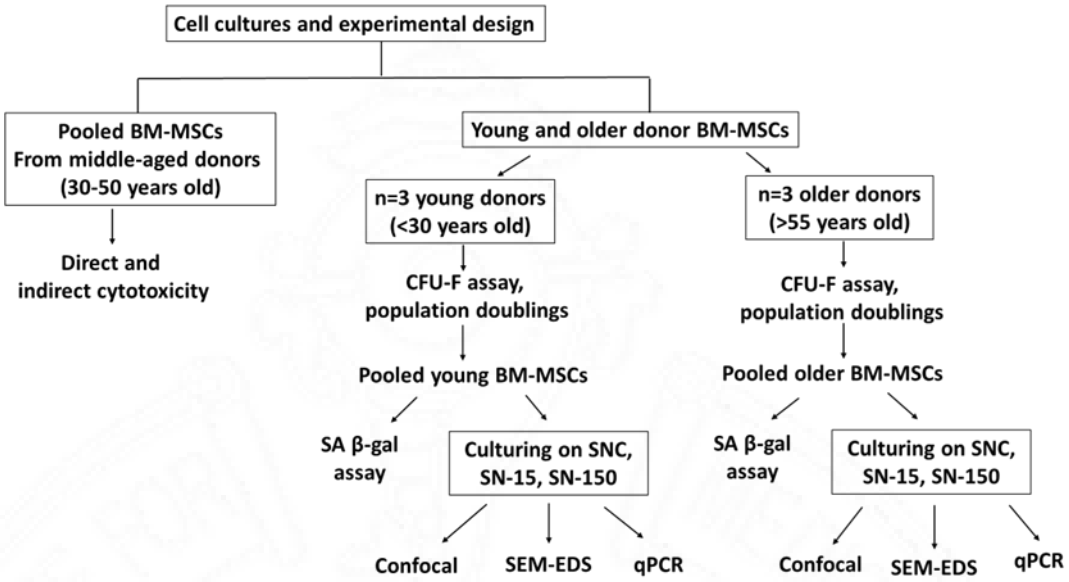

Figure 7.1. Flowchart of experimental design

7.1 MATERIALS AND METHODS

7.1.1 Samples

Cured shell nacre cement samples of size 10mm diameter x 1mm width and 4mm diameter x 1mm width, shell nacre scaffolds SN-15, SN-150 of size 10mm diameter x 1mm width and 5mm diameter x 1mm width were prepared and EO sterilized.

7.1.2 Ethical approval and donor details

Ethical approval was obtained from NREC Yorkshire and Humberside National Research Ethics Committee (06/Q1206/127 and 18/YH/0166) to collect bone marrow aspirate (BMA) samples from human donors. Frozen vials containing previously characterized BM-MSCs from donors aged between 21 and 64 years old were thawed in complete DMEM media containing 10% FBS and 1% P/S (Thermo Scientific, Loughborough, UK). The thawed cells were then cultured in StemMACS (SM,

Miltenyi Biotec, Bisley, UK) medium. The cells were expanded in culture and tracked for growth kinetics. On reaching confluency, the cells were trypsinized and used for further experiments. Out of these 10 donors, n=4 were middle age donors (aged between 30-50), n=3 was young with ages below 30 (aged between 21-26 years old), and n=3 were older donors above 55 years old (aged between 58-64 years old).

7.1.3 Direct Cytotoxicity studies

BM-MSCs from middle age donors (Figure 7.1) were used for the cytotoxicity studies. Direct contact of SNC, SN-15, SN-150 and steriStrip was studied for 1, 4, and 7 days with the BM-MSC. The monolayer of BM-MSC was taken as control. Sample movement was prevented by sticking using SteriStrip (3M), tape to avoid the disruption of the BM-MSC monolayer. After the duration, the cellular response around the material was observed for morphological changes, zone of lysis, vacuolization, membrane disruption, and cellular detachment.

7.1.4 Indirect cytotoxicity studies -XTT assay

The STEM MACS (SM) medium (Miltenyi Biotec, Bisley, UK) was used as extraction medium and the extracts were collected after 72 h, 7 days, and 14 days of contact with the sterile SNC, SN-15, SN-150 samples based on ISO standard (ISO 10993-12, 2021). Briefly, duplicate samples of SNC, SN-15, SN-150 were incubated separately in 6ml of SM media (6-well plate) and this media was then collected at 72 h, 7 days and 14 days' time points and stored as an extract at -80°C until further use. Cytotoxicity and proliferation by XTT were performed as per the manufacturer's

protocols. BM-MSCs from middle age donors (Figure 7.1) were used for the indirect cytotoxicity studies.

7.1.4.1 Cell viability

BM-MSCs were seeded at a density of 10,000 cells/well in a 96-well plate. After 24 h of incubation, the SM media was replaced with 200 µl of the SNC/ SN-15/SN-150 sample extract, 10% DMSO SM medium (positive control), and SM Medium (negative control). After 24h exposure, the treatment media were replaced with 100 µl of Dulbecco's minimal essential medium (DMEM) with 10% FCS and 50 µl of the XTT (sodium 3'-[phenylaminocarbonyl)-3,4-tetrazolium]–bis (4-methoxy-6-nitro) benzene sulfonic acid hydrate) solution (cell proliferation kit II (XTT), Roche, Germany) and incubated at dark for 4h at 37°C. The plates were then read at 450nm and 630nm (reference wavelength) and the value for the reference wave at 630nm was deducted from the 450nm to give the final optical density (OD). Test ODs were normalized to negative control ODs, to measure cell viability.

7.1.4.2 Cell proliferation

BM-MSCs were seeded at a density of 500 cells/well in a 96-well plate for 24h in SM medium. After 24 h, the SM media was replaced with 200 µl of treatment media containing either the SNC sample extract or SN-15 or SN-150, the positive control (SM media with 10% DMSO), or the negative control (SM media). Cells were then cultured for 4 days in the treatment media. After 4 days, the XTT assay was carried out as described above and analyzed to quantify cell proliferation compared to the negative control.

7.1.5 Culture and expansion of older and young donor BM-MSCs

BM-MSCs collected from donors under the age of 30 were taken as young donors (n=3) and above 55 as older donors (n=3) (Table 7.1). On reaching confluency, the cells were trypsinized and used for further experiments.

Table 7.1 List of donors used during the study

Sex	Age
Female	64
Male	59
Male	58
Male	22
Male	21
Male	26

7.1.5.1 Calculation of population doubling time

The population doubling (PD) of the individual donors hBM-MSC was studied from the passage 0 (P0) to passage 4 (43) using the formula $\log_2$(cells trypsinized/ cells seeded) and the average cumulative population doubling of young (n=3) and older donors (n=3) were compared.

7.1.5.2 Colony forming unit-fibroblast (CFU-F) assay

CFU-F assay was performed as previously described (El-Jawhari et al., 2017; Ganguly et al., 2019). $2x10^3$ BM-MSCs were seeded in duplicate into 100mm Petri dishes (Corning, New York) containing 10 ml SM media and cultured for 2 weeks as per the standard colony forming unit fibroblast (CFU-F) assay protocol. After 24 to 48 hours, complete media was changed, and half media change was performed twice a week. After the duration, media was removed, washed in PBS, fixed with 3.7% formaldehyde (Fisher Scientific, Loughborough, UK), and stained with 1% w/v methylene blue (Sigma, Dorset, UK). The plates were allowed to dry and then scanned at 1200 dpi for further analysis.

7.1.5.3 Analysis of colony area and integrated density

The colony area and integrated density of the scanned duplicate images of all the donors were further analyzed using Image J. Scanned images were converted into 8-bit images and calibrated. Each colony was selected manually and simultaneously both colony area and density were calculated. Compared the colony area and density between young and older donors by Mann Whitney test using GraphPad prism (version 9.5.1). The data were shown as violin plots.

7.1.6 Studies with pooled older and young donor BM-MSC

7.1.6.1 Cell morphology

After studying the colony-forming ability of individual donors, the older donors (n=3) and young donor(n=3) BM-MSCwere pooled separately at passage 3. Both the

pooled older donor BM-MSC and young donor BM-MSC were observed using phase contrast microscopy.

7.1.6.2 Senescence-associated beta galactosidase (SA-β-gal) assay

4×10^4 BM-MSCs from each sample were plated in duplicate wells of a 6-well plate overnight for adhesion in 1.5 ml of SM medium. After 24 h, the media was removed and the cells were washed in PBS. Then the cells were fixed using fixation buffer (1.5 ml) and incubated for 6–7 min at room temperature (RT). Followed by the wash with PBS and the cells were stained X-Gal staining mixture (1 ml) prepared as per the manufacturer's protocol (Sigma Aldrich, USA). The dishes were then sealed in parafilm and incubated at 37°C without CO_2 overnight. Next day, the cells were observed for the presence of blue (or SA-β-gal positive cells) under light microscopy. The cells were counted using the multi-point option in Image J.

7.1.6.3 In vitro osteogenesis experiments

$3x10^4$ BM-MSCs were loaded to the SN-15, SN-150 and preconditioned SNC samples, (triplicates) for microscopy studies. $1x10^6$ cells were seeded on the materials (triplicates) for Q-PCR in 24-well plates and incubated for 1 hour. After the incubation, the samples were moved to a low-attachment 24 well plate and cultured for up to 7 days with SM medium. After the cell attachment, the SM Media was replaced with OsteoDIFF Media (Milteny Biotech) for up to 14 days and half media change was performed twice weekly.

7.1.6.4 Live cell tracker green staining

The SNC samples, SN-15, SN-150 samples with cells were stained with cell tracker green (Thermo Scientific) to check the viability of BM-MSCs and cytocompatibility of the materials on day 7 and 21. The cell tracker green working medium was prepared by adding 10µl of cell tracker green solution (50µg Cell tracker green/ 10µl of DMSO) to 15 ml of serum free DMEM Medium. The cell tracker green working medium was added enough to cover the samples and allowed to stain for 30 mins at 37°C and 5% CO_2. Subsequently, the samples with cells were imaged using confocal microscopy (Leica TCS SP8 confocal microscope).

7.1.6.5 SEM EDS study

SEM-EDS analysis (Hitachi S-3400 N with Bruker ESPIRT SYSTEM) of the above samples after 14 days of osteo-induction was carried out after dehydrating the samples in different grades of ethanol from 30% to 100%. The material without cells were taken as controls.

7.1.6.6 Influence of SNC, SN-15, SN-150 on the gene expression of young and older BM-MSC

$1x10^6$ cells were loaded into the samples, as mentioned in 2.8.1. On days 14, the samples with BM-MSCs were treated with 350 µl of Buffer RL to lyse the cells inside the scaffolds with strong agitation using vortex over ice to ensure removal of all the cells with their genetic contents and prevent the RNA from degradation. Briefly, RNA was extracted from the cells from the scaffolds collected in the buffer RL using the column method per the kit protocol (Total RNA purification kit, Norgen Biotek, Canada). Reverse transcription was performed using reverse transcriptase master mix

(Fluidgm) to convert the extracted RNA into cDNA. The cDNA was pre-amplified with the pooled Taqman assay and the preamplification reaction mix for 14 cycles (95°C – 2 min, 95°C – 15 s, 60°C – 4 min, hold at 4°C) using Fluidigm.

The 48.48 chip was primed, and the sample (diluted pre-amplified cDNA) and assay (Taqman assays) mix were loaded into the respective compartments. The chip was then run on the Biomark real-time PCR system using a GE 48 × 48 standard protocol (Ganguly, El-Jawhari, et al., 2022; Ganguly, Fiz, et al., 2022; Sanjurjo-Rodriguez et al., 2020). Gene expression was performed for 48 genes (the panel associated with MSC function, Supplementary) using standard Taqman assay (Thermofisher Scientific) and the 48.48 integrated fluidic chip (IFC) with the manufacture recommended reagents and protocols (Fluidigm corporation, USA). Hypoxanthine phosphoribosyl transferase1 (HPRT1) was used as a housekeeping gene (Ganguly, Fiz, et al., 2022). The cycle threshold (ct) values of the gene of interest were normalized to the housekeeping gene, and the fold expression of the genes was calculated using the formula $2^{-\Delta\Delta Ct}$ where ΔΔCT= ΔCT of the target gene of the test - ΔCT of the target gene of control (BM-MSCs only).

The fold expression of the genes was filtered and adjusted with log transform data. Hierarchical clustering of the genes was performed by the complete linkage method and the similarity metric used was Spearman rank correlation method. The gene clustering was done with Cluster 3.0 software. The resulting heat maps are visualized using Java Tree View software.

7.1.7 Statistics

All statistical analysis were performed using GraphPad Prism software (version 9.5.1). Mann Whitney Test was used to analyze the unpaired data. Further unpaired t test ordinary ANOVA (analysis of variance) was used to compare between the mean of the data. The differences between mean were statistically significant only if $p \leq 0.05$. The symbols used to indicate the level of significance were as follows: ns - $p>0.05$, * - $p\leq 0.05$, ** - $p<0.01$, *** - $p<0.001$, **** - $p<0.0001$.

7.2 RESULTS AND DISCUSSION

Senescence in bone is elicited by oxidative stress, altered mitochondrial metabolism, aberrant epigenetic modification, DNA damage, telomere dysfunction, heterochromatin changes, mutation and oncogene expression. All of these factors contribute to the ageing of bone microenvironment (Chen et al., 2016; Pignolo et al., 2019; Ganguly et al., 2019). Both *in vitro* and *in vivo* studies have shown a shift towards adipogenesis rather than osteogenesis in older BM-MSCs (Meunier et al., 1971; Justesen et al., 2001; Nuttall et al., 1998; Rodríguez et al., 2000; Stolzing et al., 2008; Zhou et al., 2008). Therefore, it is crucial to evaluate the osteogenic potential of any bone substitute material with senescent BM-MSCs of older donors. Hence, only after confirming the osteogenic potential with older BM-MSCs, a bone substitute material would be considered truly osteogenic. *In vitro* osteogenesis of PCL nanofibrous mat, graphene-incorporated methacrylate gelatin, and rattan wood have been studied with older BM-MSCs. However, it is important to note that in all of these studies, the senescence of older BM-MSCs was not investigated or confirmed (Ganguly, El-Jawhari, et al., 2022; Li et al., 2005, 2021). This *in vitro* study is the first

to compare the osteogenic potential of the SNC, SN-15 and SN-150 samples using senescent older donor BM-MSC and young donor BM-MSC.

7.2.1 Direct cytotoxicity studies

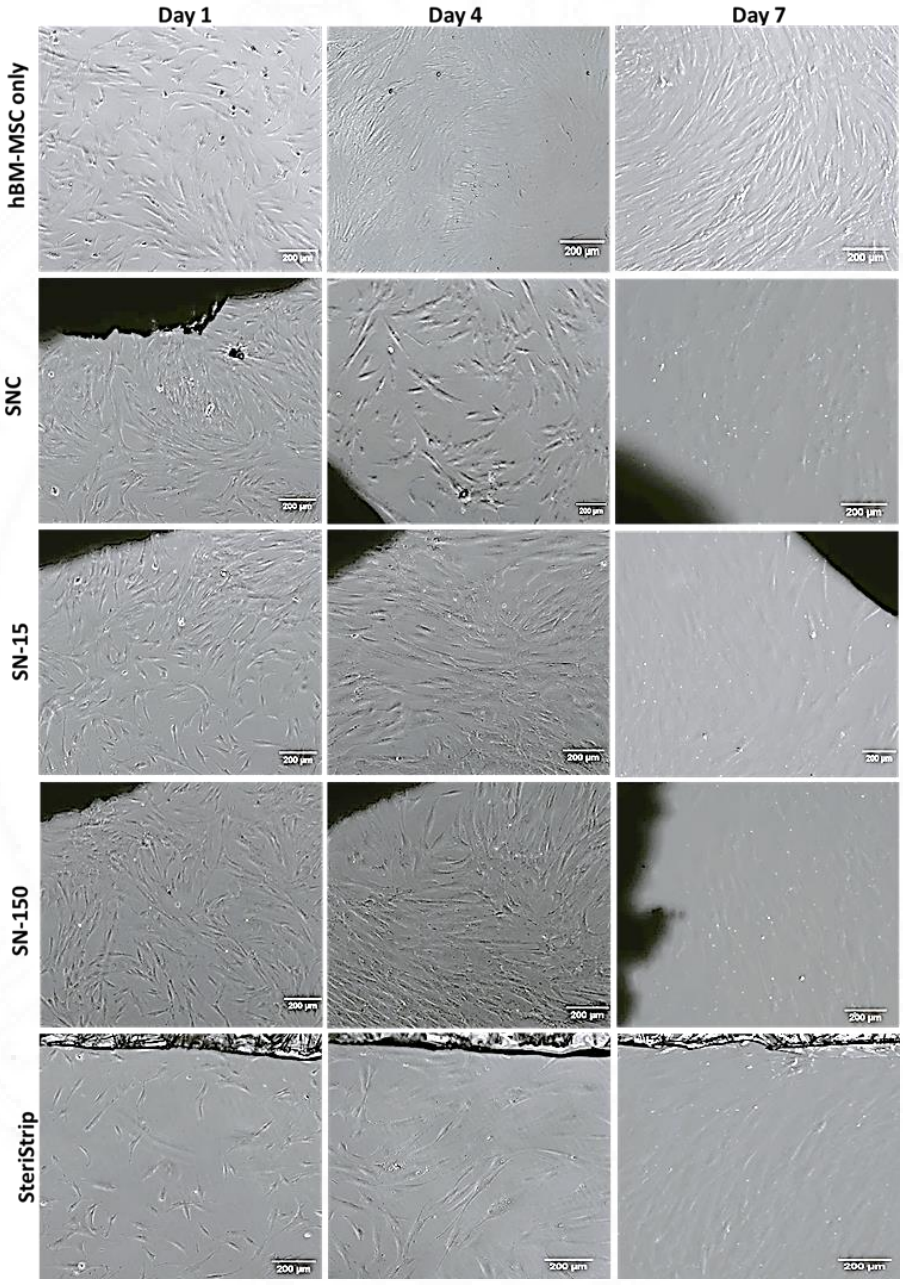

Figure 7.2.1 Direct cytotoxicity: Light microscopy images of direct contact of shell nacre cement samples and SteriStrip (used to stick the samples) with BM-MSCs for up to 7 days. Scale bar represents 200µm

Direct contact studies of the SNC, SN-15, SN-150 samples (Figure 7.2.1) with BM-MSCs showed no signs of cytotoxicity up to 7 days. After contact with the SNC, SN-15, SN-150 samples, BM-MSCs retained the spindle morphology and the cell morphology was similar as seen in the cell only control. The cells were found very close contact and attached to the samples and no zone of lysis was observed. Likewise, SteriStrip also showed no features of cytotoxicity in all durations. During day 7 observation, the monolayer was highly confluent and the same features was seen in cell only control, SteriStrip and SNC, SN-15 and SN-150 samples. All these seven-day observation indicated the non-cytotoxic nature of the SNC, SN-15 and SN-150 samples.

7.2.2 Indirect cytotoxicity studies

The cell viability studies were conducted with the SNC/ SN-15/SN-150 sample extract for a duration of 24 h. The cells were exposed to the sample extracts for 24h and the viability was assessed at the end of this period to determine if the extracts had any toxic effects on the cells.

Cell viability (%) of BM-MSCs (Figure 7.2.2) was more than 90% for all the sample extract and similar to the negative control whereas the 10% DMSO medium exerted 42.8% as expected. On the other hand, the cell proliferation studies were carried out for longer duration of four days with SNC/ SN-15/SN-150 sample extract. After 4 days of contact, the cell proliferation (%) of BM-MSCs (Figure 7.2.3) was more than 88% for all the sample extract and STEM MACS medium whereas the 10% DMSO medium showed only 43.7% as anticipated**.**

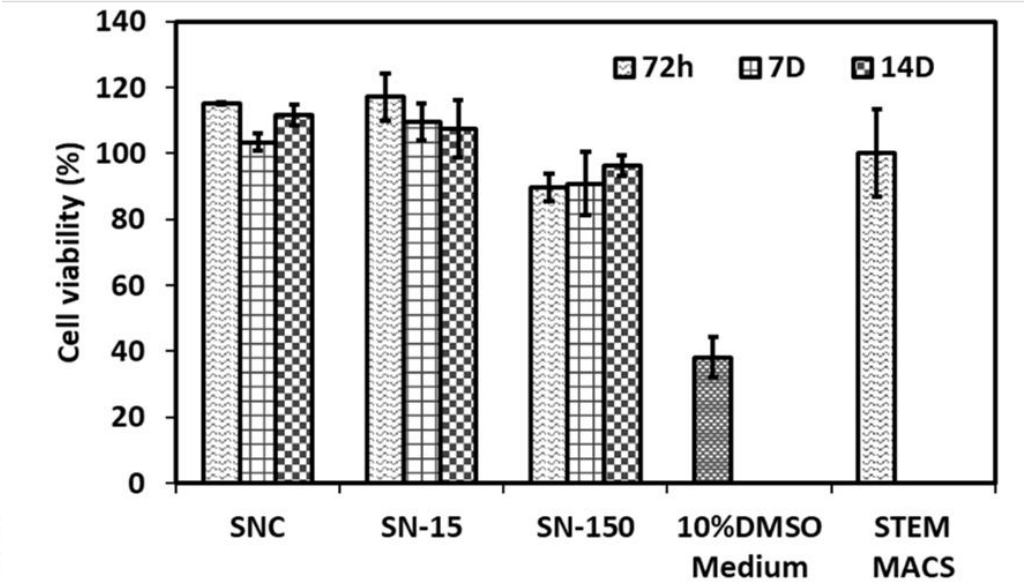

Figure 7.2.2. Indirect cytotoxicity with BM-MSCs: Cell viability (%) of BM-MSCs after 24 h contact with sample extract of SNC, SN-15, SN-150 collected after 72 h, 7 day, and 14 days. Controls are DMSO medium and SM medium

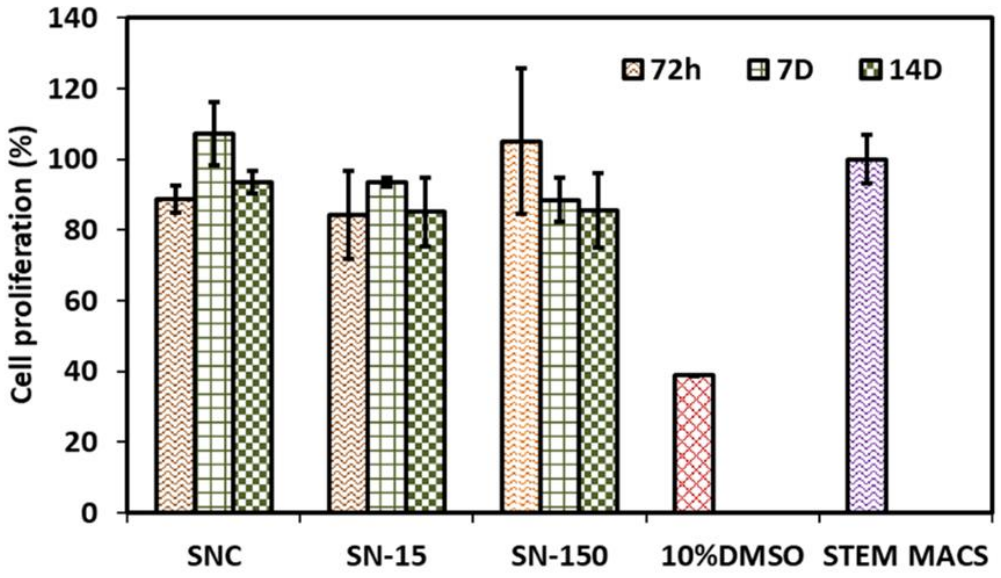

Figure 7.2.3. Indirect cytotoxicity with BM-MSCs: Cell proliferation % of BM-MSCs after 4 days contact with sample extract of SNC, SN-15, SN-150 collected after 72 h, 7 day, and 14 days. Controls were 10% DMSO medium and SM medium

7.2.3 Culture and expansion of older and young donor BM-MSCs

BM-MSCs collected from donors less than 30 years of age were categorized as young and while those obtained from donors over the age of 55 were classified as older. This classification was based on the fact that bone formation continues until mid-twenties (Breeland et al., 2023). It was reported that the fitness of BM-MSCs declines with advancing age, resulting in changes in both proliferative capacity and morphology. Hence, the population doubling time and CFU-F analysis were carried out.

7.2.3.1 Calculation of population doubling time

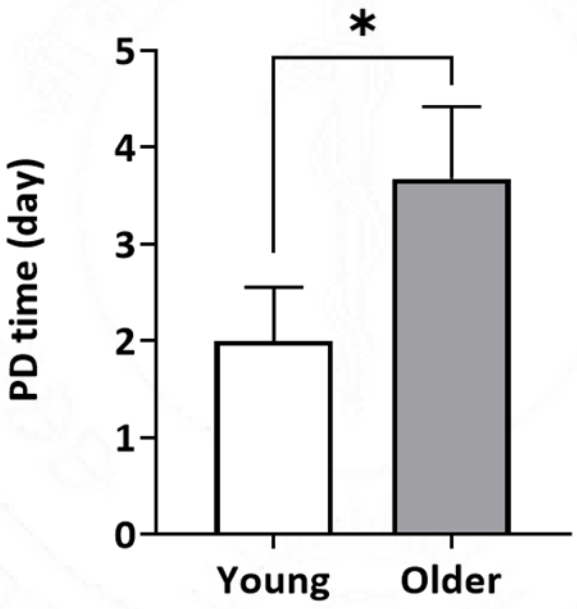

Figure 7.3.1 Older donor BM-MSCs exhibited significantly higher population doubling time than young donor BM-MSCs. Unpaired t test. Two tailed, p=0.0334

Both the young and older donor BM-MSCs were grown from P0 to P4. From the estimated number of cells seeded and trypsinized, the population doubling time was

calculated. The cumulative population doubling with respect to cumulative days were calculated for all the donors. The average cumulative population doubling time (Figure 7.3.1) of older donor BM-MSCs were significantly higher than the young donor BM-MSCs (Unpaired t test p=0.0334). This finding is consistent with previous studies that have reported a longer PD time for older donor BM-MSCs (Carvalho et al., 2021; Zhou et al., 2008).

7.2.3.2 CFU-F assay

The CFU-F assay was carried out in duplicate for all the donors to increase the reliability and validity of the result. During visual comparison, all the methylene blue stained CFU-F plates (Figure 7.3.2 a) of young donor BM-MSCs were more intense when compared to the older donor BM-MSCs. Further, Image J analysis of the all the scanned CFU-F plates confirmed the same where the colony area (Figure 7.3.2 b) and colony integrated density (Figure 7.3.2 c) of young donor BM-MSCs were better than older donor BM-MSCs.

During the colony analysis of CFU-f assay, the significant reduction in the colony area and integrated density was observed indicating a decrease in the proliferation potential of the older donor BM-MSC. This findings were similar with the previous report highlighting the reduction in proliferative capacity of BM-MSC from older donors (Ganguly et al., 2019).

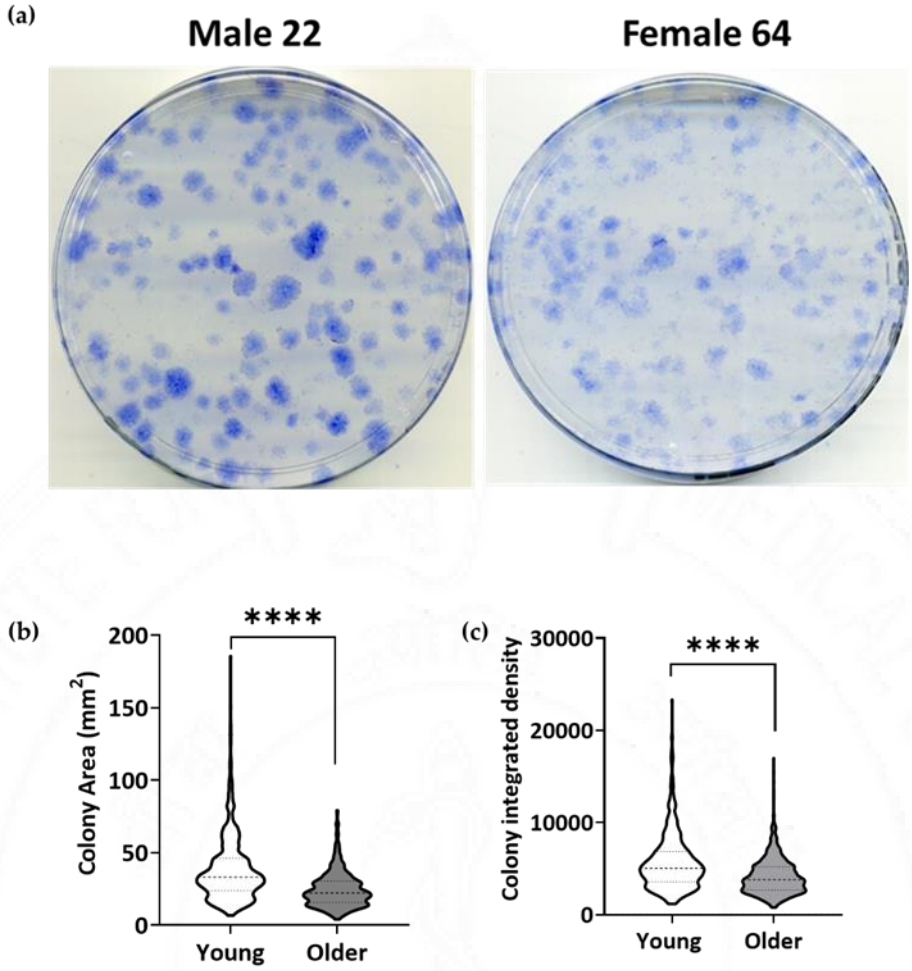

Figure 7.3.2 CFU-F assay: a) Representative images of methylene blue stained CFU-F plates b) Violin plots showing the colony area and d) colony density of BM-MSC of young (n=3) and older donors (n=3 Mann Whitney test **** - $p < 0.0001$

7.2.4 Studies with pooled young and older donor BM-MSCs

7.2.4.1 Cell morphology

Both the young (n=3) and older donor BM-MSC (n=3) were pooled separately to minimize donor variation within the groups. Microscopic images (Figure 7.4.1) of pooled older donor BM-MSCs showed the presence of large flattened cells whereas the young donor BM-MSCs exhibited the normal elongated spindle shaped cells. Alterations in cell morphology is a sign of senescence and similar observation was documented in a previous study (Asumda and Chase, 2011).

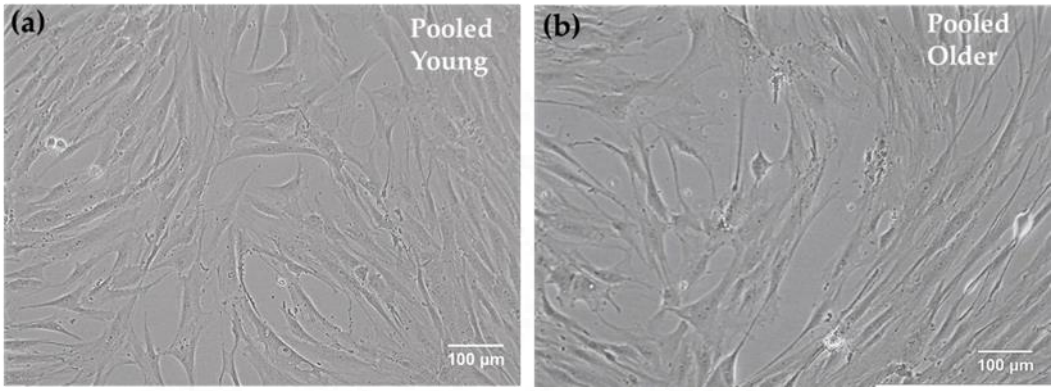

Figure 7.4.1 Microscopic images of pooled cultures. The pooled young BM-MSCs depicted the spindle-shaped morphology whereas the pooled older cultures showed the large flattened morphology. The scale bar represents 100 µm (10X).

7.2.4.2 SA-β gal assay

Both the pooled young and older donor BM-MSCs were subjected to SA-β Gal staining procedure. The percentage of blue-colored β-galactosidase positive cells in pooled older donor BM-MSC (65%) was significantly higher than pooled young donor BM-MSC (35%) (Figure 7.4.2 c). β- galactosidase is a marker of cellular senescence and SA-β gal assay is a widely accepted procedure to study the senescence of any cells (Debacq-Chainiaux et al., 2009). It was reviewed that β-gal positive cells exhibited the features of senescence-like shortening of telomeres and higher expression of phosphorylated inhibitor of cyclin depended kinase 4A ($p16^{INK4a}$) (Liu et al., 2020). In the current experiment, it was found that 65% of older BM-MSCs were β-gal positive, indicating cellular senescence, and this percentage was significantly higher than the young BM-MSCs. These results are consistent with previous studies which reported a high number of β-gal positive cells in older donor BM-MSCs (Block et al., 2017; Chen et al., 2019; Zhou et al., 2008). Therefore, low proliferation, large flattened morphology and β-gal positivity indicated the senescence of older donor BM-MSC.

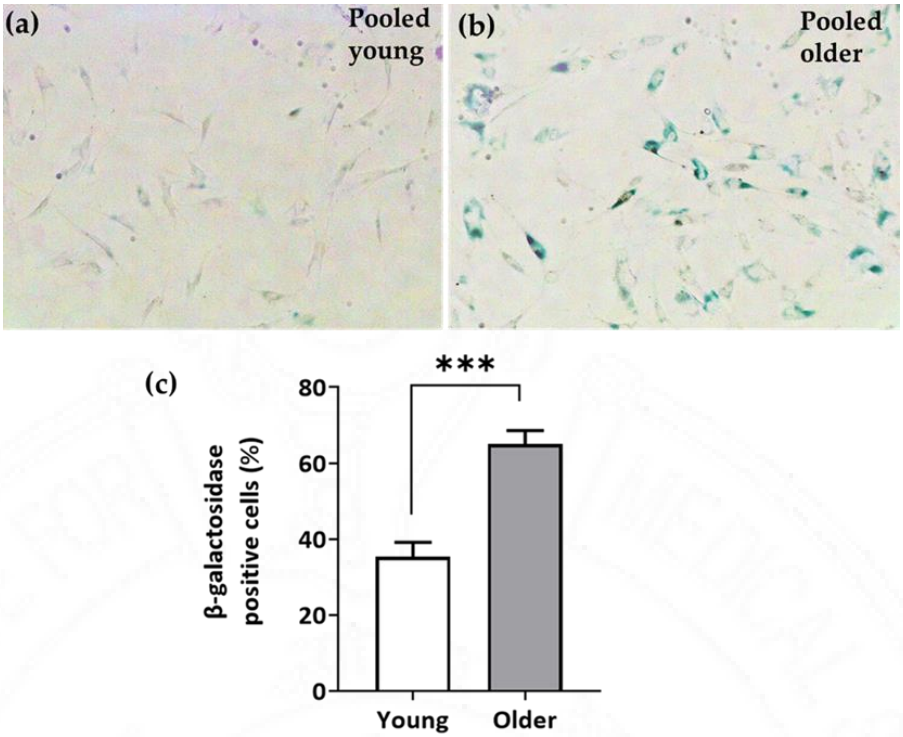

Figure 7.4.2 SA-β Gal assay: a) Representative microscopic images of the pooled young donor BM-MSC and b) pooled older donor BM-MSC after the staining procedure; c) The percentage of blue-coloured β-galactosidase positive cells in pooled older donor was significantly higher than pooled young donor BM-MSCs. Unpaired t test. Two tailed, *** p=0.0006. Data are shown as mean and standard deviation of the mean

7.2.5 *In vitro* osteogenesis

7.2.5.1 Cell Tracker Green staining

Confocal imaging of cell tracker green stained SNC samples with cells on days 7 and 21 confirmed the presence of viable young and older donor BM-MSCs in both groups. During the day 7 observation (Figure 7.5.1), both the older and young donor BM-MSCs demonstrated excellent attachment and seen as a distinct layer of cells over the samples. However, during the day 21 observation, only a smaller number of pooled young donor BM-MSCs were observed on the SNC sample, whereas a noticeable group of cells were observed in the case of older donor BM-MSCs. Similarly, both the young and older donor BM-MSCs remained viable in the SN-15 (Figure 7.5.2) and

SN-150 (Figure 7.5.3) sample for up to 21 days. However, a smaller number of young BM-MSCs were seen on day 7 observation in SN-150 samples.

Overall, all the SNC, SN-15 and SN-150 samples were cell friendly and both young and older donor BM-MSC survived in the sample for up to 21 days. However, on day 7, a small number of young BM-MSCs were observed in SN-150. This decrease in cell number could be attributed to the potential draining of cells during the loading process. Furthermore, a smaller number of young donor BM-MSCs on day 21 in SNC samples could be detachment of cells when highly confluent or as a result of osteo-differentiation of the BM-MSCs and complete mineralization, leading to fewer viable young BM-MSCs remaining in the SNC sample.

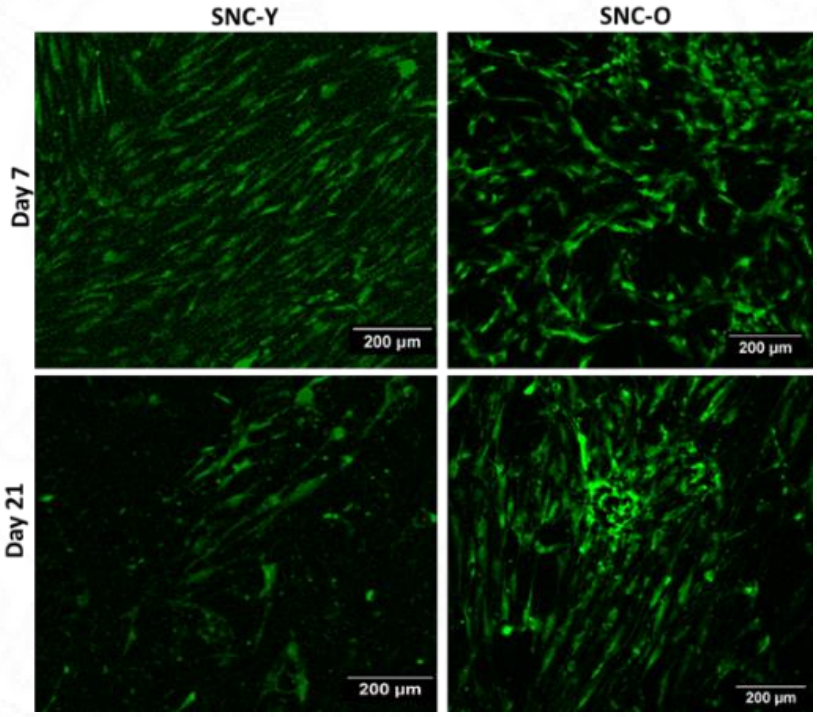

Figure 7.5.1 Confocal microscopy images on day 7 and 21 days after staining with cell tracker green indicated the presence of viable BM-MSCs in SNC samples. Scale bar represents 200 µm.

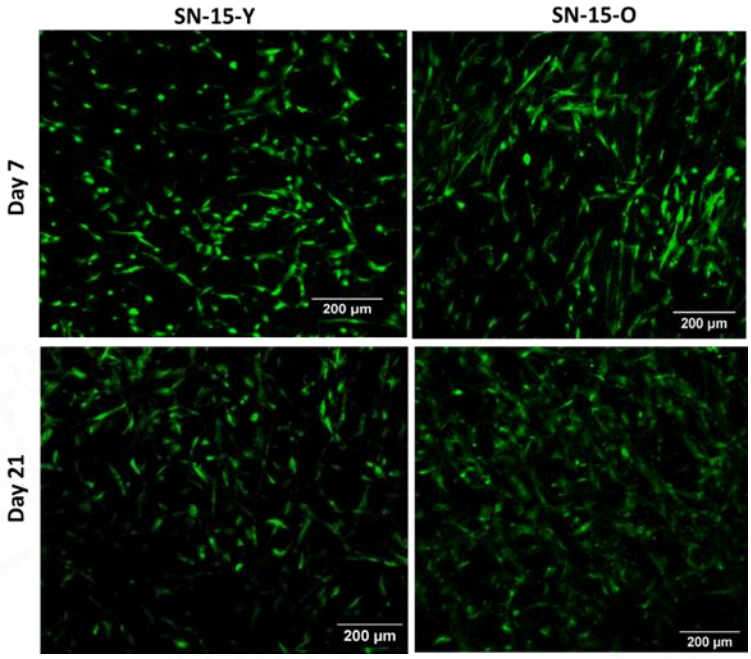

Figure 7.5.2 Confocal microscopy images on day 7 and 21 days after staining with cell tracker green indicated the presence of viable BM-MSCs in SN-15 samples. Scale bar represents 200 µm

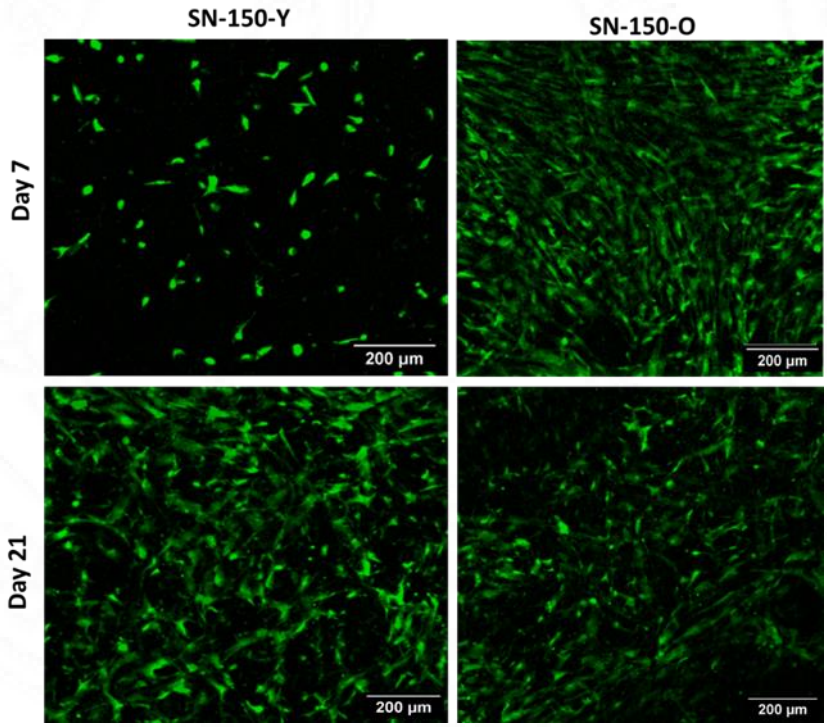

Figure 7.5.3 Confocal microscopy images on day 7 and 21 days after staining with cell tracker green indicated the presence of viable BM-MSCs in SN-150 samples. Scale bar represents 200 µm

7.2.5.2 SEM-EDS study

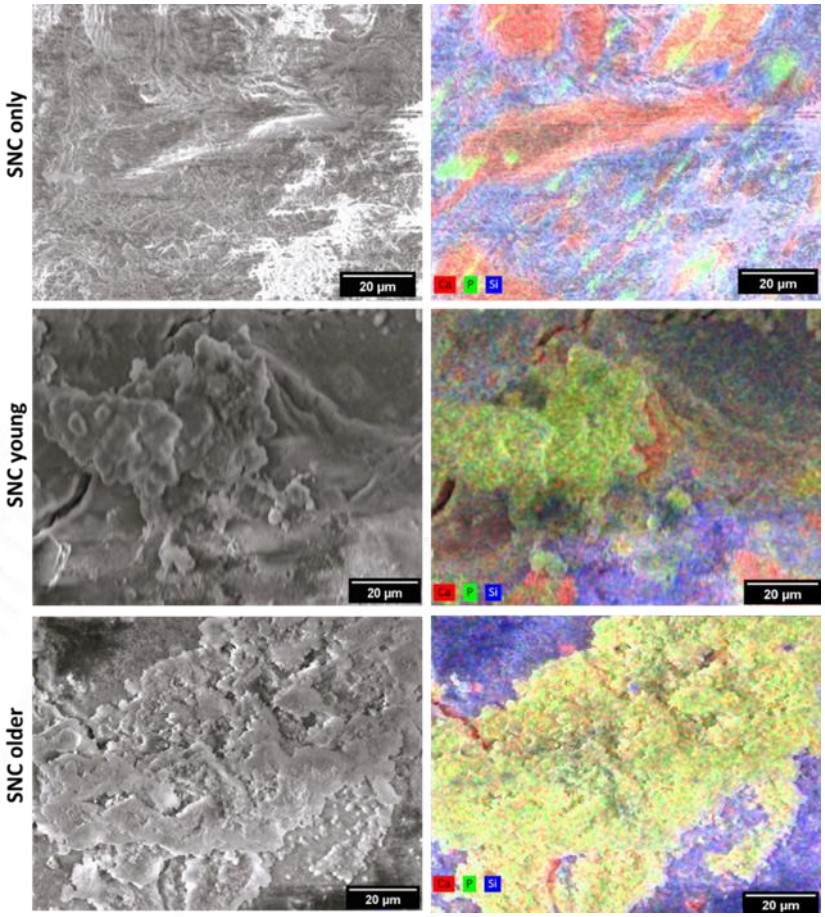

Figure 7.6.1 SEM-EDS imaging of the SNC 72 samples exhibited hydroxyapatite mineralization in both the young and older donor BM-MSCs on day 14. The colour code of the image is as follows: red represents calcium, green represents phosphorous and blue represents silicon. The scale bar represents 20µm.

In vitro mineralization of differentiated BM-MSCs was investigated using SEM-EDS. SNC 72 samples without the cells served as the material control and underwent the same treatment medium as of SNC 72 with young donor BM-MSC and older donor BM-MSC. Remarkable hydroxyapatite mineralization was observed in both the SNC samples with young and older donor BM-MSCs (Figure 7.6.1).

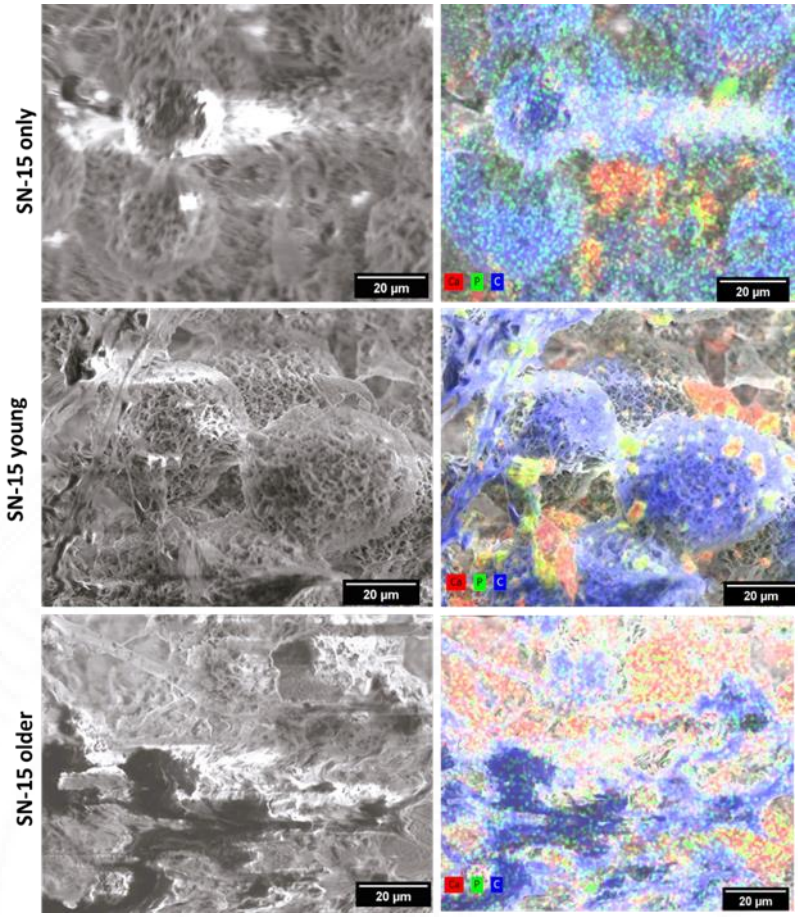

Figure 7.6.2. SEM-EDS imaging of the SN-15 samples indicated hydroxyapatite mineralization in both the young and older donor BM-MSCs on day 14. The colour code of the image is as follows: red represents calcium, green represents phosphorous and blue represents silicon. The scale bar represents 20µm.

In the SN-15 group, the material control was SN-15 samples without cells and subjected with the same treatment as SN-15 young and SN-15 older. Both the SN-15 young and SN-15 older showed calcium phosphate mineralization (Figure 7.6.2). Similarly, in the case of SN-150 group, SN-150 without cell was the control used and no mineralization was seen even after the same treatment medium. Both the SN-150 young and older donor BM-MSC showed hydroxyapatite mineralization (Figure 7.6.3).

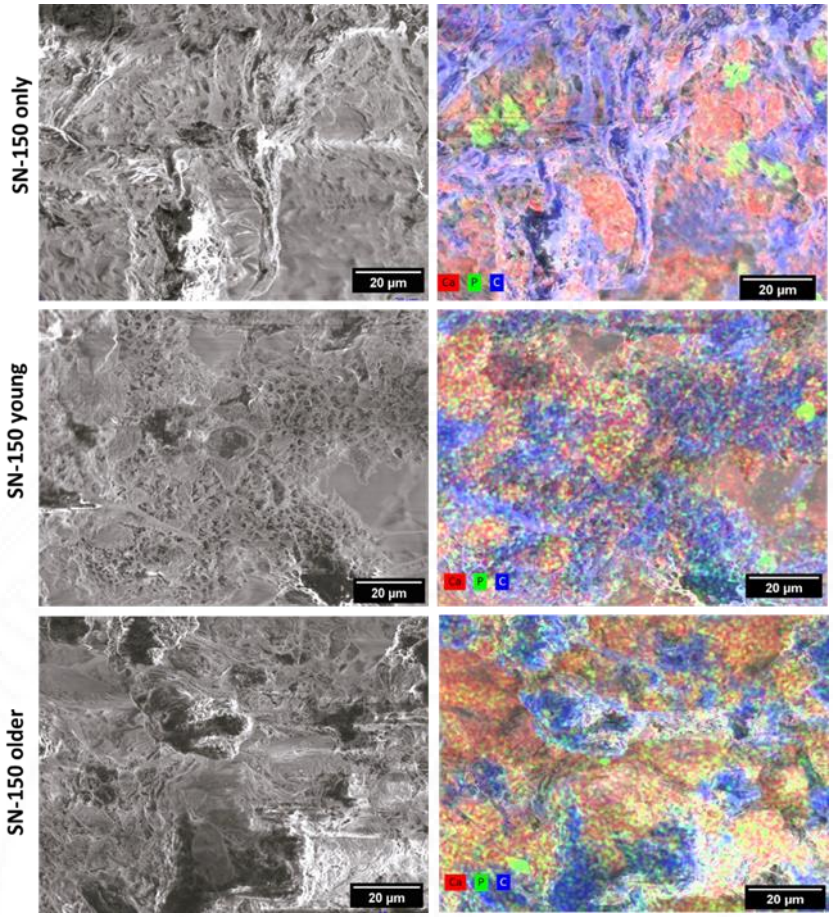

Figure 7.6.3 SEM-EDS imaging of the SN-150 samples exhibited hydroxyapatite mineralization in both the young and older donor BM-MSCs on day 14. The colour code of the image is as follows: red represents calcium, green represents phosphorous and blue represents silicon. The scale bar represents 20µm.

Among the three materials, SNC showed higher mineralization compared to SN-15 and SN-150. Since, SNC was a flat and non-porous material, hydroxyapatite mineralization was clearly observed. On the other hand, SN-150 had 35% porosity, whereas SN-15 had 70 % porosity. During confocal imaging, cells were observed inside the scaffold for both SN-15 and SN-150. Consequently, during the surface imaging with SEM, less hydroxyapatite mineralization was observed in SN-15 and SN-150 compared to SNC 72. However, all the three materials, SNC 72, SN-15 and SN-150 samples demonstrated hydroxyapatite mineralization, providing evidence for

the osteogenic potential of the materials and osteo-differentiation of both the young and older donor BM-MSCs.

Previous studies reported that the senescent older donor BM-MSCs were committed towards adipogenesis lineage rather than osteogenesis (Stolzing et al., 2008; Zhou et al., 2008). In addition to the decline in the quality and quantity of the BM-MSC, the microenvironment of the bone is reversed during ageing (Block et al., 2017). In this study, both the shell nacre integrated cement and scaffolds, induced osteo-differentiation of both young and older donor BM-MSCs with the evidence of hydroxyapatite mineralisation. Although the older donor BM-MSCs were more senescent than the young, SNC 72, SN-15 and SN-150 samples enriched the microenvironment and the older donor BM-MSCs performed equivalent to the young donor BM-MSC in cell attachment and osteogenesis.

7.2.5.3 Influence of SNC 72, SN-15, SN-150 on the gene expression of young and older donor BM-MSC

The effect of SNC 72, SN-15, SN-150 on the gene expression of young and older donor BM-MSCs was studied on day 14 and 21. All the SNC 72, SN-15, SN-150 with young donor BM-MSC and older donor BM-MSC were subjected to the osteo-differentiation medium. Two set of cells only controls were maintained for young donor BM-MSC and older donor BM-MSC for the day 14 and 21. One set of cells only control was treated with SM medium and the other set with osteo-differentiation medium. The fold expression was calculated by the ΔΔ CT method. The fold expression of the test was normalized with HPTR1 and the target gene of the cell only control with osteo-differentiation medium to assess the effect of SNC 72/ SN-15

and SN-150. Hierarchical clustering of the genes was performed by complete linkage method using the Spearman rank correlation method (similarity metric).

Three clusters were seen both in samples and genes (Figure 7.7). The first small cluster (pink box) consisted of the samples SN-15 YW3 and SN-150 Y W3. This was followed by the large middle cluster, which included all the week 2 samples of young and older donor BM-MSC with SNC 72, SN-15 and SN-150. The third sample cluster (yellow) comprised the week 3 samples of older donor BM-MSC with SNC, SN-15 and SN-150. Among the gene clusters, first large gene cluster (SNC O W3, SN-15 O W3 and SN-150 O W3) which showed the higher expression of the genes involved in osteogenesis (BGLAP, Col I A1, SPARC, ANKH, ALP, OMD, RUNX2), cartilage homeostasis (COMP, SERPINE1, ADAMTS4, TIMP1, TIMP2, TIMP3 and MMP-2), angiogenesis (CXCL2 and VEGF A) and autocrine support of BM-MSC (TGFBR2, PDGFRB and FGFR2). The middle gene cluster included the late genes of osteogenesis such as IBSP, OPN, PDPN and the cartilage homeostasis gene MMP-13. Further, both the young and older donor BM-MSC expressed the positive stem cell marker CD 73 and CD 90, irrespective of material interaction, The third gene cluster included the expression of genes such as Col10 A, SOX9, MMP-3, BMP-2. EGFR and GREM1 of all the week 2 samples of young and older donor BM-MSC with SNC, SN-15 and SN-150. These genes were not expressed by the cluster 3 samples. Similarly, the expression of the genes PPAR-γ (marker of adipogenesis) and the cell cycle controls (P53, P16, P21) were completely absent in cluster 3 samples. This indicated the arrest of proliferation and higher level of ossification (endochondral).

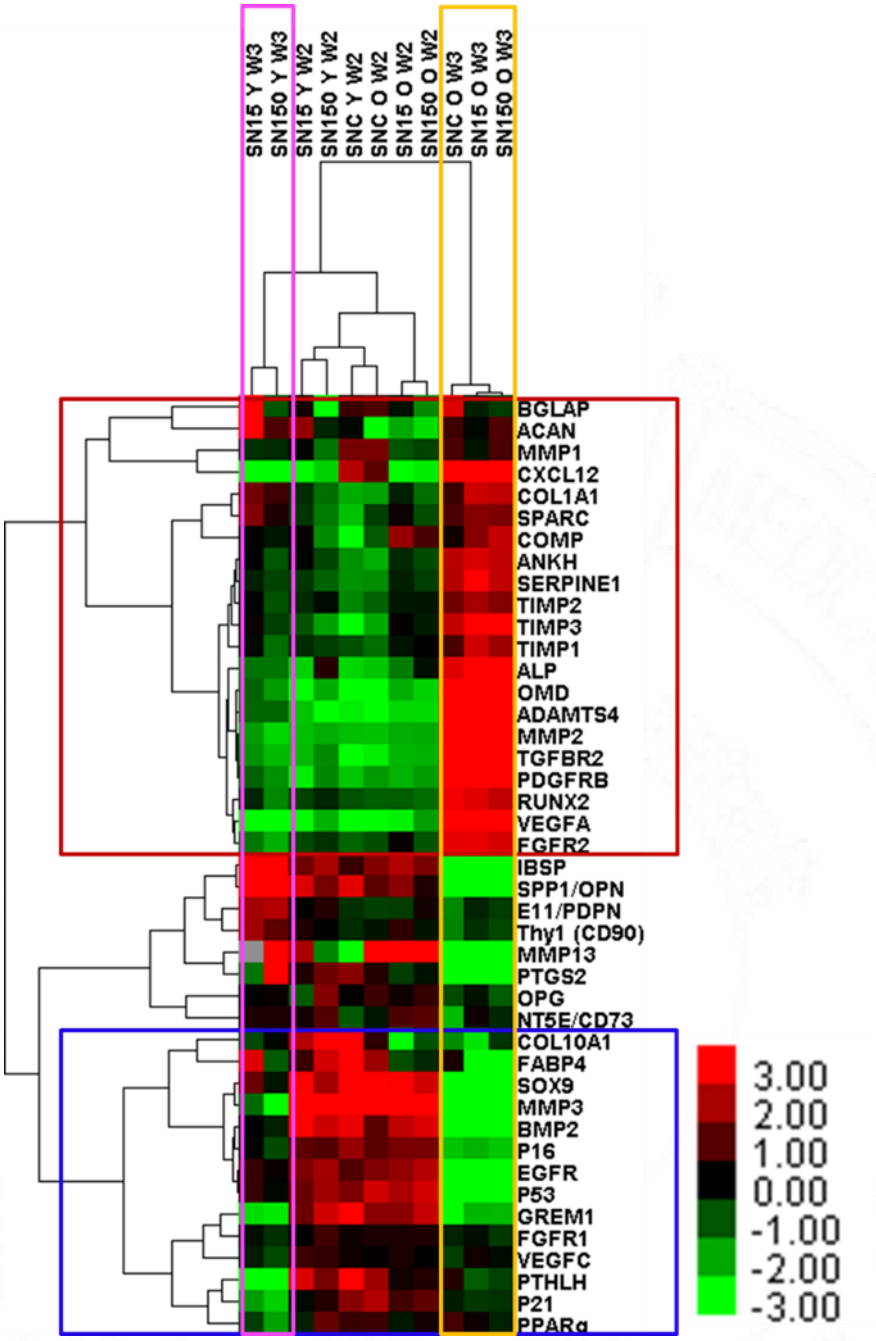

Figure 7.7 Hierarchical clustering of the gene by complete linkage (Spearman rank correlation method) Each row represents gene and the gene names are shown on the right side. Each columns represents samples and sample names are shown on the top. The gene expression levels are represented by color scale, ranging from red for the highest and green for the lowest expression. Data are shown as heat map with average value (n=2) of fold expression

Gene expression studies demonstrated the osteogenic potential of SNC, SN-15 and SN-150 with the proof of high expression of the transcription factor RUNX2, early

osteogenic genes such as ALP, Col 1A1, SPARC or osteonectin, ANKH, osteomodulin and the late osteogenic genes such as osteocalcin and podoplanin.

RUNX2 is the master controller of osteogenesis and controls the expression of genes involved in osteogenesis. It is essential for the differentiation of mesenchymal stem cells into osteoblast and their maturation into osteocytes (Schroeder et al., 2005). In the present study, older donor BM-MSC of week3 showed higher expression of RUNX2. Alkaline phosphatase is a marker of osteoblast activity (Christenson, 1997; Sabokbar et al., 1994) and expression of ALP in the present study confirmed the osteogenic potential of the materials. Previous studies demonstrated that OMD as a marker of osteoblast differentiation (Kawada et al., 2006) and as a positive controller of osteogenesis through BMP2/SMAD pathway (Lin et al., 2021). Osteocalcin / (BGLAP) is an abundant non-collagenous protein and marker for osteoblast mineralization or bone formation (Tsao et al., 2017).

It was reported that absence of ANKH gene in mice reduced the osteogenesis and increased the adipogenesis (Kim et al., 2010; Minashima et al., 2017). In the present study, expression of ANKH induced the osteogenesis and reduced the expression of adipogenic genes. Although the senescence of older donor BM-MSCs was proven, SNC, SN-15 and SN-150 upregulated the expression of RUNX2 than peroxisome proliferator activator receptor γ (PPAR- γ). In contrast, Ganguly *et al*., demonstrated that the bimorphic rattan wood scaffold upregulated the expression of genes involved in adipogenesis and osteogenesis in BM-MSCS which were collected from the donors of age 36-65 years (n=6) (Ganguly, El-Jawhari, et al., 2022). MMP1 is an interstitial collagenase participating in the remodelling of extracellular matrix (ECM) and

findings by Wu *et al.*, proved that MMP-1 induced the osteogenic differentiation of human BM-MSC via the JNK-ERK (c-Jun N -terminal kinase and the extracellular regulated protein kinase ERK) pathway (Wu et al., 2020). In the present study, expression of MMP-1 was found which again confirmed the osteogenesis of BM-MSC.

CXCL12 is a chemokine that plays an active role in the migration, homing, and engraftment of MSC and ultimately leading to the accumulation of stem cells in the bone marrow (Y Han et al., 2022). In the present study, higher expression of CXCL12 indicated the attraction of a greater number of MSCs towards SNC, SN-15 and SN-150 which indirectly exhibited the better microenvironment prompted by these materials. It is known that VEGF A is a prime factor responsible for angiogenesis but it also plays an important role in osteogenesis (Berendsen and Olsen, 2014; Hu and Olsen, 2016). Liu *et al.*, reported that intracellular VEGF controls the balance between adipogenesis and osteogenesis in mice (Liu et al., 2012). In this study, a very high expression of VEGF A indicated an ambient microenvironment for both osteogenesis and angiogenesis. Overall, the gene expression studies proved the osteogenic and angiogenic potential of SNC, SN-15 and SN-150, which improved the microenvironment of older donor BM-MSCs and young donor BM-MSC. In the presence of shell nacre integrated materials, older donor BM-MSC performed equivalent to that of young donor BM-MSC.

In brief, direct and indirect cytotoxicity studies with BM-MSC proved the non-cytotoxic nature of SNC, SN-15 and SN-150. Older donor BM-MSCs showed reduced proliferation capacity and higher senescence than young donor BM-MSC. All the three

materials induced osteogenic differentiation of both the BM-MSC with the proof of hydroxyapatite mineralisation. q-PCR confirmed the osteogenic and angiogenic potential of both the older donor BM-MSCs and young donor BM-MSC. Although a higher proportion of BM-MSCs of older donors were senescent, shell nacre integrated materials SNC 72, SN-15, SN-150 improved the microenvironment of older donor BM-MSC and performed equivalent to that of young donor BM-MSC.

8 SUMMARY AND CONCLUSIONS

8.1 SUMMARY

Shell nacre powder is renowned for its remarkable osteogenic and angiogenic properties and holds immense promise for bone defect management applications. This work focused on harnessing the potential of shell nacre powder derived from the shells of *Pinctada fucata,* a resource that has been underutilized in this field. *Pinctada fucata* shells were identified by the golden metallic hue inner nacreous layer. SEM imaging revealed the characteristic brick-and-mortar arrangement of the inner nacreous layer. HCl-based and acetic acid-based methods were attempted to remove the outer prismatic layer of the shells. The observations from the SEM imaging concluded that the acetic acid-based method retained the brick-and-mortar structure of the nacreous layer, whereas the HCL method disrupted the characteristic structure. Dried nacreous shells were ball-milled, sieved and purified to obtain shell nacre powder. Shell nacre powder revealed an irregular morphology of size less than 0.5 µm. FTIR studies confirmed the presence of both organic and inorganic constituents. From TGA analysis, it was found that the shell nacre powder contained 5% organic content and 95 % inorganic content. Raman and XRD studies confirmed the aragonite form of calcium carbonate and matching to the JCPDS of aragonite (JCPDS 01-071-2392). Trace element analysis confirmed the absence of deleterious heavy metals. Direct contact and cell adhesion studies proved the non-cytotoxic nature and cytocompatibility of shell nacre powder. Therefore, the first objective of processing of shell nacre and characterization of shell nacre powder is achieved.

The second objective shell nacre PCL composite scaffolds were accomplished by the TIPS method using the green solvent dimethyl carbonate. Scaffolds SN-15 containing 13% shell nacre powder and SN-150 containing 60% shell nacre powder were selected based on the compressive modulus values. During SEM imaging, SN-15 scaffolds revealed a porous interconnected lamellar structure that contained interconnected microspheres with pores. On the other hand, SN-150 scaffolds were porous with random aligned structure. SN-15 exhibited 70% porosity with pore size ranging from 30 to 150 µm whereas SN-150 scaffold showed 35% porosity with pore size ranging from 10 to 200 µm. FTIR analysis revealed the presence of shell nacre and PCL peaks in both the scaffolds. TGA analysis confirmed the quantity of shell nacre and PCL in the scaffolds. After 150 days aging in PBS, SN-150 (75%) exhibited higher percentage of reductions in compressive than SN-15 (51%) and PCL (30%). Both SN-15 and SN-150 showed significant rapid hydroxyapatite mineralization from day 2 and large mineralized structure were seen in SN-15 due to the porous interconnected microsphere structures. Direct contact and MTT assay proved the non-cytotoxic nature of the scaffolds.

In vitro osteogenic potential of the scaffolds was studied using rat BM-MSCs for 7, 14 and 21 days Both immunofluorescence and flow cytometry analysis of rat BM-MSCs showed positive for the mesenchymal stem cell marker CD90, CD105 and negative for the hematopoietic stem cell marker CD34. *In vitro* osteogenic potential of SN-15 and SN-150 scaffolds were compared with the clinical control G-Bone (Surgiwear, India) and the positive control. Without any osteo-differentiation medium, rat BM-MSCs after contact with SN-15 and SN-150 showed higher ALP activity equivalent to that of positive control and G-Bone. Both SN-15 and SN-150 showed

higher expression of BMP-2, RUNX-2 and ALP than G-Bone and positive control during day 7, 14 and 21 which was distinctly seen in the gene cluster map. Regarding the extracellular matrix proteins, SN-150 showed higher collagen I expression and SN-15 showed higher osteocalcin expression than G-Bone and positive control. Furthermore, ALP and osteocalcin immunostaining, again fortified the results of osteogenesis and proved the osteogenic potential of both SN-15 and SN-150. The fabricated composite scaffolds of shell nacre and PCL demonstrated desirable characteristics including, interconnected porosity, bioactivity, non-cytotoxicity and osteogenic properties. Consequently, the second objective was successfully accomplished.

The third objective is to develop bone void filling cement that exhibits low polymerization shrinkage, minimal exotherm, higher mechanical properties, bioactivity, biocompatibility and osteogenesis. To accomplish this, modifications were made to both the resin and filler components of the cement. Among the various resin matrices, ormocer resin stands out as a multifunctional glass like resin with properties such as low polymerization shrinkage, higher mechanical properties and biocompatibility. It has been extensively explored for its application in dental cements. So, considering all the merits of the ormocer resin strategy, shell nacre containing ladder structured siloxane methacrylate resins were synthesized by modified-sol gel method. During the 8h reaction, the precursor 3-TMSPM underwent hydrolysis and followed by polycondensation to form the SNLSM resins. All the resins were transparent with refractive index of ~ 1.47 respectively and no significant change in RI was found, after the addition of shell nacre. FTIR of all the resins confirmed the presence of ladder structured siloxane backbone with shell nacre integration and intact

methacrylate side chain in all the resins except LSM. Similarly, Raman spectrum showed the formation of four membered siloxane unit and integration of shell nacre. Both TGA and DSC analysis proved the thermal stability and flexibility of siloxane chains present in all the resins. LSM exhibited no T_{50} whereas SNLSM2 exhibited T_{50} at 672°C. Similarly, LSM exhibited T_g at -47°C, whereas SNLSM2 showed T_g at -50°C. This confirmed the integration of shell nacre in the siloxane network. As SNLSM2 evidenced the presence of ladder structured siloxane backbone and methacrylate side chain, it was selected for further characterizations. ^{13} C NMR of SNLSM2 confirmed the completed polycondensation of silanol which was understood by the absence of O-CH_3 groups. TEM images of SNLSM2 and LSM again confirmed the presence of ladder structured siloxane backbone, which was seen as a continuous chain of siloxane units. SNLSM2 exhibited Newtonian property with viscosity of 144.32 $Pa^{-}s$ at 25°C and 75.714 Pa^{-} at 37°C. All the above characterizations of SNLSM2 confirmed the presence of ladder structured siloxane backbone with shell nacre integration. Thus, the subobjective of the objective three was accomplished.

In order to achieve the objective of shell nacre cement development using the synthesized SNLSM2 resin and shell nacre powder. The quantity of BPO, DMAPEA, BPO and shell nacre powder were optimized. The working time of the shell nacre cement was 3 min with setting time of 6 min respectively. Different amounts of shell nacre (24%, 48%, and 72%) were added to the SNLSM2 resin and the impact on the physicochemical properties of the cement was studied. Among the compositions, SNC 72 exhibited significantly low linear polymerization shrinkage (0.4%), higher compressive (>100 MPa) and flexural strength (> 35 MPa). SNC 72 was radiopaque and the exotherm generated during the cement curing was minimal. Cytotoxicity

studies with L929 cells revealed the non-cytotoxic nature of the cement. After SBF treatment, the SEM EDS analysis of the SNC 72 confirmed the bioactive nature of the shell nacre cement, as evidenced by the significant hydroxyapatite formation indicated by the presence of calcium and phosphorus peaks. Furthermore, after aging in PBS, the compressive strength reduction percentage was 0%, 11% and 40% at 4,8 and 12 months, respectively. Similarly, after aging in SBF, the CS reduction percentages were 3%,10% and 28% at 4, 8 and 12 months. These results showed the slow degradation pattern of shell nacre cement. The biocompatibility of SNC 72 was confirmed through acute systemic toxicity, animal intracutaneous (intradermal) reactivity test, and pyrogen test, which proved that the material satisfied the requirements of the test as per ISO 10993-parts10 and 11 standards. SNC 72 exhibited osseointegration during *in situ* setting in 2mm femoral cortical defect in rats. SNC 72 adhered firmly to the bone without any signs of inflammation and infection, whereas the clinical control PMMA cement showed inadequate adhesion. Overall, this study demonstrated the successful development of shell nacre cement and its advantageous properties

As both *in vitro* and *in vivo* studies have shown a shift towards adipogenesis rather than osteogenesis in BM-MSCs of older donors, any bone substitute material would be considered truly osteogenic only after confirming the material's osteogenic potential with older BM-MSCs. Hence, the osteogenic potential of shell nacre PCL composite scaffolds and shell nacre cement, was studied with BM-MSCs from older donors, followed by the direct and indirect cytotoxicity studies with human BM-MSCs, which once again confirmed the non-cytotoxic nature of SN-15, SN-150 and SNC 72. BM-MSCs from old donors (n=3, age>55) and young donors (n=3, age<30) were expanded and evaluated for colony-forming potential and senescence assay.

Older BM-MSCs exhibited reduced proliferation and colony forming potential and higher number of β gal positive cells than young BM-MSCs. Both the pooled and old BM-MSCs were seeded on the shell nacre scaffolds and shell nacre cement. Confocal imaging of the live cell tracker green stained cells confirmed the presence of viable BM-MSCs on SN-15, SN-150, SNC-72 for up to 21 days. Scanning electron microscopy (SEM) with energy dispersive spectroscopy (EDS) revealed the hydroxyapatite mineralization of young and older BM-MSCs. Furthermore, qPCR analysis demonstrated that the SN-15, SN-150, SNC 72 upregulated the expression of genes involved in osteogenesis and angiogenesis of older donor BM-MSCs leading to an improved bone healing microenvironment. Overall, this study provided more insights into the osteogenic potential of shell nacre PCL composite scaffolds and shell nacre cement with older BM-MSCs regardless of senescence.

8.2 Conclusions

With this motto “Nature is healing always”, this study explored the potential of shell nacre, whose origin as a bone substitute dated back to the Mayan age.

Shell nacre

- Acetic acid-based processing method was developed to obtain shell nacre powder while preserving its inherent properties.
- The obtained shell nacre powder comprised of both organic (5%) and inorganic (aragonite) (95%) constituents and free of harmful heavy metals.
- Shell nacre powder lacked cytotoxicity and exhibited cyto-compatible properties.

Shell nacre PCL -Composite scaffolds

- With the aim of *in situ* bone tissue engineering, two types of shell nacre PCL composite scaffolds were fabricated by TIPS method using a green solvent dimethyl carbonate.
- SN-15 is a porous microsphere structured scaffold with 70% porosity and compressive modulus of about 6 MPa. SN-150 is a random porous scaffold with a porosity of 30% with compressive modulus of about 10 MPa.
- Both SN-15 and SN-150 scaffolds are non-cytotoxic, bioactive and exhibited features of degradation.
- Without any osteoinduction, both SN-15 and SN-150 scaffolds exhibited higher ALP activity, higher gene expression of BMP-2, RUNX-2, ALP and performed equivalent to that of positive control and better than that of clinical control G-Bone.
- SN-15 exhibited superior bioactivity and osteogenic properties than SN-150 due to its interconnected microsphere structure.

Shell nacre containing ladder structured siloxane methacrylate resin

- SNLSM2 is an ormocer resin synthesized by modified sol-gel method using the precursor 3-TMSPM.
- Spectroscopy and thermal studies revealed the formation of ladder structured siloxane backbone and intact methacrylate side chain.
- SNLSM2 played a significant role in achieving low shrinkage, improved mechanical properties and minimal exotherm generation of the shell nacre cement.

Shell nacre cement

- SNC 72 is a pioneering bone void filling cement made of shell nacre powder and ladder structured siloxane methacrylate resin. It possessed both the desired physico-chemical and biological properties.
- SNC 72 exhibited low linear polymerization shrinkage, minimal exotherm generation, higher mechanical properties and non-cytotoxic nature.
- SNC 72 is biocompatible and satisfied the acute systemic toxicity, animal intracutaneous (intradermal) reactivity test, and pyrogen test as per the ISO 10993 part 1, 10 and 11.
- The *in situ* cured SNC 72 demonstrated osseointegration in the femoral defect of Sprague Dawley rats after 6 weeks and 12 weeks.

***In vitro* osteogenesis with older donor BM-MSCs**

- SN-15, SN-150, and SNC are found to be non-cytotoxic with human BM-MSCs. Older donor BM-MSCs showed a reduced proliferation capacity and higher proportion of senescent cells than young donor BM-MSCs.
- Both young and older donor BM-MSC remained viable in SN-15, SN-150, and SNC for up to 21 days which proved the cytocompatible nature of the materials
- Although the older donor BM-MSCs were more senescent than the young donor BM-MSCs, shell nacre integrated scaffolds and cement improved the microenvironment of older donor BM-MSCs and promoted both osteogenesis and angiogenesis in older donor BM-MSCs regardless of senescence.

- This study underscores the need to evaluate the osteogenesis of any bone substitute material with BM-MSCs from older donors, considering the more prevalence of orthopaedic surgeries in the geriatric population.

Overall, three different types of shell nacre integrated biomaterials have been developed such as shell nacre PCL composite scaffolds (SN-15 and SN-150), shell nacre containing ormocer resin (SNLSM2) and bone void filling shell nacre cement (SNC 72). It is important to note that these materials serve different applications, making direct comparisons challenging. Among the scaffolds, SN-15 stands out as a superior choice than SN-150 due to its interconnected microsphere structure, which demonstrated better bioactivity and osteogenesis. Among the resins, SNLSM2 would be a promising candidate resin for hard tissue restorative applications due to its siloxane backbone and methacrylate side-chain. SNC 72 would be the best candidate for a bone void filling cement, offering substantial advantages over existing options in the market with its impressive physico-chemical and biological properties.

8.3 Future perspectives

- Composite scaffolds of shell nacre and PCL are the promising candidate for bone defect management. Further research, focusing on *in vivo* critical sized osteoporotic model for longer duration will reveal the potential of these scaffolds. Additionally, *in vivo* degradation and inflammatory studies may extend the potential of these scaffolds.
- SNLSM2 holds tremendous potential for hard tissue restorative applications. Further research into the 3 D printability of the resin may enhance the versatility of the SNLSM2 resin.

- Taken together, the findings from this study proved that the SNC 72 has the potential to become a leading bone void filling cement for bone defect management. Further research and testing will be necessary to fully explore its potential and refine its formula for clinical use. Additionally, examining the flow properties and formulating as an injectable cement will enhance the versatility of the cement
- Future investigations into *in vivo* long term degradation studies, *in vivo* critical sized defects in osteoporotic models will provide even more evidence for the superiority of shell nacre scaffolds and cement.
- Further investigation with larger numbers of donors for BM-MSC with an expanded age range from 18 to 80 will provide more insights into the performance of all the materials.

References

Abdelrazek EM, Hezma AM, El-khodary A, et al. (2016) Spectroscopic studies and thermal properties of PCL/PMMA biopolymer blend. *Egyptian Journal of Basic and Applied Sciences* 3(1): 10–15.

Agarwal V, Tjandra ES, Iyer KS, et al. (2014) Evaluating the effects of nacre on human skin and scar cells in culture. *Toxicol. Res.* 3(4): 223–227.

Agbaje OBA, Dominguez JG and Jacob DE (2021) Organic biopolymers of venus clams: Collagen-related matrix in the bivalve shells with crossed-lamellar ultrastructure. *Biochemistry and Biophysics Reports* 26: 100939.

Albrektsson T and Johansson C (2001) Osteoinduction, osteoconduction and osseointegration. *European Spine Journal: Official Publication of the European Spine Society, the European Spinal Deformity Society, and the European Section of the Cervical Spine Research Society* 10 Suppl 2(Suppl 2): S96-101.

Al-Odayni A-B, Alfotawi R, Khan R, et al. (2019) Synthesis of chemically modified BisGMA analog with low viscosity and potential physical and biological properties for dental resin composite. *Dental Materials* 35(11): 1532–1544.

Alrahlah A, Al-Odayni A-B, Al-Mutairi HF, et al. (2021) A Low-Viscosity BisGMA Derivative for Resin Composites: Synthesis, Characterization, and Evaluation of Its Rheological Properties. *Materials* 14(2): 338.

Alt V, Walter N, Rupp M, et al. (2023) Bone defect filling with a novel rattan-wood based not-sintered hydroxyapatite and beta-tricalcium phosphate material (b.Bone^{TM}) after tricortical bone graft harvesting – A consecutive clinical case series of 9 patients. *Trauma Case Reports* 44: 100805.

Artaki I, Bradley M, Zerda TW, et al. (1985a) NMR and Raman study of the hydrolysis reaction in sol-gel processes. *The Journal of Physical Chemistry* 89(20). American Chemical Society: 4399–4404.

Artaki I, Bradley M, Zerda TW, et al. (1985b) NMR and Raman study of the hydrolysis reaction in sol-gel processes. *The Journal of Physical Chemistry* 89(20). American Chemical Society: 4399–4404.

ASTM F640 (2023) Standard Test Methods for Determining Radiopacity for Medical Use. Available at: https://www.astm.org/f0640-23.html.

ASTM F1609-08 (2014) Standard Specification for Calcium Phosphate Coatings for Implantable Materials. Available at: https://www.astm.org/f1609-08r14.html (accessed 8 April 2023).

ASTM F2103 (2018) Standard Guide for Characterization and Testing of Chitosan Salts as Starting Materials Intended for Use in Biomedical and Tissue-

Engineered Medical Product Applications. Available at: https://www.astm.org/f2103-18.html (accessed 28 February 2023).

Asumda FZ and Chase PB (2011) Age-related changes in rat bone-marrow mesenchymal stem cell plasticity. *BMC Cell Biology* 12: 44.

Atlan G, Balmain N, Berland S, et al. (1997) Reconstruction of human maxillary defects with nacre powder: histological evidence for bone regeneration. *Comptes Rendus de l'Académie des Sciences - Series III - Sciences de la Vie* 320(3): 253–258.

Atlan G, Delattre O, Berland S, et al. (1999) Interface between bone and nacre implants in sheep. *Biomaterials* 20(11): 1017–1022.

Aurégan J-C and Bégué T (2014) Induced membrane for treatment of critical sized bone defect: a review of experimental and clinical experiences. *International Orthopaedics* 38(9): 1971–1978.

Baatti A, Erchiqui F, Bébin P, et al. (2017) A two-step Sol-Gel method to synthesize a ladder polymethylsilsesquioxane nanoparticles. *Advanced Powder Technology* 28(3): 1038–1046.

Babensee JE, Anderson JM, McIntire LV, et al. (1998) Host response to tissue engineered devices. *Advanced Drug Delivery Reviews* 33(1). Tissue Engineering: 111–139.

Balmain J, Hannoyer B and Lopez E (1999) Fourier transform infrared spectroscopy (FTIR) and X-ray diffraction analyses of mineral and organic matrix during heating of mother of pearl (nacre) from the shell of the mollusc Pinctada maxima. *Journal of Biomedical Materials Research* 48(5): 749–754.

Bartl R and Bartl C (2017) Structure and Architecture of Bone. In: Bartl R and Bartl C (eds) *Bone Disorders : Biology, Diagnosis, Prevention, Therapy*. Cham: Springer International Publishing, pp. 11–20. Available at: https://doi.org/10.1007/978-3-319-29182-6_2 (accessed 5 June 2023).

Behera PR (2017) Pinctada fucata (Gould, 1850). Kochi: ICAR - Central Marine Fisheries Research Institute, pp. 401–407. Available at: http://eprints.cmfri.org.in/12412/ (accessed 10 April 2023).

Behera S, Naskar D, Sapru S, et al. (2017) Hydroxyapatite reinforced inherent RGD containing silk fibroin composite scaffolds: Promising platform for bone tissue engineering. *Nanomedicine: Nanotechnology, Biology and Medicine* 13(5): 1745–1759.

Bellaaj-Zouari A, Chérif K, Elloumi-Hannachi I, et al. (2011) Characterization of mineral and organic phases in nacre of the invasive pearl oyster Pinctada radiata (Leach, 1814). 52: 337.

Berendsen AD and Olsen BR (2014) How Vascular Endothelial Growth Factor-A (VEGF) Regulates Differentiation of Mesenchymal Stem Cells. *Journal of Histochemistry and Cytochemistry* 62(2): 103–108.

Berland S, Delattre O, Borzeix S, et al. (2005) Nacre/bone interface changes in durable nacre endosseous implants in sheep. *Biomaterials* 26(15): 2767–2773.

Bharadwaz A and Jayasuriya AC (2020) Recent trends in the application of widely used natural and synthetic polymer nanocomposites in bone tissue regeneration. *Materials Science and Engineering: C* 110: 110698.

Bian T, Zhao K, Meng Q, et al. (2019) The construction and performance of multi-level hierarchical hydroxyapatite (HA)/collagen composite implant based on biomimetic bone Haversian motif. *Materials & Design* 162: 60–69.

Block TJ, Marinkovic M, Tran ON, et al. (2017) Restoring the quantity and quality of elderly human mesenchymal stem cells for autologous cell-based therapies. *Stem Cell Research & Therapy* 8(1): 239.

Blokhuis TJ (2017) Management of traumatic bone defects: Metaphyseal versus diaphyseal defects. *Injury* 48. Complications of intramedullary nailing - Evolution of treatment: S91–S93.

Bobbio A (1972) The first endosseous alloplastic implant in the history of man. *Bulletin of the History of Dentistry* 20(1): 1–6.

Bohner M (2000) Calcium orthophosphates in medicine: from ceramics to calcium phosphate cements. *Injury* 31: D37–D47.

Boros K and Freemont T (2017) Physiology of ageing of the musculoskeletal system. *Best Practice & Research Clinical Rheumatology* 31(2). Ageing and musculoskeletal health: 203–217.

Boskey AL (2013) Bone composition: relationship to bone fragility and antiosteoporotic drug effects. *BoneKEy Reports* 2: 447.

Boyd D, Towler MR, Wren A, et al. (2008) Comparison of an experimental bone cement with surgical Simplex P, Spineplex and Cortoss. *Journal of Materials Science. Materials in Medicine* 19(4): 1745–1752.

Breeland G, Sinkler MA and Menezes RG (2023) Embryology, Bone Ossification. In: *StatPearls*. Treasure Island (FL): StatPearls Publishing. Available at: http://www.ncbi.nlm.nih.gov/books/NBK539718/ (accessed 2 April 2023).

Bridget Jeyatha W, Paul W, Mani S, et al. (2022) Synthesis and characterization of ladder structured ormocer resin of siloxane backbone and methacrylate side chain. *Materials Letters* 310: 131192.

Brown JF (1963) Double chain polymers and nonrandom crosslinking. *Journal of Polymer Science Part C: Polymer Symposia* 1(1): 83–97.

Burr DB (2019) Changes in bone matrix properties with aging. *Bone* 120: 85–93.

Campana V, Milano G, Pagano E, et al. (2014) Bone substitutes in orthopaedic surgery: from basic science to clinical practice. *Journal of Materials Science. Materials in Medicine* 25(10): 2445–2461.

Camprasse S, Camprasse G, Pouzol M, et al. (1990) Artificial dental root made of natural calcium carbonate (bioracine). *Clinical Materials* 5(2). EMRS interfaces in biomaterials sciences: 235–250.

Cao S, Zhao Y, Hu Y, et al. (2020) New perspectives: In-situ tissue engineering for bone repair scaffold. *Composites Part B: Engineering* 202: 108445.

Cao Y, Croll TI, Oconnor AJ, et al. (2006) Systematic selection of solvents for the fabrication of 3D combined macro- and microporous polymeric scaffolds for soft tissue engineering. *Journal of Biomaterials Science. Polymer Edition* 17(4): 369–402.

Capuana E, Lopresti F, Carfì Pavia F, et al. (2021) Solution-Based Processing for Scaffold Fabrication in Tissue Engineering Applications: A Brief Review. *Polymers* 13(13). 13. Multidisciplinary Digital Publishing Institute: 2041.

Carvalho MS, Alves L, Bogalho I, et al. (2021) Impact of Donor Age on the Osteogenic Supportive Capacity of Mesenchymal Stromal Cell-Derived Extracellular Matrix. *Frontiers in Cell and Developmental Biology* 9: 747521.

Chen L, Hu J, Ran J, et al. (2014) Preparation and evaluation of collagen-silk fibroin/hydroxyapatite nanocomposites for bone tissue engineering. *International Journal of Biological Macromolecules* 65: 1–7.

Chen Q, Shou P, Zheng C, et al. (2016) Fate decision of mesenchymal stem cells: adipocytes or osteoblasts? *Cell Death & Differentiation* 23(7). 7. Nature Publishing Group: 1128–1139.

Chen X, Wang L, Hou J, et al. (2019) Study on the Dynamic Biological Characteristics of Human Bone Marrow Mesenchymal Stem Cell Senescence. *Stem Cells International* 2019: 9271595.

Chen X-D (2010) Extracellular matrix provides an optimal niche for the maintenance and propagation of mesenchymal stem cells. *Birth Defects Research. Part C, Embryo Today: Reviews* 90(1): 45–54.

Chiang C-C, Hsieh M-K, Wang C-Y, et al. (2021) Cytotoxicity and cell response of preosteoblast in calcium sulfate-augmented PMMA bone cement. *Biomedical Materials (Bristol, England)* 16(5).

Christenson RH (1997) Biochemical Markers of Bone Metabolism: An Overview. *Clinical Biochemistry* 30(8): 573–593.

Clarke BL and Khosla S (2010) Physiology of Bone Loss. *Radiologic Clinics* 48(3). Elsevier: 483–495.

Coots BK (2012) Alveolar Bone Grafting: Past, Present, and New Horizons. *Seminars in Plastic Surgery* 26(4): 178–183.

Corrado A, Cici D, Rotondo C, et al. (2020) Molecular Basis of Bone Aging. *International Journal of Molecular Sciences* 21(10). 10. Multidisciplinary Digital Publishing Institute: 3679.

Crane GM, Ishaug SL and Mikos AG (1995) Bone tissue engineering. *Nature Medicine* 1(12): 1322–1324.

Crystal E. Porter and Frank D. Blum (2000) Thermal Characterization of PMMA Thin Films Using Modulated Differential Scanning Calorimetry. Macromolecules 2000 33 (19), 7016-7020 DOI: 10.1021/ma000302l.

Cui X, Huang C, Zhang M, et al. (2017) Enhanced osteointegration of poly(methylmethacrylate) bone cements by incorporating strontium-containing borate bioactive glass. *Journal of The Royal Society Interface* 14(131). Royal Society: 20161057.

Dar PMUD, Mir N, Katiyar AK, et al. (2023) Outcome predictors of patients who underwent limb amputation/s following trauma at a level I trauma center in North India. *European Journal of Trauma and Emergency Surgery*. Epub ahead of print 26 May 2023. DOI: 10.1007/s00068-023-02273-1.

de Muizon CJ, Iandolo D, Nguyen DK, et al. (2022) Organic Matrix and Secondary Metabolites in Nacre. *Marine Biotechnology* 24(5): 831–842.

Deb S, Aiyathurai L, Roether JA, et al. (2005) Development of high-viscosity, two-paste bioactive bone cements. *Biomaterials* 26(17): 3713–3718.

Debacq-Chainiaux F, Erusalimsky JD, Campisi J, et al. (2009) Protocols to detect senescence-associated beta-galactosidase (SA-βgal) activity, a biomarker of senescent cells in culture and in vivo. *Nature Protocols* 4(12). 12. Nature Publishing Group: 1798–1806.

Delattre O, Catonne Y, Berland S, et al. (1997) Use of mother of pearl as a bone substitute - Experimental study in sheep. *European Journal of Orthopaedic Surgery & Traumatology* 7(2): 143–147.

Demers C, Hamdy CR, Corsi K, et al. (2002) Natural coral exoskeleton as a bone graft substitute: a review. *Bio-Medical Materials and Engineering* 12(1): 15–35.

Deshpande R, Shukla S, Kale A, et al. (2022) Silk Fibroin Microparticle Scaffold for Use in Bone Void Filling: Safety and Efficacy Studies. *ACS Biomaterials Science & Engineering* 8(3). American Chemical Society: 1226–1238.

Díaz E, Sandonis I and Valle MB (2014) In Vitro Degradation of Poly(caprolactone)/nHA Composites. *Journal of Nanomaterials* 2014. Hindawi: e802435.

Díaz E, Aresti J and León J (2021) Evaluation of physicochemical and mechanical properties with the in vitro degradation of PCL/nHA/MWCNT composite scaffolds. *Journal of Reinforced Plastics and Composites* 40(3–4). SAGE Publications Ltd STM: 134–142.

Didekhani R, Sohrabi MR, Soleimani M, et al. (2020) Incorporating PCL nanofibers with oyster shell to improve osteogenic differentiation of mesenchymal stem cells. *Polymer Bulletin* 77(2): 701–715.

Dirckx N, Van Hul M and Maes C (2013) Osteoblast recruitment to sites of bone formation in skeletal development, homeostasis, and regeneration. *Birth Defects Research. Part C, Embryo Today: Reviews* 99(3): 170–191.

Dirè S, Borovin E and Ribot F (2018) Architecture of Silsesquioxanes. In: Klein L, Aparicio M, and Jitianu A (eds) *Handbook of Sol-Gel Science and Technology: Processing, Characterization and Applications*. Cham: Springer International Publishing, pp. 3119–3151. Available at: https://doi.org/10.1007/978-3-319-32101-1_119 (accessed 4 January 2023).

Dominici M, Le Blanc K, Mueller I, et al. (2006) Minimal criteria for defining multipotent mesenchymal stromal cells. The International Society for Cellular Therapy position statement. *Cytotherapy* 8(4): 315–317.

Dou DD, Zhou G, Liu HW, et al. (2019) Sequential releasing of VEGF and BMP-2 in hydroxyapatite collagen scaffolds for bone tissue engineering: Design and characterization. *International Journal of Biological Macromolecules* 123: 622–628.

Du M, Li Q, Chen J, et al. (2021) Design and characterization of injectable abalone shell/calcium sulfate bone cement scaffold for bone defect repair. *Chemical Engineering Journal* 420: 129866.

Duan H, Cao C, Wang X, et al. (2020) Magnesium-alloy rods reinforced bioglass bone cement composite scaffolds with cortical bone-matching mechanical properties and excellent osteoconductivity for load-bearing bone in vivo regeneration. *Scientific Reports* 10(1). 1. Nature Publishing Group: 18193.

Duplat D, Chabadel A, Gallet M, et al. (2007) The in vitro osteoclastic degradation of nacre. *Biomaterials* 28(12): 2155–2162.

El-Alfy BS and Ali AM (2015) Management of segmental skeletal defects by the induced membrane technique. *Indian Journal of Orthopaedics* 49(6): 643–648.

El-Jawhari JJ, Cuthbert R, McGonagle D, et al. (2017) The CD45lowCD271high Cell Prevalence in Bone Marrow Samples May Provide a Useful Measurement of the Bone Marrow Quality for Cartilage and Bone Regenerative Therapy. *The Journal of Bone and Joint Surgery. American Volume* 99(15): 1305–1313.

Elsalanty ME and Genecov DG (2009) Bone grafts in craniofacial surgery. *Craniomaxillofacial Trauma & Reconstruction* 2(3): 125–134.

Elzein T, Nasser-Eddine M, Delaite C, et al. (2004) FTIR study of polycaprolactone chain organization at interfaces. *Journal of Colloid and Interface Science* 273(2): 381–387.

Erbe EM, Clineff TD and Gualtieri G (2001) Comparison of a new bisphenol-a-glycidyl dimethacrylate-based cortical bone void filler with polymethyl methacrylate. *European Spine Journal* 10(2): S147–S152.

Fabbri P, Cannillo V, Sola A, et al. (2010) Highly porous polycaprolactone-45S5 Bioglass® scaffolds for bone tissue engineering. *Composites Science and*

Technology 70(13). ICCM-17: Composites In Biomedical Applications: 1869–1878.

Farr JN and Khosla S (2019) Cellular Senescence in Bone. *Bone* 121: 121–133.

Feng X (2009) Chemical and Biochemical Basis of Cell-Bone Matrix Interaction in Health and Disease. *Current chemical biology* 3(2): 189–196.

Fernandez AC, Mohanty M, Varma HK, et al. (2006) Safety and efficacy of Chitra-CPC calcium phosphate cement as bone substitute. *Current Science* 91(12). Temporary Publisher: 1678–1686.

Fernandez de Grado G, Keller L, Idoux-Gillet Y, et al. (2018) Bone substitutes: a review of their characteristics, clinical use, and perspectives for large bone defects management. *Journal of Tissue Engineering* 9: 2041731418776819.

Fielding G and Bose S (2013) SiO2 and ZnO dopants in three-dimensionally printed tricalcium phosphate bone tissue engineering scaffolds enhance osteogenesis and angiogenesis in vivo. *Acta Biomaterialia* 9(11): 9137–9148.

Fillingham Y and Jacobs J (2016) Bone grafts and their substitutes. *The Bone & Joint Journal* 98-B(1_Supple_A). Bone & Joint: 6–9.

Flausse A, Henrionnet C, Dossot M, et al. (2013) Osteogenic differentiation of human bone marrow mesenchymal stem cells in hydrogel containing nacre powder. *Journal of Biomedical Materials Research Part A* 101(11): 3211–3218.

Florencio-Silva R, Sasso GR da S, Sasso-Cerri E, et al. (2015) Biology of Bone Tissue: Structure, Function, and Factors That Influence Bone Cells. *BioMed Research International* 2015: 421746.

Fortune Business Insights (2023a) Bone Graft Substitutes Market Size, Share & Analysis [2030]. Available at: https://www.fortunebusinessinsights.com/bone-graft-substitutes-market-103106 (accessed 18 September 2023).

Fortune Business Insights (2023b) Bone Void Fillers Market Size, Share, Growth | Forecast [2030]. Available at: https://www.fortunebusinessinsights.com/industry-reports/bone-void-fillers-market-101015 (accessed 18 September 2023).

Galea GL, Zein MR, Allen S, et al. (2021) Making and shaping endochondral and intramembranous bones. *Developmental Dynamics* 250(3): 414–449.

Ganguly P, El-Jawhari JJ, Burska AN, et al. (2019) The Analysis of *In Vivo* Aging in Human Bone Marrow Mesenchymal Stromal Cells Using Colony-Forming Unit-Fibroblast Assay and the $CD45^{low}CD271^{+}$ Phenotype. *Stem Cells International* 2019. Hindawi: e5197983.

Ganguly P, Fiz N, Beitia M, et al. (2022) Effect of Combined Intraosseous and Intraarticular Infiltrations of Autologous Platelet-Rich Plasma on Subchondral Bone Marrow Mesenchymal Stromal Cells from Patients with Hip

Osteoarthritis. *Journal of Clinical Medicine* 11(13). 13. Multidisciplinary Digital Publishing Institute: 3891.

Ganguly P, El-Jawhari JJ, Vun J, et al. (2022) Evaluation of Human Bone Marrow Mesenchymal Stromal Cell (MSC) Functions on a Biomorphic Rattan-Wood-Derived Scaffold: A Comparison between Cultured and Uncultured MSCs. *Bioengineering* 9(1). 1. Multidisciplinary Digital Publishing Institute: 1.

Gao C, Peng S, Feng P, et al. (2017) Bone biomaterials and interactions with stem cells. *Bone Research* 5: 17059.

Gerhard EM, Wang W, Li C, et al. (2017) Design strategies and applications of nacre-based biomaterials. *Acta Biomaterialia* 54: 21–34.

Giannoudis PV, Dinopoulos H and Tsiridis E (2005) Bone substitutes: an update. *Injury* 36 Suppl 3: S20-27.

Giannoudis PV, Einhorn TA and Marsh D (2007) Fracture healing: The diamond concept. *Injury* 38. 4th European Clinical Symposium on Bone and Tissue Regeneration: S3–S6.

Giannoudis PV, Harwood PJ, Tosounidis T, et al. (2016) Restoration of long bone defects treated with the induced membrane technique: protocol and outcomes. *Injury* 47. Restoration of cartilage and bone loss: S53–S61.

Gilbert JL, Hasenwinkel JM, Wixson RL, et al. (2000) A theoretical and experimental analysis of polymerization shrinkage of bone cement: A potential major source of porosity. *Journal of Biomedical Materials Research* 52(1): 210–218.

Gillman CE and Jayasuriya AC (2021) FDA-approved bone grafts and bone graft substitute devices in bone regeneration. *Materials Science and Engineering: C* 130: 112466.

Gleeson JP, Plunkett NA and O'Brien FJ (2010) Addition of hydroxyapatite improves stiffness, interconnectivity and osteogenic potential of a highly porous collagen-based scaffold for bone tissue regeneration. *European Cells & Materials* 20: 218–230.

Goonasekera CS, Jack KS, Cooper-White JJ, et al. (2016) Dispersion of hydroxyapatite nanoparticles in solution and in polycaprolactone composite scaffolds. *Journal of Materials Chemistry B* 4(3). The Royal Society of Chemistry: 409–421.

Goto K, Tamura J, Shinzato S, et al. (2005) Bioactive bone cements containing nano-sized titania particles for use as bone substitutes. *Biomaterials* 26(33): 6496–6505.

Grohmann CVS, Sinhoreti MAC, Soares EF, et al. (2022) Effect of a polymerization inhibitor on the chemomechanical properties and consistency of experimental resin composites. *Brazilian Dental Journal* 33(3): 92–98.

Gu X, Li Y, Qi C, et al. (2022) Biodegradable magnesium phosphates in biomedical applications. *Journal of Materials Chemistry B* 10(13). The Royal Society of Chemistry: 2097–2112.

Guarino V, Causa F and Ambrosio L (2007) Porosity and Mechanical Properties Relationship in PCL Porous Scaffolds. *Journal of Applied Biomaterials and Biomechanics* 5(3). SAGE Publications: 149–157.

Guarino V, Scaglione S, Sandri M, et al. (2014) MgCHA particles dispersion in porous PCL scaffolds: in vitro mineralization and in vivo bone formation. *Journal of Tissue Engineering and Regenerative Medicine* 8(4): 291–303.

Haas K-H (2000) Hybrid Inorganic–Organic Polymers Based on Organically Modified Si-Alkoxides. *Advanced Engineering Materials* 2(9): 571–582.

Hadjidakis DJ and Androulakis II (2006) Bone remodeling. *Annals of the New York Academy of Sciences* 1092: 385–396.

Han Y, Yang J, Fang J, et al. (2022) The secretion profile of mesenchymal stem cells and potential applications in treating human diseases. *Signal Transduction and Targeted Therapy* 7(1). 1. Nature Publishing Group: 1–19.

Han Z, Wang B, Ren B, et al. (2022) Characterization and Biomechanical Study of a Novel Magnesium Potassium Phosphate Cement. *Life* 12(7): 997.

Hasandoost L, Rodriguez O, Alhalawani A, et al. (2020) The Role of Poly(Methyl Methacrylate) in Management of Bone Loss and Infection in Revision Total Knee Arthroplasty: A Review. *Journal of Functional Biomaterials* 11(2): 25.

He Z, Zhai Q, Hu M, et al. (2015) Bone cements for percutaneous vertebroplasty and balloon kyphoplasty: Current status and future developments. *Journal of Orthopaedic Translation* 3(1): 1–11.

Hristov S, Visscher L, Winkler J, et al. (2022) A Novel Technique for Treatment of Metaphyseal Voids in Proximal Humerus Fractures in Elderly Patients. *Medicina* 58(10). 10. Multidisciplinary Digital Publishing Institute: 1424.

Hu K and Olsen BR (2016) The roles of vascular endothelial growth factor in bone repair and regeneration. *Bone* 91: 30–38.

Iandolo D, Laroche N, Nguyen DK, et al. (2022) Preclinical safety study of nacre powder in an intraosseous sheep model. *BMJ Open Science* 6(1).

Idumah CI, Zurina M, Hassan A, et al. (2019) Chapter 8 - Recently Emerging Trends in Bone Replacement Polymer Nanocomposites. In: Swain SK and Jawaid M (eds) *Nanostructured Polymer Composites for Biomedical Applications*. Micro and Nano Technologies. Elsevier, pp. 139–166. Available at: https://www.sciencedirect.com/science/article/pii/B9780128167717000089 (accessed 9 June 2023).

Infante A and Rodríguez CI (2018) Osteogenesis and aging: lessons from mesenchymal stem cells. *Stem Cell Research & Therapy* 9(1): 244.

ISO 10993-1 (2018) Biological evaluation of medical devices — Part 1: Evaluation and testing within a risk management process.

ISO 10993-5 (2009) Biological evaluation of medical devices — Part 5: Tests for in vitro cytotoxicity.

ISO 10993-10 (2021) Biological evaluation of medical devices — Part 10: Tests for skin sensitization.

ISO 10993-11 (2017) Biological evaluation of medical devices — Part 11: Tests for systemic toxicity.

ISO 10993-12 (2021) ISO 10993-12:2021 - Biological evaluation of medical devices — Part 12: Sample preparation and reference materials. Available at: https://www.iso.org/standard/75769.html (accessed 8 May 2023).

ISO 23317 (2014) ISO 23317:2014 Implants for surgery — In vitro evaluation for apatite-forming ability of implant materials.

Jacobs E, Saralidze K, Roth AK, et al. (2016) Synthesis and characterization of a new vertebroplasty cement based on gold-containing PMMA microspheres. *Biomaterials* 82: 60–70.

Jayabalan M, Thomas V and Sreelatha PK (2000) Studies on poly(propylene fumarate-co-ethylene glycol) based bone cement. *Bio-medical materials and engineering* 10(2): 57–71.

Jayasree R and Sampath Kumar T (2015) Acrylic cement formulations modified with calcium deficient apatite nanoparticles for orthopaedic applications. *Journal of Composite Materials* 49(23). SAGE Publications Ltd STM: 2921–2933.

Jena KK, Alhassan SM, Tiwari A, et al. (2018) Functional Nano-Coating Materials by Michael Addition and Ring-opening Polymerization: Reactivity, Molecular Architecture and Refractive index. *Scientific Reports* 8(1). 1. Nature Publishing Group: 11912.

Jia Y, Zhang P, Sun Y, et al. (2019) Regeneration of large bone defects using mesoporous silica coated magnetic nanoparticles during distraction osteogenesis. *Nanomedicine: Nanotechnology, Biology and Medicine* 21: 102040.

Johari N, Madaah Hosseini HR and Samadikuchaksaraei A (2017) Optimized composition of nanocomposite scaffolds formed from silk fibroin and nano-TiO2 for bone tissue engineering. *Materials Science and Engineering: C* 79: 783–792.

Justesen J, Stenderup K, Ebbesen EN, et al. (2001) Adipocyte tissue volume in bone marrow is increased with aging and in patients with osteoporosis. *Biogerontology* 2(3): 165–171.

Kalampounias AG (2011) IR and Raman spectroscopic studies of sol–gel derived alkaline-earth silicate glasses. *Bulletin of Materials Science* 34(2): 299–303.

Kasha S, Rathore SS and Kumar H (2019) Antibiotic Cement Spacer and Induced Membrane Bone Grafting in Open Fractures with Bone Loss: A Case Series. *Indian Journal of Orthopaedics* 53(2): 237–245.

Kashirina A, Yao Y, Liu Y, et al. (2019) Biopolymers as bone substitutes: a review. *Biomaterials Science* 7(10). The Royal Society of Chemistry: 3961–3983.

Kawada M, Hamajima S and Abiko Y (2006) Osteomodulin Gene Expression in Human Bone Marrow-Derived Mesenchymal Stem Cells into Osteoblastic Differentiation. *International Journal of Oral-Medical Sciences* 4(3): 170–176.

Kawanabe K, Tamura J, Yamamuro T, et al. (1993) A new bioactive bone cement consisting of BIS-GMA resin and bioactive glass powder. *Journal of Applied Biomaterials* 4(2): 135–141.

Keating JF, Simpson AHRW and Robinson CM (2005) The management of fractures with bone loss. *The Journal of Bone and Joint Surgery. British volume* 87-B(2). The British Editorial Society of Bone & Joint Surgery: 142–150.

Khandaker M, Vaughan MB, Morris TL, et al. (2014) Effect of additive particles on mechanical, thermal, and cell functioning properties of poly(methyl methacrylate) cement. *International Journal of Nanomedicine* 9: 2699–2712.

Kim D, Lee J, Min Seok J, et al. (2021) Three-dimensional bioprinting of bioactive scaffolds with thermally embedded abalone shell particles for bone tissue engineering. *Materials & Design* 212: 110228.

Kim H, Lee K, Ko C-Y, et al. (2012) The role of nacreous factors in preventing osteoporotic bone loss through both osteoblast activation and osteoclast inactivation. *Biomaterials* 33(30): 7489–7496.

Kim HJ, Minashima T, McCarthy EF, et al. (2010) Progressive ankylosis protein (ANK) in osteoblasts and osteoclasts controls bone formation and bone remodeling. *Journal of Bone and Mineral Research: The Official Journal of the American Society for Bone and Mineral Research* 25(8): 1771–1783.

Kim Yun Hyeok, Choi G-M, Bae JG, et al. (2018a) High-Performance and Simply-Synthesized Ladder-Like Structured Methacrylate Siloxane Hybrid Material for Flexible Hard Coating. *Polymers* 10(4). 4. Multidisciplinary Digital Publishing Institute: 449.

Kim Yun Hyeok, Choi G-M, Bae JG, et al. (2018b) High-Performance and Simply-Synthesized Ladder-Like Structured Methacrylate Siloxane Hybrid Material for Flexible Hard Coating. *Polymers* 10(4): 449.

Kokubo T and Takadama H (2006) How useful is SBF in predicting in vivo bone bioactivity? *Biomaterials* 27(15): 2907–2915.

Kokubo T, Yoshihara S, Nishimura N, et al. (1991) Bioactive Bone Cement Based on CaO─SiO2─P2O5 Glass. *Journal of the American Ceramic Society* 74(7): 1739–1741.

Komori T (2013) Functions of the osteocyte network in the regulation of bone mass. *Cell and Tissue Research* 352(2): 191–198.

Kon E, Salamanna F, Filardo G, et al. (2021) Bone Regeneration in Load-Bearing Segmental Defects, Guided by Biomorphic, Hierarchically Structured Apatitic Scaffold. *Frontiers in Bioengineering and Biotechnology* 9.

Korbut A, Włodarczyk M, Rudnicka K, et al. (2021) Three Component Composite Scaffolds Based on PCL, Hydroxyapatite, and L-Lysine Obtained in TIPS-SL: Bioactive Material for Bone Tissue Engineering. *International Journal of Molecular Sciences* 22(24). 24. Multidisciplinary Digital Publishing Institute: 13589.

Kovar FM and Wozasek GE (2011) Bone graft harvesting using the RIA (reaming irrigation aspirator) system – a quantitative assessment. *Wiener klinische Wochenschrift* 123(9): 285–290.

Krishnan V and Lakshmi T (2013) Bioglass: A novel biocompatible innovation. *Journal of Advanced Pharmaceutical Technology & Research* 4(2): 78–83.

Kumar MN, Belehalli P and Ramachandra P (2014) PET/CT study of temporal variations in blood flow to the femoral head following low-energy fracture of the femoral neck. *Orthopedics* 37(6): e563-570.

Kün-Darbois J-D, Libouban H, Camprasse G, et al. (2021) In vivo osseointegration and erosion of nacre screws in an animal model. *Journal of Biomedical Materials Research. Part B, Applied Biomaterials* 109(6): 780–788.

Lamghari M, Almeida MJ, Berland S, et al. (1999) Stimulation of bone marrow cells and bone formation by nacre: in vivo and in vitro studies. *Bone* 25(2, Supplement 1): 91S-94S.

Lamghari M, Antonietti P, Berland S, et al. (2001) Arthrodesis of Lumbar Spine Transverse Processes Using Nacre in Rabbit. *Journal of Bone and Mineral Research* 16(12): 2232–2237.

Lamghari M, Berland S, Laurent A, et al. (2001) Bone reactions to nacre injected percutaneously into the vertebrae of sheep. *Biomaterials* 22(6): 555–562.

Lee K, Kim H, Kim JM, et al. (2012) Nacre-driven water-soluble factors promote wound healing of the deep burn porcine skin by recovering angiogenesis and fibroblast function. *Molecular Biology Reports* 39(3): 3211–3218.

Lewis G (2008) Alternative acrylic bone cement formulations for cemented arthroplasties: present status, key issues, and future prospects. *Journal of Biomedical Materials Research. Part B, Applied Biomaterials* 84(2): 301–319.

Li W-J, Tuli R, Huang X, et al. (2005) Multilineage differentiation of human mesenchymal stem cells in a three-dimensional nanofibrous scaffold. *Biomaterials* 26(25): 5158–5166.

Li Z, Xiang S, Lin Z, et al. (2021) Graphene oxide-functionalized nanocomposites promote osteogenesis of human mesenchymal stem cells via enhancement of BMP-SMAD1/5 signaling pathway. *Biomaterials* 277: 121082.

Libouban H, Pascaretti-Grizon F, Camprasse G, et al. (2016) In vivo erosion of orthopedic screws prepared from nacre (mother of pearl). *Orthopaedics & Traumatology: Surgery & Research* 102(7): 913–918.

Lin W, Zhu X, Gao L, et al. (2021) Osteomodulin positively regulates osteogenesis through interaction with BMP2. *Cell Death & Disease* 12(2): 147.

Lin X, Ge J, Wei D, et al. (2019) Surface degradation–enabled osseointegrative, angiogenic and antiinfective properties of magnesium-modified acrylic bone cement. *Journal of Orthopaedic Translation* 17. Degenerative musculoskeletal diseases: pathology and treatments: 121–132.

Liu C, Han Z and Czernuszka JT (2009) Gradient collagen/nanohydroxyapatite composite scaffold: Development and characterization. *Acta Biomaterialia* 5(2): 661–669.

Liu J, Ding Y, Liu Z, et al. (2020) Senescence in Mesenchymal Stem Cells: Functional Alterations, Molecular Mechanisms, and Rejuvenation Strategies. *Frontiers in Cell and Developmental Biology* 8: 258.

Liu Q, Kim JH, Cho M, et al. (2023) Bioactive magnesium-based whitlockite ceramic as bone cement additives for enhancing osseointegration and bone regeneration. *Materials & Design* 229: 111914.

Liu Y, Berendsen AD, Jia S, et al. (2012) Intracellular VEGF regulates the balance between osteoblast and adipocyte differentiation. *The Journal of Clinical Investigation* 122(9): 3101–3113.

Liu Y, Huang Q and Feng Q (2013) 3D scaffold of PLLA/pearl and PLLA/nacre powder for bone regeneration. *Biomedical Materials* 8(6). IOP Publishing: 065001.

Liu Z, Tang Y, Kang T, et al. (2015) Synergistic effect of HA and BMP-2 mimicking peptide on the bioactivity of HA/PMMA bone cement. *Colloids and Surfaces. B, Biointerfaces* 131: 39–46.

Liu Z, He X, Chen S, et al. (2023) Advances in the use of calcium silicate-based materials in bone tissue engineering. *Ceramics International*. Epub ahead of print 7 March 2023. DOI: 10.1016/j.ceramint.2023.03.063.

Lizymol PP (2004a) Effects of diluent's concentration upon the properties of organically modified ceramics based composites for application in dentistry. *Journal of Applied Polymer Science* 94(2): 469–473.

Lizymol PP (2004b) Thermal studies: A comparison of the thermal properties of different oligomers by thermogravimetric techniques. *Journal of Applied Polymer Science* 93(2): 977–985.

Lizymol PP (2010) Studies on shrinkage, depth of cure, and cytotoxic behavior of novel organically modified ceramic based dental restorative resins. *Journal of Applied Polymer Science* 116(5): 2645–2650.

Lopez E, Vidal B, Berland S, et al. (1992) Demonstration of the capacity of nacre to induce bone formation by human osteoblasts maintained in vitro. *Tissue and Cell* 24(5): 667–679.

Lotke PA, Wong RY and Ecker ML (1991) The use of methylmethacrylate in primary total knee replacements with large tibial defects. *Clinical Orthopaedics and Related Research* (270): 288–294.

Lu J, Wang Z, Zhang H, et al. (2022) Bone Graft Materials for Alveolar Bone Defects in Orthodontic Tooth Movement. *Tissue Engineering. Part B, Reviews* 28(1): 35–51.

Ma T, Liao J, Zhang Y, et al. (2023) Study on modification of hydroxyapatite/magnesium phosphate bone cement by N-acetyl-l-cysteine. *Ceramics International* 49(11, Part A): 16545–16553.

Malhotra A, Pelletier MH, Yu Y, et al. (2014) A Sheep Model for Cancellous Bone Healing. *Frontiers in Surgery* 1.

Mancuso F, Beltrame A, Colombo E, et al. (2017) Management of metaphyseal bone loss in revision knee arthroplasty. *Acta Bio Medica : Atenei Parmensis* 88(Suppl 2): 98–111.

Mark JE (2004) Some Interesting Things about Polysiloxanes. *Accounts of Chemical Research* 37(12). American Chemical Society: 946–953.

Marongiu G, Verona M, Cardoni G, et al. (2020) Synthetic Bone Substitutes and Mechanical Devices for the Augmentation of Osteoporotic Proximal Humeral Fractures: A Systematic Review of Clinical Studies. *Journal of Functional Biomaterials* 11(2). 2. Multidisciplinary Digital Publishing Institute: 29.

Marsell R and Einhorn TA (2011) THE BIOLOGY OF FRACTURE HEALING. *Injury* 42(6): 551–555.

Masquelet AC, Fitoussi F, Begue T, et al. (2000) [Reconstruction of the long bones by the induced membrane and spongy autograft]. *Annales De Chirurgie Plastique Et Esthetique* 45(3): 346–353.

Mathew L, Joseph R and Krishnan VK (1997) Effect of Amine Activators on the Properties of Chemical Cured Dental Composites. *Journal of Biomaterials Applications* 11(3). SAGE Publications Ltd STM: 349–359.

MEGA BIOPHARMA (n.d.) Orthopaedics | Bone repair. Available at: https://megabiopharma.com/en/orthopaedics/ (accessed 11 March 2023).

Megat Abdul Wahab R, Abdullah N, Zainal Ariffin SH, et al. (2020) Effects of the Sintering Process on Nacre-Derived Hydroxyapatite Scaffolds for Bone

Engineering. *Molecules* 25(14). 14. Multidisciplinary Digital Publishing Institute: 3129.

Meunier P, Aaron J, Edouard C, et al. (1971) Osteoporosis and the Replacement of Cell Populations of the Marrow by Adipose Tissue: A Quantitative Study of 84 Iliac Bone Biopsies. *Clinical Orthopaedics and Related Research*® 80: 147.

Minashima T, Quirno M, Lee YJ, et al. (2017) The Role of the Progressive Ankylosis Protein (ANK) in Adipogenic/Osteogenic Fate Decision of Precursor Cells. *Bone* 98: 38–46.

Moore WR, Graves SE and Bain GI (2001) Synthetic bone graft substitutes. *ANZ Journal of Surgery* 71(6): 354–361.

Moreira CA, Dempster DW and Baron R (2019) Anatomy and Ultrastructure of Bone – Histogenesis, Growth and Remodeling. In: *Endotext [Internet]*. MDText.com, Inc. Available at: https://www.ncbi.nlm.nih.gov/sites/books/NBK279149/ (accessed 6 June 2023).

Mousa WF, Kobayashi M, Shinzato S, et al. (2000) Biological and mechanical properties of PMMA-based bioactive bone cements. *Biomaterials* 21(21): 2137–2146.

Moutahir-belqasmi F, Balmain N, Lieberrher M, et al. (2001) Effect of water soluble extract of nacre (Pinctada maxima) on alkaline phosphatase activity and Bcl-2 expression in primary cultured osteoblasts from neonatal rat calvaria. *Journal of Materials Science: Materials in Medicine* 12(1): 1–6.

Nair BP, Sindhu M and Nair PD (2016) Polycaprolactone-laponite composite scaffold releasing strontium ranelate for bone tissue engineering applications. *Colloids and Surfaces. B, Biointerfaces* 143: 423–430.

Nam YS and Park TG (1999) Porous biodegradable polymeric scaffolds prepared by thermally induced phase separation. *Journal of Biomedical Materials Research* 47(1): 8–17.

Nandi SK, Roy S, Mukherjee P, et al. (2010) Orthopaedic applications of bone graft & graft substitutes: a review. *Indian Journal of Medical Research* 132(1): 15.

Nauth A, Schemitsch E, Norris B, et al. (2018) Critical-Size Bone Defects: Is There a Consensus for Diagnosis and Treatment? *Journal of Orthopaedic Trauma* 32: S7.

Ni G. X., Chiu KY, Lu WW, et al. (2006) Strontium-containing hydroxyapatite bioactive bone cement in revision hip arthroplasty. *Biomaterials* 27(24): 4348–4355.

Ni G.X., Chiu KY, Lu WW, et al. (2006) Strontium-containing hydroxyapatite bioactive bone cement in revision hip arthroplasty. *Biomaterials* 27(24): 4348–4355.

Nisal A, Sayyad R, Dhavale P, et al. (2018) Silk fibroin micro-particle scaffolds with superior compression modulus and slow bioresorption for effective bone regeneration. *Scientific Reports* 8(1). 1. Nature Publishing Group: 7235.

Nussbaum DA, Gailloud P and Murphy K (2004) The Chemistry of Acrylic Bone Cements and Implications for Clinical Use in Image-guided Therapy. *Journal of Vascular and Interventional Radiology* 15(2). Elsevier: 121–126.

Nuttall ME, Patton AJ, Olivera DL, et al. (1998) Human Trabecular Bone Cells Are Able to Express Both Osteoblastic and Adipocytic Phenotype: Implications for Osteopenic Disorders. *Journal of Bone and Mineral Research* 13(3): 371–382.

O'dowd-Booth CJ, White J, Smitham P, et al. (2011) Bone Cement: Perioperative Issues, Orthopaedic Applications and Future Developments. *Journal of Perioperative Practice* 21(9). SAGE Publications: 304–308.

Ormsby R, McNally T, Mitchell C, et al. (2011) Effect of MWCNT addition on the thermal and rheological properties of polymethyl methacrylate bone cement. *Carbon* 49(9): 2893–2904.

Owens GJ, Singh RK, Foroutan F, et al. (2016) Sol–gel based materials for biomedical applications. *Progress in Materials Science* 77: 1–79.

Pan P, Geng Y, Hu L, et al. (2022) Biologically enhanced 3D printed micro-nano hybrid scaffolds doped with abalone shell for bone regeneration. *Advanced Composites and Hybrid Materials* 6(1): 10.

Parekh N, Hushye C, Warunkar S, et al. (2017) In vitro study of novel microparticle based silk fibroin scaffold with osteoblast-like cells for load-bearing osteo-regenerative applications. *RSC Advances* 7(43). Royal Society of Chemistry: 26551–26558.

Paz E, Forriol F, Del Real JC, et al. (2017) Graphene oxide versus graphene for optimisation of PMMA bone cement for orthopaedic applications. *Materials Science & Engineering. C, Materials for Biological Applications* 77: 1003–1011.

Pei J, Wang Y, Zou X, et al. (2021) Extraction, Purification, Bioactivities and Application of Matrix Proteins From Pearl Powder and Nacre Powder: A Review. *Frontiers in Bioengineering and Biotechnology* 9.

Piccirilli E, Cariati I, Primavera M, et al. (2022) Augmentation in fragility fractures, bone of contention: a systematic review. *BMC Musculoskeletal Disorders* 23(1): 1046.

Pignolo RJ, Samsonraj RM, Law SF, et al. (2019) Targeting Cell Senescence for the Treatment of Age-Related Bone Loss. *Current Osteoporosis Reports* 17(2): 70–85.

Ponzetti M and Rucci N (2021) Osteoblast Differentiation and Signaling: Established Concepts and Emerging Topics. *International Journal of Molecular Sciences* 22(13): 6651.

Pountos I and Giannoudis PV (2016) Is there a role of coral bone substitutes in bone repair? *Injury* 47(12): 2606–2613.

Przesławski G, Szcześniak K, Gajewski P, et al. (2022) Influence of Initiator Concentration on the Polymerization Course of Methacrylate Bone Cement. *Polymers* 14(22): 5005.

Quatman CE, Wiseman J and Phieffer L (2018) Academic Geriatric Orthopaedics: A New paradigm for Inpatient Care. *Current geriatrics reports* 7(4): 272–277.

Rahman MS, Akhtar N, Jamil HM, et al. (2015) TGF-β/BMP signaling and other molecular events: regulation of osteoblastogenesis and bone formation. *Bone Research* 3(1). 1. Nature Publishing Group: 1–20.

Ramesh K, Melzner F, Griffith AW, et al. (2018) In vivo characterization of bivalve larval shells: a confocal Raman microscopy study. *Journal of the Royal Society, Interface* 15(141): 20170723.

Reito A and Ylitalo A (2020) Polymethyl Methacrylate Cement Fill as a Definitive Treatment for Massive Bone Defect After Infected Internal Fixation in Bicondylar Tibial Fracture: A Case Report. *JBJS Case Connector* 10(3): e19.00286.

Remya KR, Chandran S, Mani S, et al. (2018) Hybrid polycaprolactone/polyethylene oxide scaffolds with tunable fiber surface morphology, improved hydrophilicity and biodegradability for bone tissue engineering applications. *Journal of Biomaterials Science, Polymer Edition* 29(12). Taylor & Francis: 1444–1462.

Rodríguez JP, Montecinos L, Ríos S, et al. (2000) Mesenchymal stem cells from osteoporotic patients produce a type I collagen-deficient extracellular matrix favoring adipogenic differentiation. *Journal of Cellular Biochemistry* 79(4): 557–565.

Rolvien T and Amling M (2016) Bone biology in the elderly: clinical importance for fracture treatment. *Innovative Surgical Sciences* 1(2): 49–55.

Rousseau M, Lopez E, Stempflé P, et al. (2005) Multiscale structure of sheet nacre. *Biomaterials* 26(31): 6254–6262.

Rousseau M, Boulzaguet H, Biagianti J, et al. (2008) Low molecular weight molecules of oyster nacre induce mineralization of the MC3T3-E1 cells. *Journal of Biomedical Materials Research Part A* 85A(2): 487–497.

Rowe P, Koller A and Sharma S (2023) Physiology, Bone Remodeling. In: *StatPearls*. Treasure Island (FL): StatPearls Publishing. Available at: http://www.ncbi.nlm.nih.gov/books/NBK499863/ (accessed 6 June 2023).

Ruan R, Zheng M, Gao J, et al. (2018) Improved Biological Properties of Calcium Phosphate Cement by Nacre Incorporation: An In Vitro Study. *Journal of Biomaterials and Tissue Engineering* 8(1): 67–79.

Russell TA, Leighton RK, and Alpha-BSM Tibial Plateau Fracture Study Group (2008) Comparison of autogenous bone graft and endothermic calcium phosphate cement for defect augmentation in tibial plateau fractures. A multicenter, prospective, randomized study. *The Journal of Bone and Joint Surgery. American Volume* 90(10): 2057–2061.

Sabokbar A, Millett PJ, Myer B, et al. (1994) A rapid, quantitative assay for measuring alkaline phosphatase activity in osteoblastic cells in vitro. *Bone and Mineral* 27(1): 57–67.

Safadi FF, Barbe MF, Abdelmagid SM, et al. (2009) Bone Structure, Development and Bone Biology. In: Khurana JS (ed.) *Bone Pathology*. Totowa, NJ: Humana Press, pp. 1–50. Available at: https://doi.org/10.1007/978-1-59745-347-9_1 (accessed 5 June 2023).

Sahu AK, Lenka BS and Panda CK (2019) Masquelet technique for treatment of open tibia fracture with bone loss: An observational study. *International Journal of Orthopaedics Sciences* 5(3): 387–390.

Sahu N, Baligar P, Midha S, et al. (2015) Nonmulberry Silk Fibroin Scaffold Shows Superior Osteoconductivity Than Mulberry Silk Fibroin in Calvarial Bone Regeneration. *Advanced Healthcare Materials* 4(11): 1709–1721.

Salerno A and Domingo C (2015) Pore structure properties of scaffolds constituted by aggregated microparticles of PCL and PCL-HA processed by phase separation. *Journal of Porous Materials* 22(2): 425–435.

Sandhya S, Mohanan PV, Sabareeswaran A, et al. (2017) Preclinical safety and efficacy evaluation of 'BioCaS' bioactive calcium sulfate bone cement. *Biomedical Materials* 12(1). IOP Publishing: 015022.

Sanjurjo-Rodriguez C, Altaie A, Mastbergen S, et al. (2020) Gene Expression Signatures of Synovial Fluid Multipotent Stromal Cells in Advanced Knee Osteoarthritis and Following Knee Joint Distraction. *Frontiers in Bioengineering and Biotechnology* 8.

Schemitsch EH (2017) Size Matters: Defining Critical in Bone Defect Size! *Journal of Orthopaedic Trauma* 31: S20.

Schildhauer TA, Bauer TW, Josten C, et al. (2000) Open reduction and augmentation of internal fixation with an injectable skeletal cement for the treatment of complex calcaneal fractures. *Journal of Orthopaedic Trauma* 14(5): 309–317.

Schroeder TM, Jensen ED and Westendorf JJ (2005) Runx2: a master organizer of gene transcription in developing and maturing osteoblasts. *Birth Defects Research. Part C, Embryo Today: Reviews* 75(3): 213–225.

Sengupta D, Waldman SD and Li S (2014) From In Vitro to In Situ Tissue Engineering. *Annals of Biomedical Engineering* 42(7): 1537–1545.

Sheen JR, Mabrouk A and Garla VV (2023) Fracture Healing Overview. In: *StatPearls*. Treasure Island (FL): StatPearls Publishing. Available at: http://www.ncbi.nlm.nih.gov/books/NBK551678/ (accessed 7 June 2023).

Shen Y, Yang S, Liu J, et al. (2014) Engineering Scaffolds Integrated with Calcium Sulfate and Oyster Shell for Enhanced Bone Tissue Regeneration. *ACS Applied Materials & Interfaces* 6(15). American Chemical Society: 12177–12188.

Siddiqui N, Asawa S, Birru B, et al. (2018) PCL-Based Composite Scaffold Matrices for Tissue Engineering Applications. *Molecular Biotechnology* 60(7): 506–532.

Siffert RS (1951) THE ROLE OF ALKALINE PHOSPHATASE IN OSTEOGENESIS. *The Journal of Experimental Medicine* 93(5): 415–426.

Silve C, Lopez E, Vidal B, et al. (1992) Nacre initiates biomineralization by human osteoblasts maintained In Vitro. *Calcified Tissue International* 51(5): 363–369.

Simu M-R, Pall E, Radu T, et al. (2018) Development of a novel biomaterial with an important osteoinductive capacity for hard tissue engineering. *Tissue and Cell* 52: 101–107.

Singh L, Brennan TA, Russell E, et al. (2016) Aging alters bone-fat reciprocity by shifting in vivo mesenchymal precursor cell fate towards an adipogenic lineage. *Bone* 85: 29–36.

Sivakumar R, Mohideen MG, Chidambaram M, et al. (2016) Management of Large Bone Defects in Diaphyseal Fractures by Induced Membrane Formation by Masquelet's Technique. *Journal of Orthopaedic Case Reports* 6(3): 59–62.

Soleymani Eil Bakhtiari S, Bakhsheshi-Rad HR, Karbasi S, et al. (2020) Polymethyl Methacrylate-Based Bone Cements Containing Carbon Nanotubes and Graphene Oxide: An Overview of Physical, Mechanical, and Biological Properties. *Polymers* 12(7): E1469.

Solomin L, Komarov A, Semenistyy A, et al. (2022) Universal long bone defect classification. *Journal of Limb Lengthening & Reconstruction* 8(1): 54.

Stolzing A, Jones E, McGonagle D, et al. (2008) Age-related changes in human bone marrow-derived mesenchymal stem cells: Consequences for cell therapies. *Mechanisms of Ageing and Development* 129(3): 163–173.

Sultana N and Hayat Khan T (2013) Polycaprolactone Scaffolds and Hydroxyapatite/Polycaprolactone Composite Scaffolds for Bone Tissue Engineering. *Journal of Bionanoscience* 7(2): 169–173.

Sun J and Bhushan B (2012) Hierarchical structure and mechanical properties of nacre: a review. *RSC Advances* 2(20). The Royal Society of Chemistry: 7617–7632.

Tampieri A, Sprio S, Ruffini A, et al. (2009) From wood to bone: multi-step process to convert wood hierarchical structures into biomimetic hydroxyapatite scaffolds for bone tissue engineering. *Journal of Materials Chemistry* 19(28). The Royal Society of Chemistry: 4973–4980.

Tamura J, Kawanabe K, Yamamuro T, et al. (1995) Bioactive bone cement: The effect of amounts of glass powder and histologic changes with time. *Journal of Biomedical Materials Research* 29(5): 551–559.

Tan Q-C, Jiang X-S, Chen L, et al. (2023) Bioactive graphene oxide-functionalized self-expandable hydrophilic and osteogenic nanocomposite for orthopaedic applications. *Materials Today Bio* 18: 100500.

Tarafder S, Davies NM, Bandyopadhyay A, et al. (2013) 3D printed tricalcium phosphate bone tissue engineering scaffolds: effect of SrO and MgO doping on in vivo osteogenesis in a rat distal femoral defect model. *Biomaterials Science* 1(12). The Royal Society of Chemistry: 1250–1259.

Thomas JD and Kehoe JL (2023) Bone Nonunion. In: *StatPearls*. Treasure Island (FL): StatPearls Publishing. Available at: http://www.ncbi.nlm.nih.gov/books/NBK554385/ (accessed 9 June 2023).

Thomas MV and Puleo DA (2009) Calcium sulfate: Properties and clinical applications. *Journal of Biomedical Materials Research Part B: Applied Biomaterials* 88B(2): 597–610.

Tiede-Lewis LM and Dallas SL (2019) Changes in the Osteocyte Lacunocanalicular Network with Aging. *Bone* 122: 101–113.

Tsao Y-T, Huang Y-J, Wu H-H, et al. (2017) Osteocalcin Mediates Biomineralization during Osteogenic Maturation in Human Mesenchymal Stromal Cells. *International Journal of Molecular Sciences* 18(1): 159.

Unno M, Suto A and Matsumoto T (2013) Laddersiloxanes — silsesquioxanes with defined ladder structure. *Russian Chemical Reviews* 82(4). IOP Publishing: 289.

Vaishya R, Chauhan M and Vaish A (2013) Bone cement. *Journal of Clinical Orthopaedics and Trauma* 4(4): 157–163.

Verma D, Katti K and Katti D (2006) Photoacoustic FTIR spectroscopic study of undisturbed nacre from red abalone. *Spectrochimica Acta Part A: Molecular and Biomolecular Spectroscopy* 64(4): 1051–1057.

Verma D, Katti K and Katti D (2007) Nature of water in nacre: a 2D Fourier transform infrared spectroscopic study. *Spectrochimica Acta. Part A, Molecular and Biomolecular Spectroscopy* 67(3–4): 784–788.

Vibha, C. (2018) *Synthesis and characterization of novel bioactive low shrinkage inorganic-organic hybrid polymer for dental restorative applications (Doctoral dissertation, SCTIMST).* Doctoral dissertation. SCTIMST.

Vibha C and Lizymol PP (2017) Development of hydroxyapatite-reinforced biocomposites based on polymerizable multifunctional strontium containing inorganic-organic hybrid resins for biomedical applications. *Materials Letters* 197: 63–66.

Vibha C and Lizymol PP (2019) Synthesis and characterization of a novel radiopaque dimethacrylate zirconium containing pre-polymer for biomedical applications. *Materials Letters* 237: 294–297.

Voor MJ, Yoder EM and Burden RL (2011) Xenograft bone inclusion improves incorporation of hydroxyapatite cement into cancellous defects. *Journal of Orthopaedic Trauma* 25(8): 483–487.

Wang M, Ma L, Li D, et al. (2013) Preparation of polycaprolactone microspheres-aggregated scaffold with ultra big pores and fuzzy sphere surface by a one-step phase separation method. *Journal of Biomedical Materials Research. Part A* 101(11): 3219–3227.

Wang W and Yeung KWK (2017) Bone grafts and biomaterials substitutes for bone defect repair: A review. *Bioactive Materials* 2(4): 224–247.

Watson MB, Miles AW and Clift SE (1990) The influence of curing time and environment on the fracture properties of bone cement. *Clinical Materials* 6(4): 299–305.

Wee ATH and Wong YS (2009) Percutaneous Reduction and Injection of Norian Bone Cement for the Treatment of Displaced Intra-articular Calcaneal Fractures. *Foot & Ankle Specialist* 2(2). SAGE Publications: 98–106.

Weng Z, Wang C, Zhang C, et al. (2019) All-Trans Retinoic Acid Promotes Osteogenic Differentiation and Bone Consolidation in a Rat Distraction Osteogenesis Model. *Calcified Tissue International* 104(3): 320–330.

Willemin A-S, Zhang G, Velot E, et al. (2019) The effect of nacre extract on cord blood-derived endothelial progenitor cells: A natural stimulus to promote angiogenesis? *Journal of Biomedical Materials Research Part A* 107(7): 1406–1413.

Wolf-Brandstetter C, Roessler S, Storch S, et al. (2013) Physicochemical and cell biological characterization of PMMA bone cements modified with additives to increase bioactivity. *Journal of Biomedical Materials Research Part B: Applied Biomaterials* 101B(4): 599–609.

Wolter H, Glaubitt W and Rose K (1992) Multifunctional (Meth)Acrylate Alkoxysilanes a New Type of Reactive Compounds. *MRS Online Proceedings Library* 271(1): 719–724.

Wu G, Feng C, Hui G, et al. (2016) Improving the osteogenesis of rat mesenchymal stem cells by chitosan-based-microRNA nanoparticles. *Carbohydrate Polymers* 138: 49–58.

Wu M, Yao S, Xie Y, et al. (2018) A novel subchondral bone-grafting procedure for the treatment of giant-cell tumor around the knee: A retrospective study of 27 cases. *Medicine* 97(45): e13154.

Wu T, Gao S, Cui Y, et al. (2018a) Amphiphilic Bioactive Filler for Acrylic Bone Cement to Enhance Its Cell Adhesion. *Journal of Biomedical Nanotechnology* 14(4): 795–801.

Wu T, Gao S, Cui Y, et al. (2018b) Amphiphilic Bioactive Filler for Acrylic Bone Cement to Enhance Its Cell Adhesion. *Journal of Biomedical Nanotechnology* 14(4): 795–801.

Wu Y, Tang Y, Zhang X, et al. (2020) MMP-1 promotes osteogenic differentiation of human bone marrow mesenchymal stem cells via the JNK and ERK pathway. *The International Journal of Biochemistry & Cell Biology* 129: 105880.

Xiao W-D, Zhong Z-M, Tang Y-Z, et al. (2012) Repair of critical size bone defects with porous poly(D,L-lactide)/nacre nanocomposite hollow scaffold. *Saudi Medical Journal* 33(6): 601–607.

Yamamuro T, Nakamura T, Iida H, et al. (1998) Development of bioactive bone cement and its clinical applications. *Biomaterials* 19(16): 1479–1482.

Yang Z, Chen L, Hao Y, et al. (2017) Synthesis and Characterization of an Injectable and Hydrophilous Expandable Bone Cement Based on Poly(methyl methacrylate). *ACS Applied Materials & Interfaces* 9(46). American Chemical Society: 40846–40856.

Yao Q, Liu Y, Pan Y, et al. (2020) One-pot porogen free method fabricated porous microsphere-aggregated 3D PCL scaffolds for bone tissue engineering. *Journal of Biomedical Materials Research Part B: Applied Biomaterials* 108(6): 2699–2710.

Yehye WA, Rahman NA, Ariffin A, et al. (2015) Understanding the chemistry behind the antioxidant activities of butylated hydroxytoluene (BHT): a review. *European Journal of Medicinal Chemistry* 101: 295–312.

Ying R-L, Sun R-X, Li Q, et al. (2019) Synthesis of ultralong hydroxyapatite micro/nanoribbons and their application as reinforcement in collagen scaffolds for bone regeneration. *Ceramics International* 45(5): 5914–5921.

Zeinali R, del Valle LJ, Torras J, et al. (2021) Recent Progress on Biodegradable Tissue Engineering Scaffolds Prepared by Thermally-Induced Phase Separation (TIPS). *International Journal of Molecular Sciences* 22(7). 7. Multidisciplinary Digital Publishing Institute: 3504.

Zhang H, Cui Y, Zhuo X, et al. (2022) Biological Fixation of Bioactive Bone Cement in Vertebroplasty: The First Clinical Investigation of Borosilicate Glass (BSG) Reinforced PMMA Bone Cement. *ACS Applied Materials & Interfaces* 14(46). American Chemical Society: 51711–51727.

Zhang X, Du X, Li D, et al. (2018) Three dimensionally printed pearl powder/poly-caprolactone composite scaffolds for bone regeneration. *Journal of Biomaterials Science, Polymer Edition* 29(14). Taylor & Francis: 1686–1700.

Zhao Y, Tan K, Zhou Y, et al. (2016) A combinatorial variation in surface chemistry and pore size of three-dimensional porous poly(ε-caprolactone) scaffolds modulates the behaviors of mesenchymal stem cells. *Materials Science and Engineering: C* 59: 193–202.

Zhou S, Greenberger JS, Epperly MW, et al. (2008) Age-related intrinsic changes in human bone-marrow-derived mesenchymal stem cells and their differentiation to osteoblasts. *Aging Cell* 7(3): 335–343.

Appendices

APPENDIX B – SUPPLEMENTARY TABLES

Preparation of PBS

NaCl - 8 g

KCl - 0.2 g

Na_2HPO_4 - 1.44 g

KH_2PO_4 - 0.24 g

(1000 ml pH 7.4)

Preparation of Simulation Body Fluid (SBF)

Order, reagent, weight (g), used for preparing 1 L of SBF

Order	Reagent	Weight (g)
1	NaCl	8.035
2	$NaHCO_3$	0.355
3	KCl	0.255
4	K_2HPO_4	0.1759
5	$MgCl_2.6H_2O$	0.311
6	1M HCl	39 ml
7	$CaCl_2.2H_2O$	0.3713
8	Na_2SO_4	0.072
9	Tris	6.118
10	1M-HCl	0-5 ml

500ml deionised water was taken in a polythene beaker and kept in a water bath at 37°C with magnetic stirring. Reagents were added in the order given above after each component was dissolved completely. Reagent 6 was added slowly. Reagent 9 was added in small quantity to avoid local rise in pH. The pH was adjusted to 7.4 using 1M HCl. Make up the solution to 1000 ml in a 1000 ml standard flask. Checked the stability of SBF by placing 25ml of SBF in an incubator at 37°C for any precipitation.

List of genes and probes for qPCR (Fluidigm)

No	Gene Name	Gene ID	Assay	Category
1	Runt related transcription factor 2	RUNX2	Hs00231692_m1	Osteogenesis and bone remodeling
2	Alkaline phosphatase	ALP	Hs00758162_m1	
3	Integrin binding sialoprotein	IBSP	Hs00173720_m1	
4	Collagen type I alpha 1 chain	COL1A1	Hs01076777_m1	
5	Bone gamma-carboxyglutamate protein	BGLAP	Hs01587814_g1	
6	Secreted phosphoprotein 1	SPP1	Hs00959010_m1	
7	Secreted protein acidic and cysteine rich	SPARC	Hs00277762_m1	
8	Receptor activator of nuclear factor kappa- B Ligand	RANKL	Hs01092186_m1	
9	Osteoprotegerin	OPG	Hs00900360_m1	
10	Human homolog of the murine progressive ankylosis gene	ANKH	Hs01064613_m1	
11	Gremlin 1, DAN family BMP antagonist	GREM1	Hs00171951_m1	
12	Podoplanin	PDPN/E11	Hs00366766_m1	
13	Bone morphogenetic protein 2	BMP2	Hs00154192_m1	
14	Osteomodulin	OMD	Hs00192325_m1	
15	Parathyroid hormone like hormone	PTHLH	Hs00174969_m1	Chondrogenesis and cartilage homeostasis
16	Sex determining region Y box 9	SOX9	Hs00165814_m1	
17	Cartilage oligomeric matrix protein	COMP	Hs00164359_m1	
18	Aggrecan	ACAN	Hs00153936_m1	
19	Matrix metalloproteinase 1	MMP1	Hs00899658_m1	
20	Matrix metalloproteinase 3	MMP3	Hs00968308_m1	
21	Matrix metalloproteinase 13	MMP13	Hs00942589_m1	
22	Matrix metalloproteinase 9	MMP9	Hs00957562_m1	
23	A disintegrin and metalloproteinase with thrombospondin motifs 4	ADAMTS4	Hs00192708_m1	
24	A disintegrin and metalloproteinase with thrombospondin motifs 4	ADAMTS5	Hs01095524_m1	
25	Collagen type 10 alpha 1 chain	COL10A1	Hs00166657_m1	
26	Serpin family E member 1	SERPINE1	Hs00167155_m1	
27	Stathmin 2	STMN2	Hs00975800_m1	
28	Tissue inhibitor of metalloproteinase- 1	TIMP1	Hs00171558_m1	
29	Tissue inhibitor of metalloproteinase- 2	TIMP2	Hs01091319_m1	
30	Tissue inhibitor of metalloproteinase- 3	TIMP3	Hs00927214_m1	
31	Prostaglandin-endoperoxide synthase 2	PTGS2	Hs00153133_m1	
32	Peroxisome proliferator activated receptor γ	PPAR-ɣ	Hs00602622_m1	Adipogenesis and stromal support for angiogenesis
33	Fatty acid binding protein 4	FABP4	Hs00609791_m1	
34	C-X-C motif chemokine ligand 12	CXCL12	Hs00171022_m1	
35	Vascular endothelial growth factor a	VEGFA	Hs00900058_m1	
36	Vascular endothelial growth factor c	VEGFC	Hs01099206_m1	
37	Platelet derived growth factor receptor β	PDGFRB	Hs01019589_m1	MSC autocrine support
38	Epidermal growth factor receptor	EGFR	Hs01076078_m1	
39	Fibroblast growth factor receptor 1	FGFR1	Hs00241111_m1	

40	Fibroblast growth factor receptor 2	FGFR2	Hs01552926_m1	
41	Transforming growth factor beta receptor 2	TGFBR2	Hs00559661_m1	
42	Protein tyrosine phosphate receptor typeC	PTPRC	Hs00898487_s1	CD45
43	5’-nucleotidase ecto	NT5E	Hs00159686_m1	CD73
44	Thy-1 cell surface antigen	Thy1	Hs06633377_s1	CD90
45	Cyclin dependent kinase inhibitor 1A	p21/CDKN1A	Hs00355782_m1	Senescence / cell cycle
46	Tumour protein 53	p53	Hs01034249_m1	
47	Cyclin dependent kinase inhibitor 2A	p16/CDKN2A	Hs00923894_m1	
48	Hypoxanthine phosphoribosyl transferase 1	HPRT1	Hs99999909_m1	Housekeeping gene

ANNEXURES

List of patents from Thesis

Lizymol Philiphose Pampadykandathil, Bridget Jeyatha Wilson, and Venkiteswaran Kalliyanakrishnan. 2018. A process for the synthesis of shell nacre containing bio-resin for dental and orthopedic applications. Indian patent No.400578. **Date of Grant**: 30/06/2022.

Lizymol Philiphose Pampadykandathil and Bridget Jeyatha Wilson. 2020. Low-cost bioactive bone cement. Indian patent No. 410827. Date of Grant: 02/11/2022.

Bridget Jeyatha Wilson and Lizymol Philiphose Pampadykandathil. 2022. A process for the fabrication of low-cost polymeric composite osteogenic bone substitute/bone graft expander. Indian provisional application number 202241077522 dated 06.12.2022.

List of publications from Thesis

Jeyatha, W. B., Paul, W., Mani, S., & Lizymol, P. P. (2022). Synthesis and characterization of ladder structured ormocer resin of siloxane backbone and methacrylate side chain.*Materials Letters*,*310*, 131192.

Wilson, Bridget Jeyatha, and Lizymol Philipose Pampadykandathil. "Novel Bone Void Filling Cement Compositions Based on Shell Nacre and Siloxane Methacrylate Resin: Development and Characterization." *Bioengineering* 10, no. 7 (2023): 752.

Bridget Jeyatha Wilson,Neelam Iqbal, Heather Owston, Hemant Pandit, Payal Ganguly Lizymol P. P.,Elena Jones. *In vitro* osteogenic potential of shell nacre cement: A comparison between young and older donor human bone marrow mesenchymal stem cells. **Submitted for correction-3 to Leeds group**

Bridget Jeyatha Wilson, Deepa K Raj, Anil Kumar P R and Lizymol Philiphose Pampadykandathil. Fabrication and characterization of shell nacre PCL composite scaffolds by simple thermal induced phase separation method.**drafted**

Bridget Jeyatha Wilson, Lizymol P. P., Payal Ganguly, Hemant Pandit, Elena Jones. *Comparison of in vitro* osteogenesis of shell nacre PCL composite scaffolds with human BM-MSC. **Under preparation**

Bridget Jeyatha Wilson, HariKrishanan, Sabareesswaran,. Lizymol Philiphose Pampadykandathil**.** *Biological performance* of shell nacre cement in femoral cortical defect model. **Under preparation**

List of awards during PhD

- **Newton Bhabha Fund Ph.D. Placement Award** for the project entitled "Osteogenesis of shell nacre integrated composite material with mesenchymal stem cells of geriatric patients" at the University of Leeds under the mentorship of Dr. Elena Jones, Associate Professor (Stem cell Biology/Regenerative Medicine/Musculoskeletal diseases), Leeds Institute of Rheumatic and Musculoskeletal Medicine (LIRMM), St. James Hospital, University of Leeds, UK.
- **ICMR SRF**-Indian Council for Medical Research Senior Research Fellowship 2018-2022.
- Received **Best Poster Award, 6th Asian Biomaterials Congress** with the theme "Innovative Biomaterials: Technologies for Life & Society" October 25-27, 2017.

List of conferences attended

- XXVII National Conference and the 6th Asian Biomaterials Congress with the theme "Innovative Biomaterials: Technologies for Life & Society" presented a poster titled "Effect of shell nacre on physico-mechanical properties of inorganic -organic hybrid resin composites", authored by Bridget Jeyatha W., Dhanya G. R. & Lizymol P.P. at Thiruvananthapuram, October 25-27, 2017.
- Second International conference on recent trends in materials science & technology (ICMST) at VSSC, Veli from 10.10.2018 to 13.10.2018 and presented a poster entitled "Novel shell nacre containing bio-resin based composites for hard tissue replacements" authored by Bridget Jeyatha W. & Lizymol P.P.
- Attended virtual international conference on Biomedical Material Innovation from 6.12.2020 -9.12.2020 and presented a paper entitled "Synthesis and characterization of ladder like siloxane methacrylate prepolymers for hard tissue restorative applications" authored by Bridget Jeyatha W., Willi Paul & Lizymol P.P. during the conference through google meet.
- Attended Virtual World Biomaterial Congress from 13.12.20 to 16.12.20
- Presented a paper entitled "Natural Calcium containing siloxane methacrylate prepolymers for hard tissue restorative applications" authored by Bridget Jeyatha W., & Lizymol P.P. during 33rd Kerala Science Congress 25-30 Jan 2021.

Curriculum Vitae

Education

2004-2006 **M.Sc. Biotechnology**

Bharathidasan University,

Tiruchirapalli, TamilNadu, India.

2001-2004 **B.Sc. Biotechnology**

Periyar University,

Salem, Tamil Nadu, India.

Research Experience

2018-2022 **ICMR SRF** "Shell nacre integrated bioactive composite materials for bone defect treatment"

2017-2018 **Project fellow** in the KSCSTE project "Development of bioactive bone cement based on inorganic-organic hybrid resin" at Sree Chitra Tirunal Institute for Medical Science & Technology, Thiruvananthapuram, Kerala, India.

2015-2017 **Principal Investigator** of the project "*In vitro* marine molluscan mantle tissue culture for ortho and dental applications" Department of Science & Technology, Women Scientist Scheme A (DST WOSA) at TRC center of Central Marine Fisheries Research Institute, Tuticorin, TamilNadu, India

2009-2010 **Junior Research Fellow** of the DBT project on 'Indo-Norwegian platform for developing candidate vaccines to Piscine, Avian and Invertebrate species' Virology Unit, Fisheries College & Research Institute, Tuticorin, TamilNadu, India

2007-2008 **Junior Research Fellow** of the project "Developing yellow mosaic virus resistance in black gram" at School of Biotechnology, Madurai Kamaraj University, Tamil Nadu, India.

Awards

- Department of Science & Technology (DST) **Women Scientist A Award** 2015-2017 for the project entitled "*In vitro* marine molluscan mantle tissue culture for ortho and dental applications"
- Qualified GATE 2009 with a score of 393, Percentile score of 90.9
- Secured university rank -14 (B.Sc. Biotechnology)